STUDIES ON LONGITUDINAL STRUCTURE FUNCTION F_L OF PROTON AT SMALL – X

A thesis submitted in partial fulfilment of
the requirements for award of the degree of
Doctor of Philosophy

Nomita Baruah
Registration No: 017 of 2013

Department of Physics
School of Sciences
Tezpur University
Napaam, Tezpur – 784028
Assam, India

March, 2015

*To **Maa-Deuta** (my parents).*

Studies on Longitudinal Structure Function F_L of Proton at Small-x

Abstract

The knowledge of structure of the matter, its properties and interactions are important for better understanding of the origin of the universe. High Energy Physics has been dealing with the understanding of the fundamental constituents of the matter, i.e., the leptons, quarks, the intermediate gauge bosons and the interaction between them. Scattering experiments starting from Rutherford's famous experiment have played an important role in the investigation of the inner structure of matter. Deep Inelastic lepton-nucleon Scattering (DIS) provides quantitative test of Quantum Chromodynamics (QCD) i.e., the measurement of quarks and gluon densities inside the nucleon. The interaction among these constituents of nucleon can be described by different QCD evolution equations. The structure functions of the nucleon which provide the information about the partons (quarks and gluons) can be obtained as a solution of these evolution equations.

Proton is one of the familiar particles around us and it is being used in the present colliders where investigations are going on in search of new physics. So, the knowledge of its structure is essential for the detailed perturbative QCD (pQCD) calculations of any process involving proton. Among the proton structure functions, longitudinal structure function F_L is important one to study as it is directly sensitive to the gluon distribution in the proton. Theoretically and phenomenologically the measurement of F_L structure

function helps one to distinguish different models describing the QCD evolutions at small-x. Moreover, the structure function measurement remains incomplete without the inclusion of this particular structure function measurement. Experimentally it was measured at electron proton collider HERA over a wide range of Bjorken variable x and the four momentum transfer in DIS process Q^2.

In pQCD among the QCD evolution equations, Dokshitzer-Gribov-Lipatov-Altarelli-Parisi (DGLAP) evolution equation is the most fundamental one to study the Q^2 and x- evolution of structure function. Once a quark or gluon distribution function at some reference point is given, one can compute it for any value of Q^2 using this equation. The structure function of the nucleon reflects the momentum distributions of the quarks and gluons in it. It is also important to study the gluon distribution inside a hadron at small-x because gluons are expected to be dominant in this region. In the framework of the DGLAP equation the parton distributions grows at small-x as a result of their Q^2-evolution. The steep rise of $F_2(x, Q^2)$ structure function towards small-x observed at HERA also indicates a similar increase in the gluon distribution towards small values of x in pQCD. That is, the perturbative QCD predicts a strong power law rise of the gluon distribution in the small-x region. At small values of x, the behaviour of F_L is driven mainly by gluons through the transition $g \to q\bar{q}$. Therefore, once the distribution of gluon inside the proton is known, F_L structure function can be calculated from it. The behaviour of F_L structure function also shows power law rise as that of the gluon distribution function.

Along with the light flavours, the inclusion of heavy flavours (charm and beauty quarks) in the study of evolution of F_L structure function is also important. It is already well known that the scaling violations are different in case of the massless and massive pQCD calculation. Thus, in all precision measurement of structure functions, a detailed treatment of heavy flavour contribution is required. At small-x, all the heavy quark structure functions are dominated by the gluon content of the proton. Therefore,

the behaviour of these structure functions can be studied using the gluon distribution function.

In this thesis, we have studied the behaviour of proton longitudinal structure function F_L in the region of small-x up to next-to-next-to-leading orders. Here the evolution of structure function in higher orders are studied using the higher order kernels in the QCD evolution equation. The inclusion of higher order kernel in the study of the hard processes in QCD becomes significant as compared to leading one due to consistency and accuracy of the results. This consideration is particularly important for studying the physical processes at the present colliders LHC and TEVATRON. Also, in these colliders major emphasis has been given on the small-x region.

In Chapter 1, we present a brief introduction to the structure of matter, standard model of elementary particle physics, deep inelastic scattering, DIS cross section and structure function, Quantum Chromodynamics, Quark Parton Model, QCD evolution equation, Longitudinal structure function F_L, heavy quarks in the proton, small-x physics, experimental measurement of F_L structure function and the related experiments.

In Chapter 2, we have solved the QCD evolution equation for F_L structure function up to next-next-to-leading order at small-x. Here we use Taylor expansion method to obtain the analytical expression for t- and x-evolution of F_L structure function. The computed results are compared with recent H1, ZEUS data, Donnachie-Landshoff (DL) model results and the theoretical prediction of MSTW08, CT10, ABM11 and NNPDF2.3 parameterizations.

In Chapter 3, we have presented the t- and x-evolutions of F_L structure function obtained as a solution of QCD evolution equation for F_L structure function up to next-to-leading order at small-x using Regge like behaviour of structure function. The results obtained are compared with H1, ZEUS data, DL model results and the theoretical prediction of MSTW08, CT10, ABM11 and NNPDF2.3 parameterizations. We have

also compared these results with our results from Chapter 2.

In Chapter 4, we have presented the approximate relation between the F_L structure function and gluon distribution function at small-x using Taylor expansion method. From this relation we have calculated the x-evolution of F_L structure function and the results obtained are compared with H1, ZEUS data, DL model results and the theoretical prediction of MSTW08, CT10, ABM11 and NNPDF2.3 parameterizations.

In Chapter 5, the t- and x-evolutions of F_L structure function up to next-to-next-to-leading order at small-x using the Regge like behaviour of gluon distribution function obtained as a solution of DGLAP evolution equation is presented. The results obtained are compared with H1, ZEUS data, DL model results and the theoretical prediction of MSTW08, CT10, ABM11 and NNPDF2.3 parameterizations. The behaviour of DIS cross section ratio R with respect to x is also presented. We have also presented a comparative study of our results with those from Chapter 4.

In Chapter 6, we have presented the behaviour of heavy flavour structure function F_L^c, F_L^b, F_2^c and F_2^b with respect to x using Taylor expansion method and Regge like behaviour of gluon distribution function. Our results are compared with H1, ZEUS data and results of DL, Colour-Dipole (CD) model. We use these results to analyse the behaviour of heavy quark DIS cross section ratio R^h and reduced cross section σ_r^h. Finally, the behaviour of heavy quark content to the F_L structure function with respect to x is also presented here. We have also presented a comparative analysis of our results obtained by both the methods.

In Chapter 7, we have summarised the overall conclusions drawn from our work. □

ACKNOWLEDGEMENT

I would like to acknowledge all those who, directly or indirectly, made my stay at Tezpur University very enjoyable and fruitful.

First of all I would like to express my appreciation and thanks to my supervisor Prof. Jayanta Kumar Sarma for his care and guidance which have been the motivating factors behind my progress. I would like to thank him for encouraging my research and for allowing me to grow as a researcher. His advice on both research as well as on my career have been priceless.

I take the opportunity to thank Tezpur University for providing me the research facility to carry on my research work properly. I also extend my gratitude to all the administrative staffs for their invaluable help during my stay over here.

I would like to express my deepest gratitude to Prof. A. Choudhury, Prof. A. Kumar, Prof. N. S. Bhattacharyya, Prof. N. Das, Prof. R. S. Sirohi, Dr. G. A. Ahmed, Dr. D. Mohanta, Dr. P. Deb, Dr. K. Barua, Dr. A. Pathak, Dr. Ng. K. Francis, Dr. M. K. Das, Dr. D. Borah, Dr. P. Nath, Dr. P. K. Karmakar, Dr. R. Biswas, Dr. A. J. Choudhury, Dr. R. Sarmah, Dr. R. Gogoi and Dr. S. K. Das of Dept. of Physics, Tezpur University for their valuable guidance and encouragement to carry out this work.

I wish to express my sincere thanks to all the departmental staff for their help during the working days.

I would also like to acknowledge DAE BRNS for financial support that I received in some part of my research period that helped me to carry out this work.

I also want to thank all my seniors, juniors, colleagues and friends in Tezpur University for their help and good wishes. I am thankful to Sovan da, Rathin da, Mayuri ba, Nayanmani, Ananya, Saurav, Runjun, Chandrani, Nurjahan, Ruprekha and many other friends for their help and good wishes and who made my stay at the campus

joyful.

A special thanks to my family. Words cannot express how grateful I am to my mother, father, mother-in-law, father-in-law for their sincere encouragement and inspiration throughout my research work. Their prayer for me was what sustained me this far. I would also like to thank my brother Jatin, sister Bornali, brother-in-law Munti and sister-in-law Nilakshi. They were always supporting me and encouraging me with their best wishes.

At the end, I would like to express my special appreciation and thanks to my beloved husband Prabwal Jyoti Phukon for standing by me throughout the years. I truly thank him for cheering me up and supporting me during my good and bad times.

Thank You All

Date : **(Nomita Baruah)**

Contents

List of Figures

Chapter 1

Introduction

One of the basic questions in physics is about the origin of the structure of matter. From the ancient times, a great number of philosophers and scientists have been trying to answer the questions that deal with the constituents of matter forming the ultimate structure of the universe. Although most of the early notions and predictions about the structure of matter were found out to be wrong, nevertheless they formed a basis for the theories developed centuries later with the improved knowledge of physicists. It is only at the present time of the 21st century, a more precise and consistent picture of the building blocks of matter has evolved that reaches from the atomic model up to the present elementary particles. Particle physics is the field of natural science which mainly deals with the fundamental constituents of matter and the interactions among them.

The theory that currently describes all the phenomena of particle physics in terms of the properties and interactions of the elementary particles, which also includes the results of experimental and theoretical investigations of many years is known as the Standard Model (SM) of particle physics. According to this theory, the fundamental constituents of matter are the two half-integer spin families of fermions called leptons and quarks. There are three generations of leptons and quarks and they interact via the exchange of gauge bosons. They are the integer-spin elementary particles mediating the fundamental interactions. Each type of these fundamental interactions corresponds to

some kind of the gauge boson: the photon γ act as a mediator for the electromagnetic interaction; the heavy gauge bosons, Z^0 and $W^{\pm}$, carry the weak interaction; and the eight gluons g mediate the strong interaction. Thus the main component of the SM [1,2] are the electroweak theory which unifies the electromagnetic and weak interactions and the strong interactions described by Quantum Chromodynamics (QCD) [3, 4]. In addition, a new spin-zero boson, named Higgs boson has been also included recently in the model. This Higgs boson is responsible for the acquisition of mass by elementary particles. Despite being the most successful theory in particle physics, SM is not completely perfect as there are still some fundamental questions which need to be further clarified. It does not explain one of the natural phenomena gravity, the nature of dark matter and dark energy, neutrino masses and matter-antimatter asymmetry etc.

The behaviour of quarks and gluons is mainly described by QCD, the theory of strong interaction. This theory describes interactions of quarks via the exchange of gluons. Due to the non-abelian nature of QCD [5, 6], the strength of the interaction between the quarks decreases towards small distance and they behave as free particles. This behaviour is called asymptotic freedom [4]. With the increase of distance, the strength of the interaction rises and the quarks cease to behave as free particles. Rather, they behave as composite particles which explains the confinement of quarks [7]. Both these interesting phenomena of QCD implies that gluons carry colour charge and indicate the self interaction property of gluons. Thus, it is important to study the processes involving gluons.

The proton is one of the familiar particles around us. As it consists of the fundamental particles, quarks and gluons, a detailed study of its internal structure is one of the fascinating topics in QCD. The knowledge of its structure is important for perturbative QCD (pQCD) calculations of any process involving proton. Its structure also helps to explain the origin of matter. In the present particle accelerators and colliders, scattering experiments are conducted to test the theoretical predictions of the SM

and also to have the opportunity to search for new physics concerning the basic laws governing the interactions between the elementary particles. The knowledge of proton structure and QCD is a vital tool which helps to interpret the potential signals of new physics at the Large Hadron Collider (LHC) at CERN.

The scattering experiments have played an important role in the elementary particle physics research starting from Rutherford's experiment [8], which explained the structure of atom in 1911 or later the Stanford Linear Accelerator Center (SLAC) experiments, which revealed the partonic structure of nucleon in 1969 [9, 10]. SLAC allowed to study the Deep Inelastic Scattering (DIS) processes for the first time i.e., scattering at high values of momentum transfer from electrons to protons. Among the scattering experiments, the electron-proton scattering is an important one. Being leptons, electrons are small in size and possess other well known properties of leptons. These properties help the electrons to penetrate deep inside the proton and thus they are able to test the proton structure very precisely.

The electron-proton collider, Hadron Elektron Ringanlage (HERA) located at the Deutsches Elektronen Synchrotron (DESY) in Hamburg, Germany operated from year 1992 to 2007. HERA gave a unique opportunity to investigate the structure of proton over a wide kinematic range of Bjorken variable x (down to 10^{-6}) and squared four momentum transferred between lepton and proton Q^2 (up to 10^6 GeV^2) where the dynamics of DIS become dominated by gluon. It collected e^+p collision data with the H1 and ZEUS detectors at a positron beam energy of 27.5 GeV and a proton beam energies of 920, 575 and 460 GeV, which allowed a measurement of structure functions at x values $2.9 \times 10^{-5} \leq x \leq 0.01$ and Q^2 values $1.5GeV^2 \leq Q^2 \leq 800GeV^2$ [11, 12]. HERA also collected data for inclusive charm and beauty cross sections and the derived heavy flavour structure function in e^-p and e^+p neutral current collisions in the kinematical range of x values $2 \times 10^{-4} \leq x \leq 0.05$ and Q^2 values $5GeV^2 \leq Q^2 \leq 2000GeV^2$ [13].

At low values of x, the proton structure is analysed by gluon dominance. In

pQCD the gluon distribution is determined indirectly by Q^2 dependence of DIS cross section. This determination is directly affected by pQCD calculations. The proton structure is basically described in terms of structure functions, F_2, xF_3 and F_L. Among them F_L is directly related to gluon density in the proton. As its sensitivity towards gluon density is somewhat different from the scaling violation, F_L is expected to give a test of pQCD validity. Theoretically, the measurement of F_L structure function helps us to distinguish different models describing the QCD evolution at small-x. In fact, the structure function measurement remains incomplete until the measurement of longitudinal structure function is actually included in the study.

Heavy quark production at HERA is of particular interest for testing various calculations in pQCD. The heavy quark masses, as well as the transverse momentum of a jet, provide a hard scale, which is essential for the calculations in pQCD predictions [14]. As it is well known, that the scaling violations are different in the massless and massive pQCD cases, therefore, in all precision measurement, along with the light flavour, a detailed treatment of heavy flavour contribution is also required. The measurements of heavy quark uniquely constrain the parton distribution functions (PDFs) of proton, mainly its charm (c) and beauty (b) contents. The precise knowledge of PDFs is also essential at LHC. The b quark density plays an important role in Higgs production at the LHC along with the extensions to the standard model such as supersymmetric models at high values of the mixing parameter tanβ [15]. The dominant process for the charm and beauty quark production at HERA is the Boson Gluon Fusion (BGF), where the photon interacts with a gluon from the proton by the exchange of a heavy quark pair and is given as $\gamma g \rightarrow q\bar{q}X$, with $q = c, b$ [16]. This indicates that the process is sensitive to the gluon density in the proton.

In this thesis work, we have mainly studied the small-x behaviour of proton longitudinal structure function F_L. The thesis is organised as follows: in the next sections of this chapter the overview of DIS, proton structure functions and their experimental mea-

surement, quark parton model, quantum chromodynamics, QCD evolution equations, longitudinal structure function F_L, DIS experiments related to F_L structure function, small-x physics, heavy quark contribution to structure functions are given. The 2nd chapter describes the behaviour of F_L structure function from QCD evolution equation using Taylor series expansion method. In 3rd chapter, the behaviour of F_L structure function from QCD evolution equation is analysed using Regge behaviour of structure function and comparison between the results obtained in both the methods is studied. In 4th chapter, we have studied the approximate relation between F_L and gluon distribution function using Taylor expansion method and studied the evolution of F_L structure function with respect to x. In 5th chapter, the behaviour of structure function F_L is studied using the gluon distribution function obtained as a solution of the DGLAP evolution equation and comparative study of the results with the results of 4th chapter is presented. 6th chapter describes the contribution of heavy quark to F_L structure function using Taylor expansion method and Regge behaviour of gluon distribution function and the comparative analysis of the results obtained by both the methods. In chapter 7, we summarise the overall conclusion and future directions of our study.

1.1 Deep Inelastic Scattering

Deep Inelastic Scattering (DIS) is the basic tool for understanding the inside structure of nucleon and the interaction dynamics of quarks and gluons. Since the discovery of structure of proton at SLAC fixed target experiment in 1969 [9], these measurement have played an important role in the development of the theory of strong interactions, Quantum Chromodynamics. DIS is the process in which constituents of proton are probed by means of lepton-proton scattering. The process is 'inelastic' as when a quark knocks out of the proton, the proton is broken up, producing a jets of hadron. It is

called 'deep', here the proton is probed with a high energetic gauge boson i.e., with small wavelength to resolve its structure up to small distance scale. In this process when the exchange boson is a neutral particle, photon γ or a neutral vector boson Z^0, it is referred to as neutral current DIS and if the exchange particle is a charged boson, $W^{\pm}$, it is known as charged current DIS. Figure 1.1 defines the kinematics of DIS process in terms of following four-vectors, k: initial state lepton; k': final state lepton; P: final state proton and $q = k - k'$: the exchange field quantum. A measurement summing up all the final states in the hadronic system is known as inclusive measurement. The inclusive DIS process can be described in terms of the following kinematic variables:

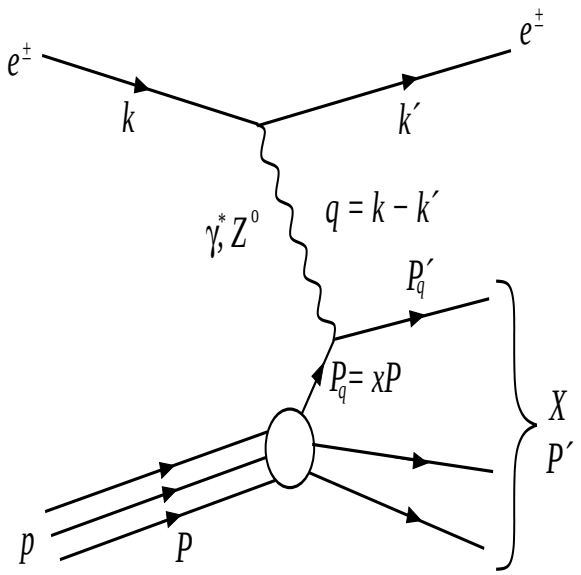

Figure 1.1: Feynmann diagram of Deep Inelastic Scattering

- The negative of the four-momentum transferred to the photon which qualitatively determines the scale of the interaction

$$Q^2 = -q^2 = -(k - k')^2 \tag{1.1}$$

- The fraction of proton momentum carried by the struck quark known as Bjorken

scaling variable

$$x = \frac{Q^2}{2P \cdot q} \tag{1.2}$$

- The inelasticity variable which corresponds to the fraction of the incoming lepton energy transfer by the exchanged boson to the proton in the proton rest frame

$$y = \frac{P \cdot q}{P \cdot k} \tag{1.3}$$

- Center of mass energy squared

$$s = (k + P)^2 \tag{1.4}$$

- The invariant mass squared W^2 of the produced hadronic final state

$$W^2 = (q + P)^2 \tag{1.5}$$

The variables Q^2, x, y and s defined above are related by the equation

$$Q^2 = (s - M_P^2)xy, \tag{1.6}$$

where M_P^2 is the mass of the proton. This relation (1.6) implies that at a given ep center of mass energy $\sqrt{s}$, any two of the variables Q^2, x, y are enough to describe the kinematics of DIS process, usually Q^2 and x are used. Here both the dimensionless variables x and y are limited to values between 0 and 1. The values of Q^2 and W^2 lies between 0 and s, M_P and $\sqrt{s}$ respectively [17].

The invariant mass squared W^2 of final hadronic state can also be written in terms of Q^2 and x as [18]

$$W^2 = M_P^2 + Q^2\Big(\frac{1-x}{x}\Big). \tag{1.7}$$

This equation (1.7) explains that at fixed Q^2, low-x interaction corresponds to large values of the invariant mass squared W^2 of final hadronic state. It also signifies the term 'deep' and 'inelastic' corresponds to $Q^2 \gg M_P^2$ and $W^2 \gg M_P^2$ respectively. Thus, the value of the proton mass M_P may be neglected in the last two equations.

1.2 DIS Cross Section and Structure Functions

In inclusive DIS experiment, one of the important quantity to measure is the scattering cross section. The cross section of the lepton-proton scattering can be written in terms of leptonic and hadronic part as [19]

$$d\sigma \sim L_{\mu\nu} W^{\mu\nu}, \tag{1.8}$$

where $L_{\mu\nu}$ denotes the leptonic tensor describing the interaction between the lepton and the virtual exchanged gauge boson and $W^{\mu\nu}$ represents the hadronic tensor which corresponds to the boson-proton interaction. Neglecting the electron mass, the leptonic tensor which is well known in Quantum Electrodynamics (QED) can be written as [20]

$$L_{\mu\nu} = 2(k'_{\mu} k_{\nu} + k'_{\nu} k_{\mu} - (k' \cdot k) g_{\mu\nu}), \tag{1.9}$$

where $g_{\mu\nu}$ denotes the metric tensor. The hadronic tensor describing the hadron vertex has the form [17]

$$\begin{aligned} W^{\mu\nu} &= -W_1 g^{\mu\nu} + \frac{W_2}{M_P^2} p^{\mu} p^{\nu} - i\varepsilon^{\mu\nu\alpha\beta} p_{\alpha} q_{\beta} \frac{W_3}{2M_P^2} + q^{\mu} q^{\nu} \frac{W_4}{M_P^2} \\ &\quad + (p^{\mu} q^{\nu} + q^{\mu} p^{\nu}) \frac{W_5}{M_P^2} + i(p^{\mu} q^{\nu} - p^{\nu} q^{\mu}) \frac{W_6}{2M_P^2}, \end{aligned} \tag{1.10}$$

where M_P is the mass of proton, W_i are Lorentz scalar function of x and Q^2 which describes the structure of proton. If the scattering process involves only γ exchange, the parity violating term W_3 and also antisymmetric term W_6 are absent. The current conservation at the hadronic vertex gives $q_{\mu} W^{\mu\nu} = q_{\nu} W^{\mu\nu} = 0$ so that

$$W_5 = -\frac{p \cdot q}{q^2} W_2, \tag{1.11}$$

$$W_4 = \Big(\frac{p \cdot q}{q^2}\Big)^2 W_2 + \frac{M_P^2}{q^2} W_1. \tag{1.12}$$

Thus, the hadronic tensor depends on W_1 and W_2 only and can be written as

$$W^{\mu\nu} = W_1\Big(- g^{\mu\nu} + \frac{q^{\mu} \cdot q^{\nu}}{q^2}\Big) + \frac{W_2}{M_P^2}\Big(p^{\mu} - \frac{p \cdot q}{q^2} q^{\mu}\Big)\Big(p^{\nu} - \frac{p \cdot q}{q^2} q^{\nu}\Big). \tag{1.13}$$

The functions W_1 and W_2 are redefined in terms of structure functions of proton F_1 and F_2 as

$$F_1(x, Q^2) = M_P W_1(x, Q^2), \tag{1.14}$$

$$F_2(x, Q^2) = \frac{p \cdot q}{M_P} W_2(x, Q^2). \tag{1.15}$$

Thus, the double differential DIS cross section can be expressed using structure function $F_1(x, Q^2)$ and $F_2(x, Q^2)$ in the form

$$\frac{d^2\sigma}{dxdQ^2} = \frac{4\pi\alpha^2}{xQ^4}\Big[\frac{y^2}{2} 2xF_1(x, Q^2) + (1-y)F_2(x, Q^2)\Big], \tag{1.16}$$

here α is the fine structure constant. The structure functions $F_1(x, Q^2)$ is proportional to the transverse component of the cross section and the difference between $F_2(x, Q^2)$ and $F_1(x, Q^2)$ gives the longitudinal part of the cross section. Thus, the longitudinal structure function is defined as

$$F_L(x, Q^2) = F_2(x, Q^2) - 2xF_1(x, Q^2). \tag{1.17}$$

Now, the cross section in terms of $F_2(x, Q^2)$ and $F_L(x, Q^2)$ structure functions can be written as

$$\frac{d^2\sigma}{dxdQ^2} = \frac{2\pi\alpha^2 Y_+}{xQ^4}\Big[F_2(x, Q^2) - \frac{y^2}{Y_+} F_L(x, Q^2)\Big], \tag{1.18}$$

where $Y_+ = 1 + (1-y)^2$ is a function of y. Since the contribution of F_L structure function to DIS cross section is proportional to the factor $\frac{y^2}{Y_+}$, the F_2 term dominates at $y < 0.5$ and the contribution of F_L structure function is significant towards the total cross section at large values of $y \geq 0.5$ [21]. In DIS experiment structure functions are extracted from the measured cross section. Therefore, it is convenient to define the reduced cross section as

$$\sigma_r = F_2(x, Q^2) - \frac{y^2}{Y_+} F_L(x, Q^2). \tag{1.19}$$

The ep scattering process can also be considered as the interaction of a flux of virtual photon and the proton. In terms of the two components of the cross section i.e., transverse and longitudinal cross section, the double differential cross section can be written as

$$\frac{d^2\sigma}{dxdQ^2} = \Gamma(y)[\sigma_T(x,Q^2) - \epsilon(y)\sigma_L(x,Q^2)]. \tag{1.20}$$

Here σ_T and σ_L corresponds to the absorption cross section for transversely and longitudinally polarised virtual photon respectively, $\Gamma(y) = \frac{\alpha^2 Y_+}{2\pi x Q^2(1-x)}$ stands for the photon flux and $\epsilon(y) = \frac{2(1-y)}{Y_+}$ defines the virtual photon polarisation.

Now, comparing the equations (1.18) and (1.20) one can express the above mentioned structure function in terms of the virtual photon absorption cross section as

$$F_2(x,Q^2) = \frac{Q^2(1-x)}{4\pi^2\alpha}[\sigma_T(x,Q^2) + \sigma_L(x,Q^2)], \tag{1.21}$$

$$F_L(x,Q^2) = \frac{Q^2(1-x)}{4\pi^2\alpha}\sigma_L(x,Q^2). \tag{1.22}$$

Equation (1.22) indicates that the longitudinal structure function is directly proportional to the longitudinal component of the cross section. From the equations (1.21) and (1.22), as the measured quantity σ cannot be negative, the two structure functions $F_2(x,Q^2)$ and $F_L(x,Q^2)$ obey the relation

$$0 \leq F_L(x,Q^2) \leq F_2(x,Q^2). \tag{1.23}$$

Another quantity which represents the relation between the cross sections of the absorption of a longitudinal and transverse polarized photon by hadron is the ratio $R(x,Q^2)$ and is given by

$$R(x,Q^2) = \frac{\sigma_L}{\sigma_T} = \frac{F_L(x,Q^2)}{F_2(x,Q^2) - F_L(x,Q^2)}. \tag{1.24}$$

At small values of x, this ratio $R(x, Q^2)$ gives the relative strength of the two components of the cross section [22]. $R(x, Q^2)$ provides the information about the spin and transverse momentum of the constituents of the nucleon [23] which is explained in the next section.

1.3 Quark Parton Model

The Quark Parton Model (QPM), introduced by Feynman, explains that the proton is made up of point like constituents known as partons [24]. The basic idea of the parton model was based on the experimental observation of Bjorken scaling [25], that is in the ep scattering experiment at SLAC it was observed that the structure function measured at fixed values of x are approximately independent of the four-momentum transfer Q^2 from the probe to the nucleon and depend only on the variable x [9, 10]. This behaviour was predicted by Bjorken and suggested that the proton is consists of point-like particle, called as parton. According to this model, the proton consists of quasi-free point-like particles which were identified as quarks, particle with spin-$\frac{1}{2}$ and electric charge $\pm\frac{1}{3}e$ or $\pm\frac{2}{3}e$, as proposed by Gell-Mann [26] and Zweig [27]. The proton consists of two u quarks with charge $+\frac{2}{3}e$ and one d quark with charge $-\frac{1}{3}e$.

In the QPM, the deep inelastic ep scattering is interpreted as the elastic scattering between the lepton and quarks. The ep cross section is then incoherent sum over all lepton-quark scattering cross section. Here incoherent means that the lepton scatters on a single quasi-free quark. With these assumptions, the structure functions F_1 and F_2 can be expressed as a sum of quark momentum distributions $xq(x)$ weighted with the square of their electric charge e_i:

$$F_1(x, Q^2) = \frac{1}{2x} \sum_i e_i^2 x q_i(x), \tag{1.25}$$

$$F_2(x, Q^2) = \sum_i e_i^2 x q_i(x), \tag{1.26}$$

here e_i is the charge of the parton i and $q_i(x)$ is the probability that the quark i carries a fraction of proton momentum in the interval $[x, x + dx]$. The sum runs over all the partons in the proton. Hence, in QPM the structure functions F_1 and F_2 depend only on the variable x as predicted by Bjorken.

The cross sections σ_T and σ_L depend on the spins of the proton constituents. As the longitudinal virtual photon cannot interact with the spin-$\frac{1}{2}$ quarks due to helicity conservation [28] at the hadronic vertex, the model predicts $\sigma_L = 0$ which leads to

$$F_L(x, Q^2) = F_2(x, Q^2) - 2xF_1(x, Q^2) = 0 \tag{1.27}$$

and consequently gives

$$F_2(x, Q^2) = 2xF_1(x, Q^2), \tag{1.28}$$

which is known as the Callan Gross relation [28] and reflects the spin-$\frac{1}{2}$ nature of the quarks. The cross section ratio R, mentioned in the section 1.2 is often used instead of F_L to describe the scattering cross section. In the framework of QPM with spin-$\frac{1}{2}$ quark, R is expected to be small, and to decrease rapidly with increasing momentum transfer Q^2. Measurement of R at SLAC also indicated that the scattering from the spin-$\frac{1}{2}$ constituents of the nucleon (quarks) dominates [29–31].

The QPM cannot explain all the properties of DIS. Since the naive QPM predicts that the proton is made up of two up (u) and one down (d) valance quarks, the total momentum of the quarks inside the proton should be 1. But the experimental results [30] show that quarks carry only half of the proton's momentum, i.e.

$$\int_0^1 [xu(x) + xd(x)]dx = 0.54. \tag{1.29}$$

This clearly suggests that there is more momentum in proton than that carried by quarks. This fact provided the first indirect evidence of the gluonic component of the proton. Another drawback is the observation of scaling violation of F_2 measured in different experiments. The scaling behaviour is observed only for values of about $x < 0.1$ and brakes for $x > 0.1$. Structure function measurement at H1 experiment [32] and some other fixed target experiment [33] shows the dependency of F_2 on Q^2. To explain the mentioned discrepancies the theory of quantum chromodynamics plays an important role, which is described in the next section.

1.4 Quantum Chromodynamics

Quantum Chromodynamics (QCD) is the theory which describe the strong interaction between the quarks and gluons inside the proton [5, 6]. The key point in this theory is that the quarks and gluons have a quantum number called colour, which is described by $SU(3)$ symmetry group and can be represented by three colours - red, green and blue. The quarks can interact by the exchange of a massless and electrically neutral spin-1 boson called gluons. QCD is a non-abelian $SU(3)$ gauge theory [6]. As a result, there are eight gluons and they also interact among themselves via the exchange of colour charge. Hadrons are considered to be colourless or colour singlets of the group $SU(3)$ constructed from the fundamental colour triplet of quarks. Only colourless particles can exist as free particles. Thus the quarks and gluons cannot be observed as free one rather they should always be confined within the hadron. This property of QCD is known as confinement. An important feature of quantum field theories is the running coupling constant, i.e., the coupling evolves with the energy scale of the interaction. Because of the non-abelian nature of gauge group $SU(3)$, opposite to $U(1)$ group of QED, the strong coupling constant α_s shows the opposite behaviour with that of the electromagnetic fine structure constant α. This leads to asymptotic freedom

which predicts that at large energy scales Q^2 the coupling between quarks and gluons decreases and they behave as free particles, while at lower energies they were confined to colourless hadron.

The strong coupling constant α_s is one of the important characteristics of strong interaction. The lowest order i.e., Leading Order (LO) of α_s does not include any gluon vertices. In Next-to-Leading Order (NLO), the interaction between quarks and gluons are included and more gluon vertices are added in higher orders. In LO approximation the coupling constant α_s is given by the equation [34]

$$\alpha_s(Q^2) = \frac{12\pi}{(33 - 2N_f)\ln\frac{Q^2}{\Lambda^2_{QCD}}}, \tag{1.30}$$

where N_f is the number of active quark flavours. Λ_{QCD} characterizes the strength of the coupling and is the order of $300 - 500MeV$. The phenomenon of confinement is described at $Q^2 < \Lambda^2_{QCD}$. Contrary to it, for large energy scales $Q^2 > 1GeV^2$, perturbative calculations are possible in QCD using order-by-order expansion in α_s [35].

According to QCD, protons not only consists of quarks but also gluons which binds the quarks inside the proton. Due to the presence of gluons, some modifications take place in the quark parton model as the quarks can interact via the exchange of gluons and can also radiate gluons. The radiated gluons can split into quark-antiquark pairs or gluons. Thus a quark seen at an energy scale Q_0^2 carrying a momentum fraction x_0 can be resolved into more quarks and gluons at a higher values of Q^2, i.e., $Q_1^2 > Q_0^2$ and lower values of $x_1 < x_0$. As a result the structure function shows Q^2 dependence violating the Bjorken scaling.

The pQCD calculations in DIS process can be expressed using factorization theorem [36]. This theorem provides a systematic way to refine the predictions of the parton model. In this theorem, the cross section involving hadron can be expressed as two distinct part: one short distance and the other long distance parts [37]. The short

distance or hard process part which is process dependent can be calculated perturbatively using renormalizable theory of QCD. On the other hand, the long distance part which is process independent and unpredictable requires experimental results. This part involves the PDFs into which infrared divergences of QCD are absorbed. Factorization theorem leads to the expression for F_2 structure function as the convolution of co-efficient function C_2^i and the parton distribution function f_i [38] :

$$F_2(x,Q^2) = \sum_{i=q,g} \int_x^1 dw C_2^i\Big(\frac{x}{w}, \frac{Q^2}{\mu_r^2}, \frac{\mu_f^2}{\mu_r^2}, \alpha_s(\mu_r^2)\Big) f_i(w,\mu_r^2,\mu_f^2). \tag{1.31}$$

Here the co-efficient function C_2^i represents the hard scattering matrix element for the interaction of the photon with a parton i which can be calculated using perturbative expansion in α_s. The parton distribution function f_i is the probability to find a parton i carrying a fraction w of the proton's momentum. In this process the summation is over all the partons. The factorization scale μ_f defines the boundary between the long distance and short distance part. The renormalization scale μ_r defines the separation between the finite and divergent contributions in the renormalization procedure. Both the scales μ_r and μ_f are arbitrary and helps to absorb the infrared and ultraviolet divergences in pQCD. There are several renormalization schemes used in the calculations of QCD. Among them the most commonly used one is the modified minimal subtraction ($\overline{MS}$) scheme [38]. Here, renormalized quark distribution absorbs the divergent part of the co-efficient functions at $\mu_r = \mu_f$. And another useful scheme is DIS scheme where one chooses $\mu_r = \mu_f = Q$. Therefore one can write the expression for F_2 as

$$F_2(x,Q^2) = \sum_i e_i^2 x f_i(x,Q^2), \tag{1.32}$$

which reflects the Q^2 dependence of the structure function. Also F_L gives non-zero value and this can be obtained from F_2 and the gluon density $G(x,Q^2)$ which is explained in the section 1.5. Since F_L is directly related to cross section ratio R, thus R is also non

zero. In QCD, the value of R is proportional to the QCD coupling constant α_s [23].

QCD Evolution Equations:

An important outcome of the factorization theorem is that the measurement of parton distribution function at one scale Q_0 allows one to calculate it for any other scale Q'. This property of parton distribution is known as evolution. The evolution equations can describe the behaviour of quark $q_i(x, Q^2)$ and gluon $g(x, Q^2)$ distribution function with the scale of interaction Q^2.

The parton distribution in the hadron cannot be calculated from the first principles, involving the building blocks of hadronic matter, the quarks and gluons, and their mutual interactions as described by QCD. With the help of the factorization theorem, the parton evolution, the Q^2 dependence of partons can be calculated within pQCD. These evolution equations of parton are known as Dokshitzer-Gribov-Lipatov-Altarelli-Parisi (DGLAP) evolution equations [35,39–41]. These describe the evolutions of quark $q_i(x, Q^2)$ and gluon $g(x, Q^2)$ distribution function with the scale of interaction Q^2 :

$$\frac{dq_i(x,Q^2)}{dlnQ^2} = \frac{\alpha_s(Q^2)}{2\pi}\int_x^1 \frac{dw}{w}\left[\sum_j q_j(w,Q^2)P_{ij}\Big(\frac{x}{w}\Big) + g(w,Q^2)P_{ig}\Big(\frac{x}{w}\Big)\right], \tag{1.33}$$

$$\frac{dg(x,Q^2)}{dlnQ^2} = \frac{\alpha_s(Q^2)}{2\pi}\int_x^1 \frac{dw}{w}\left[\sum_j q_j(w,Q^2)P_{gj}\Big(\frac{x}{w}\Big) + g(w,Q^2)P_{gg}\Big(\frac{x}{w}\Big)\right]. \tag{1.34}$$

Here, the function $P_{ij}\Big(\frac{x}{w}\Big)$ is known as the splitting functions which describes the probability that a parton i with momentum fraction x is emitted by a parton j with the larger momentum fraction $w(w > x)$ [42]. They are calculable in pQCD as a power series of α_s:

$$P_{ij}(w,\alpha_s) = \frac{\alpha_s}{2\pi}P^0_{ij}(w) + \Big(\frac{\alpha_s}{2\pi}\Big)^2 P^1_{ij}(w) + ... \tag{1.35}$$

The DGLAP equation is formally derived in the leading logarithmic approximation (LLA), where the terms of $(\alpha_s ln(Q^2))^n$ are summed up to all orders. These $(\alpha_s ln(Q^2))^n$ terms correspond to the ladder diagrams with n gluons emission as shown in figure 1.2. The LLA approximation is that the emissions are strongly ordered by transverse momentum of gluons k_T as

$$Q^2 \gg k^2_{T_n} \gg .... \gg k^2_{T_2} \gg k^2_{T_1}. \tag{1.36}$$

The approximation is valid at large enough Q^2 where α_s is small and all the contributing

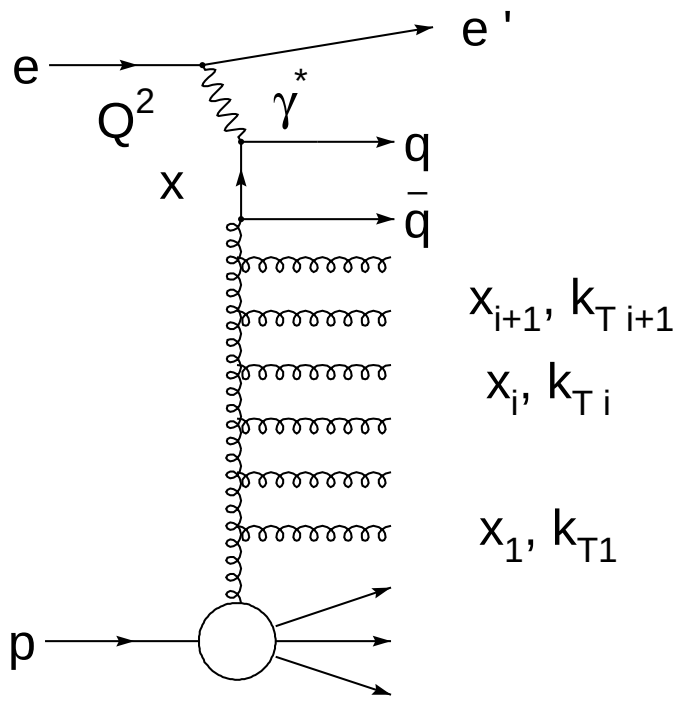

Figure 1.2: Ladder diagram for DIS in LLQ^2

terms proportional to $\alpha_s ln(\frac{1}{x})$ can be neglected.

A special case for which the DGLAP equations can be solved analytically occurs when in addition to the above conditions also strong ordering in x is required,

$$x_n \ll x_{n-1} \ll ..... \ll x_1 \ll x_0. \tag{1.37}$$

The large logarithmic terms arising from the integration are then of the form proportional to $(\alpha_s(Q^2)ln(Q^2/Q_0^2)ln(1/x))^n$, which need to be resumed. This is the double leading log approximation (DLL).

In general the structure function can be evaluated by solving the evolution equations like Dokshitzer-Gribov-Lipatov-Altarelli-Parisi (DGLAP) equation, Balitskij-Kuraev-Fadin-Lipatov (BKFL) equation [43,44] , Ciafaloni-Catani-Fiorani-Marchesini (CCFM) equation [45, 46], Gribov-Levin-Ryskin (GLR) equation [47], Modified DGLAP (MD-DGLAP) equation [48–50], Jalilian-Marian-Iancu-McLerran-Weigert-Leonidov-Kovner (JIMWLK) equation [51, 52], Balitsky-Kovchegov (BK) equation, [53, 54] etc. Among these the DGLAP evolution equation is the most familiar re-summation approach. Once a quark structure function at some reference point is given, one can compute it for any value of Q^2 using this equation. In the framework of the DGLAP equation the parton distributions grows at small-x as a result of their Q^2-evolution [41, 55].

1.5 Longitudinal Structure Function

The proton longitudinal structure function F_L, measured in DIS experiment, is one of the important observables to study. The measurement of F_L structure function is of great theoretical importance since it may allow us to distinguish between the behaviour of the different partonic distributions in the nucleon at small-x. F_L structure function is a very sensitive QCD characteristic as it is directly sensitive to the gluon density in the proton [56]. In the naive QPM, helicity is not conserved at the hadronic vertex during the interaction between the longitudinally polarised virtual photon and a quark, as illustrated in figure 1.3(a). So, the longitudinally polarized virtual photons do not couple to the spin-$\frac{1}{2}$ quarks with negligible transverse momentum and this leads to $F_L = 0$ [56]. On the other hand, in QCD improved parton model, quarks interact through gluons, and also can radiate gluons, figure 1.3(b). The gluon radiation results

in a transverse momentum component of the quark and now helicity is conserved at the hadronic vertex. As a result, quark can couple to longitudinally polarised virtual photon and the Callan-Gross relation is no longer satisfied exactly. Thus in QCD, the F_L structure function is non-zero.

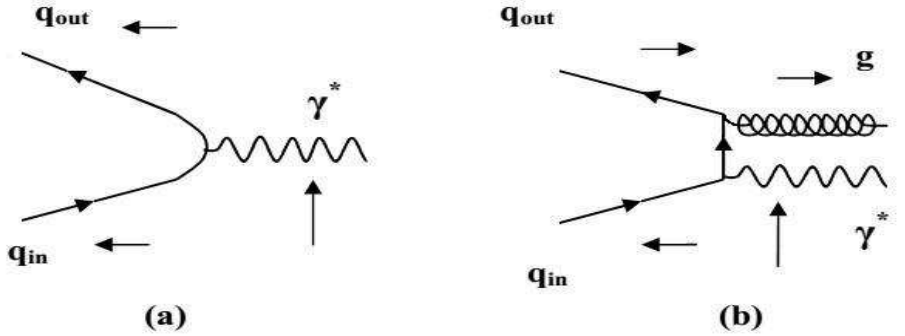

Figure 1.3: Helicity conservation at hadronic vertex in QPM (a) and QCD improved parton model (b). The arrows represent the spin orientations [57].

The one-loop virtual correction to $\gamma q \to q$ process does not contribute to the longitudinal part of the hadronic tensor $W^L_{\gamma q}$ [58] and to the order α_s the calculation of longitudinal part of this tensor gives

$$W^L_{\gamma q} = \frac{1}{3}\frac{\alpha_s}{2\pi} e_q^2 \frac{Q^2}{w} + O(\epsilon) \tag{1.38}$$

and

$$W^L_{\gamma g} = \frac{1}{2}\frac{\alpha_s}{2\pi} e_q^2 \frac{Q^2(1-w)}{w} + O(\epsilon) \tag{1.39}$$

for the contributing processes $\gamma q \to qg$ and $\gamma g \to q\bar{q}$ respectively. The contributions of ϵ-order are defined by the factorization scheme. Thus the structure functions of the gluon emission processes are expressed by the relations [59]

$$F_1^{\gamma q}(x, Q^2) = \frac{1}{2x} F_2^{\gamma q}(x, Q^2) - \sum_{q,\bar{q}} e_q^2 \frac{\alpha_s}{2\pi} \int_x^1 \frac{dw}{w} \frac{4}{3} \frac{x}{w} q(w, Q^2) \tag{1.40}$$

and

$$F_1^{\gamma g}(x,Q^2) = \frac{1}{2x}F_2^{\gamma q}(x,Q^2) - \sum_{q,\bar{q}} e_q^2 \frac{1}{2}\frac{\alpha_s}{2\pi}\int_x^1 \frac{dw}{w} g(w,Q^2) 4\frac{x}{w}\Big(1-\frac{x}{w}\Big). \tag{1.41}$$

Combining the above results, the expression for F_L structure function at LO can be written as

$$\begin{aligned} F_L(x,Q^2) &= F_2(x,Q^2) - 2xF_1(x,Q^2) \\ &= \frac{\alpha_s}{4\pi}\int_x^1 \frac{dw}{w}\Bigg[\frac{16}{3}\Big(\frac{x}{w}\Big)^2 \sum_{q,\bar{q}} e_q^2 wq(w,Q^2) \\ &\quad +8\sum_{q,\bar{q}} e_q^2\Big(\frac{x}{w}\Big)^2\Big(1-\frac{x}{w}\Big) wg(w,Q^2)\Bigg]. \end{aligned} \tag{1.42}$$

The equation (1.41) in terms of F_2 structure function and gluon distribution function can be expressed as

$$\begin{aligned} F_L(x,Q^2) &= \frac{\alpha_s}{4\pi}\int_x^1 \frac{dw}{w}\Bigg[\frac{16}{3}\Big(\frac{x}{w}\Big)^2 \sum_{q,\bar{q}} e_q^2 F_2(w,Q^2) \\ &\quad +8\sum_{q,\bar{q}} e_q^2\Big(\frac{x}{w}\Big)^2\Big(1-\frac{x}{w}\Big) wg(w,Q^2)\Bigg]. \end{aligned} \tag{1.43}$$

This equation (1.42) is known as Altarelli-Martinelli equation [18, 59]. Here the first term in the integral corresponds to the gluon radiation off a quark and the second term represents the gluon splitting into a quark anti-quark pair. Again the above equation for F_L structure function in terms of co-efficient function is given by [59, 60]

$$x^{-1}F_L = C_{L,ns} \otimes q_{ns} + < e^2 > (C_{L,s} \otimes q_s + C_{L,g} \otimes g). \tag{1.44}$$

Here q_{ns}, q_s and g are the flavour non-singlet, flavour singlet and gluon distribution function, $< e^2 >= \frac{5}{18}$ is the average squared charge for N_f (number of active light flavours) and the symbol $\otimes$ represents the standard Mellin convolution. $C_{L,a}(a = q, g)$'s

are the co-efficient functions which can be written by the perturbative expansion as follows [60]

$$C_{L,a}(\alpha_s, x) = \sum_{n=1} \left(\frac{\alpha_s}{4\pi}\right)^n C^n_{L,a}(x). \tag{1.45}$$

At small values of x, the gluon contribution to F_L dominates over the quark contribution [61] and F_L is driven mainly by gluons through the transition $g \to q\bar{q}$. Therefore, the measurement of F_L structure function can give the gluon distribution inside the proton. It also provides an important cross check of the standard picture of low-x dynamics [62].

1.6 Heavy Quarks in Proton

The heavy quarks in the proton play an pivotal role in particle physics and their production in *ep* collision provides an exciting testing ground for pQCD. The measurement of the charm and beauty quark production cross section in DIS is important for understanding the parton densities in the nucleon. The top quark is the heaviest one among the heavy quarks and due to its heavy mass it quickly decays without forming hadron. The creation of top quark pair is not possible within the range of centre of mass energy at HERA.

In the neutral current DIS process, the production of heavy quarks is mainly described by two mechanisms:

- According to the first mechanism, named as intrinsic heavy quark production, one assumes that, along with the light quarks u, d and s and the gluon g, the wave function of the proton also consists of the heavy quarks c, b, t [25, 63]. Within the context of QCD improved parton model the virtual photon interacts with the heavy quark which emerges directly from the proton.

- In the case of second mechanism known as extrinsic heavy quark production the

proton wave function does not contain the heavy quark components. In the lowest order perturbation theory the heavy quark and heavy anti-quark appear in pairs and are produced via BGF process as shown in figure 1.4.

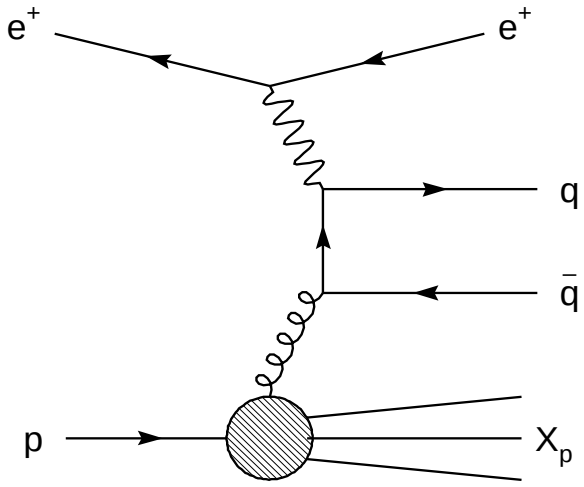

Figure 1.4: Leading order Boson Gluon Fusion (BGF) diagram for heavy quark production in ep-collisions.

In this process the quarks can be heavy if the center of mass energy squared of the $\gamma g \to q\bar{q}$ interaction is :

$$(\gamma + g)^2 > 2m_q^2, \tag{1.46}$$

where m_q^2 is the mass of the heavy quark and the photon and gluon four momentum are respectively γ and g.

The charm quark anti-quark ($c\bar{c}$) pair can be produced above the charm threshold, $Q^2 \approx (2m_c)^2$ and above the beauty threshold, the $b\bar{b}$ pair can be created. Charm contributes to the cross section mainly at small-x and higher Q^2, where the sea quark dominates the cross section. Among the charm and beauty contribution to the cross section, beauty quark contributes less to the cross section due to the coupling to its electric charge, $e_b = -\frac{1}{3}$ [57].

The dominant process for the charm and beauty quark production at HERA is the BGF shown in figure 1.4, where the photon interacts with a gluon from the proton by

the exchange of a heavy quark pair [16, 64]. Due to the presence of gluon in the initial state, this process is directly sensitive to the gluon density inside the proton. This type of process is the dominant one in DIS scattering and is particularly important at small values of x and large Q^2, due to the large gluon density [64].

The differential cross section for the charm and beauty production which directly follows from equation 1.18 can be written as

$$\frac{d^2\sigma^h}{dxdQ^2} = \frac{2\pi\alpha^2 Y_+}{xQ^4}\Big[F_2^h(x,Q^2) - \frac{y^2}{Y_+}F_L^h(x,Q^2)\Big] \tag{1.47}$$

where $h = c, b$. Both the quantities F_2^h and F_L^h are dominated by the gluon content in the proton. In the standard factorization approach to pQCD the structure functions F_k can be written as [65, 67]

$$F_k^h(x,Q^2,m_h^2) = e_h^2\frac{\alpha_s(\mu^2)}{\pi}\int_{ax}^1 \frac{dw}{w}C_{k,g}^h(w,\zeta)G\Big(\frac{x}{w},\mu^2\Big), \tag{1.48}$$

where $k = 2, L$, $a = 1 + 4\zeta(\zeta = \frac{m_h^2}{Q^2})$ and the renormalization scale μ is assumed to be either $\mu^2 = 4m_h^2$ or $\mu^2 = 4m_h^2 + Q^2$. $C_{k,g}^h$ is the heavy quark co-efficient function represented in $\overline{MS}$ scheme [67]. The heavy quark co-efficient functions differ significantly from those of the light quarks. So, the scaling violations of heavy flavour part in $F_{2,L}(x,Q^2)$ are different from those of the light flavour contribution [64]. Both for the measurement of the QCD scale Λ_{QCD} and for the extraction of the light parton densities a correct description of the heavy flavour contribution is required.

The charm and beauty production cross section has been measured in DIS using different techniques like D or D^* meson analysis [68–70], the long lifetime of heavy flavoured hadrons [71–73] or their semi leptonic decays [74].

1.7 Small-x Physics

The study of the small-x region in DIS is important for understanding the structure of the proton. The region of small-x below 0.001 is mainly dominated by the gluon

distribution in the proton [61]. In this region, the gluons in the proton form a strongly correlated system of interacting particle. The gluon densities grow rapidly as $x \to 0$ for all values of Q^2. Such types of small-x behaviour of gluon distribution function was extracted at HERA, which is shown in figure 1.5.

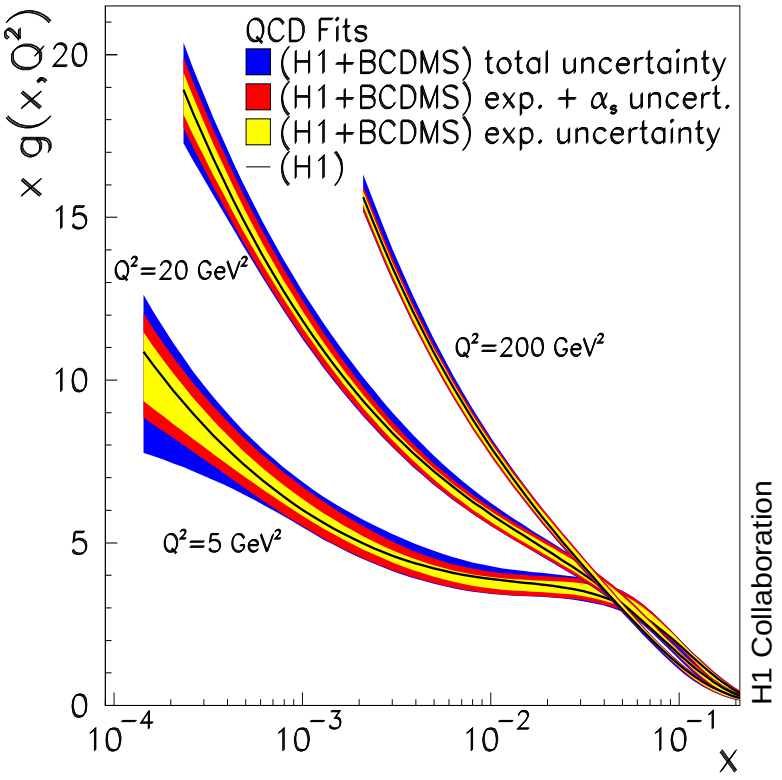

Figure 1.5: Gluon distribution function extracted at HERA [11].

This strong rise leads to a rise of the proton structure function F_2 and F_L. Such types of behaviour is well described in the framework of DGLAP evolution equations [35, 39, 41]. However, at very small values of x, when the density of gluons becomes large enough they starts overlapping in the phase space. In this case the recombination and annihilation of gluons becomes important, otherwise this strong rise leads to the violation of unitarity [75]. This effect is known as parton saturation. Such types of phenomena are explained by non-linear evolution equations.

The small-x region of the DIS offers a unique possibility to investigate the Regge

limit of pQCD [76–79]. DIS corresponds to the region where both ν and Q^2 are large. The small-x limit of DIS corresponds to case when $2M\nu >> Q^2$ which is equivalent to $s >> Q^2$ i.e., to the limit when the center of mass energy squared, s, is large and much greater than Q^2. The limit of large ν and $2M\nu >> Q^2$ is therefore the Regge limit of DIS [76]. Regge trajectory represents the exchange of a family of resonances having distinct spins. It can be asserted with confidence that the Regge theory is one of the most successful approaches for the description of high-energy scattering of hadrons. This high-energy behavior can be described by two contributions: an effective Pomeron with its intercept $\alpha_P \simeq 1.08$ slightly above unity and the leading meson Regge trajectories with the intercept $\alpha_R(0) \approx 0.5$ [80]. In Regge theory the structure function (cross section) is expected to increase approximately like a power of x towards small-x. However, at small-x the behaviour of the structure function is mainly driven by the gluons. Therefore, the behaviour of the power law rise of gluon distribution function at small-x observed at HERA is given by [81] $G(x, Q^2) \propto x^{-\lambda_g}$, where λ_g is the gluon distribution function exponent.

HERA collider made it possible to experimentally explore the small-x region. The high-energy or small-x region of DIS experiment at HERA provides a good opportunity to study the high-energy limit of QCD. One of the first observations at HERA was the strong rise of structure function F_2 towards small-x which reflects the rise of gluon density in the proton in this kinematical region [32, 82]. This was the remarkable starting point for further investigation of the structure of proton at DESY. At very small-x, saturation of the growth of the parton densities is expected, as otherwise unitarity bounds would be violated. Models based on saturation are hugely successful in describing HERA data, particularly in the low x and low Q^2 region where DGLAP approach fails.

1.8 Measurement of F_L Structure Function

Measurement of F_L structure function is a technically challenging experimental task. This structure function has a significant contribution to the cross section at high inelasticity y [21]. The direct method to obtain the F_L is to measure the DIS cross section at fixed values of x and Q^2 and different y [11]. The values of the structure function F_L were determined according to equation (1.19) by a straight-line fits to the reduced cross section as a function of y^2/Y_+ at given values of x and Q^2 and different values of center of mass energies s [11]. From the relation $Q^2 = sxy$, it is clear that the variation in y value can be obtained by varying s, the center of mass energy. Since $s = 4E_eE_p$, this could be done by varying the electron, proton or both beam energies. But in the experiment it was decided to lower the proton beam energy because reducing the electron beam energy would have required to lower the energy of the scattered electron below the trigger threshold. This would have affected the scattered electron angle more than that reduction the proton beam energy. Another advantage of lowering the proton beam is the maximum cancellation of systematics when making a relative measurement of the cross section [83]. Figure 1.5 illustrates the measurement of F_L from σ_r by the H1 collaboration [11]. Here the reduced cross section σ_r is plotted for six values of x at $Q^2 = 6.5GeV^2$, measured for proton beam energies 920, 575 and 460 GeV. The inner error bars represents the statistical error, the outer error bars show statistical and systematic uncertainties added in quadrature. The slope of the straight-line fits is determined by the structure function $F_L(x, Q^2)$ [11].

The direct measurement of F_L in the past fixed target experiments EMC (European Muon Collaboration) [84], NMC (New Muon Collaboration) [85], BCDMS (Bologna CERN Dubna Munich Saclay) [33] and SLAC [86] have been done by measuring the cross section ratio R. These measurements are at relatively high x where the sensitivity to the gluon densities is small.

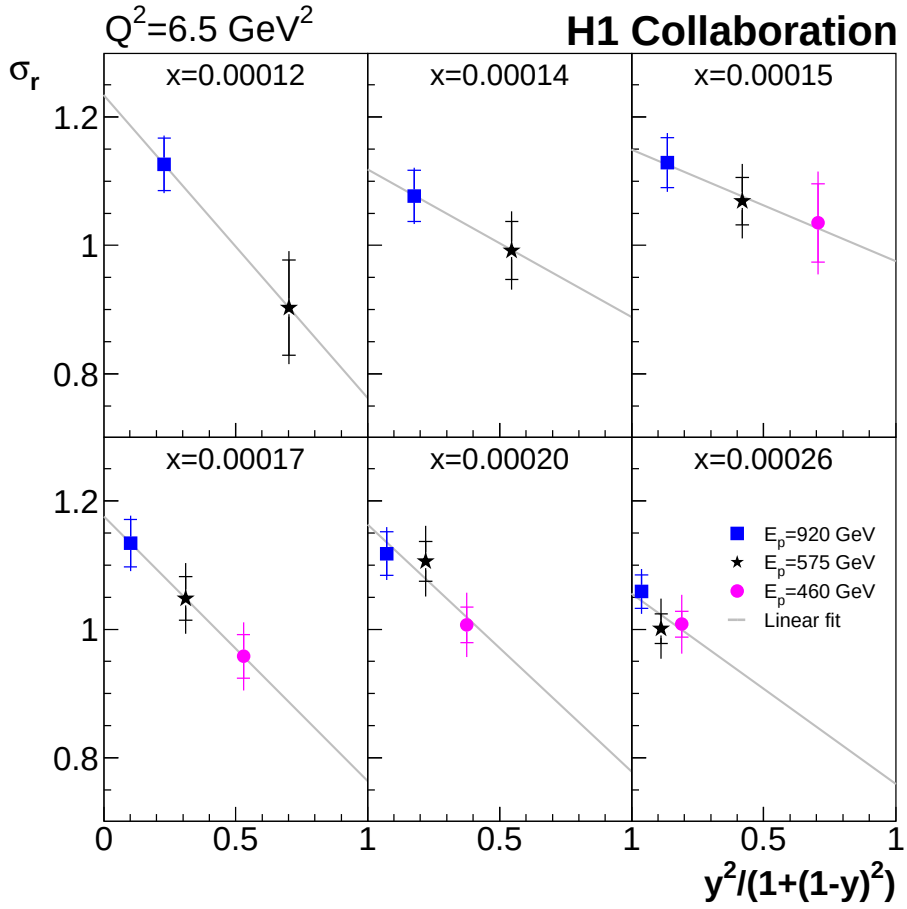

Figure 1.6: The reduced DIS cross section as a function of $y^2/(1+(1-y)^2)$ [11]

At HERA collider $F_L(x, Q^2)$ was mainly measured by H1 and ZEUS detector. An important advantage of HERA, compared to fixed target DIS lepton-nucleon experiments, is the wide range of y (inelasticity) values covered [56]. HERA collected ep collision data at a positron beam energy of 27.5 GeV and a proton beam energies of 920, 575 and 460 GeV, which allowed a measurement of structure functions at x values $2.9 \times 10^{-5} \leq x \leq 0.01$ and Q^2 values $1.5 GeV^2 \leq Q^2 \leq 800 GeV^2$ [11, 12].

1.9 Some of the DIS Experiments Related to F_L

European Muon Collaboration(EMC) : In the muon scattering experiment performed by European Muon Collaboration (EMC) at CERN (Conseil Europeen pour la Recherche Nucleaire) SPS (Super Proton Synchrotron), the structure function F_2 and R were measured with muon beams energies 120, 200, 240 and 280 GeV. Here the target materials were proton (p), deuterium (D), iron (Fe), calcium (Ca), copper (Cu), tin (Sn) and carbon (C). The kinematical range of measurement were: $0.0175 \leq x \leq 0.75$ and $2.5 \leq Q^2 \leq 170 GeV^2$ for $F_2(p)$ and $0.114 \leq x \leq 0.231$ and $15 \leq Q^2 \leq 65 GeV^2$ for $R(p)$ [84]; $0.05 \leq x \leq 0.65$ and $9 \leq Q^2 \leq 200 GeV^2$ for $F_2(Fe)$ [87]; $0.0025 \leq x \leq 0.75$ and $0.25 \leq Q^2 \leq 170 GeV^2$ for $F_2(D)$ [88, 89]; $0.0031 \leq x \leq 0.612$ and $0.52 \leq Q^2 \leq 46.4 GeV^2$ for the ratios $F_2(C)/F_2(D)$, $F_2(Cu)/F_2(D)$, $F_2(Ca)/F_2(D)$ and $F_2(Sn)/F_2(D)$ [89–92].

New Muon Collaboration (NMC) : The New Muon Collaboration (NMC) measured the structure function F_2 and R in muon scattering experiment at the CERN SPS with muon beams of energies 90, 120, 200, and 280 GeV. The target materials were p, D, helium (He), lithium (Li), C, Ca, Fe, Sn and lead (Pb). The kinematical range of measurement were: $0.001 \leq x \leq 0.6$ and $0.5 \leq Q^2 \leq 75 GeV^2$ for $F_2(p)$ and $F_2(D)$ [85, 93, 94]; $0.0045 \leq x \leq 0.11$ and $1.38 \leq Q^2 \leq 20.6 GeV^2$ for $R(p)$ [85]; $0.003 \leq x \leq 0.7$ and $0.12 \leq Q^2 \leq 100 GeV^2$ for the ratio $F_2(p)/F_2(D)$ [95–97]; $0.007 \leq x \leq 0.8$ and $0.6 \leq Q^2 \leq 18.3 GeV^2$ for the ratios $F_2(Ca)/F_2(Li)$, $F_2(C)/F_2(Li)$ and $F_2(Ca)/F_2(C)$ [98]; $0.0035 \leq x \leq 0.65$ and $0.5 \leq Q^2 \leq 90 GeV^2$ for the ratios $F_2(He)/F_2(D)$, $F_2(C)/F_2(D)$ and $F_2(Ca)/F_2(D)$ [99].

Bologna CERN Dubna Munich Saclay Collaboration (BCDMS) : The Bologna CERN Dubna Munich Saclay Collaboration measured the structure function

F_2 and R in muon scattering experiment at CERN. The incident muon beam energies are 100, 120, 200, 280 GeV and the target material used were p, D, C, Fe and nitrogen (N). The kinematical range of measurement were: $0.07 \leq x \leq 0.75$ and $7.5 \leq Q^2 \leq 230 GeV^2$ for $F_2(p)$ [33]; $0.07 \leq x \leq 0.65$ and $15 \leq Q^2 \leq 85 GeV^2$ for $R(p)$, $R(D)$ and $R(C)$ [33, 100, 101]; $0.07 \leq x \leq 0.75$ and $8.75 \leq Q^2 \leq 252.5 GeV^2$ for $F_2(C)$ and $F_2(D)$ [100, 101]; $0.02 \leq x \leq 0.7$ and $14 \leq Q^2 \leq 200 GeV^2$ for the ratios $F_2(Fe)/F_2(D)$ and $F_2(N)/F_2(D)$ [102, 103].

Stanford Linear Accelerator Center (SLAC) : In the deep inelastic electron scattering experiment performed at SLAC, structure function F_2 and R were measured with electron beam energies up to 50 GeV. Here the main target material used were p, D, Fe and gold (Au). The kinematical range of measurement were: $0.2 \leq x \leq 0.5$ and $1 \leq Q^2 \leq 10 GeV^2$ for $F_2(D)$, $F_2(Fe)$, $F_2(Au)$ and $R(D)$, $R(Fe)$, $R(Au)$ [23]; $0.03 \leq x \leq 0.1$ and $1.3 \leq Q^2 \leq 2.7 GeV^2$ for $R(C)$ [104].

H1 : The H1 collaboration determined the structure function F_2 and F_L from the cross section measurement in electron proton scattering experiment with the H1 detector at HERA. Here the data were taken with the lepton beam energy of 27.6 GeV and a proton beam energies of 920, 575 and 460 GeV. The measurement covers the region $10^{-6} \leq x \leq 0.1$ and $1.5 \leq Q^2 \leq 10^4 GeV^2$ for F_2 and $2.9 \times 10^{-5} \leq x \leq 0.1$ and $1.5 \leq Q^2 \leq 800 GeV^2$ for F_L up to $y = 0.85$ [11, 12, 32, 105]. Inclusive charm and beauty cross sections are also measured in $e^- p$ and $e^+ p$ neutral current collisions at HERA with the H1 detector in the kinematic region $5 \leq Q^2 \leq 2 \times 10^3 GeV^2$ and $2 \times 10^{-4} \leq x \leq 0.05$ [13, 71, 72].

ZEUS : The ZEUS collaboration determined the structure function F_2 and F_L from the cross section measurement in electron proton scattering experiment with the ZEUS detector at HERA. The data were taken with the lepton beam energy of 27.6 GeV and a proton beam energies of 920, 820, 575 and 460 GeV. The measurement

covers the region $10^{-4} \leq x \leq 0.1$ and $10 \leq Q^2 \leq 10^4 GeV^2$ for F_2 and $10^{-4} \leq x \leq 0.1$ and $5 \leq Q^2 \leq 130 GeV^2$ for F_L with y value $0.09 \leq y \leq 0.78$ [106–108]. The charm and beauty structure functions F_2^c and F_2^b were also measured with the ZEUS detector at HERA. Data covers the region $10 \leq Q^2 \leq 10^3 GeV^2$ and $10^{-4} \leq x \leq 0.1$ [73, 74, 109].

References

[1] Glashow, S. L. Partial-symmetries of weak interactions, *Nucl. Phys.* **22** (4), 579–588, 1961.

[2] Salam, A. and Ward, J. C. Electromagnetic and weak interactions, *Phys. Lett.*, **13** (2), 168-171, 1964.

[3] Gross, D. J. and Wilczek, F. Asymptotically free gauge theories, *Phys. Rev. D* **8** (10), 3633–3652, 1973.

[4] Politzer, H. D. Asymptotic freedom: an approach to strong interactions, *Phys. Rept.* **14** (4), 129–180, 1974.

[5] Gross, D. J. and Wilczek, F. Ultraviolet behavior of non-abelian gauge theories, *Phys. Rev. Lett.* **30** (26), 1343–1346, 1973.

[6] Weinberg, S. Non-abelian gauge theories of the strong interactions, *Phys. Rev. Lett.* **31** (7), 494–497, 1973.

[7] Wilson, K. G. Confinement of qnarks, *Phys. Rev. D* **10** (8), 2445–2459, 1974.

[8] Rutherford, E. The scattering of α and β particles by matter and the structure of the atom, *Philos. Mag.* **21** (125), 669–688, 1911.

[9] Bloom, E. D., et al. High-energy inelastic *ep* scattering at6-degrees and 10-degrees, *Phys. Rev. Lett.* **23** (16), 930–934, 1969.

[10] Breidenbach, M., et al. Observed behaviour of highly inelastic electron-proton scattering, *Phys. Rev. Lett.* **23** (16), 935–939, 1969.

[11] Aaron, F. D., et al. Measurement of the inclusive $e^{\pm}p$ scattering cross section at high inelasticity y and of the structure function F_L, *Eur. Phys. J. C* **71** (3), 1579-1–50, 2011.

[12] Andreev, V., et al. Measurement of Inclusive *ep* Cross Sections at High Q^2 at $\sqrt{s} = 225$ and $252GeV$ and of the Longitudinal Proton Structure Function F_L at HERA, *Eur. Phys. J. C* **74** (4), 2814-1–26, 2014.

[13] Aaron, F. D., et al. Measurement of the charm and beauty structure functions using the H1 vertex detector at HERA, *Eur. Phys. J. C.* **65** (1-2), 89–109, 2010.

[14] Toll, T. and Frixione, S. Charm and bottom photoproduction at HERA with MC@NLO, *Phys. Lett. B* **703** (4), 452–461, 2011.

[15] Campbell, J., et al. Higgs-boson production in association with a single bottom quark *Phys. Rev. D* **67** (9), 095002-1–13, 2003.

[16] Carvalho, F., et al. Charm and longitudinal structure functions within the Kharzeev-Levin-Nardi model, *Phys. Rev. C* **79** (3), 035211-1–6, 2009.

[17] Devenish, R. and Cooper-Sarkar, A. M. *Deep Inelastic Scattering*, Oxford University Press, New York, 2011.

[18] Roberts, R. G. *The structure of the proton*, Cambridge University Press, New York, 1990.

[19] Halzen, F. and Martin, A. D. *Quark and Leptons: An Introductory Course in Modern Particle Physics*, John Wiley and Sons, New York, 1984.

[20] Bjorken, J. D. and Drell, S. D. *Relativistic Quantum Fields*, McGraw-Hill Book Company, New York, 1965.

[21] Glazov, S. Measurement of DIS Cross Section at HERA, *Braz. J. Phys.* **37** (2C), 793–797, 2007.

[22] Abramowicz, H., et al. Deep inelastic cross-section measurements at large y with the ZEUS detector at HERA, *Phys. Rev. D* **90** (7), 072002-1–27, 2014.

[23] Dasu, S., et al. Measurement of kinematic and nuclear dependence of $R = \sigma_L/\sigma_T$ in deep inelastic electron scattering, *Phys. Rev. D* **49** (11), 5641–5674, 1994.

[24] Feynman, R. P. Very high-energy collisions of hadrons, *Phys. Rev. Lett.* **23** (24), 1415-1417, 1969.

[25] Bjorken, J. D. Asymptotic Sum Rules at Infinite Momentum, *Phys. Rev.* **179** (5), 1547-1553, 1969.

[26] Gell-Mann, M. A schematic model of baryons and mesons, *Phys. Lett.* **8** (3), 214–215, 1964.

[27] Zweig, G. An $SU(3)$ model for strong interaction symmetry and its breaking, CERN report 8419/TH. 412, 1964.

[28] Callan, C. and Gross, D. J. High-energy electroproduction and the constitution of the electric current, *Phys. Rev. Lett.* **22** (4), 156–159, 1969.

[29] Miller, G., et al. Inelastic Electron-Proton Scattering at Large Momentum Transfers and the Inelastic Structure Functions of the Proton, *Phys.Rev. D* **5** (3), 528-544, 1972.

[30] Bodek, A., et al. Experimental Studies of the Neutron and Proton Electromagnetic Structure Functions, *Phys.Rev. D* **20** (7), 1471-1552, 1979.

[31] Mesteyer, M. D., et al. Ratio σ_L/σ_T from deep-inelastic electron scattering, *Phys.Rev. D* **27** (1), 285-288, 1983.

[32] Abt, I., et al. Measurement of the proton structure function $F_2(x, Q^2)$ in the low-x region at HERA, *Nucl. Phys. B* **407** (3), 515–535, 1993.

[33] Benvenuti, A., et al. A High Statistics Measurement of the Proton Structure Functions $F_2(x, Q^2)$ and R from Deep Inelastic Muon Scattering at High Q^2, *Phys. Lett. B* **223** (3-4), 485–489, 1989.

[34] Hinchliffe, I. and Manohar, A. V. The QCD Coupling Constant, *Ann. Rev. Nucl. Part. Sci.* **50** (2000), 643–678, 2000.

[35] Altarelli, G. and Parisi, G. Asymptotic freedom in parton language, *Nucl. Phys. B.* **126** (2), 298–318, 1977.

[36] Collins, John C., et al. Factorization of Hard Processes in QCD, *Adv. Ser. Direct. High Energy Phys.* **5** (1988), 1-91, 1988.

[37] Collins, John C., et al. Factorization for short distance hadron-hadron scattering, *Nucl. Phys. B* **261** 104–142, 1985.

[38] Narison, S. *QCD as a theory of hadrons: From Partons to Confinement*, Cambridge University Press, New York, 2004.

[39] Gribov, V. N. and Lipatov, L. N. Deep inelastic ep scattering in perturbation theory, *Sov. J. Nucl. Phys.* **15** (4), 438–450, 1972.

[40] Lipatov, L. N. The parton model and perturbation theory, *Sov. J. Nucl. Phys.* **20** (1), 94–102, 1975.

[41] Altarelli, G. Partons in quantum chromodynamics, *Phys. Rep* **81** (1), 1–129, 1982.

[42] Cooper-Sarkar, A. M., Devenish R. C. E., and Roeck, A. D. E. Structure functions of the nucleon and their interactions, *Int. J. Mod. Phys. A* **13** (20), 3385–3586, 1998.

[43] Kuraev, E. A., Lipatov, L. N., and Fadin, V. S. The Pomeranchuk singularity in nonabelian gauge theories, *Sov. Phys. JETP* **45** (2), 199–204, 1977.

[44] Balitskii, Y. Y. and Lipatov, L. N. The Pomeranchuk Singularity in Quantum Chromodynamics, *Sov. J. Nucl. Phys.* **28** (6), 822–829, 1978.

[45] Catani, S., Fiorani, F. and Marchesini, G. QCD coherence in initial state radiation, *Phys. Lett. B* **234** (3), 339–345, 1990.

[46] Ciafaloni, M. QCD coherence in initial state radiation, *Nucl. Phys. B* **296** (1), 49–74, 1988.

[47] Gribov, L. V., Levin, E. M. and Ryskin, M. G. Semihard processes in QCD, *Phys. Rep.* **100** (1-2), 1–150, 1983.

[48] Zhu, W. A new approach to parton recombination in the QCD evolution equations, *Nucl. Phys. B* **551** (1-2), 245–274, 1999.

[49] Zhu, W. and Ruan, J. H. A new modified Altarelli-Parisi evolution equation with parton recombination in proton, *Nucl. Phys. B* **559** (1-2), 378–392, 1999.

[50] Zhu, W., Shen, Z. Q. and Ruan, J. H. Parton recombination effect in polarized parton distributions, *Nucl. Phys. B* **692** (3) 417–433, 2004.

[51] Jalilian Marian, J., et al. The BFKL equation from the Wilson renormalization group, *Nucl. Phys. B* **504** (1-2), 415–431, 1997.

[52] Iancu, E., Leonidov, A. and McLerran, L. Nonlinear gluon evolution in the color glass condensate: I, *Nucl. Phys. A* **692** (3-4), 583–645, 2001.

[53] Balitsky, I. Operator expansion for high-energy scattering, *Nucl. Phys. B* **463** (1), 99–157, 1996.

[54] Kovchegov, Yu. Small-x F_2 structure function of a nucleus including multiple Pomeron exchanges, *Phys. Rev. D* **60** (3), 034008,1–8, 1999.

[55] Lipatov, L. N. Small-x physics in perturbative QCD, *Phys. Rept.* **286**, (3), 131–198, 1997.

[56] Gogitidze, N. Determination of the longitudinal structure function F_L at HERA, *J. Phys. G: Nucl. Part. Phys.* **28** (5), 751–765, 2002.

[57] Tuning, N. *Proton structure functions at HERA*, PhD thesis, University of Amsterdam, Netherland, 2001.

[58] Dissertori, G., Knowles, I.G. and Schmelling, M. *Quantum Chromodynamics: High Energy Experiments and Theory*, Oxford University Press, North Carolina, U.S.A, 2003.

[59] Altarelli, G. and Martinelli, G. Transverse momentum of jets in electroproduction fromquantum chromodynamics, *Phys. Lett. B* **76** (1), 89–94, 1978.

[60] Moch, S., Vermaseren, J. A. M. and Vogt, A. The longitudinal structure function at the third order, *Phys. Lett. B* **606** (1-2), 123–129, 2005.

[61] Cooper-Sarkar, A. M., et al. Measurement of the longitudinal structure function and the small x gluon density of the proton, *Z. Phys. C* **39** (2), 281–290, 1988.

[62] Galzov, A. Recent measurements of the proton structure functions at HERA, *Acta Phys. Pol. B Proc. Suppl.* **1** (2), 371–378, 2008.

[63] Feynmann, R. P. Very high-energy collisions of hadrons, *Phys. Rev. Lett.* **23** (24), 1415–1417, 1969.

[64] Behnke, O. Open Charm and Beauty Production at HERA, *Nucl. Phys. B (Proc. Suppl.)* **222-224** 140-150, 2012.

[65] Gluck, M., Reya, E. and Vogt, A. Dynamical parton distributions of the proton and small x physics, *Z. Phys. C* **67** (3), 433–447, 1995.

[66] Gluck, M., Reya, E. and Vogt, A. Dynamical parton distributions revisited, *Eur. Phys. J. C* **5** (3), 461–470, 1998.

[67] Catani, S., Ciafaloni, M. and Hautmann, F. High energy factorization and small-x heavy flavour production, *Nucl. Phys. B* **366** (1), 135–188, 1991.

[68] Breitweg, J., et al. Measurement of $D^{*\pm}$ production and the charm contribution to F_2 in deep inelastic scattering at HERA, *Eur. Phys. J. C* **12** (1), 35–52, 2000.

[69] Adloff, C., et al. Measurement of $D^{*\pm}$ meson production and F_2^c in deep-inelastic scattering at HERA, *Phys. Lett. B* **528**, (3-4), 199–214, 2002.

[70] Abramowicz, H., et al. Measurement of D^+ and Λ_c^+ production in deep inelastic scattering at HERA, *J. High Energy Phys.* **2010** (11), 009-1-27, 2010.

[71] Aktas, A., et al. Measurement of $F_2^{c\bar{c}}$ and $F_2^{b\bar{b}}$ at high Q^2 using the H1 vertex detector at HERA, *Eur. Phys. J. C* **40** (3), 349–359, 2005.

[72] Aktas, A., et al. Measurement of $F_2^{c\bar{c}}$ and $F_2^{b\bar{b}}$ at low Q^2 and x using the H1 vertex detector at HERA, *Eur. Phys. J. C* **45**, (1), 23–33, 2006.

[73] Chekanov, S., et al. Measurement of $D^{\pm}$ and D^0 production in deep inelastic scattering using a lifetime tag at HERA, *Eur. Phys. J. C* **63** (2), 171–188, 2009.

[74] Chekanov, S., et al. Measurement of charm and beauty production in deep inelastic ep scattering from decays into muons at HERA, *Eur. Phys. J. C* **65** (1-2), 65–79, 2010.

[75] Mueller, A. H. and Qiu, J. Gluon recombination and shadowing at small values of x, *Nucl. Phys. B* **268** (2), 427–452, 1986.

[76] Collins, P. D. B. *Introduction to regge theory and high energy physics*, Cambridge University Press, New York, 1977.

[77] Soyez, G. Small-Q^2 extension of DGLAP-constrained Regge residues, *Phys. Lett. B* **603** (3-4), 189–194, 2004.

[78] Drescher, H. J., et al. Parton based Gribov Regge theory, *Phys. Rep.* **350** (2-4), 93–289, 2001.

[79] Desgrolard, P. and Martynov, E. Regge models of the proton structure function with and without hard pomeron: A comparative analysis, *Eur. Phys. J. C* **22** (3), 479–492, 2001.

[80] Donnachie, A. and Landshoff, P. V. Perturbative QCD and Regge theory: closing the circle, *Phys. Lett. B* **533** (3-4), 277–284, 1992.

[81] Kotikov, A. V. and Parente, G. The gluon distribution as a function of F_2 and $dF_2/dlnQ^2$ at small x. The next-to-leading analysis, *Phys. Lett. B* **379** (1-4), 195–201, 1996.

[82] Derrick, M., et al. Measurement of the Proton Structure Function F_2 in ep Scattering at HERA, *Phys. Lett. B* **316** (2-3), 412–426, 1993.

[83] Adloff, C. Measurement of inclusive jet cross sections in photoproduction at HERA, *Eur. Phys. J. C* **29** (4), 497–513, 2003.

[84] Aubert, J. J., et al. A detailed study of the proton structure functions in deep inelastic muon-proton scattering, *Nucl. Phys. B* **259** (2-3), 189–265, 1985.

[85] Arneodo, M., et al. Measurement of the proton and deuteron structure functions, F_2^p and F_2^d, and of the ratio σ_L/σ_T, *Nucl. Phys. B* **483** (1-2), 3-43, 1997.

[86] Whitlow, L. W., et al. A precise extraction of $R = \sigma_L/\sigma_T$ from a global analysis of the SLAC deep inelastic $e - p$ and $e - d$ scattering cross sections, *Phys. Lett. B* **250** (1-2), 193–198, 1990.

[87] Aubert, J. J., et al. A detailed study of the nucleon structure functions in deep inelastic muon scattering in iron, *Nucl. Phys. B* **272** (1), 158–192, 1986.

[88] Aubert, J. J., et al. Measurements of the nucleon structure functions F_2^N in deep inelastic muon scattering from deuterium and comparison with those from hydrogen and iron, *Nucl. Phys. B* **293**, 740–786, 1987.

[89] Arneodo, M., et al. Measurements of the nucleon structure function in the range $0.002 < x < 0.17$ and $0.2 < Q^2 < 8GeV^2$ in deuterium, carbon and calcium, *Nucl. Phys. B* **333** (1), 1–47, 1990.

[90] Ashman, J., et al. Measurement of the ratios of deep inelastic muon-nucleus cross sections on various nuclei compared to deuterium, *Phys. Lett. B* **202** (4), 603–610, 1988.

[91] Arneodo, M., et al. Shadowing in deep inelastic muon scattering from nuclear targets, *Phys. Lett. B* **211** (4), 493–499, 1988.

[92] Ashman, J., et al. A Measurement of the ratio of the nucleon structure function in copper and deuterium, *Z. Phys. C* **57** (2), 211–218, 1993.

[93] Arneodo, M., et al. Accurate measurement of F_2^d/F_2^p and $R^d - R^p$, *Nucl. Phys. B* **487** (1-2), 3–26, 1997.

[94] Arneodo, M., et al. Measurement of the proton and the deuteron structure functions, F_2^p and F_2^d, *Phys. Lett. B* **364** (2), 107–115, 1995.

[95] Allasia, D., et al. Measurement of the neutron and the proton F2 structure function ratio, *Phys. Lett. B* **249** (2), 366–372, 1990.

[96] Amaudruz, P., et al. Gottfried sum from the ratio F_2^n/F_2^p, *Phys. Rev. Lett.* **66** (21), 2712–2715, 1991.

[97] Armadruz, P., et al. The ratio F_2^n/F_2^p in deep inelastic muon scattering, *Nucl. Phys. B* **371** (1-2), 3–31, 1992.

[98] Amaudruz, P., et al. Precision measurement of structure function ratios for $Li-6$, $C-12$ and $Ca-40$, *Z. Phys. C* **53** (1), 73–77, 1992.

[99] Amaudruz, P., et al. Precision measurement of the structure function ratios $F_2(He)/F_2(D)$, $F_2(C)/F_2(D)$ and $F_2(Ca)/F_2(D)$, *Z. Phys. C* **51** (3), 387–394, 1991.

[100] Benvenuti, A. C., et al. A high statistics measurement of the nucleon structure function $F_2(x, Q^2)$ from deep inelastic muon-carbon scattering at high Q^2, *Phys. Lett. B* **195** (1), 91–96, 1987.

[101] Benvenuti, A. C., et al. A high statistics measurement of the deuteron structure functions $F_2(x, Q^2)$ and R from deep inelastic muon scattering at high Q^2, *Phys. Lett. B* **237** (3-4), 592–598, 1990.

[102] Benvenuti, A. C., et al. Nuclear effects in deep inelastic muon scattering on deuterium and iron targets, *Phys. Lett. B* **189** (4), 483–487, 1987.

[103] Bari, G., et al. A measurement of nuclear effects in deep inelastic muon scattering on deuterium, nitrogen and iron targets, *Phys. Lett. B* **163** (1-4), 282–286, 1985.

[104] Abe, K., et al. Measurements of $R = \sigma_L / \sigma_T$ for $0.03 < x < 0.1$ and fit to world data, *Phys. Lett. B* **452** (1-2), 194–200, 1999.

[105] Adloff, C., et al. Measurement of neutral and charged current cross-sections in positron proton collisions at large momentum transfer, *Eur. Phys. J. C* **13** (4), 609–639, 2000.

[106] Breitweg, J., et al. Measurement of the proton structure function F_2 at very low Q^2 at HERA, *Phys. Lett. B* **487** (1-2), 53–73, 2000.

[107] Chekanov, S., et al. Measurement of the neutral current cross-section and F_2 structure function for deep inelastic e^+p scattering at HERA, *Eur. Phys. J. C* **21** (3), 443–471, 2001.

[108] Chekanov, S., et al. Measurement of the longitudinal proton structure function at HERA, *Phys. Lett. B* **682** (1), 8–22, 2009.

[109] Chekanov, S., et al. Measurement of D mesons production in deep inelastic scattering at HERA, *J. High Energy Phys.* **2007** (07) 074-1–37, 2007. □

Chapter 2

Evolution of Longitudinal Structure Function F_L Using Taylor Series Expansion Method at Small-x

In this chapter, we study the behaviour of the longitudinal structure function F_L of proton from its QCD evolution equation in NNLO approximation at small-x. Here we use the Taylor series expansion method to solve the evolution equation. The solution of this equation provides the expressions for $t=\left[ln(\frac{Q^2}{\Lambda^2})\right]$- and x-evolution equations for the computation of the longitudinal structure function. Our calculated results are compared with the recent H1 [1–5], ZEUS [6] experimental data, results of Donnachie-Landshoff (DL) models [7] and the theoretical predictions of MSTW08 [8], CT10 [9], ABM11 [10], NNPDF2.3 [11, 12] parameterizations. We have also compared our x-evolution results with the gluon dominating F_L structure function obtained by Boroun et al. [13]. Our predicted results show good agreement with the recent data and related fit and can be described within the framework of pQCD.

2.1 Theory

At small values of x, the density of gluons in the proton is considerably larger than densities of quarks and antiquarks. Thus, at small-x the structure of proton is mainly described by the distribution of gluons only. At small-x ($x \leq 10^{-3}$) the gluon contribution to the F_L structure function dominates over the singlet and non-singlet contribu-

tion [14]. Now the QCD evolution equation for gluon dominating F_L structure function is given by [15]

$$\frac{\partial F_L^g(x,Q^2)}{\partial lnQ^2} = K_G(x,Q^2) \otimes F_L^g(x,Q^2). \tag{2.1}$$

Here $K_G(x,Q^2)$ is the gluon kernel known perturbatively up to the first few orders in $\alpha_s(Q^2)$. The symbol $\otimes$ represents the standard Mellin convolution and is given by

$$A(x) \otimes B(x) = \int_0^1 \frac{dy}{y} A(y) B\Big(\frac{x}{y}\Big). \tag{2.2}$$

The kernel $K_G(x,Q^2)$ can be written as

$$K_G(x,Q^2) = \frac{\alpha_s(Q^2)}{4\pi} K_G^0(x) + \Big(\frac{\alpha_s(Q^2)}{4\pi}\Big)^2 K_G^1(x) + \Big(\frac{\alpha_s(Q^2)}{4\pi}\Big)^3 K_G^2(x) \tag{2.3}$$

up to NNLO, where $K_G^0(x)$, $K_G^1(x)$ and $K_G^2(x)$ are the gluon splitting kernel [16, 17] in LO, NLO and NNLO respectively. The expressions for $K_G^0(x)$, $K_G^1(x)$ are defined in Appendix A. $K_G^2(x)$ is available in co-efficient function form in Refs. [18, 19] and its expression is given in Appendix A. Using all these and simplifying QCD evolution equations for the longitudinal structure function in LO, NLO and NNLO, we get

$$\frac{\partial F_L^g(x,t)}{\partial t} - \frac{\alpha_s(t)}{4\pi}\left[\frac{80}{9}\int_x^1 dw w^2(1-w) F_L^g\Big(\frac{x}{w},t\Big)\right] = 0, \tag{2.4}$$

$$\frac{\partial F_L^g(x,t)}{\partial t} - \frac{\alpha_s(t)}{4\pi}\left[\frac{80}{9}\int_x^1 dw w^2(1-w) F_L^g\Big(\frac{x}{w},t\Big)\right] - \Big(\frac{\alpha_s(t)}{4\pi}\Big)^2 I_1^G(x,t) = 0 \tag{2.5}$$

and

$$\frac{\partial F_L^g(x,t)}{\partial t} - \frac{\alpha_s(t)}{4\pi}\left[\frac{80}{9}\int_x^1 dw w^2(1-w) F_L^g\Big(\frac{x}{w},t\Big)\right] - \Big(\frac{\alpha_s(t)}{4\pi}\Big)^2 I_1^G(x,t) - \Big(\frac{\alpha_s(t)}{4\pi}\Big)^3 I_2^G(x,t) = 0, \tag{2.6}$$

where

$$I_1^G(x,t) = \frac{160}{9}\int_x^1 dw f(w) F_L^g\Big(\frac{x}{w},t\Big) \tag{2.7}$$

and

$$I_2^G(x,t) = \int_x^1 dw K_G^2(w) F_L^g\Big(\frac{x}{w},t\Big). \tag{2.8}$$

Here $t = ln\frac{Q^2}{\Lambda^2}$, Λ is the QCD cut-off parameter and the function $f(w)$ is defined in Appendix A. The strong coupling constant in higher order has the form [20, 21]

$$\alpha_s(t) = \frac{4\pi}{\beta_0 t}\Big[1 - \frac{\beta_1}{\beta_0^2}\frac{lnt}{t} + \frac{1}{\beta_0^3 t^2}\Big\{\frac{\beta_1^2}{\beta_0}(ln^2 t - lnt - 1) + \beta_2\Big\} + O\Big(\frac{1}{t^3}\Big)\Big], \tag{2.9}$$

where

$$\beta_0 = 11 - \frac{2}{3}N_f, \tag{2.10}$$

$$\beta_1 = 102 - \frac{38}{3}N_f \tag{2.11}$$

and

$$\beta_2 = \frac{2857}{2} - \frac{5033}{18}N_f + \frac{325}{54}N_f^2 \tag{2.12}$$

are the one loop, two loop and three loop correction to the QCD β-function, N_f being the number of flavours. Here we take $N_f = 4$.

Equations (2.4), (2.5) and (2.6) can be solved by Taylor series expansion method as described in ref. [22, 23]. Considering the variable $u = 1 - w$, and since $x < w < 1$, we have $0 < u < 1 - w$; so the series $\frac{x}{w} = \frac{x}{1-u}$ is convergent for $|u| < 1$ and using the Taylor expansion method and neglecting the higher order terms, $F_L^g\Big(\frac{x}{w},t\Big)$ can be approximated for small-x as

$$\begin{aligned} F_L^g\Big(\frac{x}{w},t\Big) &= F_L^g\Big(x+\frac{xu}{1-u},t\Big) \\ &= F_L^g(x,t)+\frac{xu}{1-u}\frac{\partial F_L^g(x,t)}{\partial x}. \end{aligned} \tag{2.13}$$

Using (2.13) in equations (2.4), (2.5) and (2.6) and performing u-integrations we get

$$\frac{\partial F_L^g(x,t)}{\partial t}-\frac{1}{t}\Big[A_1(x)\frac{\partial F_L^g(x,t)}{\partial x}+B_1(x)F_L^g(x,t)\Big]=0, \tag{2.14}$$

$$\frac{\partial F_L^g(x,t)}{\partial t}-\frac{1}{t}\Big(1-b\frac{lnt}{t}\Big)\Big[A_2(x)\frac{\partial F_L^g(x,t)}{\partial x}+B_2(x)F_L^g(x,t)\Big]=0 \tag{2.15}$$

and

$$\begin{aligned} &\frac{\partial F_L^g(x,t)}{\partial t}-\frac{1}{t}\Big(1-b\frac{lnt}{t}+\frac{b^2}{t^2}(ln^2t-lnt-1)+\frac{c}{t^2}\Big) \\ &\qquad\Big[A_3(x)\frac{\partial F_L^g(x,t)}{\partial x}+B_3(x)F_L^g(x,t)\Big]=0, \end{aligned} \tag{2.16}$$

where

$$A_1(x)=\frac{1}{\beta_0}P_2(x),\quad B_1(x)=\frac{1}{\beta_0}P_1(x),\quad A_2(x)=\frac{1}{\beta_0}(P_2(x)+T_0Q_2(x)),$$

$$B_2(x)=\frac{1}{\beta_0}(P_1(x)+T_0Q_1(x)),\quad A_3(x)=\frac{1}{\beta_0}(P_2(x)+T_0Q_2(x)+T_1R_2(x)),$$

$$B_3(x)=\frac{1}{\beta_0}(P_1(x)+T_0Q_1(x)+T_1R_1(x)),$$

$$P_1(x)=\frac{80}{9}\Big(\frac{1}{12}-\frac{x^3}{3}+\frac{x^4}{4}\Big),\qquad P_2(x)=\frac{80}{9}x\Big(\frac{1}{12}-\frac{x^2}{2}+\frac{2x^3}{3}-\frac{x^4}{4}\Big),$$

$$Q_1(x) = \frac{160}{9}\int_x^1 f(w)dw, \qquad Q_2(x) = \frac{160}{9}x\int_x^1 \frac{(1-w)}{w}f(w)dw,$$

$$R_1(x) = \int_x^1 K_G^2(w)dw, \qquad R_2(x) = x\int_x^1 \frac{(1-w)}{w}K_G^2(w)dw,$$

$$b = \frac{\beta_1}{\beta_0^2} \qquad \text{and} \qquad c = \frac{\beta_2}{\beta_0^3}.$$

Here we consider two numerical parameters T_0 and T_1, such that $T^2(t) = T_0.T(t)$ and $T^3(t) = T_1.T(t)$ with $T(t) = \frac{\alpha_s(t)}{4\pi}$. These numerical parameters are obtained for a particular range of Q^2 under study. As described in ref. [23], these two parameters are chosen in such a way that the difference between $T^2(t)$, $T_0.T(t)$ and $T^3(t)$, $T_1.T(t)$ are negligible in our required range. This is explained in figure 2.1. Here, we have considered the values of $T_0 = 0.0278$ and $T_1 = 0.000892$ within the range $1.5 \leq Q^2 \leq 800GeV^2$.

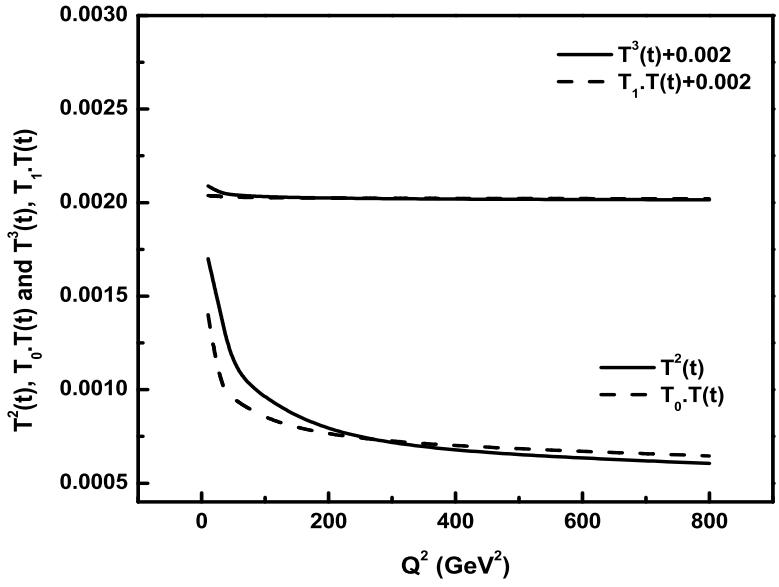

Figure 2.1: $T^2(t) = T_0.T(t)$ and $T^3(t) = T_1.T(t)$ versus $Q^2(GeV^2)$.

The general solution of equation (2.14) is $F(U,V)=0$, where $F(U,V)$ is an arbitrary function [22]. Now, $U(x,t,F_L^g)=C_1$ and $V(x,t,F_L^g)=C_2$ with C_1 and C_2, two constants, form a solution of the Lagrange's equation

$$\frac{dx}{A_1(x)}=-\frac{dt}{t}=-\frac{dF_L^g(x,t)}{B_1(x)F_L^g(x,t)} \tag{2.17}$$

from which we obtain

$$U(x,t,F_L^g)=t\cdot\exp\left[\int\frac{dx}{A_1(x)}\right] \tag{2.18}$$

and

$$V(x,t,F_L^g)=F_L^g(x,t)\cdot\exp\left[\int\frac{B_1(x)}{A_1(x)}dx\right]. \tag{2.19}$$

It thus has no unique solution. The simplest possibility is that a linear combination of U and V is to satisfy $F(U,V)=0$ so that $\alpha\cdot U+\beta\cdot V=0$, where α and β are arbitrary constants [22]. This combination gives

$$F_L^g(x,t)=-\Big(\frac{\alpha}{\beta}\Big)\cdot t\cdot\exp\left[\int\Big(\frac{1}{A_1(x)}-\frac{B_1(x)}{A_1(x)}\Big)dx\right]. \tag{2.20}$$

Now defining

$$F_L^g(x,t_0)=-\Big(\frac{\alpha}{\beta}\Big)\cdot t_0\cdot\exp\left[\int\Big(\frac{1}{A_1(x)}-\frac{B_1(x)}{A_1(x)}\Big)dx\right]$$

at $t=t_0$, where $t_0=ln\Big(\frac{Q_0^2}{\Lambda^2}\Big)$ at any lower value $Q=Q_0$, we get from equation (2.20)

$$F_L^g(x,t)=F_L^g(x,t_0)\Big(\frac{t}{t_0}\Big). \tag{2.21}$$

Again defining

$$F_L^g(x_0,t)=-\Big(\frac{\alpha}{\beta}\Big)\cdot t\cdot\exp\left[\int\Big(\frac{1}{A_1(x)}-\frac{B_1(x)}{A_1(x)}\Big)dx\right]_{x=x_0},$$

at any higher values of $x = x_0$, we obtain from equation (2.20)

$$F_L^g(x,t) = F_L^g(x_0,t)\exp\left[\int_{x_0}^{x}\Big(\frac{1}{A_1(x)} - \frac{B_1(x)}{A_1(x)}\Big)dx\right]. \tag{2.22}$$

Equations (2.21) and (2.22) give the t- and x-evolutions of longitudinal structure function F_L^g in LO respectively. Similarly, from equations (2.15) and (2.16), we obtain the t- and x-evolutions for F_L structure function in NLO and NNLO as

$$F_L^g(x,t) = F_L^g(x,t_0)\frac{t^{(1+b/t)}}{t_0^{(1+b/t_0)}}\exp\left[b\Big(\frac{1}{t} - \frac{1}{t_0}\Big)\right], \tag{2.23}$$

$$F_L^g(x,t) = F_L^g(x_0,t)\exp\left[\int_{x_0}^{x}\Big(\frac{1}{A_2(x)} - \frac{B_2(x)}{A_2(x)}\Big)dx\right] \tag{2.24}$$

and

$$F_L^g(x,t) = F_L^g(x,t_0)\frac{t^{(1+b/t)}}{t_0^{(1+b/t_0)}}\exp\left[\begin{array}{c} b\Big(\frac{1}{t} - \frac{1}{t_0}\Big) + \Big(\frac{b^2}{2} - \frac{c}{2}\Big)\Big(\frac{1}{t^2} - \frac{1}{t_0^2}\Big) \\ -\frac{b^2}{2}\Big(\frac{ln^2 t}{t^2} - \frac{ln^2 t_0}{t_0^2}\Big) \end{array}\right], \tag{2.25}$$

$$F_L^g(x,t) = F_L^g(x_0,t)\exp\left[\int_{x_0}^{x}\Big(\frac{1}{A_3(x)} - \frac{B_3(x)}{A_3(x)}\Big)dx\right] \tag{2.26}$$

respectively.

In our calculations, we used up to first order term $O(x)$ in Taylor expansion of $F_L^g\Big(\frac{x}{w},t\Big)$ and neglecting the higher order terms in small-x approximation. Now instead of neglecting the higher order terms $O(x^2)$ from the Taylor expansion series let us retain the second order term and neglecting the higher order terms $O(x^3)$, $F_L^g\Big(\frac{x}{w},t\Big)$ can then be approximated as

$$F_L^g\Big(\frac{x}{w},t\Big) \cong F_L^g(x,t) + \frac{xu}{1-u}\frac{\partial F_L^g(x,t)}{\partial x} + \frac{1}{2}\Big(\frac{xu}{1-u}\Big)^2\ \frac{\partial^2 F_L^g(x,t)}{\partial x^2}, \tag{2.27}$$

which gives from equation (2.4)

$$\frac{\partial F_L^g(x,t)}{\partial t} - \frac{1}{t}\Big[B_1(x)F_L^g(x,t) + A_1(x)\frac{\partial F_L^g(x,t)}{\partial x} + C_1(x)\frac{\partial^2 F_L^g(x,t)}{\partial x^2}\Big] = 0, \qquad (2.28)$$

where $C_1(x) = \frac{1}{\beta_0}\Big(\frac{x^2}{8} - \frac{x^3}{2} + \frac{3x^4}{4} - \frac{x^5}{2} + \frac{x^6}{8}\Big)$. $A_1(x)$ and $B_1(x)$ are given earlier.

The equation (2.28) is a second order partial differential equation and this can be solved by Monges method [24]. According to this method, the solution of second order partial differential equation

$$Rr + Ss + Tt = V \qquad (2.29)$$

can be obtained from the subsidiary equations

$$Rdy^2 + Sdxdy + Tdx^2 = 0 \qquad (2.30)$$

and

$$Rdpdy + Sdqdx - Vdxdy = 0, \qquad (2.31)$$

where R, S, T and V are functions of x, y, z, p and q. Here z, p, q, r, s and t are defined as follows

$$z = z(x,y) = F_L^g(x,t), \quad p = \frac{\partial z}{\partial x}, \quad q = \frac{\partial z}{\partial y}, \quad r = \frac{\partial^2 z}{\partial x^2} = \frac{\partial p}{\partial x},$$

$$s = \frac{\partial^2 z}{\partial x \partial y} = \frac{\partial p}{\partial y} = \frac{\partial q}{\partial x} \qquad \text{and} \qquad t = \frac{\partial^2 z}{\partial y^2} = \frac{\partial q}{\partial y}.$$

Comparing equations (2.28) and (2.29) we get

$$R = C_1(x), \quad S = 0, \quad T = 0 \quad \text{and}$$

$$V = t\frac{\partial F_L^g(x,t)}{\partial t} - A_1(x)\frac{\partial F_L^g(x,t)}{\partial x} - B_1(x)F_L^g(x,t).$$

Substituting the values of R, S, T and V in subsidiary equations (2.30) and (2.31) we ultimately obtain $V = 0$, which gives

$$\frac{\partial F_L^g(x,t)}{\partial t} - \frac{1}{t}\Big[A_1(x)\frac{\partial F_L^g(x,t)}{\partial x} + B_1(x)F_L^g(x,t)\Big] = 0, \qquad (2.32)$$

which is exactly same as the equation (2.14). Similarly, the other two equations (2.15) and (2.16) become same when we include the second order term in the Taylor expansion series. Thus it is clear that the inclusion of the second order term does not modify the solutions of the evolution equations. Similarly, if one introduce more higher order terms in Taylor expansion series, then for these cases also the term can be neglected due to smaller values of x [25, 26].

Thus we have obtained an analytical expression for the t- and x-evolutions of longitudinal structure function F_L^g. From the final expressions (2.21), (2.23) and (2.25), it is observed that our results, i.e., the t-evolutions depend upon the expressions of $\alpha_s(t)$ only. From these expressions we can easily calculate the t-evolutions of F_L^g by taking an input distribution at a given value of Q_0^2. The x-evolutions of F_L^g is determined from the expressions (2.22), (2.24) and (2.26) by taking an input distribution at a given value of x_0. Here, we have calculated the x-evolution up to NLO only. Due to the unavailability of the evolution kernel at NNLO we are unable to calculate the same at this order. But the co-efficient function and splitting function of quarks and gluon are available up to NNLO. So, we have calculated the structure function up to NLO in this chapter and up to NNLO in chapter 4 and 5. In chapter 4 and 5, we have calculated the structure function using the QCD evolution equation in terms of co-efficient function and splitting function of quarks and gluon and the details are described in the respective chapter.

2.2 Results and Discussions

Using the simple analytical expressions (2.21), (2.22), (2.23), (2.24) and (2.25), we have calculated the the gluon dominating longitudinal structure function F_L^g at small-x in leading, next-to-leading and next-to-next-to-leading orders. The obtained results are compared with the experimental data taken by H1 [1–5] and ZEUS collaboration [6], results of the Donnachie-Landshoff (DL) model [7] and the theoretical predictions from

MSTW08 [8], CT10 [9], ABM11 [10], NNPDF2.3 [11, 12] parameterizations. In H1 2001 data [2], the structure functions are measured in the kinematic range $1.5 \leq Q^2 \leq 150GeV^2$ and $3 \times 10^{-5} \leq x \leq 0.2$, for H1 2007 data [3,4], range is $2.5 \leq Q^2 \leq 25GeV^2$ and $5 \times 10^{-5} \leq x \leq 0.12$, for H1 2011 data [1], range is $1.5 \leq Q^2 \leq 120GeV^2$ and $2.9 \times 10^{-5} \leq x \leq 0.01$, for H1 2014 data [5], range is $35 \leq Q^2 \leq 800GeV^2$ and $6.5 \times 10^{-4} \leq x \leq 0.65$ and for ZEUS 2009 data [6], range is $20 < Q^2 < 130GeV^2$ and $5 \times 10^{-4} < x < 0.07$ respectively.

DL model [7] is based on dipole picture with a soft and a hard pomeron, large dipole couples to the soft pomeron and small dipole couples to the hard pomeron. The parameters in the model are fixed by proton-proton scattering data and proton structure function F_2^p data. The authors derived a good numerical fit to the output of the DGLAP evolution for the small-x behaviour of the gluon distribution function which is valid for Q^2 between 5 and $500GeV^2$. Here, they fitted their parameters with the H1 data sets [2]. The gluon distribution here is mainly dominated by the hard pomeron at small-x and for all Q^2. This not only describes the DGLAP evolution of hard part of the F_2, but also the longitudinal structure function. The MSTW08 PDFs [8] include updated LO, NLO and NNLO parton distribution functions determined from global analysis of hard-scattering data within the standard framework of leading-twist fixed-order collinear factorisation in the $\overline{MS}$ scheme. These parton distributions are a major update to the previously available MRST sets [27–29] and incorporate the maximum amount of information from DIS and other hard-scattering data. The CT10 PDFs of the proton describes theoretical advancements in the global QCD analysis that was used to produce the previous CTEQ6.6 [30] and CT09 [31] PDFs. This analysis includes the most recent collider data from deep-inelastic scattering, vector boson production, and single-inclusive jet production [9]. In CT10 PDFs the combined H1/ZEUS data [32] sets for DIS at HERA is also included. The ABM11 PDF fit is based on the world data for deep-inelastic scattering, fixed-target data for the Drell-Yan process and also

includes data from the LHC for the Drell-Yan process [10]. The NNPDF2.3 PDF fit, is the most accurate determination to date from the NNPDF family, and it supersedes previous existing sets. It differs from the NNPDF2.1 set because of the inclusion of LHC data [11].

Here, the proton longitudinal structure function, measured in the range $5 \leq Q^2 \leq 800GeV^2$ and $10^{-4} \leq x \leq 10^{-1}$, have been used for our analysis. The value of y used is greater than or equal to 0.5, as from this value onwards the contribution of F_L structure function is significant towards the total cross section [33]. The average values of Λ in our calculation is $0.22GeV$. In figure 2.2, F_L structure function is plotted against Q^2 for different values of x in comparison with the H1, ZEUS data and results of DL model. In figure 2.3, F_L structure function is plotted against x for different values of Q^2 in comparison with the H1, ZEUS data and the results of DL model. In figure 2.4, F_L structure function is plotted against x for different values of Q^2 in comparison with the H1, ZEUS data and the theoretical prediction of MSTW08. In figure 2.5, F_L structure function is plotted against x for different values of Q^2 in comparison with the H1, ZEUS data and theoretical prediction of CT10. Figures 2.6 and 2.7 describe our x-evolution results in comparison with the H1, ZEUS data and theoretical predictions of ABM11 and NNPDF2.3. The vertical error bars in all the plots are both statistical and systematic error for both H1 and ZEUS data. In all the graphs, the data points at lowest Q^2 values are taken as input point for t-evolution graphs and data points at highest x values are taken as input points for x-evolution graphs. To confirm that in spite of the large uncertainty in the experimental data, our results are in better agreement with the data, we add DL model results and the theoretical prediction of different parameterizations in all the figures.

It is observed from the t-evolution graphs that, our result shows good agreement with that of H1 and ZEUS data, i.e., with respect to the experimental data our result shows increasing behaviour with increasing values of Q^2. It is seen from the figure

2.2 that, our plots are in good agreement with DL model fit also and as the energy scale becomes larger, the agreement is better. But, at intermediate energy scale the agreement is not so good, the reason for this is that the DL model approach comes from a BFKL like evolution equation [7] and the Q^2-evolution in that case is somewhat different from a DGLAP approach. In all the cases, our calculated F_L structure function in LO, NLO and NNLO increase with the values of Q^2 in the given range like the results of DL model as expected from QCD. At small-x, F_L increases with Q^2 as we resolve increasing numbers of soft partons with increasing Q^2 [34]. The x-evolution results also show compatibility with the experimental data, model fit and the theoretical predictions of different parameterizations which are depicted in figure 2.3 to figure 2.7. Here the calculated values of F_L^g structure function increase with the decreasing x values. In case of the x-evolution results described in figure 2.3 to figure 2.7, the behaviour of LO, NLO curves are slightly different as we have considered the input point from different parameterizations. The behaviour of LO, NLO and NNLO curves in both the t- and x-evolutions of F_L^g structure function are different (i.e., sometimes NLO results overestimate LO prediction and vice versa) and this behaviour of the curves depend only on the expressions used for calculation of the structure function. Moreover, with reference to some recent papers [13, 35–37], we can say that the behaviour of the LO, NLO, NNLO curves depend only on the applied method. In all the figures, in spite of large uncertainty of the experimental data, all the plots show good agreement with the model fit and theoretical predictions of the parameterizations. It is observed from the x-evolution graphs that, our results show good agreement with the model fit and parameterizations and as the energy scale becomes larger, the agreement is better. In all our results for x-evolutions, we observe that the differences between LO and NLO results are extremely small and our NLO results are in better agreement with the data and fit. Moreover, in case of t-evolution the NLO and NNLO curves are almost overlapping with increasing values of Q^2 and our NNLO results are in better agreement

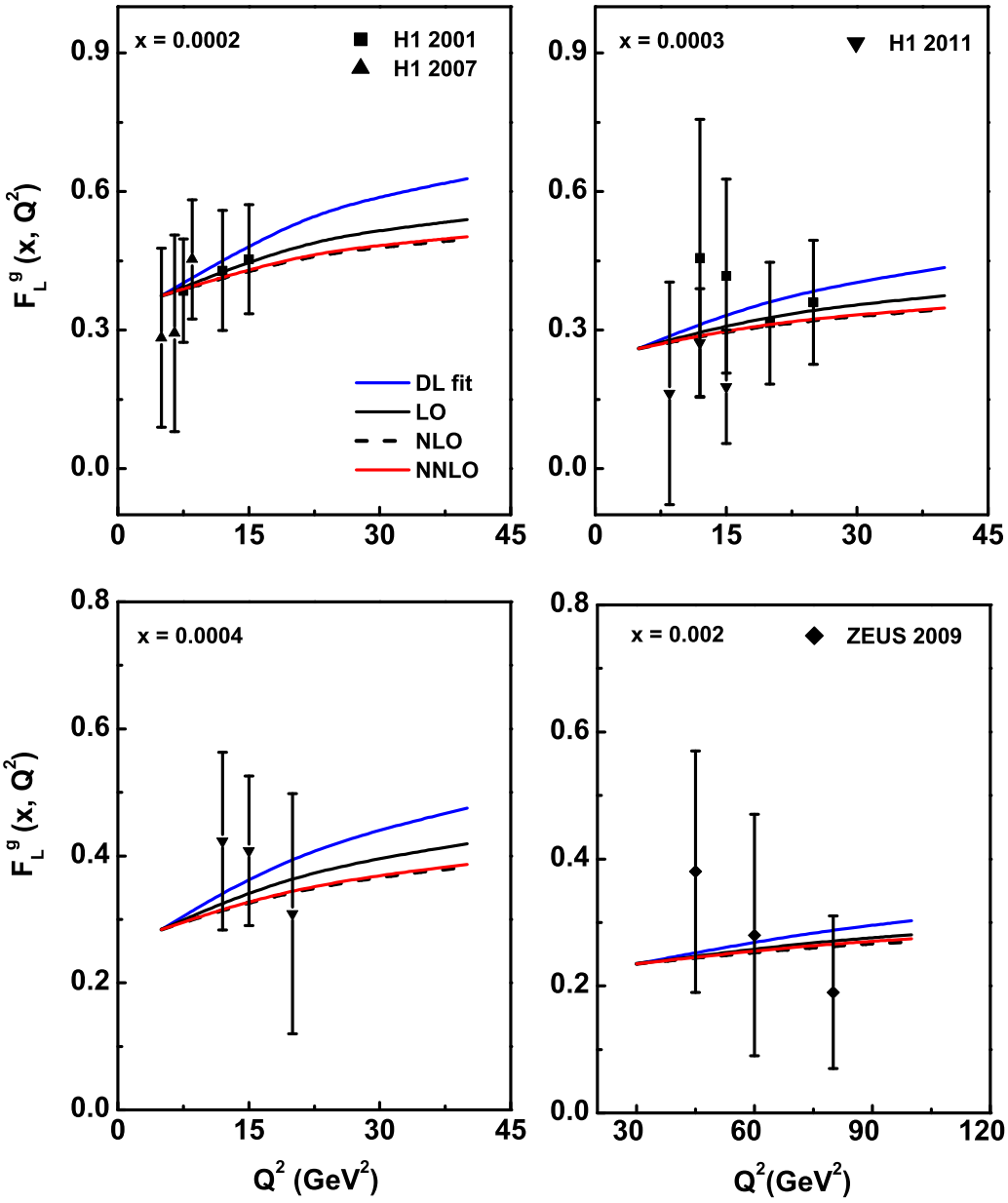

Figure 2.2: t-evolution results of F_L^g structure function up to NNLO using Taylor expansion method in comparison with the H1, ZEUS data and results of DL model.

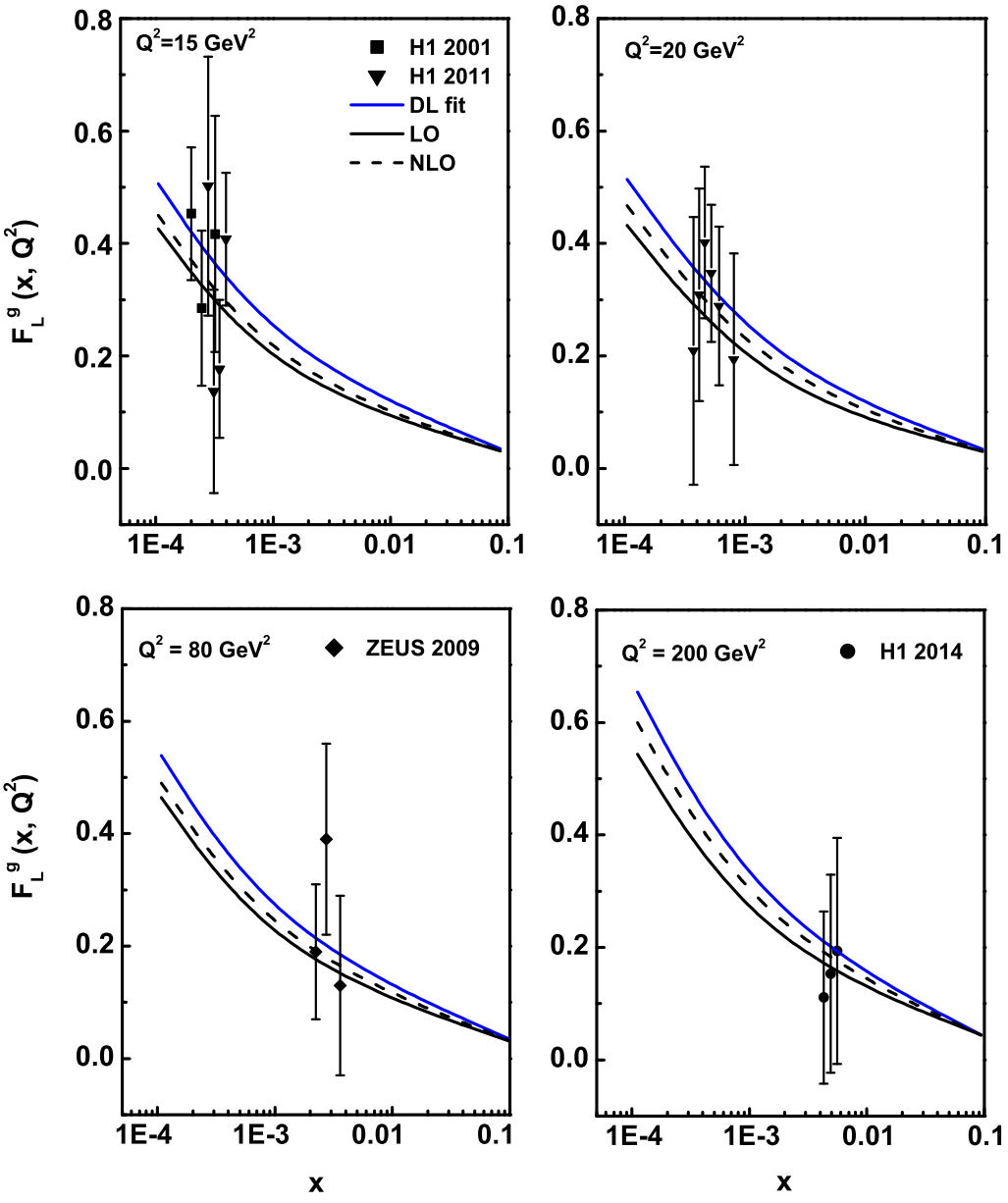

Figure 2.3: x-evolution results of F_L^g structure function up to NLO using Taylor expansion method in comparison with the H1, ZEUS data and results of DL model.

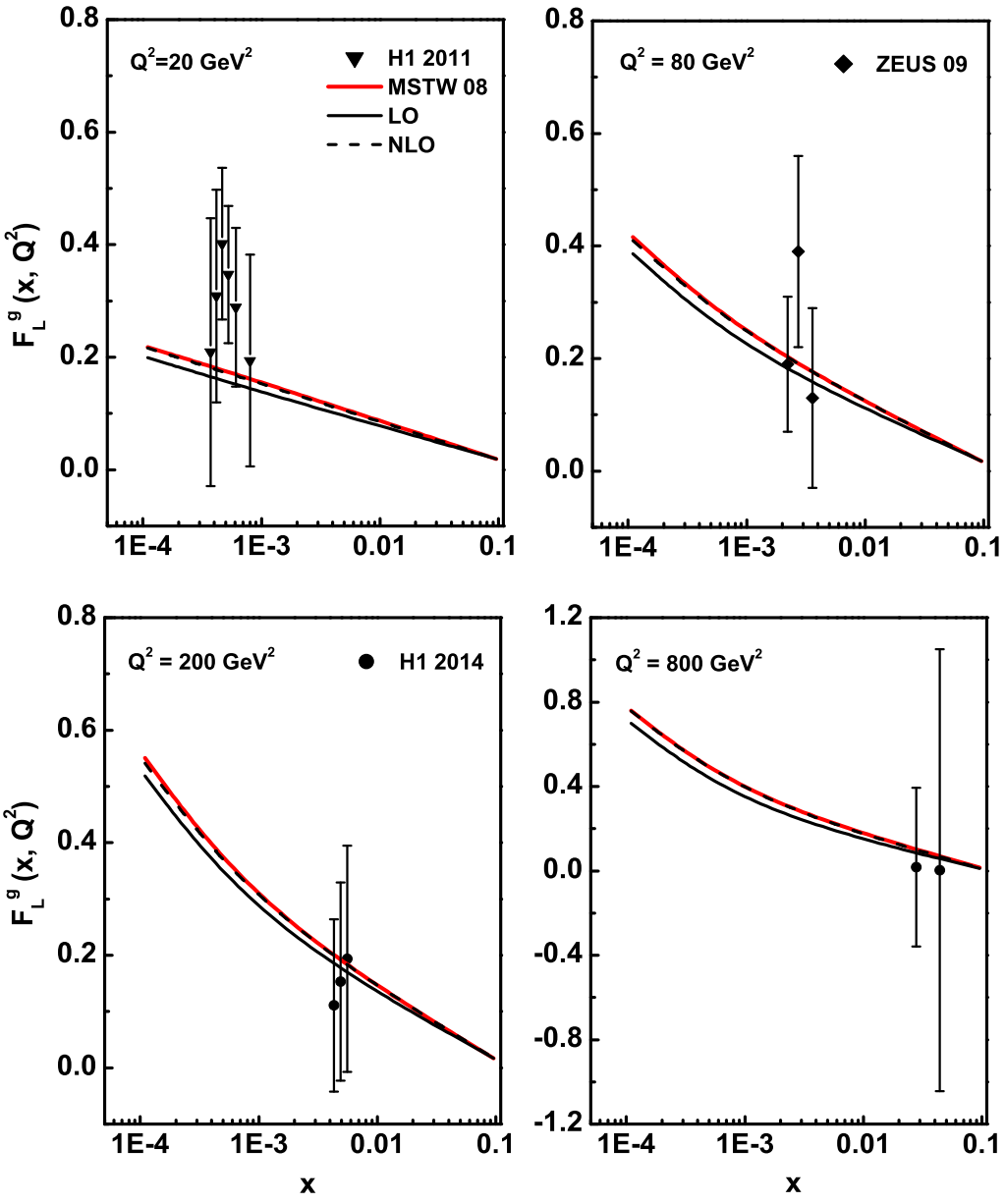

Figure 2.4: x-evolution results of F_L^g structure function up to NLO using Taylor expansion method in comparison with the H1, ZEUS data and the theoretical prediction of MSTW08.

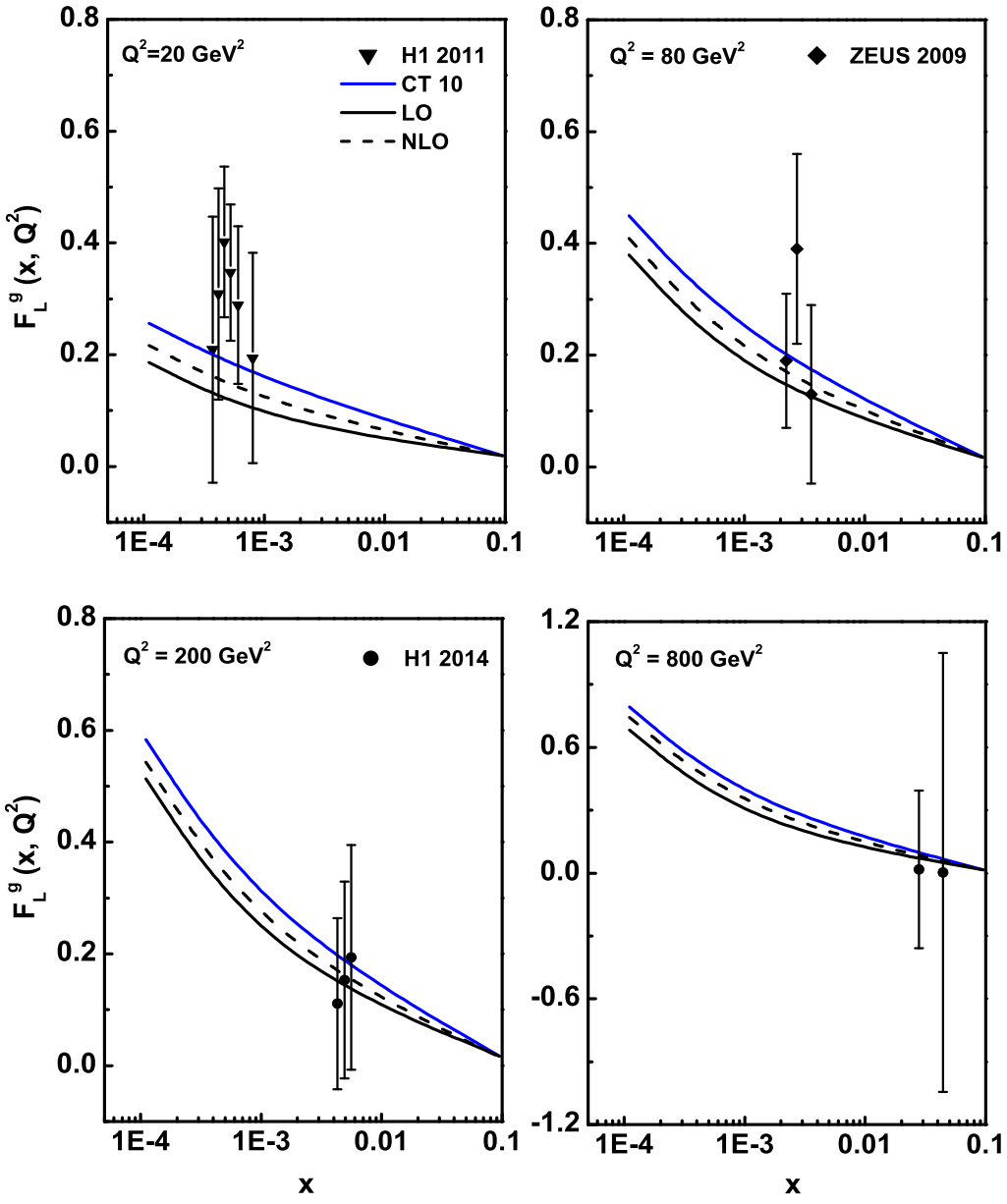

Figure 2.5: x-evolution results of F_L^g structure function up to NLO using Taylor expansion method in comparison with the H1, ZEUS data and the theoretical prediction of CT10.

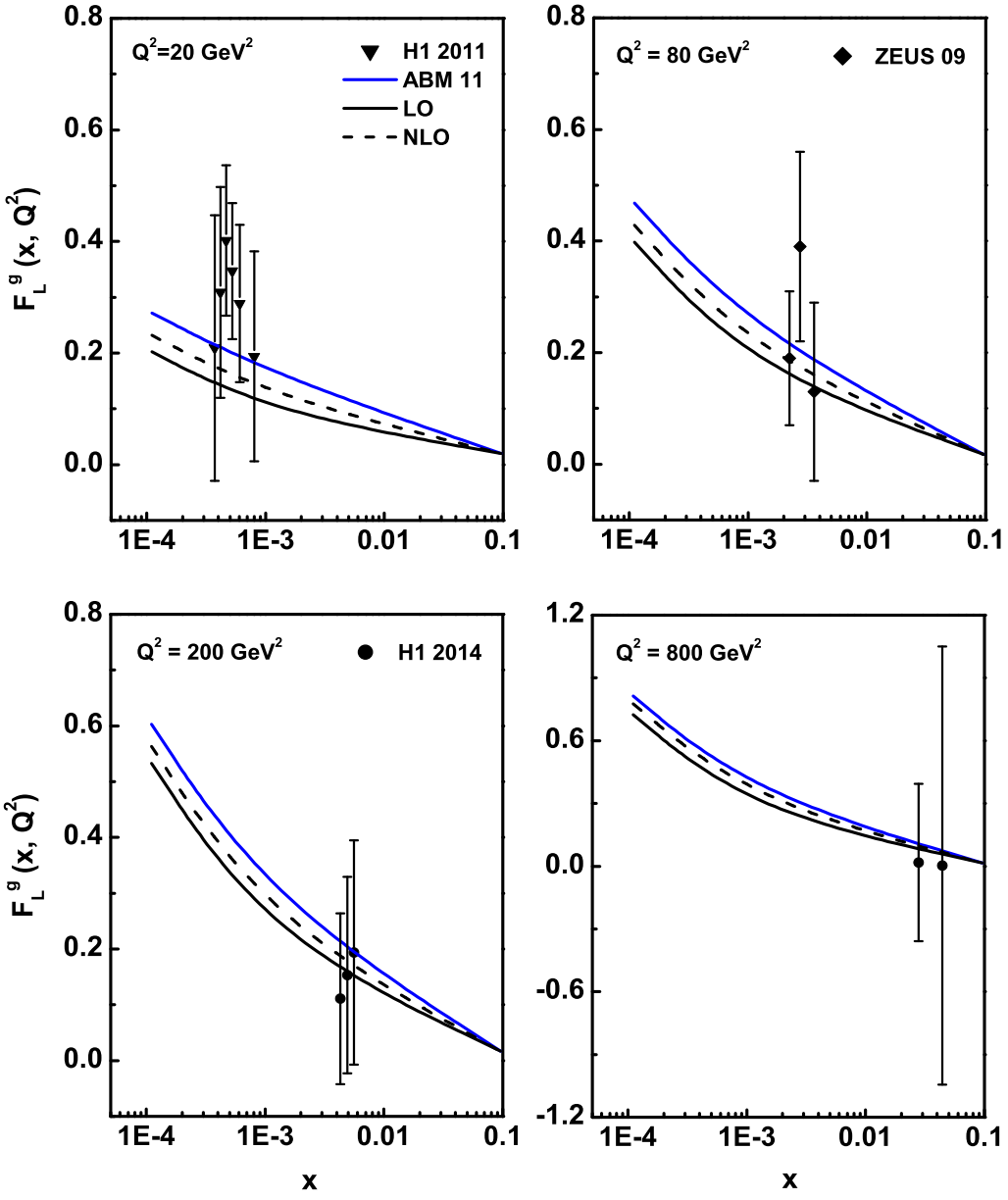

Figure 2.6: x-evolution results of F_L^g structure function up to NLO using Taylor expansion method in comparison with the H1, ZEUS data and the theoretical prediction of ABM11.

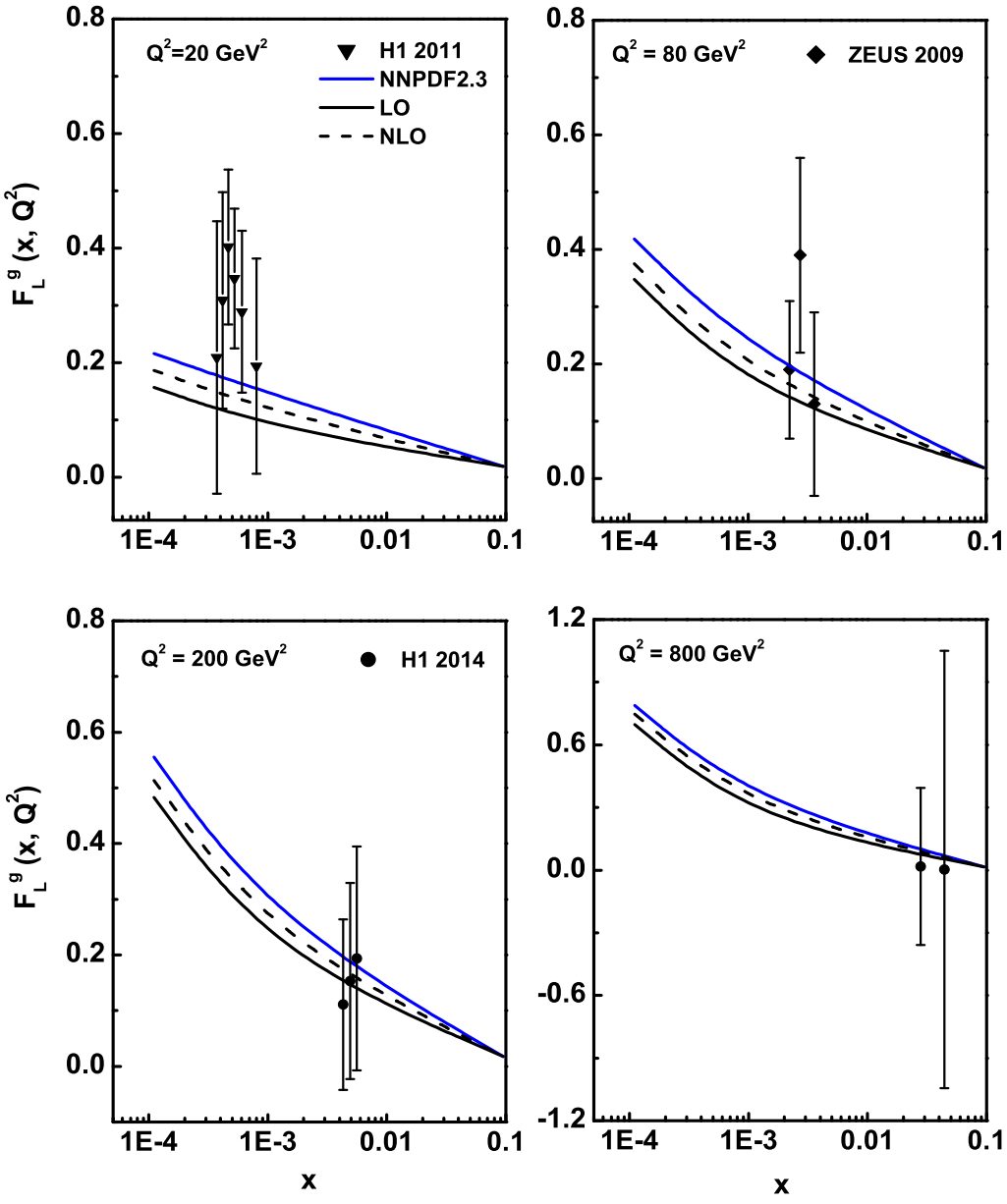

Figure 2.7: x-evolution results of F_L^g structure function up to NLO using Taylor expansion method in comparison with the H1, ZEUS data and the theoretical prediction of NNPDF2.3.

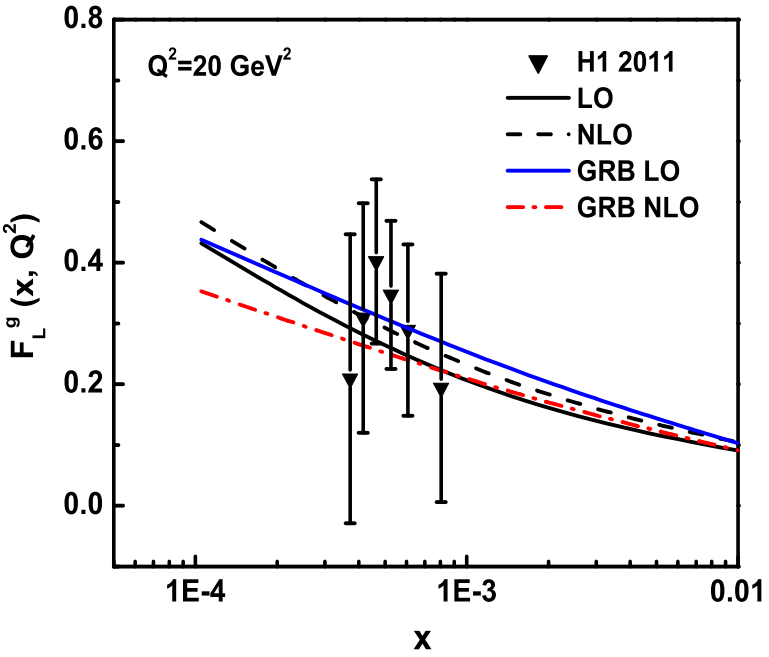

Figure 2.8: x-evolution results of F_L^g structure function up to NLO using Taylor expansion method in comparison with the H1 data and the theoretical prediction of Boroun et al. (GRB)

with data and related fits. In all the cases, the difference between different orders become less as the energy scale increases, which lies within the framework of pQCD i.e., running coupling constant becomes smaller as the energy value increases.

We have also presented a comparison of our results with the results reported in a recent paper by Boroun et al. where they have calculated the gluon dominating F_L structure function using Laguerre polynomials method [13]. Figure 2.8 shows the comparison of the results. Our results shows good agreement with the results of Boroun et al. In both the cases, the structure function increases towards small values of x as expected from QCD. Both the results does not show exactly the same behaviour as the methods for evaluating the structure function in both the cases are different, in our

case we have used 'Taylor expansion method' and they have used 'Laguerre polynomials method'.

2.3 Conclusions

In this chapter, we have obtained an analytical solution of evolution equation for gluon dominating longitudinal structure function F_L^g up to NNLO using the Taylor series expansion method. The solutions of the evolution equation provide the expressions for t- and x-evolution of F_L^g structure function. With the help of these expression, we have calculated the evolutions of F_L^g structure function by considering the input distributions from model fit and theoretical predictions of different parameterizations. Here, for the calculation of t- and x-evolution of F_L^g structure function we consider two numerical parameters T_0 and T_1. This method is simple one and less time consuming on the numerical calculations with less number of numerical parameters compared to the other methods where several parameters are included in the input function [38]. So, this method may be a viable alternative to other methods. To confirm the validity of our calculations, we have compared our results with recent experimental data. To show that in spite of the large error bars of the experimental data, our results are in good agreement with the data, we have compared our results with the results of model fit and parameterizations. The variation of F_L^g structure function with x and Q^2 shows similar nature with the H1, ZEUS experimental data as well as the results of DL model and theoretical predictions of MSTW08, CT10, ABM11 and NNPDF2.3. At small-x, our results show that the longitudinal structure function F_L^g increases with the increasing values of Q^2 and it also increases with the decreasing values os x as expected from QCD. As in our given range of x, the gluon contribution to the structure function is dominant one, so we can conclude in general that the gluon contribution to the longitudinal structure function increases with the values of Q^2 and it also increases

with the decreasing values of x.

References

[1] Aaron, F. D., et al. Measurement of the inclusive $e^{\pm}p$ scattering cross section at high inelasticity y and of the structure function F_L, *Eur. Phys. J. C.* **71** (3), 1579-1–50, 2011.

[2] Adloff, C., et al. Deep-inelastic inclusive *ep* scattering at low x and a determination of α_s, *Eur. Phys. J. C.* **21** (1), 33–61, 2001.

[3] Pardos, C. D. *Studies for the direct measurement of the proton structure function F_L with the H1 detector at HERA*, Ph.D. thesis, DESY, Zeuthen, Germany, 2007.

[4] Piec, S. *Measurement of the Proton Structure Function F_L with the H1 Detector at HERA*, Ph.D. thesis, Humboldt University of Berlin, Germany, 2009.

[5] Andreev, V., et al. Measurement of Inclusive *ep* Cross Sections at High Q^2 at $\sqrt{s} = 225$ and $252GeV$ and of the Longitudinal Proton Structure Function F_L at HERA, *Eur. Phys. J. C* **74** (4), 2814-1–26, 2014.

[6] Chekanov, S., et al. Measurement of the longitudinal proton structure function at HERA, *Phys. Lett. B* **682** (1), 8–22, 2009.

[7] Donnachie, A. and Landshoff, P. V. The protons gluon distribution, *Phys. Lett. B* **550** (3-4), 160–165, 2002.

[8] Martin, A. D., et al. Parton distributions for the LHC, *Eur. Phys. J. C* **63** (2), 189–285, 2009.

[9] Hung-Liang, Lai., et al. New parton distributions for collider physics, *Phys. Rev. D* **82** (7), 074024-1–24, 2010.

[10] Alekhin, S., Blemlein, J. and Moch, S. The ABM parton distributions tuned to LHC data, *Phys. Rev. D* **89** (5), 054028-1–21, 2014.

[11] Ball, R. D., et al. Parton distributions with LHC data, *Nucl. Phys. B* **867** (2), 244–289, 2013.

[12] Forte, S., et al. Heavy quarks in deep-inelastic scattering, *Nucl. Phys. B* **834** (1-2), 116–162, 2010.

[13] Rezaei, B. and Boroun, G. R. Analytical solution of the longitudinal structure function F_L in the leading and next-to-leading-order analysis at low x with respect to Laguerre polynomials method, *Nucl. Phys. A* **857** (1), 42–47, 2011.

[14] Cooper-Sarkar, A. M., et al. Measurement of the longitudinal structure function and the small x gluon density of the proton, *Z. Phys. C* **39** (2), 281–290, 1988.

[15] Moch, S. and Vogt, A. Threshold resummation of the structure function F_L, *J. High Energy Phys.* **2009** (04), 081-1–11, 2009.

[16] Kazakov, D. I., et al. Complete Quartic α_s^2 correction to the deep-inelastic longitudinal structure function F_L in QCD, *Phys. Rev. Lett.* **65** (13), 1535–1538, 1990.

[17] Guillen, J. S., et al. Next-to-leading order analysis of the deep inelastic $R = \sigma_L/\sigma_T$, *Nucl. Phys. B* **353** (2) 337–345, 1991.

[18] Moch, S., Vermaseren, J. A. M. and Vogt, A. The longitudinal structure function at the third order, *Phys. Lett. B* **606** (1-2), 123–129, 2005.

[19] Vermaseren, J. A. M., Vogt, A. and Moch, S. The third-order QCD corrections to deep-inelastic scattering by photon exchange, *Nucl. Phys. B* **724** (1-2), 3–182, 2005.

[20] Abbott, L. F., Atwood, W. B. and Barnett, R. M. Quantum-chromodynamic analysis of eN deep-inelastic scattering data, *Phys. Rev. D* **22** (3), 582–593, 1980.

[21] Furmanski, W. and Petronzio, R. Lepton-hadron processes beyond leading order in quantum chromodynamics, *Z. Phys. C* **11** (4), 293–314, 1982.

[22] Baishya, R., Jamil, U. and Sarma, J. K. Evolution of spin-dependent structure functions from DGLAP equations in leading order and next to leading order, *Phys. Rev. D* **79** (3), 034030-1–6, 2009.

[23] Baishya, R. and Sarma, J. K. Semi numerical solution of non-singlet Dokshitzer-GribovLipatovAltarelliParisi evolution equation up to next-to-next-to-leading order at small x, *Eur. Phys. J. C* **60** (4), 585–591, 2009.

[24] Sneddon, I. *Elements of Partial Differential Equations*, McGraw- Hill, New York, 1957.

[25] Sarma, J. K., Choudhury, D. K. and Medhi, G. K. x-distribution of deuteron structure function at low-x, *Phys. Lett. B* **403** (1-2), 139–144, 1997.

[26] Sarma, J. K. and Das, B. t evolutions of structure functions at low-x, *Phys. Lett. B* **304** (3-4), 323–328, 1993.

[27] Martin, A. D., et al. MRST2001: partons and α_S from precise deep inelastic scattering and Tevatron jet data, *Eur. Phys. J. C* **23** (1), 73–87, 2002.

[28] Martin, A. D., et al. Physical gluons and high-E_T jets, *Phys. Lett. B* **604** (1-2), 61–68, 2004.

[29] Martin, A. D., et al. Update of parton distributions at NNLO, *Phys. Lett. B* **652** (5-6), 292–299, 2007.

[30] Nadolsky, P. M., et al. Implications of CTEQ global analysis for collider observables, *Phys. Rev. D* **78** (1), 013004-1–21, 2008.

[31] Pumplin, J., et al. Collider inclusive jet data and the gluon distribution, *Phys. Rev. D* **80** (1), 014019-1–16, 2009.

[32] Aaron, F. D., et al. Combined measurement and QCD analysis of the inclusive $e\pm p$ scattering cross sections at HERA, *J. High Energy Phys.* **2010** (1), 109-1–63, 2010.

[33] Glazov, S. Measurement of DIS Cross Section at HERA, *Braz. J. Phys.* **37** (2C), 793–797, 2007.

[34] Kwiecinski, J., et al. Parton distributions at small x, *Phys. Rev. D* **42** (11), 3645–3659, 1990.

[35] Nematollahi, H., Yazdanpanah, M. M. and Mirjalili, A. NNLO longitudinal proton structure function, based on the modified χQM, *Mod. Phys. Lett. A* **27** (31),1250179-1-11 ,2012.

[36] Boroun, G. R. and Rezaei, B. Analysis of the proton longitudinal structure function from the gluon distribution function, *Eur. Phys. J. C* **72** (11), 2221-1-5, 2012.

[37] Devee, M., Baishya, R. and Sarma, J. K. Evolution of singlet structure functions from DGLAP equation at next-to-next-to-leading order at small-x, *Eur. Phys. J. C* **72** (6), 2036-1-11, 2012.

[38] Gluck, M., Reya, E. and Vogt, A. Dynamical Parton Distributions of the Proton and Small-x Physics, *Z. Phys. C* **67** (3), 433–447, 1995. □

Chapter 3

Evolution of F_L Structure Function at Small-x Using Regge Like Behaviour of Structure Function

In this chapter, the evolutions of longitudinal structure function F_L from its QCD evolution equation in next-to-leading order (NLO) at small-x is presented using the Regge like behaviour of the structure function. The proposed simple analytical expression for F_L structure function provides the t- and x-evolution equations to study the behaviour of F_L structure function at small-x. The calculated results are compared with the data of H1 [1–5], ZEUS [6] collaborations, results of Donnachie-Landshoff (DL) [7] model and theoretical predictions of MSTW08 [8], CT10 [9], ABM11 [10], NNPDF2.3 [11, 12] parameterizations. The comparison of our results with that of the results obtained by Boroun [13] is also studied here. We have also presented a comparative study of our predicted results with the results obtained in the previous chapter using Taylor expansion method. Our calculated results can be described within the framework of pQCD.

3.1 Theory

At small values of x ($x \leq 10^{-3}$), the QCD evolution equation for gluon dominating F_L^g structure function is given by [14]

$$\frac{\partial F_L^g(x,Q^2)}{\partial ln Q^2} = K_G(x,Q^2) \otimes F_L^g(x,Q^2). \tag{3.1}$$

Here $K_G(x,Q^2)$ is the gluon kernel known perturbatively up to the first few orders in $\alpha_s(Q^2)$. The symbol $\otimes$ represents the standard Mellin convolution. The kernel $K_G(x,Q^2)$ can be written as

$$K_G(x,Q^2) = \frac{\alpha_s(Q^2)}{4\pi}K_G^0(x) + \Big(\frac{\alpha_s(Q^2)}{4\pi}\Big)^2 K_G^1(x) \tag{3.2}$$

up to NLO, where $K_G^0(x)$ and $K_G^1(x)$ are the gluon splitting kernels in LO and NLO respectively. $K_G^0(x)$, $K_G^1(x)$ are given in ref. [15, 16] and their expressions are defined in Appendix A. Using all these and simplifying the QCD evolution equations for the F_L^g structure function in LO and NLO, we get

$$\frac{\partial F_L^g(x,t)}{\partial t} - \frac{\alpha_s(t)}{4\pi}\left[\frac{80}{9}\int_x^1 dw w^2(1-w)F_L^g\Big(\frac{x}{w},t\Big)\right] = 0 \tag{3.3}$$

and

$$\frac{\partial F_L^g(x,t)}{\partial t} - \frac{\alpha_s(t)}{4\pi}\left[\frac{80}{9}\int_x^1 dw w^2(1-w)F_L^g\Big(\frac{x}{w},t\Big)\right] - \Big(\frac{\alpha_s(t)}{4\pi}\Big)^2 I_1^G(x,t) = 0, \tag{3.4}$$

where

$$I_1^G(x,t) = \frac{160}{9}\int_x^1 dw f(w)F_L^g\Big(\frac{x}{w},t\Big). \tag{3.5}$$

Here $t = ln\frac{Q^2}{\Lambda^2}$, Λ is the QCD cut-off parameter and the function $f(w)$ is defined in Appendix A.

The strong coupling constant in higher order has the form [17]

$$\alpha_s(t) = \frac{4\pi}{\beta_0 t}\Big[1 - \frac{\beta_1}{\beta_0^2}\frac{lnt}{t} + O\Big(\frac{1}{t^2}\Big)\Big], \tag{3.6}$$

where β_0 and β_1 are the one loop and two loop corrections to the QCD β-function which are defined in chapter 2 (equations (2.10) and (2.11)).

Regge approach provides a very good description of the HERA data on the small-x behaviour of the structure function $F_2(x,Q^2)$ [18]. It explains the strong rise of the

structure function F_2 towards small values of x. This phenomenon is usually described with the help of the power like behaviour of the structure function at small-x as

$$F_2(x, Q^2) \propto x^{-\lambda},$$

where $\lambda > 0$. Here, the power λ is related with the intercept of the Reggeon contribution dominating at $x \to 0$, namely with the pomeron intercept, $\lambda = \alpha_p(0) - 1$. The small-$x$ behaviour of the structure function is mainly driven by the gluons in the proton and this gluon density is determined from the data on the slope $dF_2/dlnQ^2$ [19]. Thus, gluon density $G(x, Q^2)$ can be written as

$$G(x, Q^2) \sim \frac{dF_2}{dlnQ^2} \sim f(Q^2)x^{-\lambda_g},$$

where $f(Q^2)$ is a function of Q^2 and λ_g is the pomeron intercept minus one. The steep behaviour of the gluon distribution function generates a similar power like behaviour of F_2 structure function which can be expressed as $G(x, Q^2) \propto x^{-\lambda_g}$ [19]. The power of λ_g is found to be either $\lambda_g \simeq 0$ and $\lambda_g \simeq 0.5$ where the first one corresponds to soft pomeron and the second one to the hard (Lipatov) pomeron intercept [20]. As the longitudinal structure function is directly sensitive [21] to the gluon distribution function at small-x, we can use the same type of Regge behaviour to study the previous case.

Now, the Regge like behaviour of the longitudinal structure function can be expressed as

$$F_L^g(x, t) = f(t)x^{-\lambda_g}, \tag{3.7}$$

where $f(t)$ is a function of t, and λ_g is the pomeron intercept minus one. Now, $F_L^g\Big(\frac{x}{w}, t\Big)$ can be written as

$$F_L^g\Big(\frac{x}{w}, t\Big) = F_L^g(x, t)w^{\lambda_g}. \tag{3.8}$$

Using equations (3.7), (3.8) and leading order term of equation (3.6) in equation (3.3)

we get

$$\frac{\partial F_L^g(x,t)}{\partial t} = \frac{F_L^g(x,t)}{t} P(x) \tag{3.9}$$

with

$$P(x) = \frac{80}{9\beta_0} \int_x^1 dw(1-w)w^{2+\lambda_g}.$$

Integrating equation (3.9) we get

$$F_L^g(x,t) = Ct^{P(x)}, \tag{3.10}$$

where C is a constant of integration.

Applying initial conditions at $t = t_0$, $F_L(x,t) = F_L(x,t_0)$ and at $x = x_0$, $F_L(x,t) = F_L(x_0,t)$, the t and x-evolutions for F_L^g structure function in LO can be written as

$$F_L^g(x,t) = F_L^g(x,t_0)\Big(\frac{t}{t_0}\Big)^{P(x)} \tag{3.11}$$

and

$$F_L^g(x,t) = F_L^g(x_0,t)t^{[P(x)-P(x_0)]} \tag{3.12}$$

respectively. Here $F_L^g(x,t_0)$ and $F_L^g(x_0,t)$ are defined in chapter 2.

Proceeding in the similar manner from equation (3.4), we obtain the t- and x-evolutions for F_L^g structure function in NLO as

$$F_L^g(x,t) = F_L^g(x,t_0)\frac{t^{(1+\frac{b}{t})P_1(x)}}{t_0^{(1+\frac{b}{t_0})P_1(x)}} exp\Big[b\Big(\frac{1}{t}-\frac{1}{t_0}\Big)P_1(x)\Big] \tag{3.13}$$

and

$$F_L^g(x,t) = F_L^g(x_0,t)t^{(1+\frac{b}{t})[P_1(x)-P_1(x_0)]} exp\Big[\frac{b}{t}(P_1(x)-P_1(x_0))\Big] \tag{3.14}$$

respectively, where

$$P_1(x) = \frac{1}{\beta_0}[P(x) + T_0Q(x)] \qquad \text{and} \qquad Q(x) = \frac{160}{9}\int_x^1 dw w^{\lambda_g} f(w).$$

The numerical parameter T_0 is calculated for the particular range of Q^2 under study as described in ref. [22]. Here we have considered the values of $T_0 = 0.0278$ within the range $1.5 \leq Q^2 \leq 800GeV^2$ as described in chapter 2.

Thus we have obtained the analytical expressions for the t- and x-evolutions of longitudinal structure function F_L^g as the solution of its evolution equation. Equations (3.11), (3.13) and (3.12), (3.14) finally give us the t-evolutions and x-evolutions of F_L^g structure function in LO and NLO respectively.

3.2 Results and Discussions

In this chapter, we have calculated the t- and x-evolutions of the gluon dominating longitudinal structure function F_L^g at small-x in leading and next-to-leading orders using the Regge like behaviour of the structure function. The obtained results are compared with the available H1 [1–5] and ZEUS experimental data [6], results of the Donnachie-Landshoff (DL) model [7] and the theoretical predictions from MSTW08 [8], CT10 [9], ABM11 [10], NNPDF2.3 [11, 12] parameterizations at several x and Q^2 values. The kinematical ranges for H1 2001, H1 2007, H1 2011, H1 2014 and ZEUS 2009 data, are $1.5 \leq Q^2 \leq 150GeV^2$ and $3 \times 10^{-5} \leq x \leq 0.2$, $2.5 \leq Q^2 \leq 25GeV^2$ and $5 \times 10^{-5} \leq x \leq 0.12$, $1.5 \leq Q^2 \leq 120GeV^2$ and $2.9 \times 10^{-5} \leq x \leq 0.01$, $35 \leq Q^2 \leq 800GeV^2$ and $6.5 \times 10^{-4} \leq x \leq 0.65$ and $20 < Q^2 < 130GeV^2$ and $5 \times 10^{-4} < x < 0.07$ respectively.

The t- and x-evolution results of F_L^g structure function are depicted in figure 3.1 to figure 3.6, where we have compared our results with related experimental data and fit. Here, the longitudinal structure function, measured in the range $5 \leq Q^2 \leq 800GeV^2$ and $10^{-4} \leq x \leq 10^{-1}$, have been used for our analysis. The value of y used is ≥ 0.5, as from this value onwards the contribution of F_L^g structure function is significant towards the total cross section [23]. Here the value of gluon distribution function exponent λ_g is taken as 0.5 as in the region of small-x this value describes the HERA data well [24, 25]. In figure 3.1, $F_L^g(x, Q^2)$ structure function results are plotted against

Q^2 for different values of x in comparison with the H1, ZEUS data and results of DL model. In figures 3.2 to 3.6, $F_L^g(x, Q^2)$ structure function is plotted against x for different values of Q^2 in comparison with the H1, ZEUS data, the results of DL model and the theoretical predictions of F_L using standard gluon distribution function by MSTW08, CT10, ABM11 and NNPDF2.3 parameterizations. Here the vertical error bars are both statistical and systematic errors for both H1 and ZEUS data. To show that in spite of large uncertainty of the experimental data, our results lie within the framework of pQCD we have compared our results with the model fit and parameterizations. In case of the x-evolution results described in figure 3.2 to figure 3.6, the behaviour of LO, NLO curves are not exactly the same as we have considered the input point from different parameterizations. The behaviour of LO and NLO curves in both the t- and x-evolutions of F_L^g structure function are different (i.e., sometimes NLO results overestimate LO prediction and vice versa) and this behaviour of the curves depend only on the the expressions used for calculation of the structure function. Moreover, with reference to some recent papers [26–29], we can say that the behaviour of the LO, NLO curves depend only on the applied method.

It is observed from the t-evolution graphs in figure 3.1 that, our result shows almost similar behaviour with that of H1 and ZEUS data. To indicate that in spite of large uncertainty in experimental data we have compared our results with the results of DL model which also shows good agreement with results of model. Here the Q^2-dependence behaviour of structure function shows slight increasing behaviour with respect to Q^2. This is due to the presence of evolution kernel in the final expression for t-evolution of F_L^g structure function. In case of the plot $x = 0.0004$, we have used the input point from DL model to study the evolution of F_L structure function. As the input point is near the end of the error bar of F_L data and our evolution of structure function shows slightly increasing behaviour, so in this case our calculated results at some point are outside the error bars. Among all the plots, the plot at $x = 0.002$ shows better

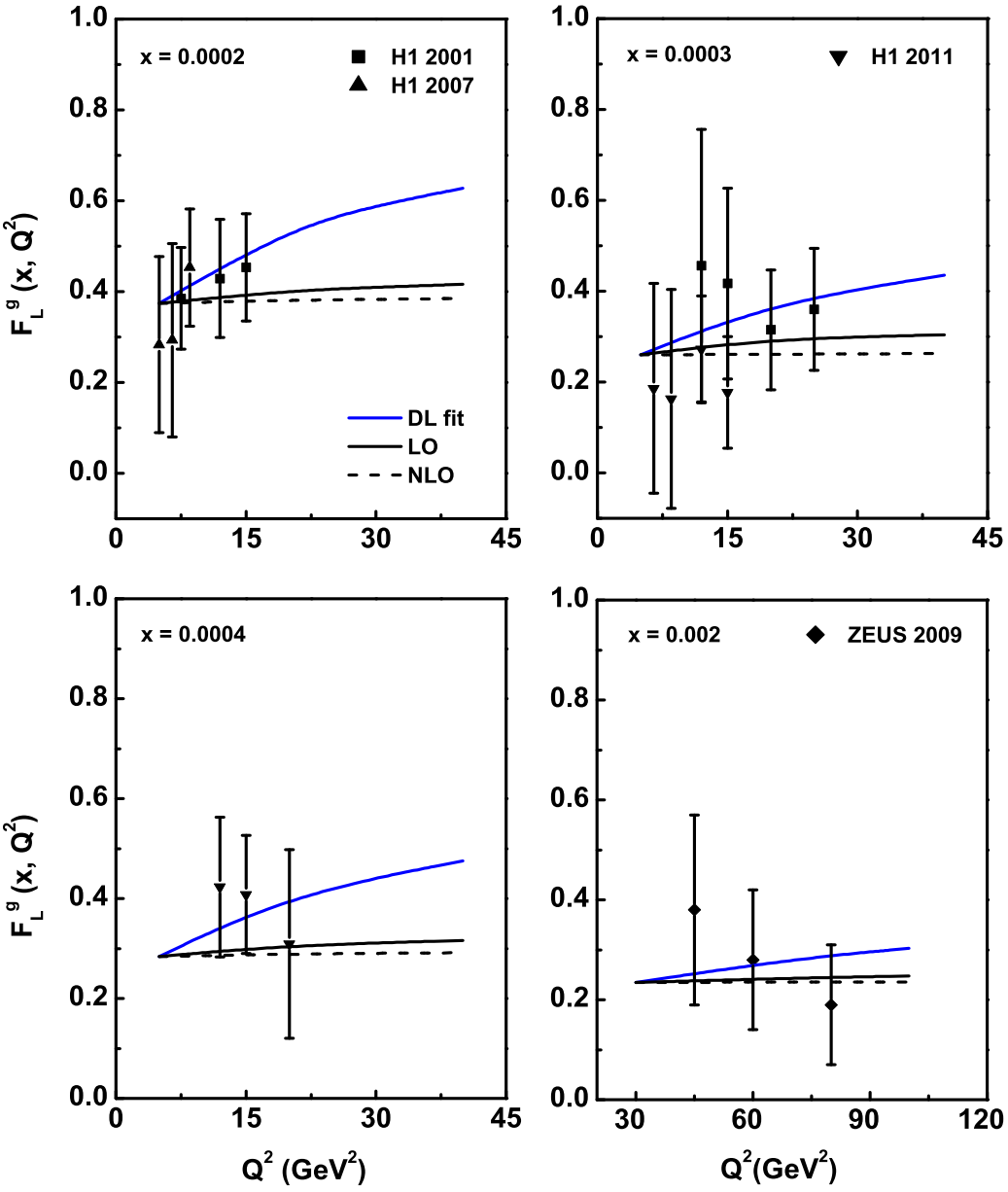

Figure 3.1: t-evolution results of F_L^g structure function up to NLO using Regge theory in comparison with the H1, ZEUS data and results of DL model.

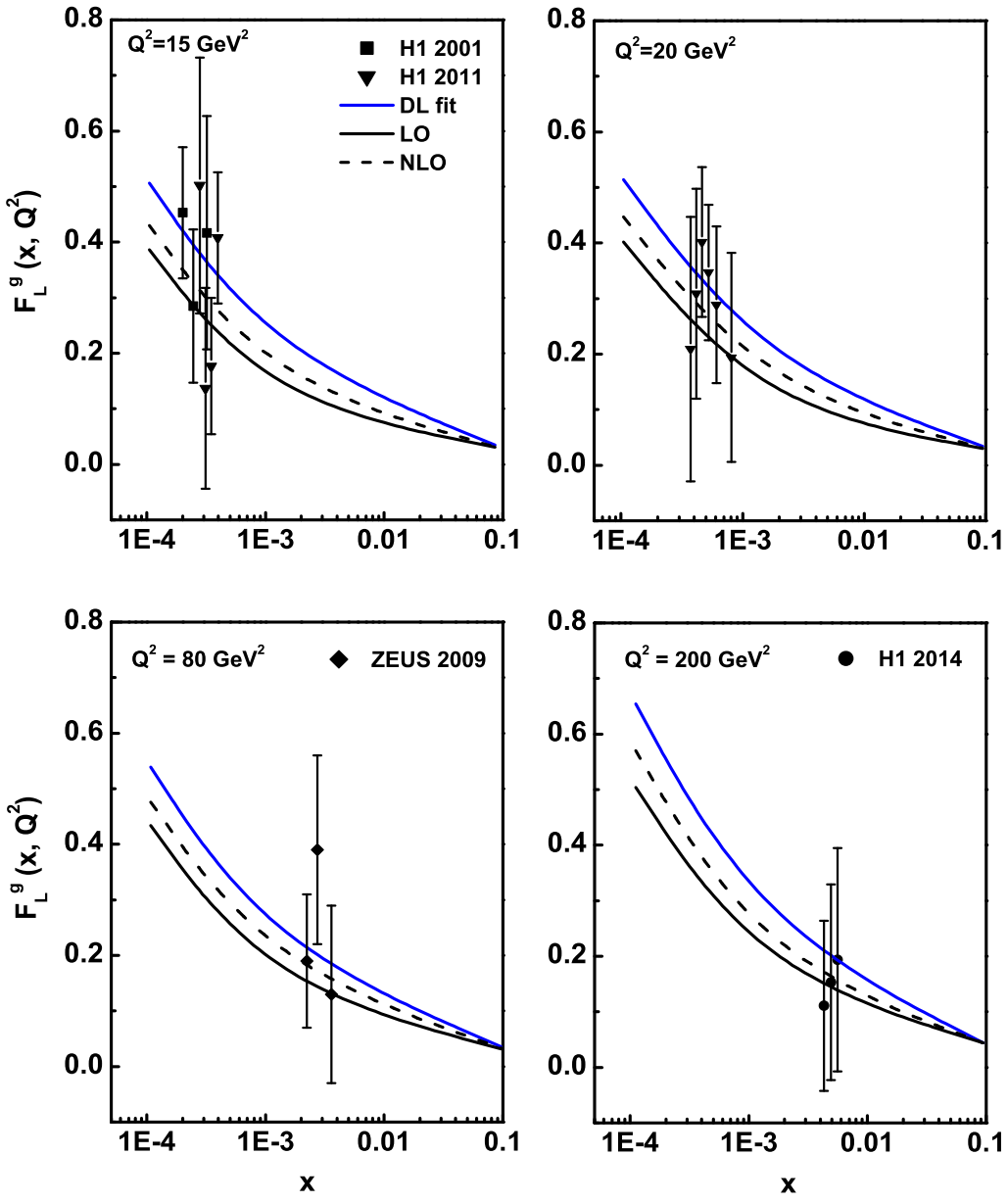

Figure 3.2: x-evolution results of F_L^g structure function up to NLO using Regge theory in comparison with the H1, ZEUS data and results of DL model.

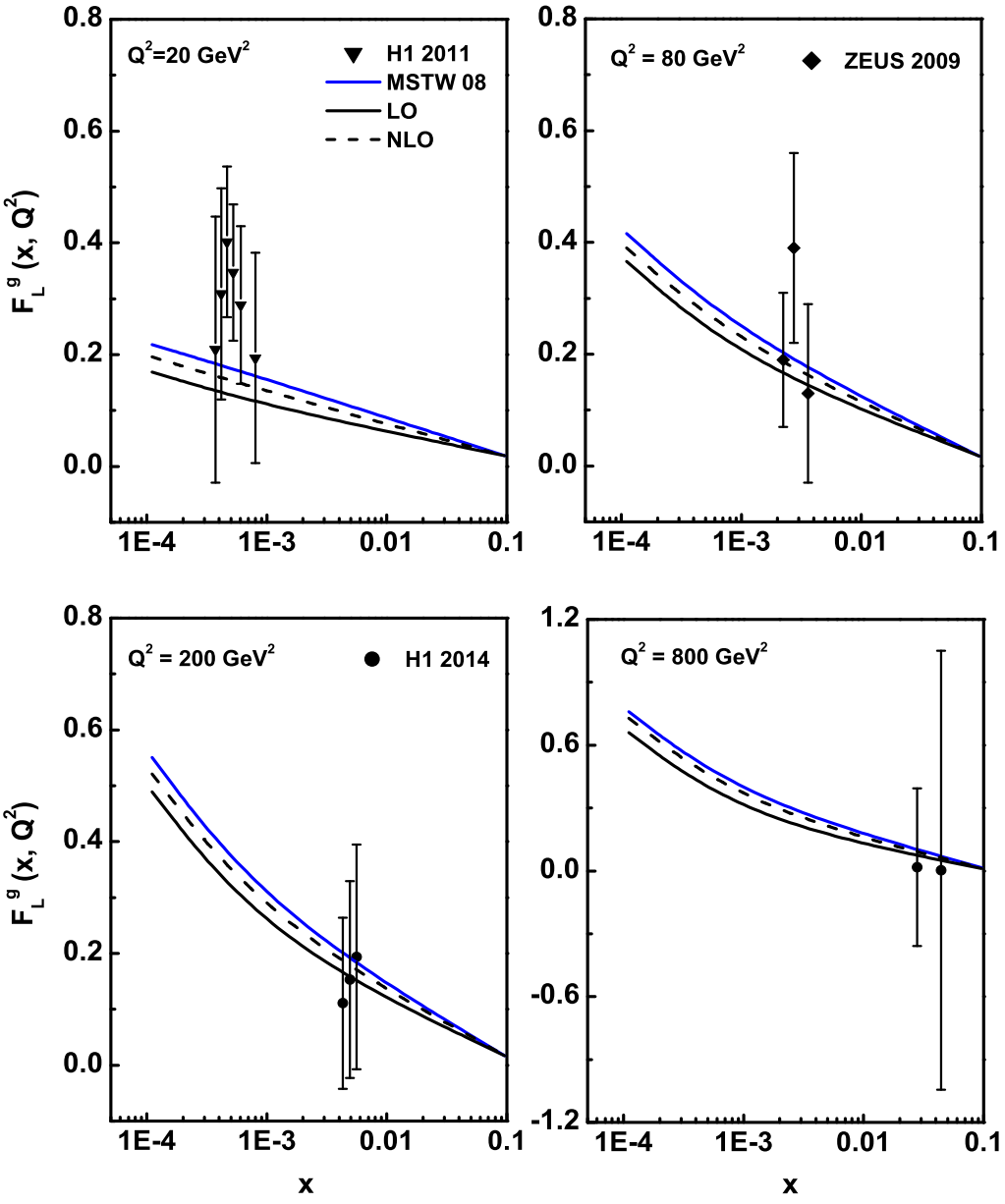

Figure 3.3: x-evolution results of F_L^g structure function up to NLO using Regge theory in comparison with the H1, ZEUS data and the theoretical prediction of MSTW08.

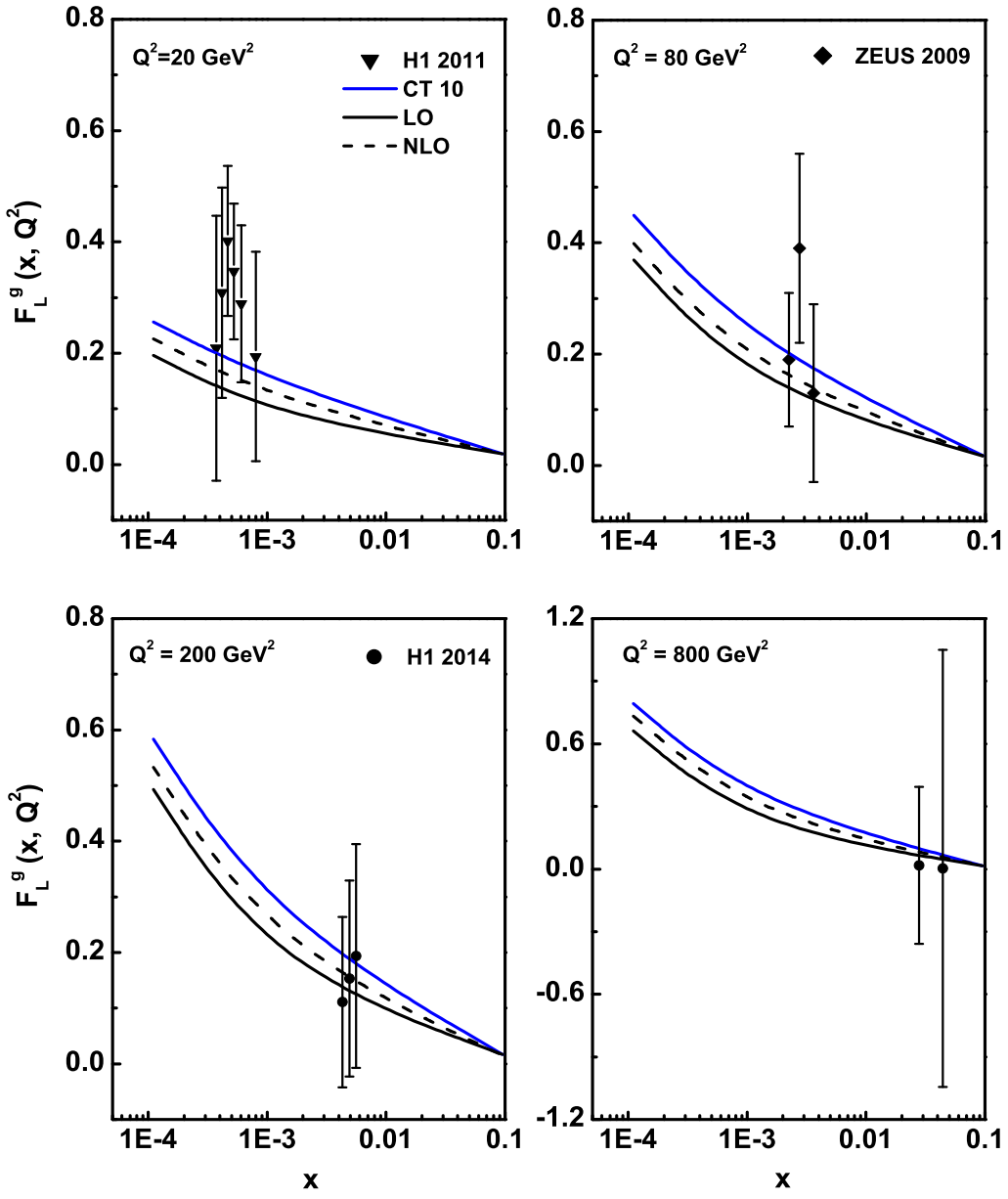

Figure 3.4: x-evolution results of F_L^g structure function up to NLO using Regge theory in comparison with the H1, ZEUS data and the theoretical prediction of CT10.

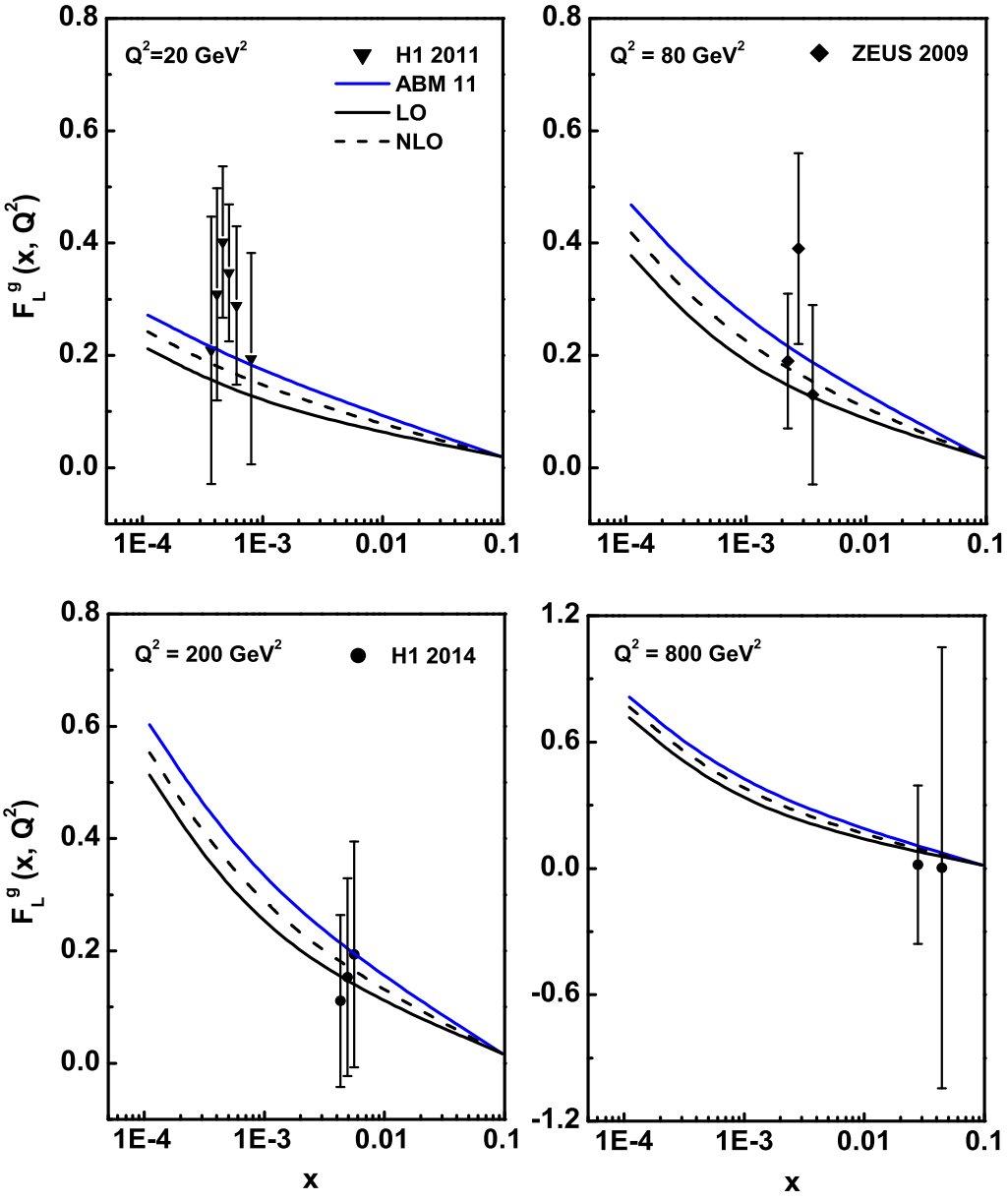

Figure 3.5: x-evolution results of F_L^g structure function up to NLO using Regge theory in comparison with the H1, ZEUS data and the theoretical prediction of ABM11.

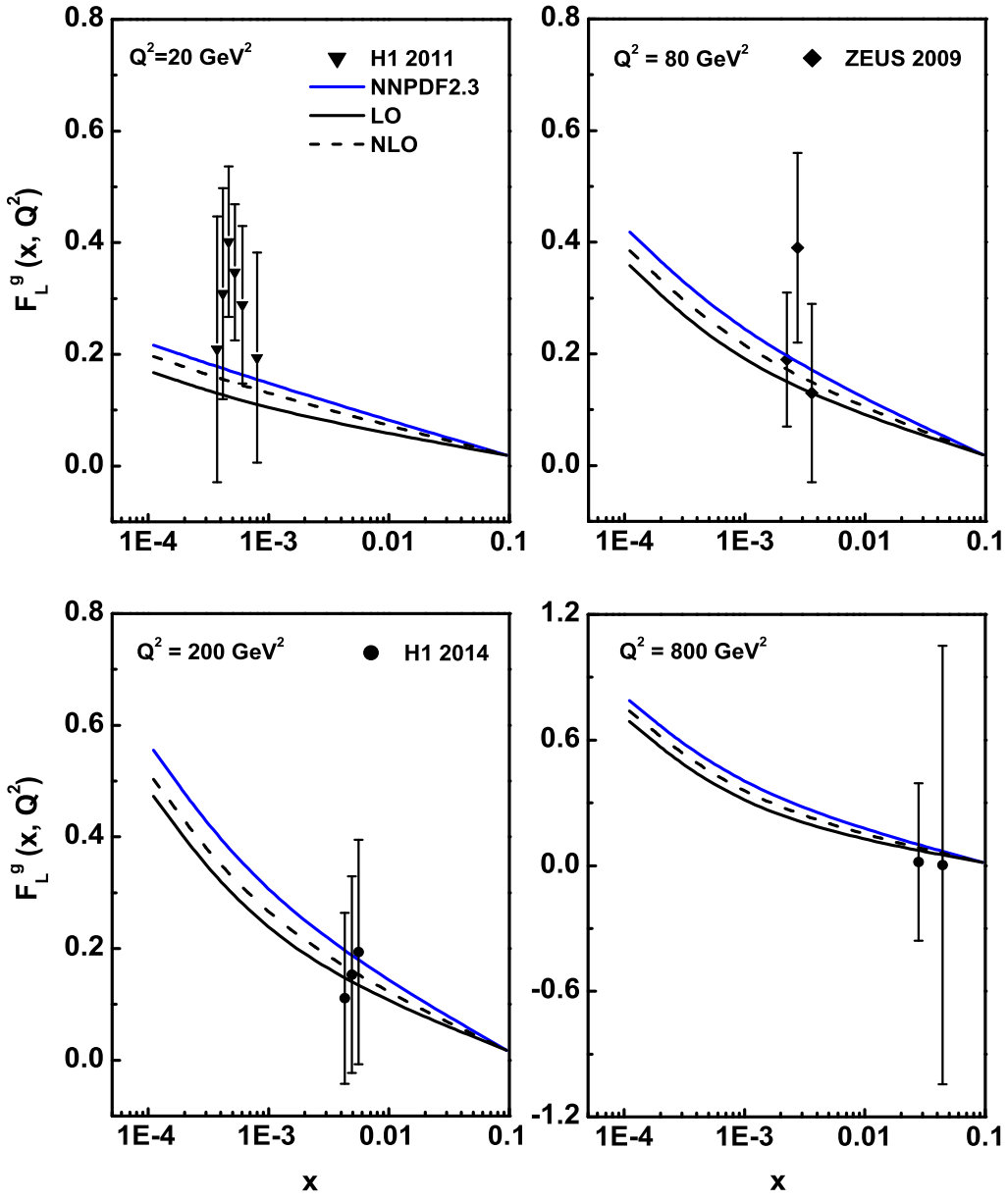

Figure 3.6: x-evolution results of F_L^g structure function up to NLO using Regge theory in comparison with the H1, ZEUS data and the theoretical prediction of NNPDF2.3.

agreement with the model fit i.e., the Q^2 dependence of structure function obtained by our approach shows better agreement with the results of model fit for this x value. In all the cases, our calculated F_L structure function in LO and NLO increase with the values of Q^2 in the given range like the results of DL models. This is an expected result from QCD also. At small-x, F_L increases with Q^2 as we resolve increasing numbers of soft partons with increasing Q^2 [30]. From the x-evolution graphs, it is observed that our result shows good agreement with those of H1, ZEUS data and those predicted by model and parameterizations. Also it is observed that compatibility with data becomes better with increasing values of Q^2.

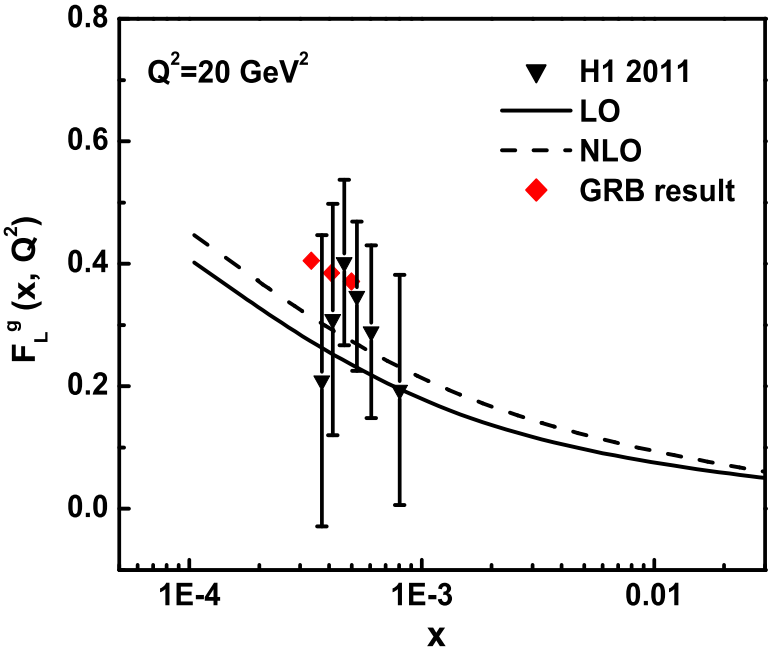

Figure 3.7: x-evolution results of F_L^g structure function up to NLO using Regge theory in comparison with the H1 data and the theoretical prediction of Boroun (GRB) [13].

We have also compared our x-evolution results with the results obtained by Boroun

[13] which is shown in figure 3.7. Here they have reported an analytical expression to determine the F_L structure function in NLO at small-x. In their approach Regge like behaviour of gluon distribution function is used which reflects good agreement of their results with recent data and fit. As depicted in figure 3.7 our result shows similar behaviour with the results in ref. [13]. In both the cases, the structure function increases towards small values of x as expected from QCD. Both the results does not show exactly the same behaviour as the methods for calculation of the structure function in both the cases are different.

3.2.1 Comparative study of our results predicted by Regge theory and Taylor expansion method

Here we have presented a comparative analysis of our results predicted by Regge theory (RT) approach and results of chapter 2 i.e., obtained by Taylor expansion (TE) method. Figures 3.8 to 3.13 show the comparison of the evolutions of F_L^g structure functions obtained by the two methods already discussed above.

The comparison of our results of the t-evolution of F_L^g structure function at small-x is presented in figure 3.8 which reflects similar nature with the results of DL model in spite of the large uncertainties of the data. The results predicted by Taylor expansion method shows better agreement with the results of the model than those obtained by the Regge theory approach. This implies that the compatibility of the t-evolution results with the model fit and data depends on the expression of evolution kernel of F_L. Due to the presence of evolution kernel in the final expression for t-evolution of F_L^g structure function in equations (3.11) and (3.13) in Reege theory approach, the growth of structure function is not sharp as that obtained by the Taylor expansion method where the final expressions for determination of t-evolution of structure function, equations (2.21) and (2.23) are independent of evolution kernel.

Figures 3.9 to 3.13 describe the comparison of the behaviour of F_L^g structure function

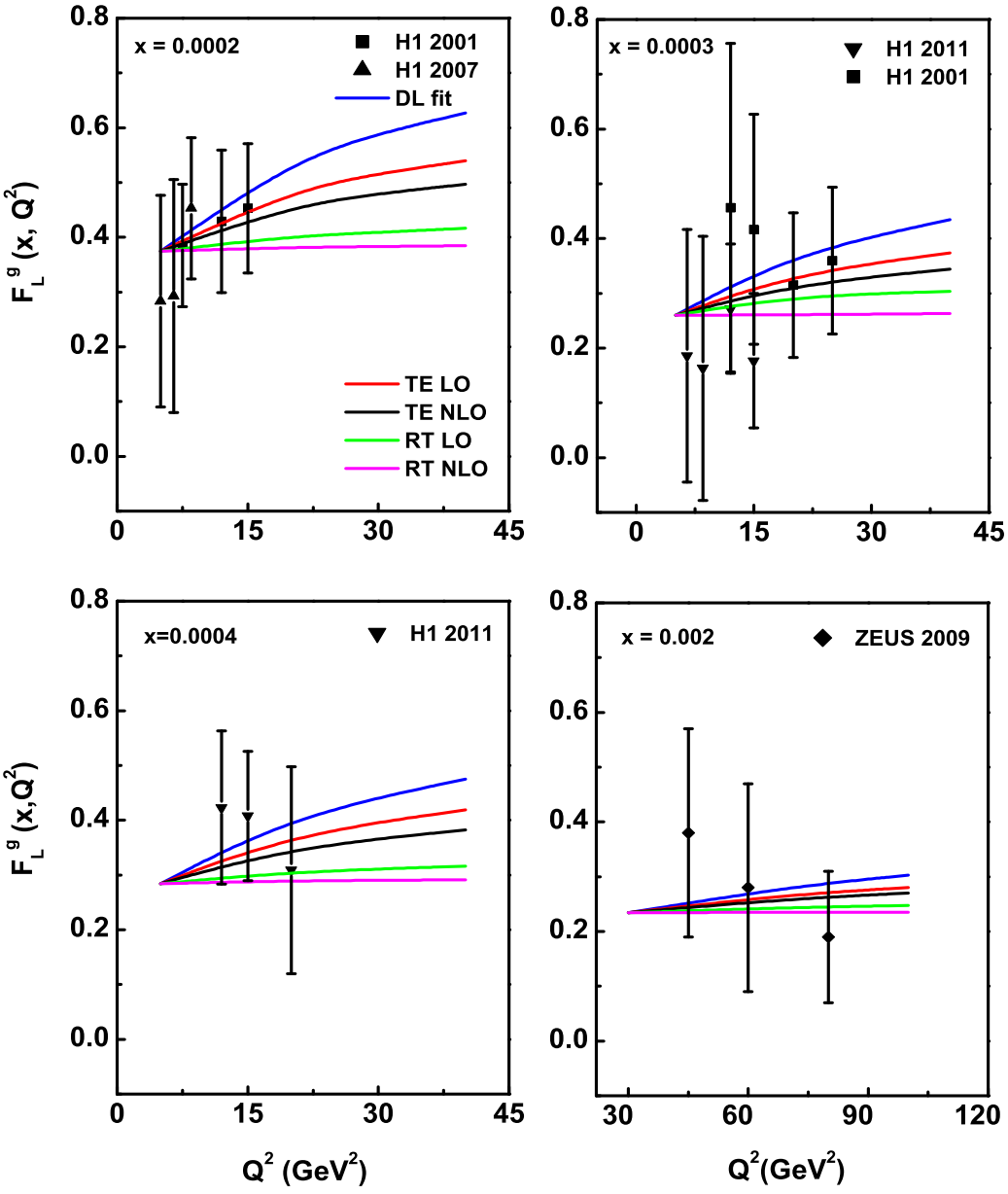

Figure 3.8: Comparison of t-evolution results of F_L^g structure function predicted by Regge theory approach and Taylor expansion method and DL model.

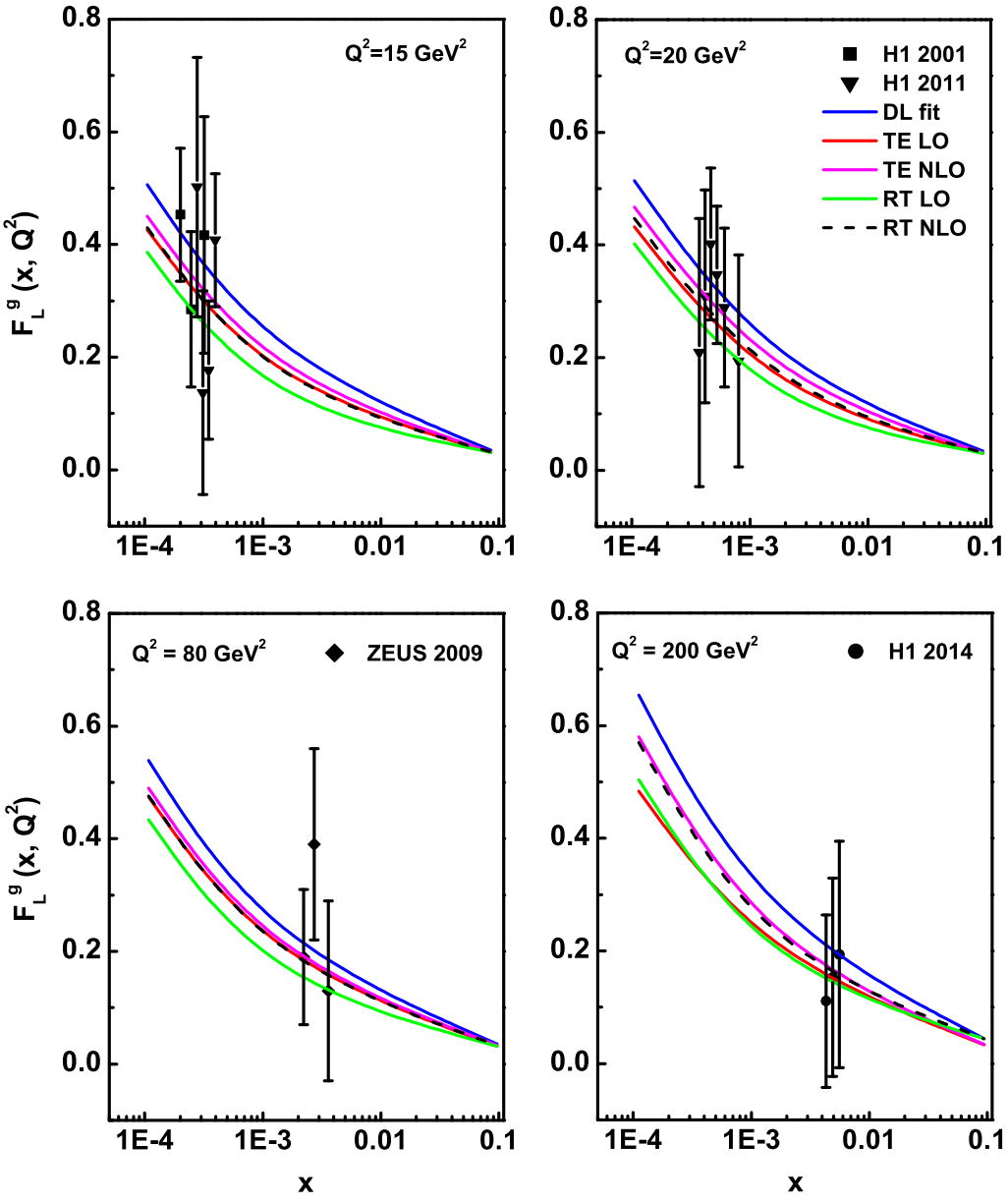

Figure 3.9: Comparison of x-evolution results of F_L^g structure function predicted by Regge theory approach and Taylor expansion method and DL model.

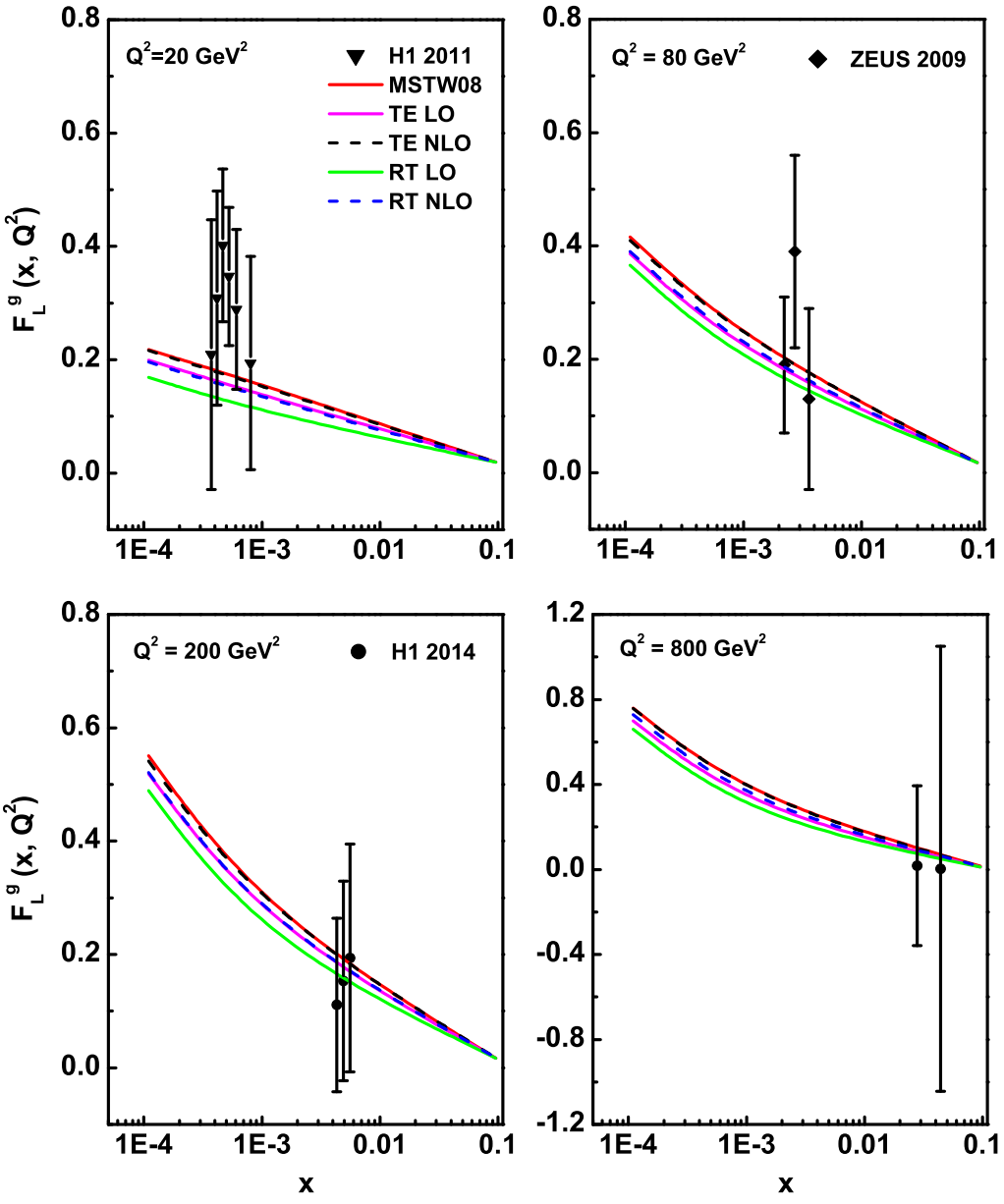

Figure 3.10: Comparison of x-evolution results of F_L^g structure function predicted by Regge theory approach and Taylor expansion method and MSTW08.

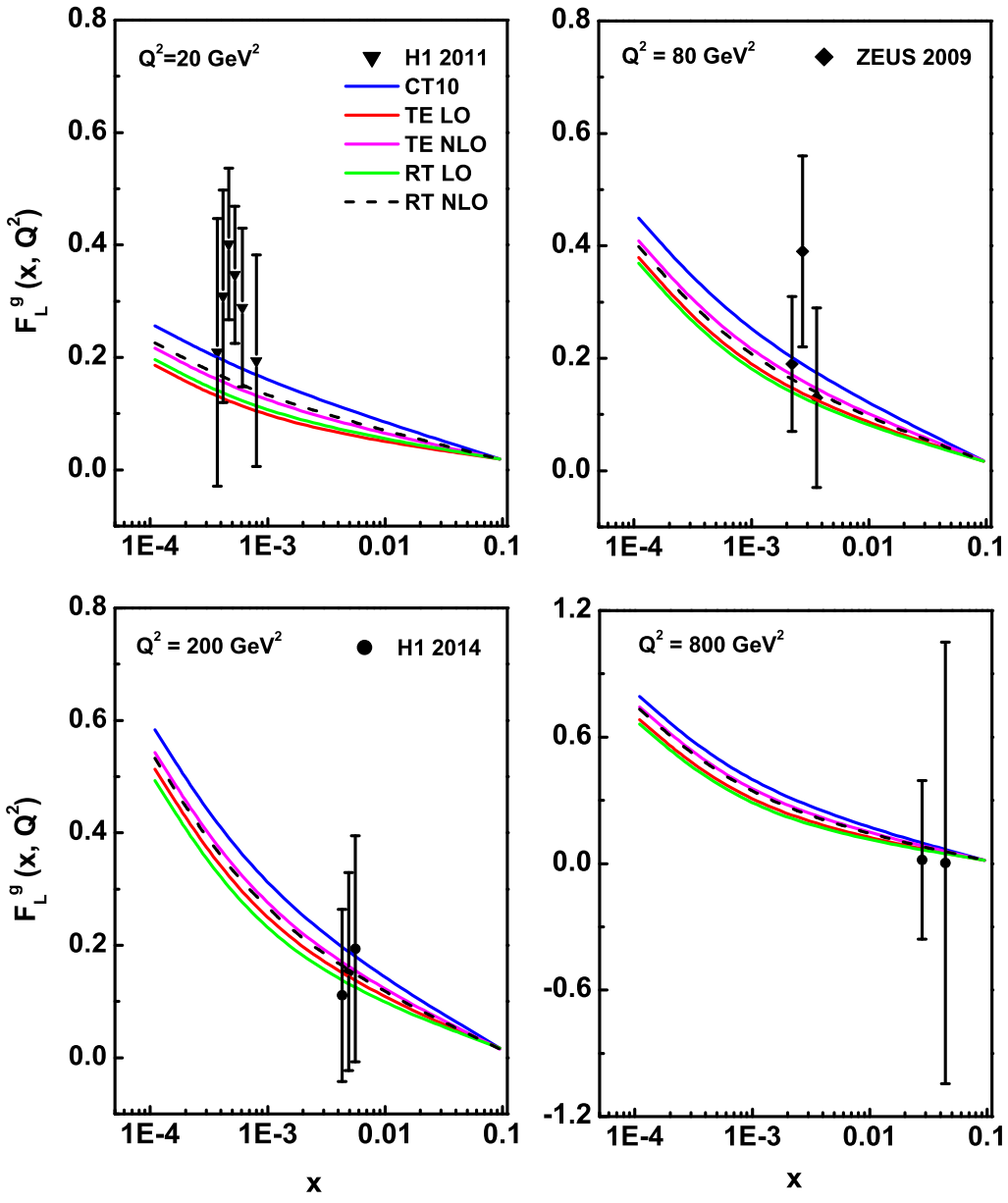

Figure 3.11: Comparison of x-evolution results of F_L^g structure function predicted by Regge theory approach and Taylor expansion method and CT10.

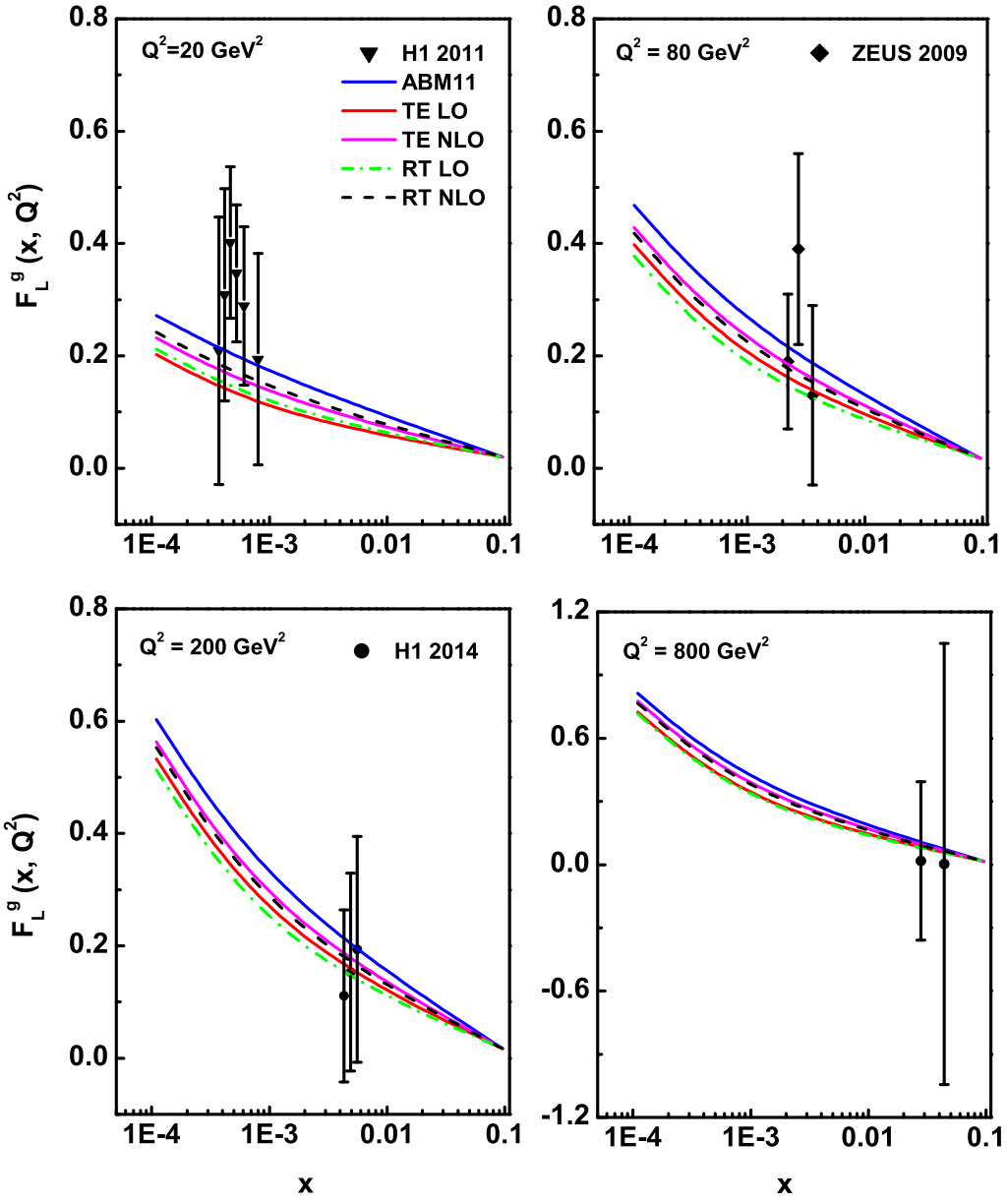

Figure 3.12: Comparison of x-evolution results of F_L^g structure function predicted by Regge theory approach and Taylor expansion method and ABM11.

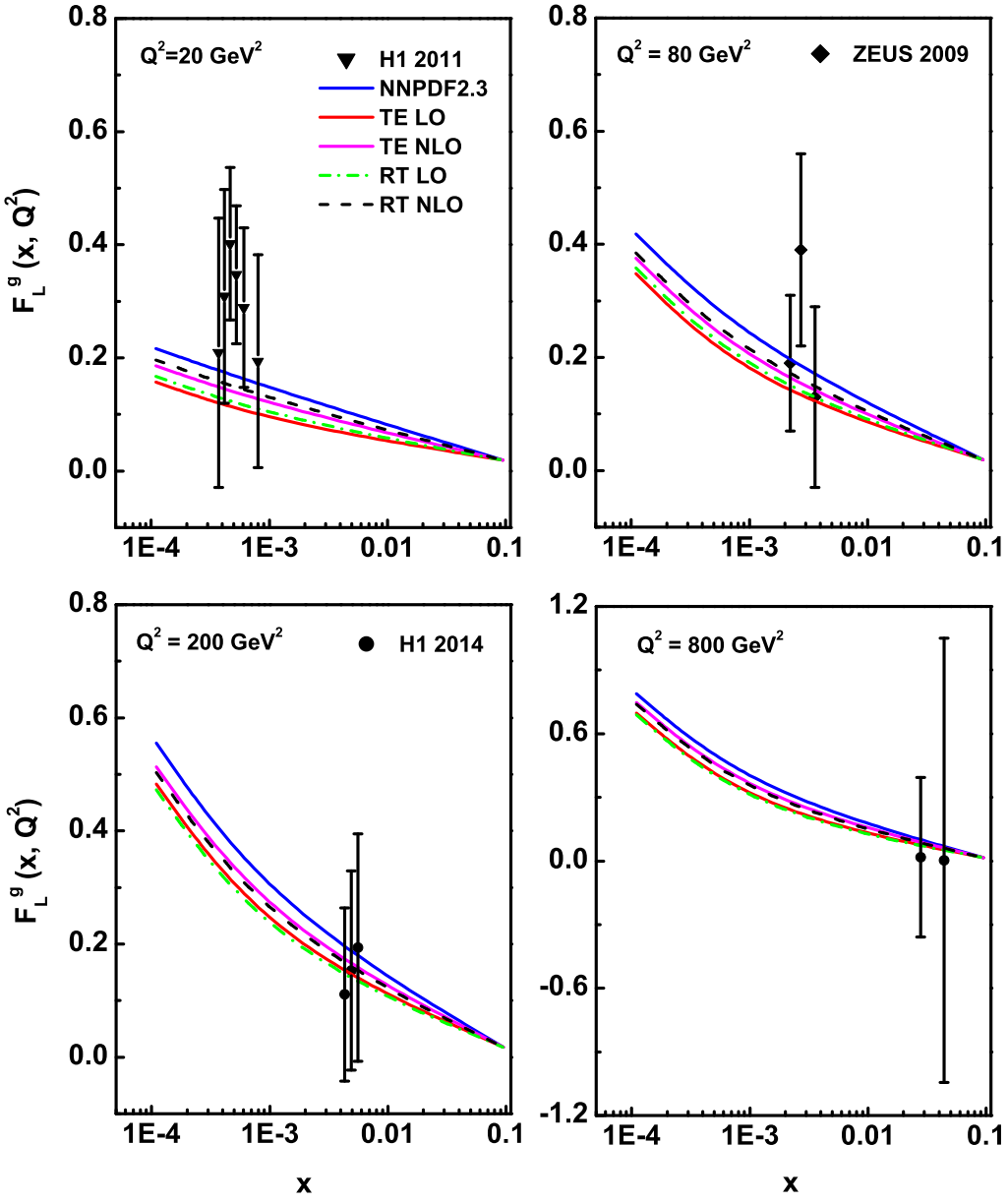

Figure 3.13: Comparison of x-evolution results of F_L^g structure function predicted by Regge theory approach and Taylor expansion method and NNPDF2.3.

with respect to x which shows good agreement with the data, model fit and parameterizations. In all the graphs, F_L^g structure function predicted by both approach increases towards small values of x. Though the results of obtained by TE approach are slightly higher than those of RT approach in almost all the cases, yet both the methods can be applied to calculate the F_L^g structure function at small-x.

3.3 Conclusions

In this chapter, we have obtained an analytical solution of evolution equation for longitudinal structure function F_L^g up to NLO using the Regge like behaviour of the structure function. Here, we have studied the behaviour of the t and x-evolutions of F_L^g structure function up to NLO only. Due to the unavailability of the evolution kernel at NNLO we are unable to calculate the same at this order. We have compared our results with the recent experimental data to confirm the validity of our calculations. The variation of F_L^g structure function with x and Q^2 shows similar nature with the experimental data as well as the model fit and parameterizations which shows the compatibility of Regge behaviour with the perturbative evolution of structure function at small-x. At small-x, our results show that the longitudinal structure function F_L^g increases as the values of Q^2 increases and x decreases. The increasing behaviour of F_L^g structure function in this approach follows the power law behaviour of structure function as predicted by Regge theory. As in our given range of x, we have considered only the gluon dominating part of the structure function, so we can say that the gluon contribution to the longitudinal structure function increases as the values of Q^2 increases and x decreases. From the comparative study of evolution of F_L structure function predicted by Regge theory approach and Taylor expansion method shows that results obtained by both the method are in good agreement with data and parameterizations.

References

[1] Aaron, F. D., et al. Measurement of the inclusive $e^{\pm}p$ scattering cross section at high inelasticity y and of the structure function F_L, *Eur. Phys. J. C.* **71** (3), 1579-1–50, 2011.

[2] Adloff, C., et al. Deep-inelastic inclusive ep scattering at low x and a determination of α_s, *Eur. Phys. J. C.* **21** (1), 33–61, 2001.

[3] Pardos, C. D. *Studies for the direct measurement of the proton structure function F_L with the H1 detector at HERA*, Ph.D. thesis, DESY, Zeuthen, Germany, 2007.

[4] Piec, S. *Measurement of the Proton Structure Function F_L with the H1 Detector at HERA*, Ph.D. thesis, Humboldt University of Berlin, Germany, 2009.

[5] Andreev, V., et al. Measurement of Inclusive ep Cross Sections at High Q^2 at $\sqrt{s} = 225$ and $252GeV$ and of the Longitudinal Proton Structure Function F_L at HERA, *Eur. Phys. J. C* **74** (4), 2814-1–26, 2014.

[6] Chekanov, S., et al. Measurement of the longitudinal proton structure function at HERA, *Phys. Lett. B* **682** (1), 8–22, 2009.

[7] Donnachie, A. and Landshoff, P. V. The protons gluon distribution, *Phys. Lett. B* **550** (3-4), 160–165, 2002.

[8] Martin, A. D., et al. Parton distributions for the LHC, *Eur. Phys. J. C* **63** (2), 189–285, 2009.

[9] Hung-Liang, Lai., et al. New parton distributions for collider physics, *Phys. Rev. D* **82** (7), 074024-1–24, 2010.

[10] Alekhin, S., Blemlein, J. and Moch, S. The ABM parton distributions tuned to LHC data, *Phys. Rev. D* **89** (5), 054028-1–21, 2014.

[11] Ball, R. D., et al. Parton distributions with LHC data, *Nucl. Phys. B* **867** (2), 244–289, 2013.

[12] Forte, S., et al. Heavy quarks in deep-inelastic scattering, *Nucl. Phys. B* **834** (1-2), 116–162, 2010.

[13] Boroun, G. R. Hard-pomeron behavior of the longitudinal structure function F_L in the next-to-leading order at low x, *Int. J. Mod. Phys. E* **18** (1), 131–140, 2009.

[14] Moch, S. and Vogt, A. Threshold resummation of the structure function F_L, *J. High Energy Phys.* **2009** (04), 081-1–11, 2009.

[15] Kazakov, D. I., et al. Complete Quartic α_s^2 correction to the deep-inelastic longitudinal structure function F_L in QCD, *Phys. Rev. Lett.* **65** (13), 1535–1538, 1990.

[16] Guillen, J. S., et al. Next-to-leading order analysis of the deep inelastic $R = \sigma_L/\sigma_T$, *Nucl. Phys. B* **353** (2) 337–345, 1991.

[17] Abbott, L. F., Atwood, W. B. and Barnett, R. M. Quantum-chromodynamic analysis of eN deep-inelastic scattering data, *Phys. Rev. D* **22** (3), 582–593, 1980.

[18] Donnachie, A. and Landshoff, P. V. Small x: two pomerons, *Phys. Lett. B* **437** (3-4), 408–416 , 1998.

[19] Kotikov, A. V. and Parente, G. The gluon distribution as a function of F_2 and $dF_2/dlnQ^2$ at small x. The next-to-leading analysis, *Phys. Lett. B* **379** (1-4), 195–201, 1996.

[20] Donnachie, A. and Landshoff, P. V. Perturbative QCD and Regge theory: closing the circle, *Phys. Lett. B* **533** (3-4), 277–284 , 2002.

[21] Cooper-Sarkar, A. M., et al. Measurement of the longitudinal structure function and the small x gluon density of the proton, *Z. Phys. C* **39** (2), 281–290, 1988.

[22] Baishya, R. and Sarma, J. K. Semi numerical solution of non-singlet DokshitzerGribovLipatovAltarelliParisi evolution equation up to next-to-next-to-leading order at small x, *Eur. Phys. J. C* **60** (4), 585–591, 2009.

[23] Glazov, S. Measurement of DIS Cross Section at HERA, *Braz. J. Phys.* **37** (2C), 793–797, 2007.

[24] Jamil, U. and Sarma, J. K. Regge behaviour of distribution functions and evolution of gluon distribution function in next-to-leading order at low-x, *Pramana J. Phys.* **71** (3), 509–519, 2008.

[25] Martin, A. D., Ryskin, M. G. and Watt, G. Simultaneous QCD analysis of diffractive and inclusive deep-inelastic scattering data, *Phys. Rev. D* **70** (9), 091502-1–5, 2004.

[26] Rezaei, B. and Boroun, G. R. Analytical solution of the longitudinal structure function F_L in the leading and next-to-leading-order analysis at low x with respect to Laguerre polynomials method, *Nucl. Phys. A* **857** (1), 42–47, 2011.

[27] Nematollahi, H., Yazdanpanah, M. M. and Mirjalili, A. NNLO longitudinal proton structure function, based on the modified χQM, *Mod. Phys. Lett. A* **27** (31),1250179-1-11 ,2012.

[28] Boroun, G. R. and Rezaei, B. Analysis of the proton longitudinal structure function from the gluon distribution function, *Eur. Phys. J. C* **72** (11), 2221-1-5, 2012.

[29] Devee, M., Baishya, R. and Sarma, J. K. Evolution of singlet structure functions from DGLAP equation at next-to-next-to-leading order at small-x, *Eur. Phys. J. C* **72** (6), 2036-1-11, 2012.

[30] Kwiecinski, J., et al. Parton distributions at small x, *Phys. Rev. D* **42** (11), 3645–3659, 1990. □

Chapter 4

F_L Structure Function from Gluon Distribution Function Using Taylor Expansion Method at Small-x

In this chapter, we have presented the relation between the F_L structure function and the gluon distribution function up to next-to-next-to-leading order analysis at small-x using Taylor expansion method. We use the Altarelli-Martinelli equation in our analysis to obtain the evolution of F_L structure function at small-x. The obtained theoretical results are compared with H1 [1–5], ZEUS [6] data, results of DL [7] model, results predicted by MSTW08 [8], CT10 [9, 10], ABM11 [11] and NNPDF2.3 [12, 13] parameterizations and results obtained by other authors.

4.1 Theory

In pQCD, the Altarelli-Martinelli equation for longitudinal structure function $F_L(x, Q^2)$ of proton in terms of co-efficient function is given by [14, 15]

$$x^{-1}F_L = C_{L,ns} \otimes q_{ns} + < e^2 > (C_{L,s} \otimes q_s + C_{L,g} \otimes g). \tag{4.1}$$

Here q_{ns}, q_s and g are the flavour non singlet, flavour singlet and gluon distribution function, $< e^2 >= \frac{5}{18}$ is the average squared charge for N_f (number of active light flavours) and the symbol $\otimes$ represents the standard Mellin convolution. $C_{L,a}(a = ns, s, g)$'s are the co-efficient functions which can be written by the perturbative expansion as follows [15]

$$C_{L,a}(\alpha_s, x) = \sum_{n=1} \Big(\frac{\alpha_s}{4\pi}\Big)^n C^n_{L,a}(x), \tag{4.2}$$

where n denotes the order in running coupling constant $\alpha_s(Q^2)$ [16] and the expression of α_s is mentioned in section 2.1 of chapter 2.

At small values of x ($x \leq 10^{-3}$) the gluon contribution to the F_L structure function dominates over the flavour singlet and non-singlet contribution [17]. Now the Altarelli Martinelli equation for gluon dominating F_L structure function is given by

$$F^g_L(x, Q^2) =< e^2 > \int_x^1 \frac{dw}{w} C_{L,g}(w, Q^2) G\Big(\frac{x}{w}, Q^2\Big). \tag{4.3}$$

Here $C_{L,g}(w, Q^2)$ is the gluon co-efficient function for F_L known perturbatively up to first few orders in running coupling constant $\alpha_s(Q^2)$ and can be written as

$$C_{L,g}(w, Q^2) = \frac{\alpha_s(Q^2)}{4\pi} C^1_{L,g}(w) + \Big(\frac{\alpha_s(Q^2)}{4\pi}\Big)^2 C^2_{L,g}(w) + \Big(\frac{\alpha_s(Q^2)}{4\pi}\Big)^3 C^3_{L,g}(w), \tag{4.4}$$

where $C^1_{L,g}(w)$, $C^2_{L,g}(w)$ and $C^3_{L,g}(w)$ are the gluon co-efficient functions for F_L in LO, NLO and NNLO respectively [15, 18, 19]. The analytical expression of the gluon co-efficient function for F_L are defined in the Appendix A.

At small values of x we can rewrite the equation (4.3) by substituting $w = 1 - z$ as

$$F^g_L(x, Q^2) =< e^2 > \int_0^{1-x} \frac{dz}{1-z} C_{L,g}(1-z, Q^2) G\Big(\frac{x}{1-z}, Q^2\Big), \tag{4.5}$$

where F^g_L is derived from the integrated gluon distribution function $G(x, Q^2)$. An approximate relationship between F^g_L and gluon distribution can be obtained from the expansion of $G\Big(\frac{x}{1-z}, Q^2\Big)$ around a particular choice of point of expansion. Since $x < w < 1$, we have $0 < z < 1 - x$; so the series $\frac{x}{w} = \frac{x}{1-z}$ is convergent for $|z| < 1$. So, we can take the point of expansion z as any value between $0 \leq z < 1$.

Using the Taylor expansion method for the gluon distribution function at an arbitrary point $z = \frac{1}{2}$, and neglecting the higher order terms at small-x, $G\Big(\frac{x}{1-z}, Q^2\Big)$ can

be written as

$$G\Big(\frac{x}{1-z},Q^2\Big)\Big|_{z=\frac{1}{2}} = G\Big(z=\frac{1}{2},Q^2\Big)+\Big(z-\frac{1}{2}\Big)\frac{\partial G\Big(z=\frac{1}{2},Q^2\Big)}{\partial x}$$
$$= G(2x,Q^2)+\Big(z-\frac{1}{2}\Big)\frac{\partial G(2x,Q^2)}{\partial x}. \quad (4.6)$$

Using equation (4.6) and leading order terms of equation (4.4) in equation (4.5) and performing the integration, we get

$$F_L^g(x,Q^2) =< e^2 > \frac{\alpha_s(Q^2)}{4\pi}P(x)G\Big(2x+\frac{Q(x)}{P(x)},Q^2\Big), \quad (4.7)$$

where

$$P(x)=\int_0^{1-x}\frac{dz}{1-z}\Big(C_{L,g}^1(1-z)\Big) \quad (4.8)$$

and

$$Q(x)=\int_0^{1-x}\frac{dz}{1-z}\Big(z-\frac{1}{2}\Big)\Big(C_{L,g}^1(1-z)\Big). \quad (4.9)$$

This result shows that the longitudinal structure function $F_L^g(x,Q^2)$ can be calculated using the low x gluon density from Donnachie Landshoff (DL) model [7] at LO. Similarly, when gluon density is expanded at $z=0.8$, the corresponding LO expression takes the form

$$F_L^g(x,Q^2) =< e^2 > \frac{\alpha_s(Q^2)}{4\pi}P(x)G\Big(5x+\frac{R(x)}{P(x)},Q^2\Big), \quad (4.10)$$

where

$$R(x)=\int_0^{1-x}\frac{dz}{1-z}(z-0.8)\Big(C_{L,g}^1(1-z)\Big). \quad (4.11)$$

Both the equations (4.7) and (4.10) show the behaviour of $F_L^g(x,Q^2)$ with respect to x. We have also checked this for $z=0.6,0.7,0.9$; but the best result is obtained in the

case of the expansion point of the gluon density at $z = 0.8$ in LO analysis, which is depicted in figure 4.1 in comparison with the experimental data and model fit.

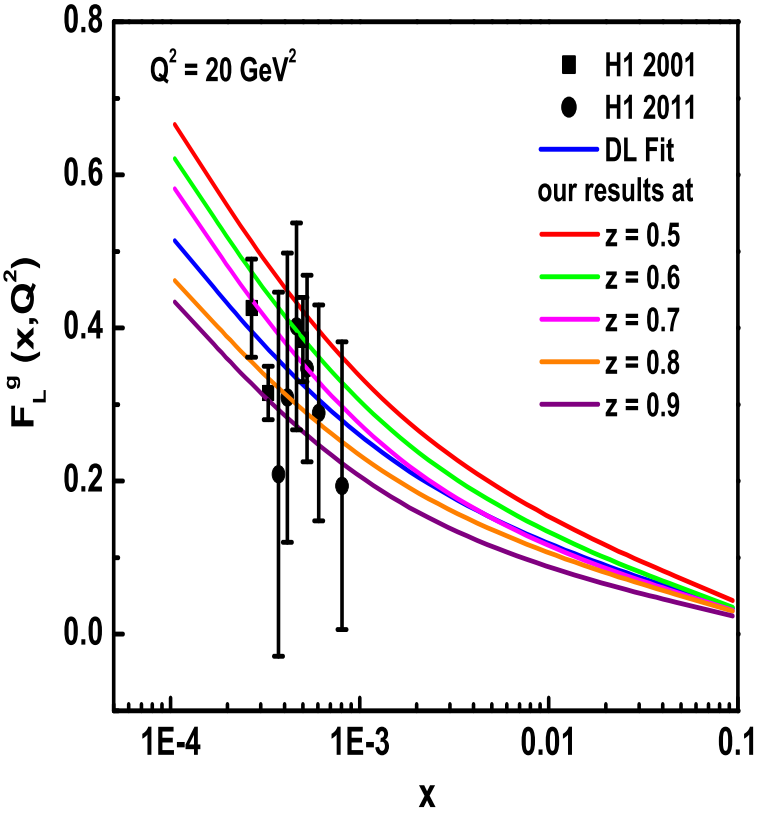

Figure 4.1: Sensitivity of our results of F_L^g structure function in LO with respect to the expansion point of gluon density at z = 0.5, 0.6, 0.7, 0.8, 0.9 in comparison with H1 data and DL model.

We have also obtained the relation between the longitudinal structure function and the gluon distribution function at small-x in NLO and NNLO analysis by considering the expansion point of the gluon density at $z = 0.8$. These are given by

$$F_L^g(x,Q^2) =< e^2 > \frac{\alpha_s(Q^2)}{4\pi} P_1(x) G\Big(5x + \frac{R_1(x)}{P_1(x)}, Q^2\Big) \tag{4.12}$$

and

$$F_L^g(x,Q^2) =< e^2 > \frac{\alpha_s(Q^2)}{4\pi} P_2(x) G\Big(5x + \frac{R_2(x)}{P_2(x)}, Q^2\Big) \tag{4.13}$$

in NLO and NNLO respectively. Here

$$P_1(x) = \int_0^{1-x} \frac{dz}{1-z}\Big(C_{L,g}^1(1-z) + T_0 C_{L,g}^2(1-z)\Big), \tag{4.14}$$

$$P_2(x) = \int_0^{1-x} \frac{dz}{1-z}\Big(C_{L,g}^1(1-z) + T_0 C_{L,g}^2(1-z) + T_1 C_{L,g}^3(1-z)\Big), \tag{4.15}$$

$$R_1(x) = \int_0^{1-x} \frac{dz}{1-z}(z-0.8)\Big(C_{L,g}^1(1-z) + T_0 C_{L,g}^2(1-z)\Big) \tag{4.16}$$

and

$$R_2(x) = \int_0^{1-x} \frac{dz}{1-z}(z-0.8)\Big(C_{L,g}^1(1-z) + T_0 C_{L,g}^2(1-z) + T_1 C_{L,g}^3(1-z)\Big). \tag{4.17}$$

Here we consider two numerical parameters T_0 and T_1, such that $T^2(t) = T_0.T(t)$ and $T^3(t) = T_1.T(t)$ with $T(t) = \frac{\alpha_s(t)}{2\pi}$. These numerical parameters are obtained for a particular range of Q^2 under study. As described in chapter 2 and ref. [20], these two parameters are chosen in such a way that the difference between $T^2(t)$, $T_0.T(t)$ and $T^3(t)$, $T_1.T(t)$ are negligible in our required range. Here, we have considered the values of $T_0 = 0.0278$ and $T_1 = 0.000892$ within the range $1.5 \leq Q^2 \leq 200GeV^2$. We have also checked the sensitivity of our results of F_L^g structure function in NLO and NNLO with respect to the expansion point of the gluon density at $z = 0.5, 0.6, 0.7, 0.8, 0.9$ which is depicted in figure 4.2. This figure shows that in case of the expansion point of gluon density at $z = 0.8$, our results show better agreement with the results of model fit and experimental data. Therefore, in all the cases of our calculated results of F_L^g structure function, i.e., in LO, NLO and NNLO analysis, the results calculated with respect to

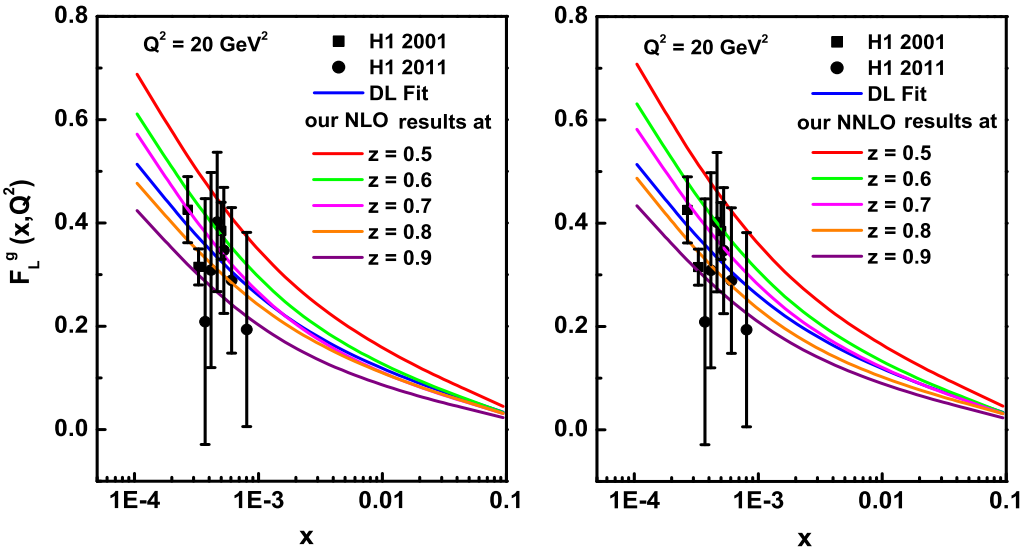

Figure 4.2: Sensitivity of our results of F_L^g structure function in NLO and NNLO with respect to the expansion point of gluon density at z = 0.5, 0.6, 0.7, 0.8, 0.9 in comparison with H1 data and DL model.

the expansion point of the gluon density at $z = 0.8$ shows compatibility with the results of model fit and data. In a similar way we have also checked the sensitivity of z values for all values of Q^2 like the values of $Q^2 = 20GeV^2$ which is found to be 0.8.

Thus using equations (4.10), (4.12) and (4.13) we have calculated the x-evolutions for F_L^g structure function in LO, NLO and NNLO respectively.

4.2 Results and Discussions

We have determined the approximate relation between the longitudinal structure function of proton and gluon distribution function at small-x in next-next-to-leading order analysis with respect to the expansion of the gluon density at an arbitrary point of expansion. With the help of these relations we have calculated the F_L^g structure

function in the range $10^{-4} \leq x \leq 0.1$ and $15 \leq Q^2 \leq 200GeV^2$ using the small-x gluon distribution function of DL model and the co-efficient functions which are given in Appendix A. The obtained results are compared with the the recent H1 [1–5], ZEUS [6] experimental data and results of DL model [7]. The related plots are depicted in figure 4.3 which indicate a good agreement with experimental data and model fit. Here, the vertical error bars are both statistical and systematic errors for both H1 and ZEUS data. To confirm that in spite of the large uncertainty in the experimental data, our results are in good agreement with the other results, we also add DL model results. We have also compared our results with the theoretical predictions of MSTW08 [8], CT10 [9,10], ABM11 [11] and NNPDF2.3 [12, 13] parameterizations. Figures 4.4 to 4.7 show the related plots for different values of $Q^2 = 20, 25, 80$ and $200GeV^2$. These plots also reflect better agreement of our results with these parameterizations. Here all the plots show compatibility with predictions of parameterizations towards higher values of Q^2 i.e., $Q^2 = 80$ and $200GeV^2$. In this procedure of evaluation of F_L^g structure function as we have taken the input distribution of gluon from DL model, so the behaviour of structure function increases towards small-x depending on values of the input distribution. Our calculated results of F_L^g structure function in all the cases i.e., LO, NLO and NNLO increases towards small values of x in the given range of x and Q^2 as expected from QCD.

In our analysis, we have determined the approximate relation between F_L^g structure function of proton and gluon distribution function at small-x in next-next-to-leading order using the Altarelli- Martinelli equation for F_L^g structure function in terms of the co-efficient functions. We have also compared our results at moderate values of $Q^2 = 20GeV^2$ with the similar results obtained by Sarkar et al (CS) [17] and Boroun et al (GRB) [21]. In ref. [17], the authors suggested a relation between F_L structure function of proton and gluon distribution function at small-x in leading order approximation

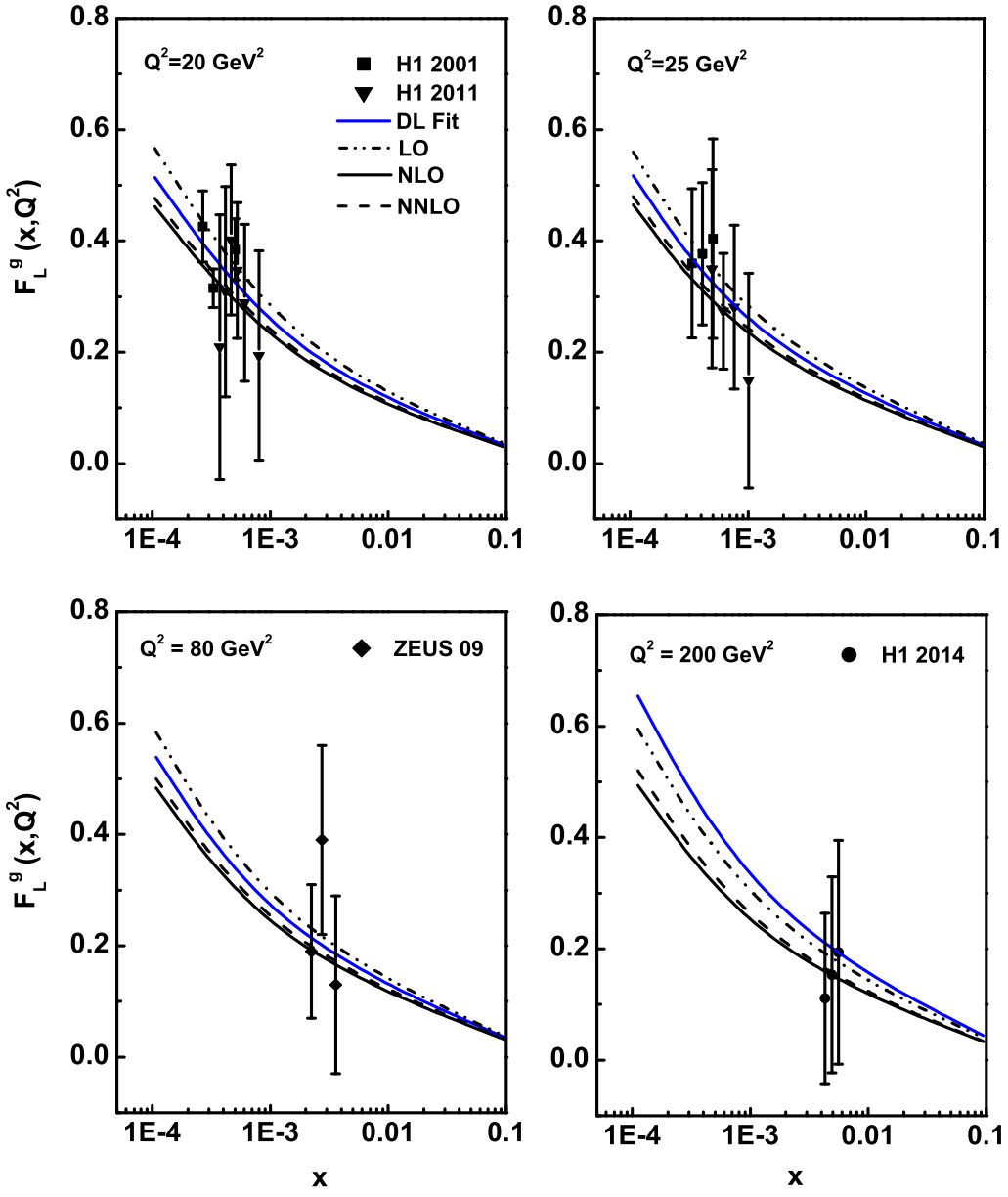

Figure 4.3: x-evolution results of F_L^g structure function up to NNLO using Taylor expansion method in comparison with the H1, ZEUS data and results of DL model.

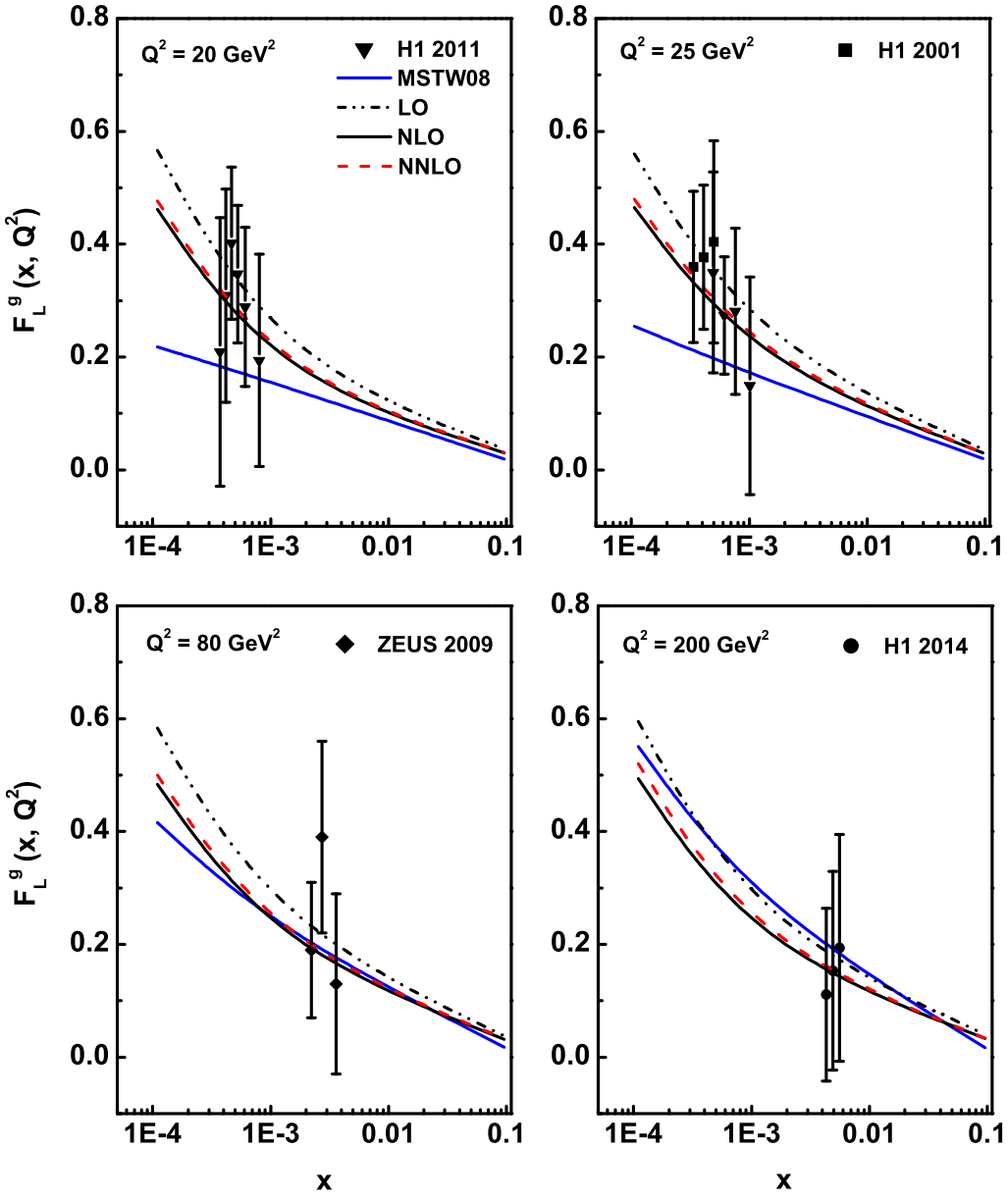

Figure 4.4: x-evolution results of F_L^g structure function up to NNLO using Taylor expansion method in comparison with the H1, ZEUS data and the theoretical prediction of MSTW08.

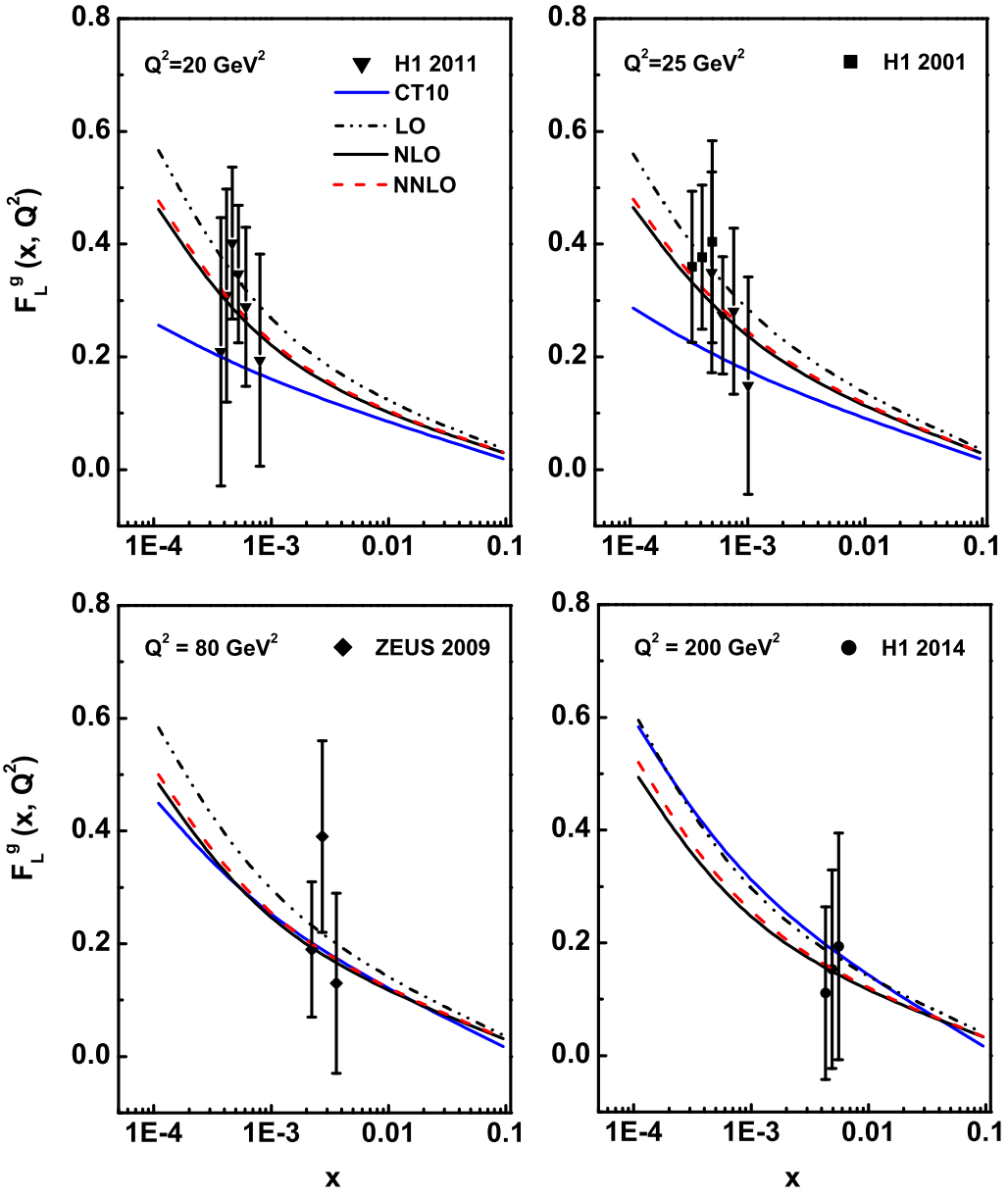

Figure 4.5: x-evolution results of F_L^g structure function up to NNLO using Taylor expansion method in comparison with the H1, ZEUS data and the theoretical prediction of CT10.

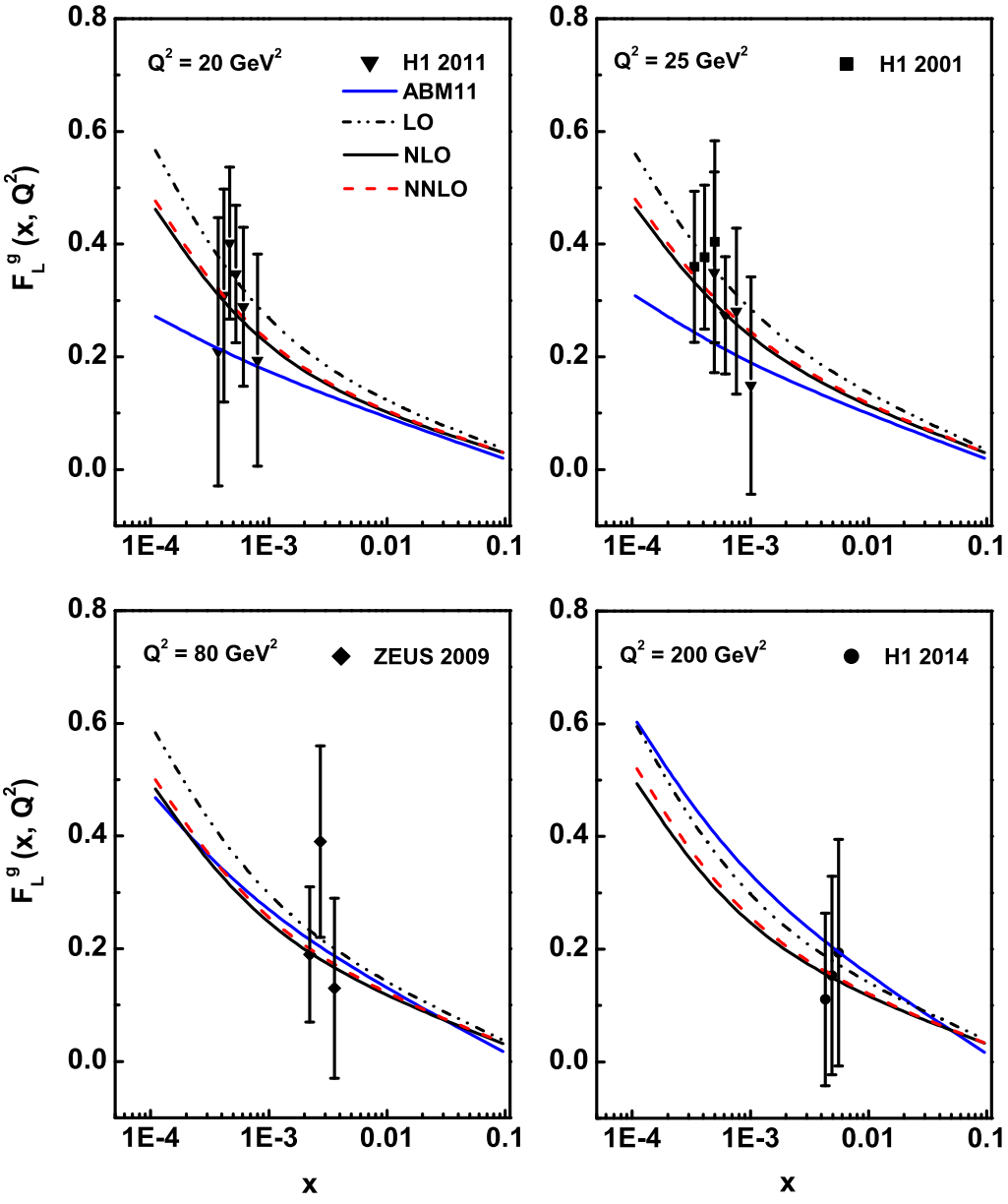

Figure 4.6: x-evolution results of F_L^g structure function up to NNLO using Taylor expansion method in comparison with the H1, ZEUS data and the theoretical prediction of ABM11.

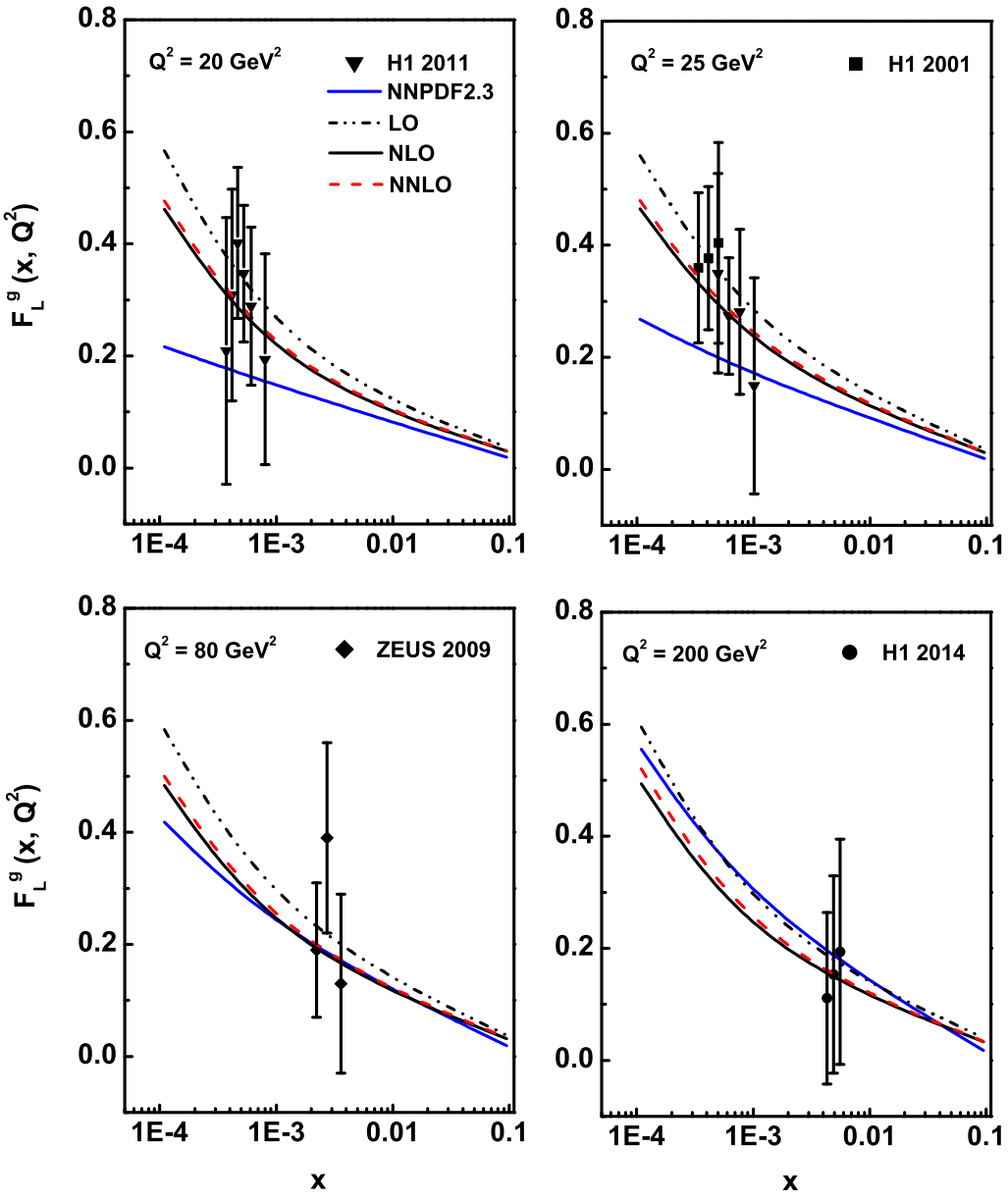

Figure 4.7: x-evolution results of F_L^g structure function up to NNLO using Taylor expansion method in comparison with the H1, ZEUS data and the theoretical prediction of NNPDF2.3.

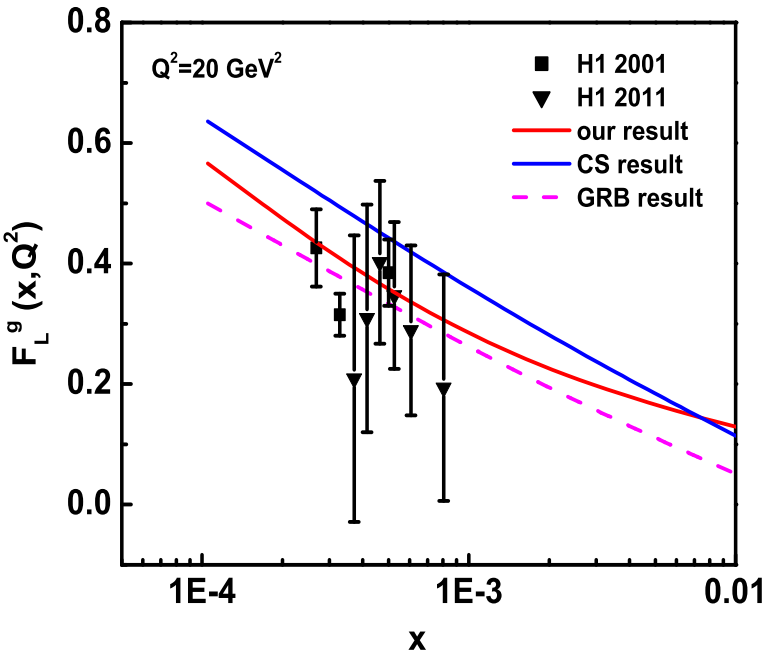

Figure 4.8: comparison of our x-evolution results of F_L^g structure function with the results of Sarkar et al (CS) and Boroun et al (GRB).

given by

$$F_L^g(x,Q^2) = \frac{2\alpha_s}{\pi}\frac{\sum_{i=1}^{N_f} e_i^2}{5.9} G(2.5x,Q^2) \tag{4.18}$$

which shows the close relation between these two quantities. In ref. [21], the authors reported an NLO analysis of the relation between F_L structure function and gluon distribution obtained by Sarkar et al. Figure 4.8 shows the comparison of our results with the above mentioned two results which reflects similar behaviour with the results obtained by Sarkar et al (CS) and Boroun et al (GRB). Thus our approximate relation can be used to study the x-evolution of F_L^g structure function at small-x up to NNLO analysis.

4.3 Conclusions

In this work, we have determined the proton longitudinal structure function up to NNLO at small-x using the approximate relation between F_L^g structure function and gluon distribution function with respect to the expansion of the gluon density at an arbitrary point of expansion i.e., at $z = 0.8$. The behaviour of F_L^g structure function with x shows good agreement with the experimental data and the model fit and parameterizations. Our predicted results also shows resemblance with the results obtained by other authors. The calculated results of F_L^g structure function in all orders lies within the framework of pQCD i.e, it increases towards low values of x. As at small-x gluon contents in the proton is dominant one we can say that gluon contribution to the F_L structure function increases as x decreases.

References

[1] Aaron, F. D., et al. Measurement of the inclusive $e^{\pm}p$ scattering cross section at high inelasticity y and of the structure function F_L, *Eur. Phys. J. C.* **71** (3), 1579-1–50, 2011.

[2] Adloff, C., et al. Deep-inelastic inclusive ep scattering at low x and a determination of α_s, *Eur. Phys. J. C.* **21** (1), 33–61, 2001.

[3] Pardos, C. D. *Studies for the direct measurement of the proton structure function F_L with the H1 detector at HERA*, Ph.D. thesis, DESY, Zeuthen, Germany, 2007.

[4] Piec, S. *Measurement of the Proton Structure Function F_L with the H1 Detector at HERA*, Ph.D. thesis, Humboldt University of Berlin, Germany, 2009.

[5] Andreev, V., et al. Measurement of Inclusive *ep* Cross Sections at High Q^2 at $\sqrt{s} = 225$ and $252GeV$ and of the Longitudinal Proton Structure Function F_L at HERA, *Eur. Phys. J. C* **74** (4), 2814-1–26, 2014.

[6] Chekanov, S., et al. Measurement of the longitudinal proton structure function at HERA, *Phys. Lett. B* **682** (1), 8–22, 2009.

[7] Donnachie, A. and Landshoff, P. V. The protons gluon distribution, *Phys. Lett. B* **550** (3-4), 160–165, 2002.

[8] Martin, A. D., et al. Parton distributions for the LHC, *Eur. Phys. J. C* **63** (2), 189–285, 2009.

[9] Hung-Liang, Lai., et al. New parton distributions for collider physics, *Phys. Rev. D* **82** (7), 074024-1–24, 2010.

[10] Jun, Gao., et al. CT10 next-to-next-to-leading order global analysis of QCD, *Phys. Rev. D* **89** (3), 033009-1–28, 2014.

[11] Alekhin, S., Bluemlein, J. and Moch, S. The ABM parton distributions tuned to LHC data, *Phys. Rev. D* **89** (5), 054028-1–21, 2014.

[12] Ball, R. D., et al. Parton distributions with LHC data, *Nucl. Phys. B* **867** (2), 244–289, 2013.

[13] Forte, S., et al. Heavy quarks in deep-inelastic scattering, *Nucl. Phys. B* **834** (1-2), 116–162, 2010.

[14] Altarelli, G. and Martinelli, G. Transverse momentum of jets in electroproduction from quantum chromodynamics, *Phys. Lett. B* **76** (1), 89–94, 1978.

[15] Moch, S., Vermaseren, J. A. M. and Vogt, A. The longitudinal structure function at the third order, *Phys. Lett. B* **606** (1-2), 123–129, 2005.

[16] Abbott, L. F., Atwood, W. B. and Barnett, R. M. Quantum-chromodynamic analysis of eN deep-inelastic scattering data, *Phys. Rev. D* **22** (3), 582–593, 1980.

[17] Cooper-Sarkar, A. M., et al. Measurement of the longitudinal structure function and the small x gluon density of the proton, *Z. Phys. C* **39** (2), 281–290, 1988.

[18] Zijlstra, E. B. and Van Neerven, W. L. Contribution of the second order gluonic Wilson coefficient to the deep inelastic structure function, *Phys. Lett. B* **273** (4), 476–482, 1991.

[19] Moch, S. and Vermaseren, J. A. M. Deep-inelastic structure functions at two loops, *Nucl. Phys. B* **573** (3), 853–907, 2000.

[20] Baishya, R. and Sarma, J. K. Semi numerical solution of non-singlet Dokshitzer-GribovLipatovAltarelliParisi evolution equation up to next-to-next-to-leading order at small x, *Eur. Phys. J. C* **60** (4), 585–591, 2009.

[21] Boroun, G. R. and Rezaei, B. Analysis of the proton longitudinal structure function from the gluon distribution function, *Eur. Phys. J. C* **72** (11), 2221-1–5, 2012. □

Chapter 5

Longitudinal Structure Function F_L and DIS Cross Section Ratio $R = \frac{\sigma_L}{\sigma_T}$ at Small-x from Regge Behaviour of Gluon Distribution Function

In this chapter, the behaviour of gluon dominated longitudinal structure function F_L^g with respect to Bjorken variable x and Q^2 , the squared four-momentum transfer between lepton and nucleon in next-next-to-leading order (NNLO) at small-x is presented using the Regge like behaviour of the gluon distribution function. Here we have calculated t- and x-evolutions of the F_L^g structure function using the gluon distribution function obtained as a result of solution of the DGLAP evolution equation at small-x. We have also studied the behaviour of the DIS cross section ratio $R = \frac{\sigma_L}{\sigma_T}$ in this kinematical region. The calculated results are compared with recent H1 [1–5], ZEUS [6] data and DL [7] model results. We have also compared our results with the theoretical results predicted by MSTW08 [8], CT10 [9,10], ABM11 [11] and NNPDF2.3 [12,13] parameterizations. The results obtained can be explained within the framework of pQCD i.e., the evolution of structure function F_L^g increases towards low values of x. And the behaviour of F_L^g structure function shows resemblance with the gluon distribution function as it is originated from gluon distribution function. Contrary to it, the behaviour of the ratio R shows constant behaviour with respect to x and fixed Q^2 i.e., its behaviour is independent of the behaviour of gluon distribution function. A comparative analysis of our x-evolution results with the results obtained in chapter 4 is also studied here

which indicate that the behaviour of structure function can be studied using both the Regge behaviour of gluon distribution function and Taylor expansion method.

5.1 Theory

In pQCD, the Altarelli-Martinelli equation for longitudinal structure function $F_L(x, Q^2)$ of proton in terms of co-efficient function is given by [14, 15]

$$x^{-1}F_L = C_{L,ns} \otimes q_{ns} + < e^2 > (C_{L,s} \otimes q_s + C_{L,g} \otimes g). \tag{5.1}$$

Here q_{ns}, q_s and g are the flavour non singlet, flavour singlet and gluon distribution function, $< e^2 >= \frac{5}{18}$ is the average squared charge for even N_f (number of active light flavours) and the symbol $\otimes$ represents the standard Mellin convolution. $C_{L,a}(a = ns, s, g)$'s represent the co-efficient functions as described in chapter 4.

At small values of x ($x \leq 10^{-3}$) the gluon contribution to the F_L structure function dominates over the flavour singlet and non-singlet contribution [16]. Now the Altarelli-Martinelli equation for gluon dominating F_L structure function is given by

$$F_L^g(x, Q^2) = \int_x^1 \frac{dw}{w} C_{L,g}(w, Q^2) G\Big(\frac{x}{w}, Q^2\Big). \tag{5.2}$$

Here $C_{L,g}(w, Q^2)$ is the gluon co-efficient function for F_L known perturbatively up to first few orders in running coupling constant $\alpha_s(Q^2)$ [17] and can be written as

$$C_{L,g}(w, Q^2) = \frac{\alpha_s(Q^2)}{4\pi} C_{L,g}^1(w) + \Big(\frac{\alpha_s(Q^2)}{4\pi}\Big)^2 C_{L,g}^2(w) + \Big(\frac{\alpha_s(Q^2)}{4\pi}\Big)^3 C_{L,g}^3(w), \tag{5.3}$$

where $C_{L,g}^1(w)$, $C_{L,g}^2(w)$ and $C_{L,g}^3(w)$ are the gluon co-efficient function for F_L in LO, NLO and NNLO respectively [15]. The required LO, NLO and NNLO approximation of the gluon co-efficient functions for F_L [15, 18, 19] are defined in Appendix A.

Using the gluon co-efficient functions and the equation (5.2), we can calculate the F_L^g structure function up to NNLO approximation. For this purpose, we have to first

determine the gluon distribution function $G(x,Q^2)$. We calculate this by solving the DGLAP evolution equation for gluon distribution function at small-x using the Regge like behaviour of the gluon distribution function. At small values of x, neglecting the quark singlet part, the DGLAP evolution equation for gluon distribution function is given by [20]

$$Q^2\frac{\partial G(x,Q^2)}{\partial Q^2} = \int_x^1 \frac{dw}{w} P_{gg}(w,Q^2) G\Big(\frac{x}{w},Q^2\Big). \tag{5.4}$$

Here $P_{gg}(w,Q^2)$ is the gluon splitting function known perturbatively up to first few orders in running coupling constant $\alpha_s(Q^2)$ and can be written as

$$P_{gg}(w,Q^2) = \frac{\alpha_s(Q^2)}{2\pi}P^1_{gg}(w) + \Big(\frac{\alpha_s(Q^2)}{2\pi}\Big)^2 P^2_{gg}(w) + \Big(\frac{\alpha_s(Q^2)}{2\pi}\Big)^3 P^3_{gg}(w), \tag{5.5}$$

up to NNLO, where $P^1_{gg}(w)$, $P^2_{gg}(w)$ and $P^3_{gg}(w)$ are the gluon splitting functions [20–22] in LO, NLO and NNLO respectively. At small-x limit the expressions for these splitting functions are defined in Appendix A.

Using the expressions for gluon splitting functions in equation (5.4) and simplifying the DGLAP evolution equations for the gluon distribution function $G(x,Q^2)$ in LO, NLO and NNLO, we get

$$\frac{\partial G(x,t)}{\partial t} = \frac{\alpha_s(t)}{2\pi}\Big[6\Big\{\Big(\frac{11}{12}-\frac{N_f}{18}\Big) + ln(1-x)\Big\}G(x,t) + 6I^1_g(x,t)\Big], \tag{5.6}$$

$$\begin{aligned}\frac{\partial G(x,t)}{\partial t} &= \frac{\alpha_s(t)}{2\pi}\Big[6\Big\{\Big(\frac{11}{12}-\frac{N_f}{18}\Big) + ln(1-x)\Big\}G(x,t) + 6I^1_g(x,t)\Big] \\ &\quad + \Big(\frac{\alpha_s(t)}{2\pi}\Big)^2 I^2_g(x,t),\end{aligned} \tag{5.7}$$

$$\begin{aligned}\frac{\partial G(x,t)}{\partial t} &= \frac{\alpha_s(t)}{2\pi}\Big[6\Big\{\Big(\frac{11}{12}-\frac{N_f}{18}\Big) + ln(1-x)\Big\}G(x,t) + 6I^1_g(x,t)\Big] \\ &\quad + \Big(\frac{\alpha_s(t)}{2\pi}\Big)^2 I^2_g(x,t) + \Big(\frac{\alpha_s(t)}{2\pi}\Big)^3 I^3_g(x,t),\end{aligned} \tag{5.8}$$

where

$$I_g^1(x,t) = \int_x^1 dw \left[\frac{wG\left(\frac{x}{w},t\right) - G(x,t)}{(1-w)} + \left\{ w(1-w) + \frac{1-w}{w} \right\} G\left(\frac{x}{w},t\right) \right], \tag{5.9}$$

$$I_g^2(x,t) = \int_x^1 dw P_{gg}^2(w) G\left(\frac{x}{w},t\right) \tag{5.10}$$

and

$$I_g^3(x,t) = \int_x^1 dw P_{gg}^3(w) G\left(\frac{x}{w},t\right). \tag{5.11}$$

Now, the Regge like behaviour of the gluon distribution function can be expressed as [23]

$$G(x,t) = f(t) x^{-\lambda_g}, \tag{5.12}$$

where $f(t)$ is a function of t and t is defined in chapter 2, and λ_g is the Regge exponent. Now, $G\left(\frac{x}{w},t\right)$ can be written as

$$G\left(\frac{x}{w},t\right) = G(x,t) w^{\lambda_g}. \tag{5.13}$$

Using equations (5.12) and (5.13) in equation (5.6) we get

$$\frac{\partial G(x,t)}{\partial t} = \frac{G(x,t)}{t} P(x), \tag{5.14}$$

where

$$\begin{aligned} P(x) &= \frac{12}{\beta_0} \left[\left(\frac{11}{12} - \frac{N_f}{18} \right) + ln(1-x) \right. \\ &\quad \left. + \int_x^1 dw \left\{ \frac{w^{1+\lambda_g} - 1}{1-w} + w^{\lambda_g} \left(w(1-w) + \frac{1-w}{w} \right) \right\} \right]. \end{aligned} \tag{5.15}$$

Integrating equation (5.14) we get

$$G(x,t) = Ct^{P(x)}, \tag{5.16}$$

where C is a constant of integration and can be determined from experimental data.

Applying initial conditions at $t = t_0$, $G(x,t) = G(x,t_0)$ and at $x = x_0$, $G(x,t) = G(x_0,t)$, the t- and x-evolutions for $G(x,t)$ gluon distribution function in LO can be written as

$$G(x,t) = G(x,t_0)\Big(\frac{t}{t_0}\Big)^{P(x)} \tag{5.17}$$

and

$$G(x,t) = G(x_0,t)t^{[P(x)-P(x_0)]} \tag{5.18}$$

respectively.

Proceeding in the similar manner from equation (5.7)and (5.8), we obtain the t- and x-evolution equations for $G(x,t)$ gluon distribution function in NLO as

$$G(x,t) = G(x,t_0)\frac{t^{(1+\frac{b}{t})Q(x)}}{t_0^{(1+\frac{b}{t_0})Q(x)}} exp\Big[b\Big(\frac{1}{t}-\frac{1}{t_0}\Big)Q(x)\Big] \tag{5.19}$$

and

$$G(x,t) = G(x_0,t)t^{(1+\frac{b}{t})[Q(x)-Q(x_0)]} exp\Big[\frac{b}{t}(Q(x)-Q(x_0))\Big] \tag{5.20}$$

respectively, and in NNLO as

$$G(x,t) = G(x,t_0)\frac{t^{(1+b/t)S(x)}}{t_0^{(1+b/t_0)S(x)}} \exp\left[\begin{array}{c} \Big\{b\Big(\frac{1}{t}-\frac{1}{t_0}\Big)+\Big(\frac{b^2}{2}-\frac{c}{2}\Big)\Big(\frac{1}{t^2}-\frac{1}{t_0^2}\Big) \\ -\frac{b^2}{2}\Big(\frac{ln^2 t}{t^2}-\frac{ln^2 t_0}{t_0^2}\Big)\Big\}S(x) \end{array}\right] \tag{5.21}$$

and

$$G(x,t) = G(x_0,t)t^{(1+b/t)\{S(x)-S(x_0)\}} \cdot \exp\left[\begin{array}{c}\left\{\frac{b}{t}+\left(\frac{b^2}{2}-\frac{c}{2}\right)\left(\frac{1}{t^2}\right)-\frac{b^2}{2}\left(\frac{ln^2t}{t^2}\right)\right\}\\ \{S(x)-S(x_0)\}\end{array}\right] \quad (5.22)$$

respectively. Here

$$Q(x) = [P(x) + T_0R(x)], \qquad R(x) = -27.11\frac{1-x^{\lambda_g}}{\lambda_g} + 98.9\Big(\frac{1-x^{1+\lambda_g}}{1+\lambda_g}\Big),$$

$$S(x) = [P(x) + T_0R(x) + T_1Y(x)], \qquad \text{and} \qquad Y(x) = -149.33\frac{(1-x^{\lambda_g-1})}{\lambda_g-1}.$$

The numerical parameters T_0 and T_1 are calculated from the data as described in chapter 2 and ref. [24]. Here $T_0 = 0.0278$ and $T_1 = 0.00013$ in our required Q^2 range $1.5 \leq Q^2 \leq 800GeV^2$.

Thus we have obtained an analytical expression for the t- and x-evolutions of gluon distribution function $G(x,t)$ in LO, NLO and NNLO. Using the above expressions of gluon distribution function along with the co-efficient functions we have calculated F_L^g structure functions in LO, NLO and NNLO.

In a similar manner, the F_2^g structure function can be determined at small-x with the help of the calculated results of gluon distribution function using the equation [25]

$$F_2^g(x,Q^2) =< e^2 > \int_x^1 dw C_{2,g}(w)G\Big(\frac{x}{w},Q^2\Big). \quad (5.23)$$

Here $C_{2,g}(w)$ is the gluon co-efficient function for F_2 and can be written as

$$C_{2,g}(w,Q^2) = \frac{\alpha_s(Q^2)}{4\pi}C^1_{2,g}(w) + \Big(\frac{\alpha_s(Q^2)}{4\pi}\Big)^2 C^2_{2,g}(w) + \Big(\frac{\alpha_s(Q^2)}{4\pi}\Big)^3 C^3_{2,g}(w) \quad (5.24)$$

up to NNLO, where $C^1_{2,g}(w)$, $C^2_{2,g}(w)$ and $C^3_{2,g}(w)$ are the gluon co-efficient functions [26] for F_2 structure function in LO, NLO and NNLO respectively and are defined in Appendix A.

The measurements of longitudinal structure function F_L are used to determine the DIS cross section ratio R which is related to the structure functions F_2 and F_L as

$$R = \frac{\sigma_L}{\sigma_T} = \frac{F_L}{F_2 - F_L}, \tag{5.25}$$

where σ_L and σ_T are the absorption cross sections of longitudinally and transversely polarized virtual photons by proton. At small-x, F_2 and F_L are gluon dominating and so equation (5.25) can be written as

$$R = \frac{F_L^g}{F_2^g - F_L^g}. \tag{5.26}$$

In analogy with the F_L structure function the ratio R is a good QCD characteristic because it equals zero in the naive parton model. Moreover at small values of x, the ratio R gives the relative strength of the two components of the absorption cross section [6, 27]. Here, we have also studied the behaviour of ratio R at small-x in LO, NLO and NNLO using the calculated values of F_L^g and F_2^g structure function.

5.2 Results and Discussions

We have calculated the t- and x-evolutions of the gluon dominating longitudinal proton structure function F_L at small-x up to next-next-to-leading order approximation using the gluon distribution function. This gluon distribution function is obtained as a result of solution of the DGLAP evolution equation for gluon distribution at small-x. To extract the gluon density inside proton, we use Regge like behaviour of the gluon distribution function. For this purpose, we use the input distribution of gluon from DL model [7], MSTW08 [8], CT10 [9, 10], ABM11 [11] and NNPDF2.3 [12, 13] to obtain t- and x-evolutions of the gluon density. As the values of Regge exponent is close to 0.5 in the region of small-x [28], we have taken its value as 0.5. Thus using the required co-efficient function which are given in Appendix A and gluon distribution

function we have calculated the F_L^g structure function in the range $10^{-4} \leq x \leq 0.1$ and $1.5 \leq Q^2 \leq 800GeV^2$.

The obtained results are compared with the available H1 [1–5], ZEUS [6] experimental data and results of DL model fit [7], MSTW08 [8], CT10 [9, 10], ABM11 [11] and NNPDF2.3 [12, 13] parameterizations. The related plots are shown in figures 5.1 to 5.6 which indicate a good agreement with the experimental data, related fit and parameterizations. In all the graphs, the lowest-Q^2 and highest-x points are taken as input for $G(x, t_0)$ and $G(x_0, t)$ respectively. Here, the vertical error bars are both statistical and systematic errors for both H1 and ZEUS data. To confirm that in spite of the large uncertainty in the experimental data, our results are in good agreement with the data, we add DL model results and the theoretical prediction of different parameterizations in all the figures. Figure 5.1 represents the t-evolution results of F_L^g structure function which show that our results are compatible with the data and the results of DL model. Here the structure function increases with the increase of Q^2. The x-evolution results are depicted in figure 5.2 to 5.6 which reflect better agreement of our results with data and results of the model and parameterizations. These graphs describe that the behaviour of structure function F_L^g increases towards small values of x. In case of the x-evolution results described in figure 5.2 to figure 5.6, the behaviour of LO, NLO curves are not exactly the same as we have considered the input point from different parameterizations. In all the graphs it is observed that our results show good agreement with data, related model fit and parameterizations as the energy scale becomes larger. It is observed from the t- and x-evolutions results that the behaviour of the LO, NLO and NNLO curves are different in both the cases. Thee reason for this is that the expressions for the calculation of t- and x-evolutions are different and the behaviour of LO, NLO, NNLO curves depends on the expressions only. Moreover, with reference to some recent papers [29–32], we can say that the pattern of LO, NLO, NNLO curves (i.e., sometimes NLO results overestimate LO prediction and vice versa)

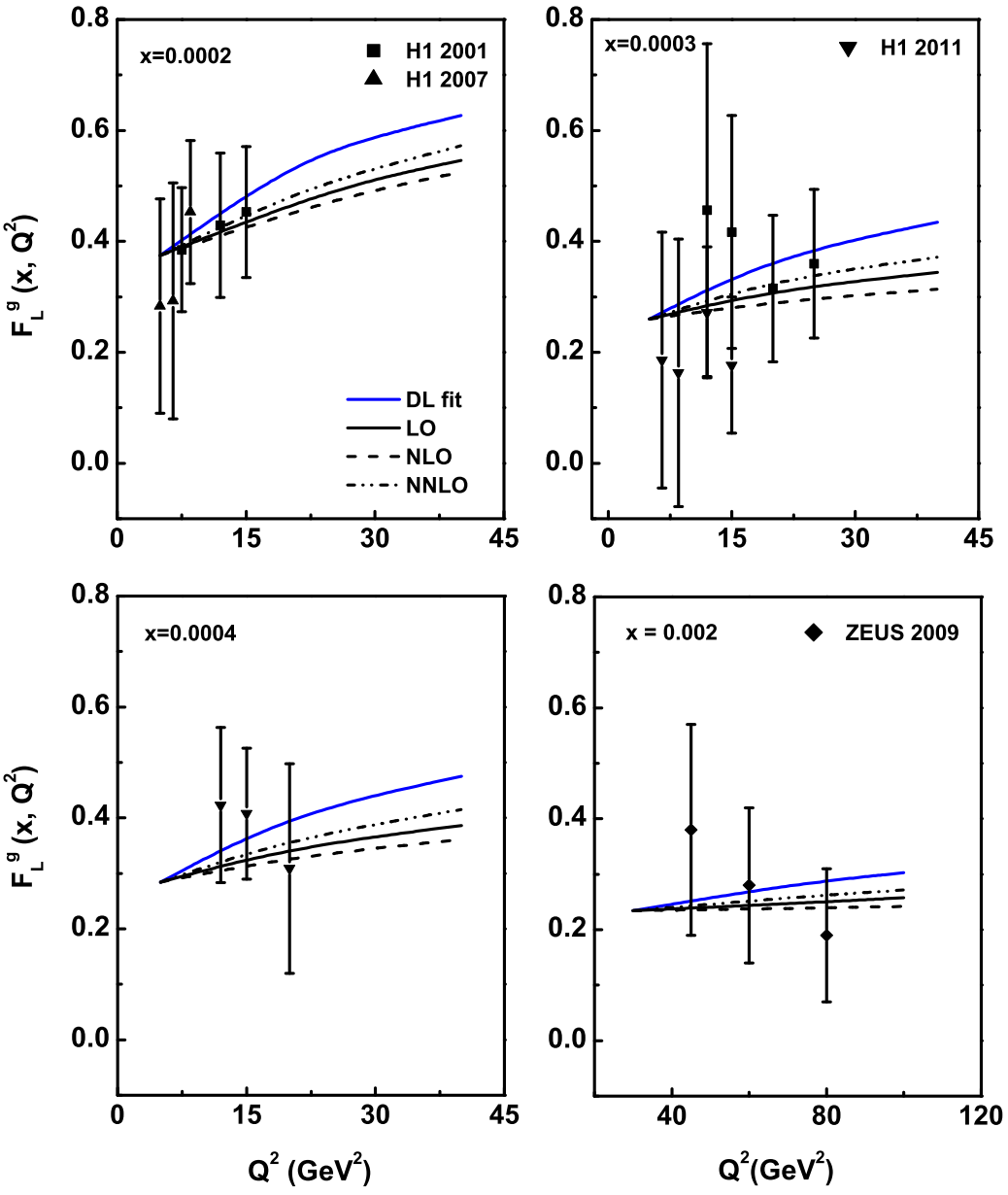

Figure 5.1: t-evolution results of F_L^g structure function up to NNLO using Regge theory in comparison with the H1, ZEUS data and results of DL model.

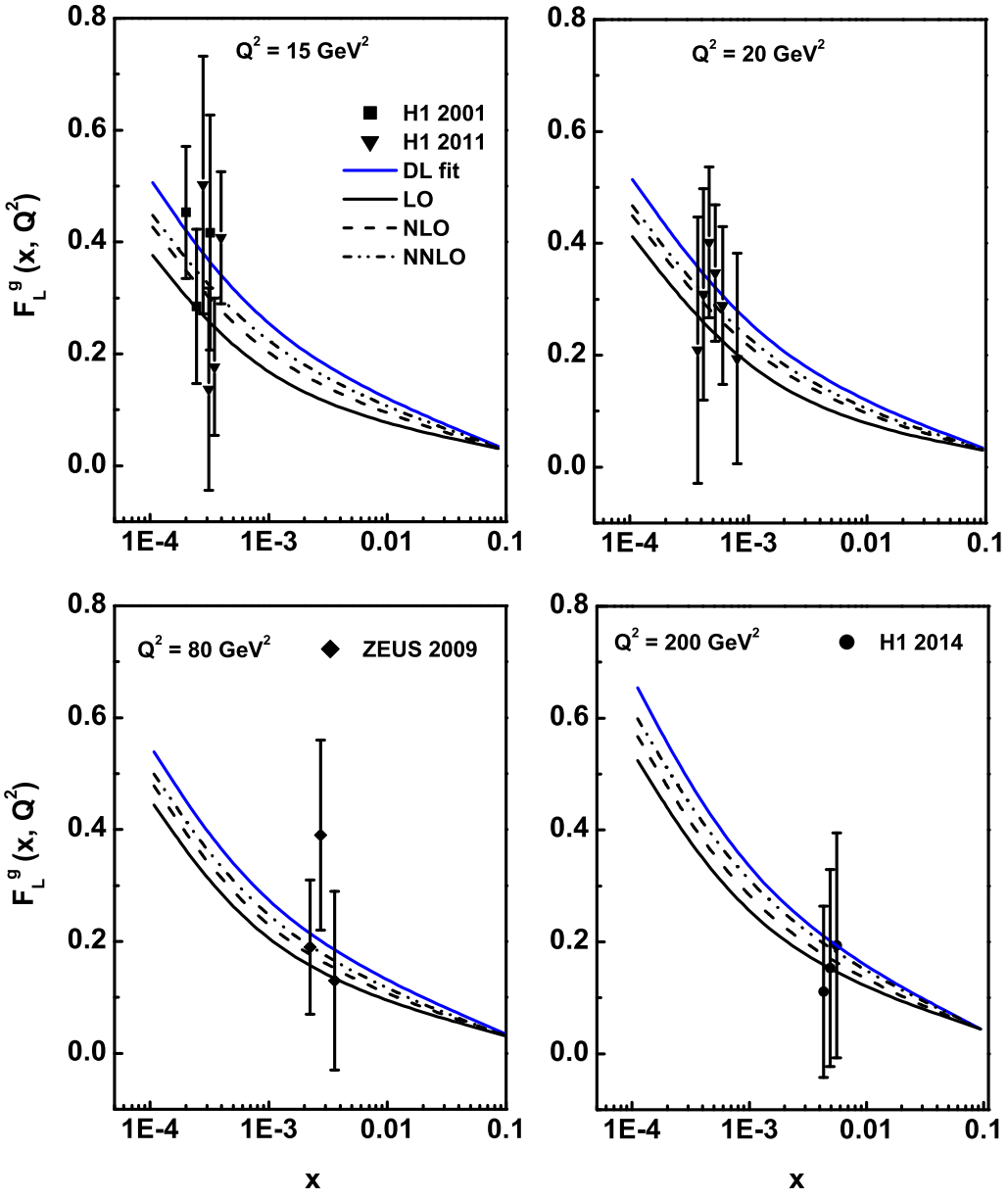

Figure 5.2: x-evolution results of F_L^g structure function up to NNLO using Regge theory in comparison with the H1, ZEUS data and results of DL model.

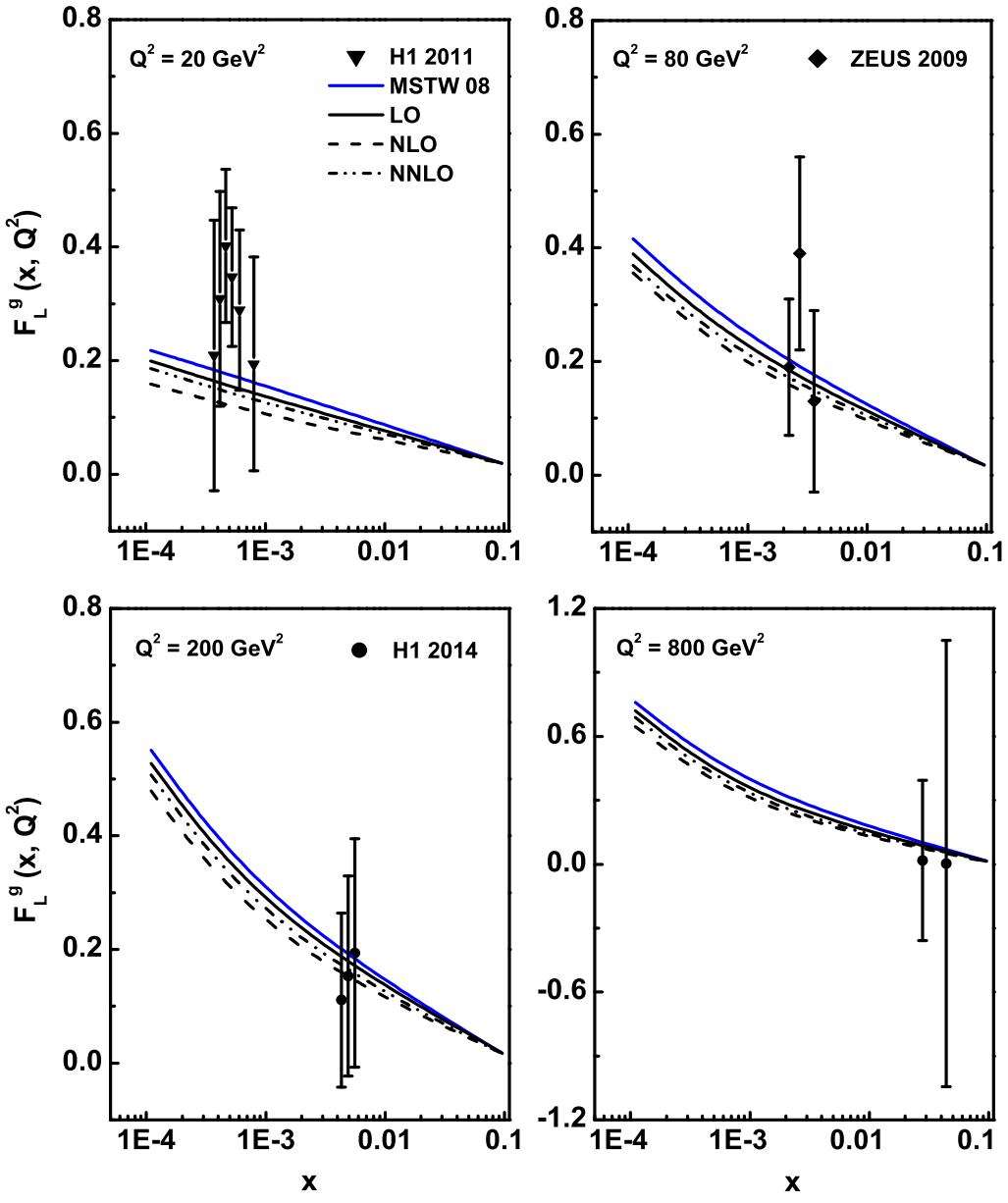

Figure 5.3: x-evolution results of F_L^g structure function up to NNLO using Regge theory in comparison with the H1, ZEUS data and the theoretical prediction of MSTW08.

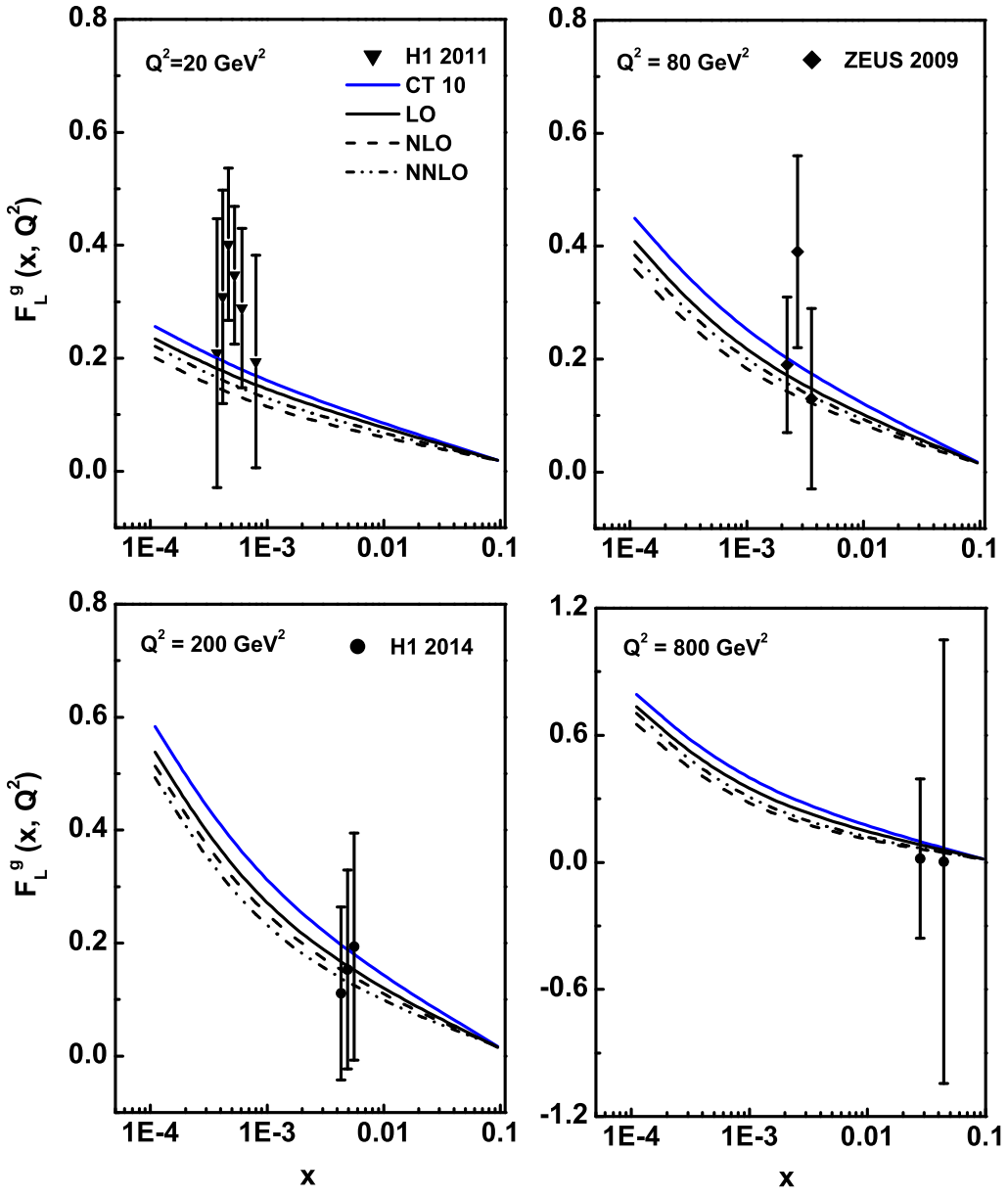

Figure 5.4: x-evolution results of F_L^g structure function up to NNLO using Regge theory in comparison with the H1, ZEUS data and the theoretical prediction of CT10.

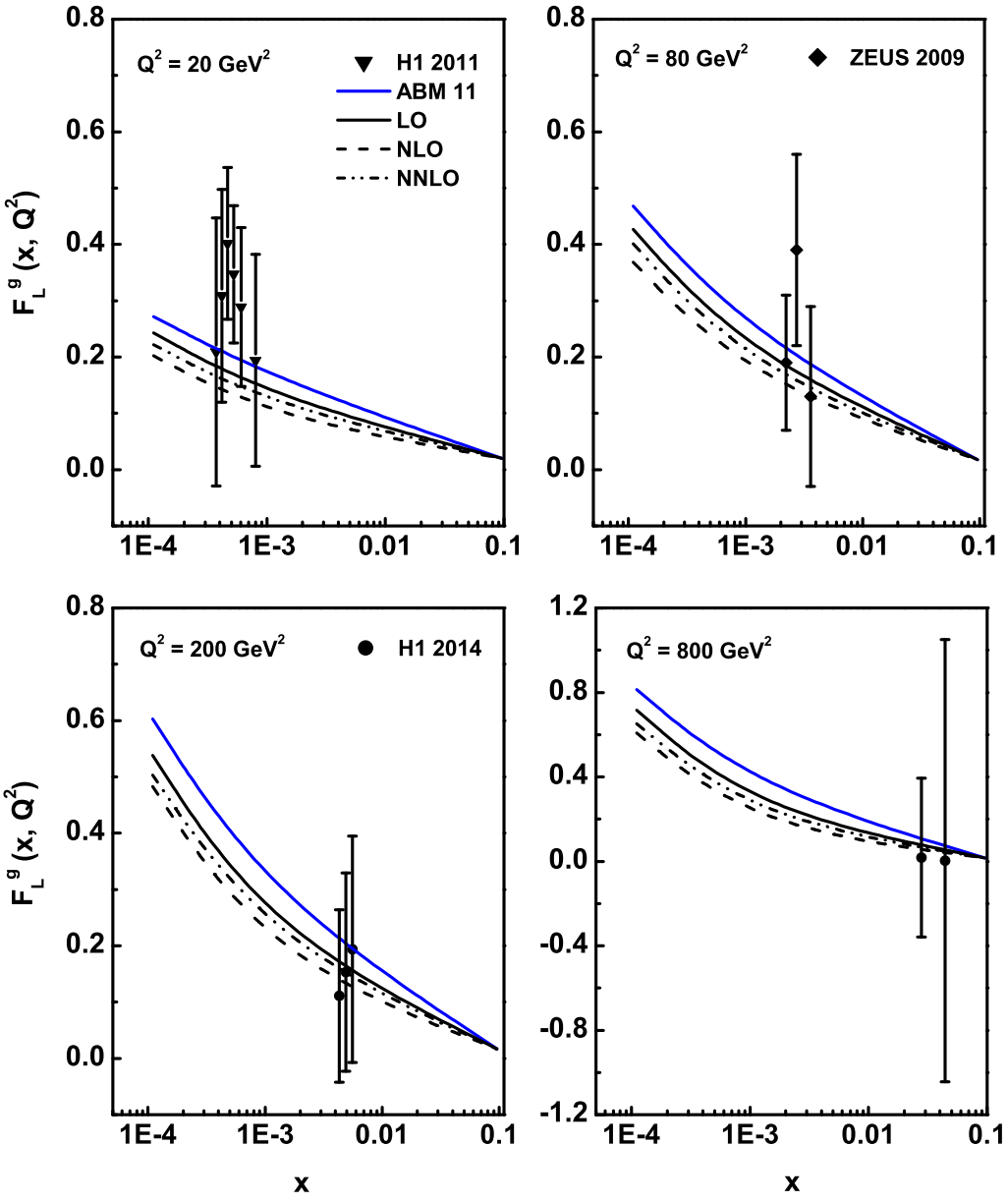

Figure 5.5: x-evolution results of F_L^g structure function up to NNLO using Regge theory in comparison with the H1, ZEUS data and the theoretical prediction of ABM11.

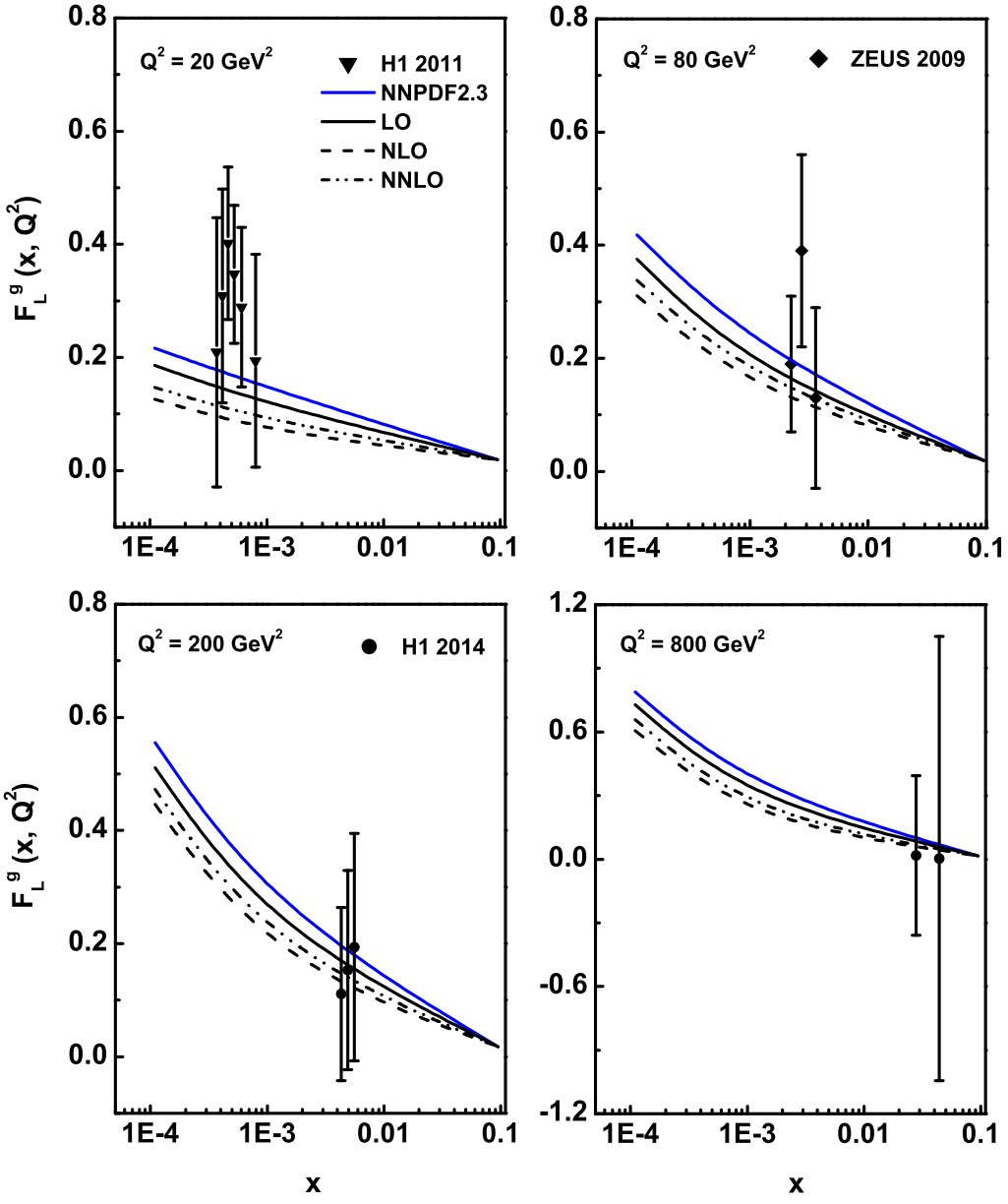

Figure 5.6: x-evolution results of F_L^g structure function up to NNLO using Regge theory in comparison with the H1, ZEUS data and the theoretical prediction of NNPDF2.3.

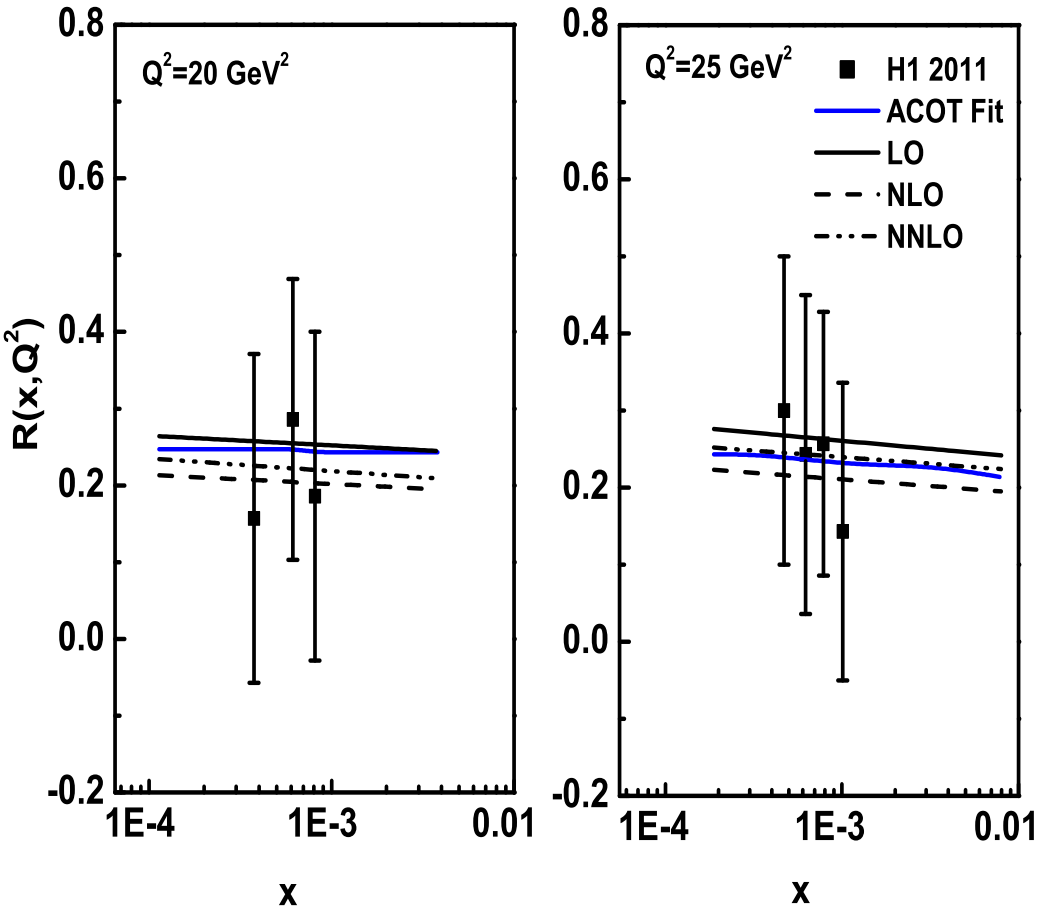

Figure 5.7: x-evolution results of R in comparison with the H1 data and the theoretical prediction of ACOT fit.

depend only on the applied method.

We have also calculated the cross section ratio R using the results of the F_2^g and F_L^g structure functions from equations (5.2) and (5.23). In figure 5.7, the ratio R is plotted against x for different values of Q^2 in comparison with the H1 data and the prediction of DGLAP fit in the ACOT scheme [33]. ACOT scheme incorporates the heavy quark mass into the theoretical calculations of massive partonic cross section.

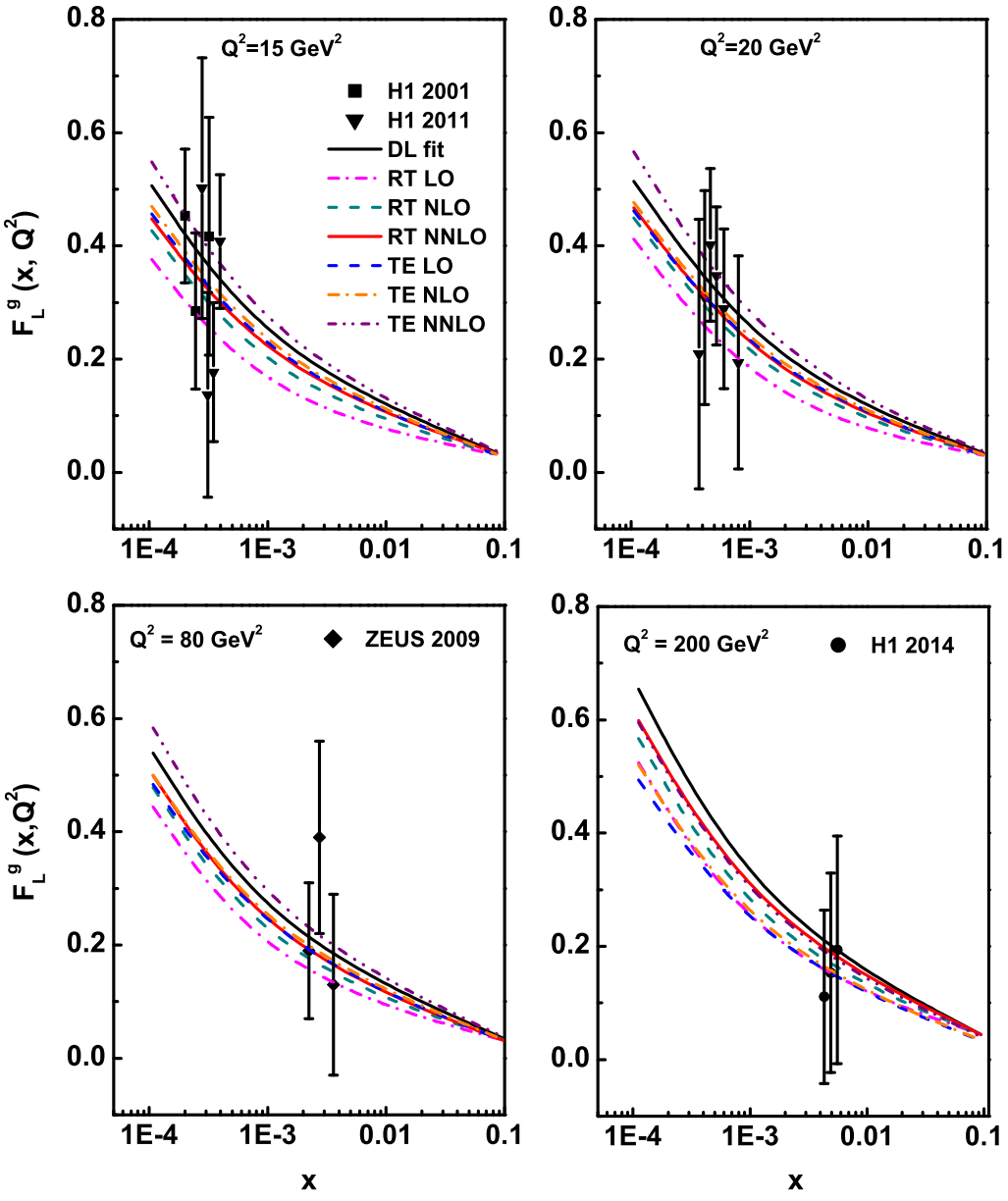

Figure 5.8: Comparison of x-evolution results of F_L^g structure function up to NNLO using Regge theory (RT) and Taylor expansion (TE) method in comparison with the H1, ZEUS data and the of DL model.

Here they have used the QCDNUM program [34] for the DGLAP evolution which helps to generate the PDFs from an initial distribution based on the Les Houches benchmark set [35]. Together with the precise HERA data, these calculations facilitate accurate determination of PDFs. We have analyzed the behaviour of the ratio R for two values of $Q^2 = 20GeV^2, 25GeV^2$ which indicate good agreement with the experimental data and fit. It has been observed in the H1 experimental results that for $Q^2 \geq 3.5GeV2$, the ratio R is consistent with a constant behaviour [1]. Our analysis also shows constant behavior with respect to x for fixed values of Q^2. The constant behaviour of the cross section ratio implies that its behaviour is independent of the behaviour of gluon distribution function with respect to x at small-x.

5.2.1 Comparative study of our results obtained by Regge theory and Taylor expansion method

We have also presented a comparison of our x-evolution results and the results obtained in the chapter 4 which is shown in figure 5.8. These two results are actually the results of F_L^g structure function obtained by Regge theory (RT) and Taylor expansion (TE) method. The comparison of the results of F_L structure function obtained in both the cases shows similar behaviour with the model fit and data. Thus one can determine the evolution of structure function using both the methods.

5.3 Conclusions

In this chapter, we have calculated the gluon dominating longitudinal structure function F_L^g of proton up to NNLO approximation from DGLAP evolution equation for gluon distribution function at small-x using the Regge like behaviour of the gluon distribution function. The evolutions of F_L structure function with x and Q^2 reflects similar nature with the experimental data which shows the compatibility of Regge behaviour with the perturbative evolution of structure function at small-x. To confirm the validity of our

calculations we compare our results with the recent experimental data taken by H1 and ZEUS collaborations along with the DL model results and the theoretical prediction of different parameterizations. Our results are in good agreement with the data and related fits. As in our given range of x, the gluon contribution to the structure function is dominant one, so we can conclude in general that the gluon contribution to the longitudinal structure function increases with the decreasing values of x. We have also calculated the cross section ratio R which indicates good agreement with the H1 data and DGLAP fit in the ACOT scheme. Its variation with small values of Bjorken variable x and fixed Q^2 shows constant behaviour similar to that of the experimental data and fit. From the constant behaviour of the cross section ratio R with respect to x, we can conclude that its behaviour does not depend on the behaviour of gluon distribution function with respect to x and fixed Q^2 at small-x. The comparative analysis of our x-evolution results with that of the results obtained in chapter 4 show good agreement with data and the related model fit. In chapter 4, Taylor expansion method is used to evaluate the structure function. Thus, we can conclude that both Regge theory and Taylor expansion method can be used to study the behaviour of the structure function in small-x region.

References

[1] Aaron, F. D., et al. Measurement of the inclusive $e^{\pm}p$ scattering cross section at high inelasticity y and of the structure function F_L, *Eur. Phys. J. C.* **71** (3), 1579-1–50, 2011.

[2] Adloff, C., et al. Deep-inelastic inclusive ep scattering at low x and a determination of α_s, *Eur. Phys. J. C.* **21** (1), 33–61, 2001.

[3] Pardos, C. D. *Studies for the direct measurement of the proton structure function F_L with the H1 detector at HERA*, Ph.D. thesis, DESY, Zeuthen, Germany, 2007.

[4] Piec, S. *Measurement of the Proton Structure Function F_L with the H1 Detector at HERA*, Ph.D. thesis, Humboldt University of Berlin, Germany, 2009.

[5] Andreev, V., et al. Measurement of Inclusive *ep* Cross Sections at High Q^2 at $\sqrt{s} = 225$ and $252GeV$ and of the Longitudinal Proton Structure Function F_L at HERA, *Eur. Phys. J. C* **74** (4), 2814-1–26, 2014.

[6] Chekanov, S., et al. Measurement of the longitudinal proton structure function at HERA, *Phys. Lett. B* **682** (1), 8–22, 2009.

[7] Donnachie, A. and Landshoff, P. V. The protons gluon distribution, *Phys. Lett. B* **550** (3-4), 160–165, 2002.

[8] Martin, A. D., et al. Parton distributions for the LHC, *Eur. Phys. J. C* **63** (2), 189–285, 2009.

[9] Hung-Liang, Lai., et al. New parton distributions for collider physics, *Phys. Rev. D* **82** (7), 074024-1–24, 2010.

[10] Jun, Gao., et al. CT10 next-to-next-to-leading order global analysis of QCD, *Phys. Rev. D* **89** (3), 033009-1–28, 2014.

[11] Alekhin, S., Bluemlein, J. and Moch, S. The ABM parton distributions tuned to LHC data, *Phys. Rev. D* **89** (5), 054028-1–21, 2014.

[12] Ball, R. D., et al. Parton distributions with LHC data, *Nucl. Phys. B* **867** (2), 244–289, 2013.

[13] Forte, S., et al. Heavy quarks in deep-inelastic scattering, *Nucl. Phys. B* **834** (1-2), 116–162, 2010.

[14] Altarelli, G. and Martinelli, G. Transverse momentum of jets in electroproduction from quantum chromodynamics, *Phys. Lett. B* **76** (1), 89–94, 1978.

[15] Moch, S., Vermaseren, J. A. M. and Vogt, A. The longitudinal structure function at the third order, *Phys. Lett. B* **606** (1-2), 123–129, 2005.

[16] Cooper-Sarkar, A. M., et al. Measurement of the longitudinal structure function and the small x gluon density of the proton, *Z. Phys. C* **39** (2), 281–290, 1988.

[17] Abbott, L. F., Atwood, W. B. and Barnett, R. M. Quantum-chromodynamic analysis of eN deep-inelastic scattering data, *Phys. Rev. D* **22** (3), 582–593, 1980.

[18] Zijlstra, E. B. and Van Neerven, W. L. Contribution of the second order gluonic Wilson coefficient to the deep inelastic structure function, *Phys. Lett. B* **273** (4), 476–482, 1991.

[19] Moch, S. and Vermaseren, J. A. M. Deep-inelastic structure functions at two loops, *Nucl. Phys. B* **573** (3), 853–907, 2000.

[20] Furmanski, W. and Petronzio, R. Singlet parton densities beyond leading order, *Phys. Lett. B* **97** (3-4), 437–442, 1980.

[21] Altarelli, G. and Parisi, G. Asymptotic freedom in parton language, *Nucl. Phys. B* **126** (2), 298–318, 1977.

[22] Ellis, R. K., Kunszt, Z. and Levin, E. M. The evolution of parton distributions at small x, *Nucl. Phys. B* **420** (3), 517–549, 1994.

[23] Kotikov, A. V. and Parente, G. The gluon distribution as a function of F_2 and $dF_2/dlnQ^2$ at small x. The next-to-leading analysis, *Phys. Lett. B* **379** (1-4), 195–201, 1996.

[24] Baishya, R. and Sarma, J. K. Semi numerical solution of non-singlet DokshitzerGribovLipatovAltarelliParisi evolution equation up to next-to-next-to-leading order at small x, *Eur. Phys. J. C* **60** (4), 585–591, 2009.

[25] Vermaseren, J. A. M., Vogt, A. and Moch, S. The third-order QCD corrections to deep-inelastic scattering by photon exchange, *Nucl. Phys. B* **724** (1-2), 3–182, 2005.

[26] Neerven, W. L. Van and Vogt, A. NNLO evolution of deep-inelastic structure functions: the singlet case, *Nucl. Phys. B* **588** (1-2), 345–373, 2000.

[27] Aaron, F. D., et al. Combined measurement and QCD analysis of the inclusive e p scattering cross sections at HERA, *J. High Energy Phys.* **2010** (1), 109-1–63, 2010.

[28] Martin, A. D., Ryskin, M. G. and Watt, G. Simultaneous QCD analysis of diffractive and inclusive deep-inelastic scattering data, *Phys. Rev. D* **70** (9), 091502-1–5, 2004.

[29] Rezaei, B. and Boroun, G. R. Analytical solution of the longitudinal structure function F_L in the leading and next-to-leading-order analysis at low x with respect to Laguerre polynomials method, *Nucl. Phys. A* **857** (1), 42–47, 2011.

[30] Nematollahi, H., Yazdanpanah, M. M. and Mirjalili, A. NNLO longitudinal proton structure function, based on the modified χQM, *Mod. Phys. Lett. A* **27** (31),1250179-1-11 ,2012.

[31] Boroun, G. R. and Rezaei, B. Analysis of the proton longitudinal structure function from the gluon distribution function, *Eur. Phys. J. C* **72** (11), 2221-1-5, 2012.

[32] Devee, M., Baishya, R. and Sarma, J. K. Evolution of singlet structure functions from DGLAP equation at next-to-next-to-leading order at small-x, *Eur. Phys. J. C* **72** (6), 2036-1-11, 2012.

[33] Kramer, M., Olness, F. I. and Soper, D. E. Treatment of heavy quarks in deeply inelastic scattering, *Phys. Rev. D* **62** (9), 096007-1–9, 2000.

[34] Botje, M. QCDNUM: Fast QCD evolution and convolution, *Comput. Phys. Commun.* **182** (2), 490–532, 2011.

[35] Giele, W., et al. The QCD/SM Working Group: Summary Report, FERMILAB-Conf-02/410 (2004), arXiv:hep-ph/0204316. □

Chapter 6

Heavy Quark Contribution to Longitudinal Structure Function F_L and the Ratio $R^h = \frac{F_L^h}{F_2^h}$ at Small-x

The dominant process for the heavy quark (charm and beauty quarks) production at HERA is the boson gluon fusion (BGF), where the photon interacts with a gluon from the proton by the exchange of a heavy quark pair and is given as $\gamma g \to q\bar{q}X$, with $q = c, b$ [1]. This reflects that the process is sensitive to the gluon density in the proton. Thus, the structure functions $F_k^h(k = 2, L; h = c, b)$ are dominated by the gluon content of the proton. The charm structure function F_2^c and the beauty structure function F_2^b are obtained from the measured charm and beauty cross sections after applying small corrections for the longitudinal structure functions F_L^c and F_L^b. At small values of x, F_L becomes non-negligible and its contribution should be properly taken into account while F_2 is extracted from the measured values of cross section. The same is also true for the contributions F_L^h to F_2^h due to the heavy quarks. In this chapter, the behaviour of heavy quark structure functions F_k^h with respect to Bjorken variable x are studied using Taylor expansion method and Regge behaviour of structure function at small-x. Here, we use the input distribution of gluon from Donnachie-Landshoff (DL) model [2] to determine the heavy flavour structure function of proton. The obtained results are compared with the recent HERA data [3, 4] and results of DL, Colour Dipole [5] models (CDM) and MSTW08 [6] parameterization which show good agreement with data and fit. We have used our results of heavy flavour structure function to analyze the behaviour of heavy

quark DIS cross section ratio $R^h(x,Q^2)$ and reduced cross section σ_r^h in heavy quark lepto-production at small values of x. We have also studied the behaviour of the heavy quark content of the F_L structure functions with respect to x.

6.1 Theory

6.1.1 Heavy quark contribution to F_L structure function using Taylor expansion method

In the small-x region, the heavy quark structure function is given by [7–9]

$$F_k^h(x,Q^2,m_h^2) = e_h^2 \frac{\alpha_s(\mu^2)}{\pi} \int_{ax}^1 \frac{dw}{w} C_{k,g}^h(w,\zeta) G\Big(\frac{x}{w},\mu^2\Big), \tag{6.1}$$

where $a = 1 + 4\zeta(\zeta = \dfrac{m_h^2}{Q^2})$, $m_h; (h = c,b)$ is the mass of the heavy quark and the renormalization scale μ is assumed to be either $\mu^2 = 4m_h^2$ or $\mu^2 = 4m_h^2 + Q^2$. $C_{k,g}^h; (k = 2, L)$ is the heavy quark co-efficient function which can be written up to NLO as [9]

$$C_{k,g}^h(w,\zeta) \rightarrow C_{k,g}^{(0)}(w,\zeta) + a_s(\mu^2)\Big[C_{k,g}^{(1)}(w,\zeta) + \overline{C}_{k,g}^{(1)}(w,\zeta) ln\frac{\mu^2}{m_h^2}\Big]. \tag{6.2}$$

Here $a_s(\mu^2) = \dfrac{\alpha_s(\mu^2)}{4\pi}$ and in NLO analysis

$$\alpha_s(\mu^2) = \frac{4\pi}{\beta_0 ln(\mu^2/\Lambda^2)} - \frac{4\pi\beta_1}{\beta_0^3} \frac{lnln(\mu^2/\Lambda^2)}{ln(\mu^2/\Lambda^2)}. \tag{6.3}$$

The co-efficient functions $C_{k,g}^{(0)}$ and $C_{k,g}^{(1)}$, $\overline{C}_{k,g}^{(1)}$ are at LO and NLO respectively. These have been computed up to NLO in ref. [7–10] and the expressions are given in Appendix B.

At small values of x we can rewrite the equation (6.1) by substituting $w = 1 - z$ as

$$F_k^h(x,Q^2) =< e^2 > \frac{\alpha_s(\mu^2)}{\pi} \int_0^{1-ax} \frac{dz}{1-z} C_{k,g}^h(1-z,\zeta) G\Big(\frac{x}{1-z},\mu^2\Big), \tag{6.4}$$

where F_k^h is derived from the integrated gluon distribution function $G(x,\mu^2)$. An approximate relationship between F_k^h and gluon distribution can be obtained from the expansion of $G\Big(\frac{x}{1-z},\mu^2\Big)$ around a particular choice of point of expansion. Since $ax < w < 1$, we have $0 < z < 1-ax$; so the series $\frac{x}{w} = \frac{x}{1-z}$ is convergent for $|z| < 1$. So, we can take the point of expansion z as any value between $0 \leq z < 1$.

Using the Taylor expansion method for the gluon distribution function at an arbitrary point $z = 0.8$ as described in chapter 4, and neglecting the higher order terms at small-x, $G\Big(\frac{x}{1-z},\mu^2\Big)$ can be written as

$$\begin{aligned} G\Big(\frac{x}{1-z},\mu^2\Big)\Big|_{z=0.8} &= G(z=0.8,\mu^2) + (z-0.8)\frac{\partial G(z=0.8,\mu^2)}{\partial x} \\ &= G(5x,\mu^2) + (z-0.8)\frac{\partial G(5x,\mu^2)}{\partial x}. \end{aligned} \tag{6.5}$$

Using equation (6.5) and leading order terms of equation (6.2) in equation (6.4) and performing the integration, we get

$$F_k^h(x,Q^2) = e_h^2\frac{\alpha_s(\mu^2)}{\pi}A(x)G\Big(5x+\frac{B(x)}{A(x)},\mu^2\Big) \tag{6.6}$$

where

$$A(x) = \int_0^{1-ax}\frac{dz}{1-z}[C_{k,g}^0(1-z)], \tag{6.7}$$

$$B(x) = \int_0^{1-ax}\frac{dz}{1-z}(z-0.8)[C_{k,g}^0(1-z)], \tag{6.8}$$

This result shows that the charm and beauty quark structure functions $F_k^h(x,Q^2)(k = 2, L; h = c, b)$ can be calculated using the low x gluon density from DL model [2] at LO. Similarly, we have also obtained the expression for the structure functions $F_k^h(x,Q^2)$ in NLO using the respective co-efficient function which is given by

$$F_k^h(x,Q^2) = e_h^2\frac{\alpha_s(\mu^2)}{\pi}P(x)G\Big(5x+\frac{Q(x)}{P(x)},\mu^2\Big), \tag{6.9}$$

$$P(x) = \int_0^{1-ax} \frac{dz}{1-z}\Big[C^0_{k,g}(1-z) + T_0\{C^1_{k,g}(1-z) + C^1_{k,g}(1-z)\}\Big] \tag{6.10}$$

and

$$Q(x) = \int_0^{1-ax} \frac{dz}{1-z}(z-0.8)\Big[C^0_{k,g}(1-z) + T_0(C^1_{k,g}(1-z) + C^1_{k,g}(1-z))\Big]. \tag{6.11}$$

Here, the numerical parameter T_0 is calculated from the data as described in chapter 2 and ref. [11]. Here $T_0 = 0.0278$ in our required Q^2 range $15 \leq Q^2 \leq 600GeV^2$.
Thus, we have calculated the charm and beauty quark structure functions F_L^c and F_2^c, F_L^b and F_2^b from the above equations (6.6) and (6.9)using the small-x gluon density from Donnachie Landshoff model [2].

The measurement of heavy quark structure function F_k^h are used to study the behaviour of DIS cross section ratio R^h which is related to the structure functions at small-x as

$$R^h = \frac{F_L^h}{F_2^h}. \tag{6.12}$$

Thus using the expressions for F_k^h, we get the LO and NLO relation for R^h as

$$R^h = \frac{A_L(x)}{A_2(x)} \tag{6.13}$$

and

$$R^h = \frac{P_L(x)}{P_2(x)}. \tag{6.14}$$

respectively.

The above expressions (6.13) and (6.14) show that the ratio is independent of the gluon distribution function and it depends only on the co-efficient function. Here, $A_L(x)$, $A_2(x)$, $P_L(x)$ and $P_2(x)$ are obtained by putting $k = L, 2$ in equations (6.7)and (6.10).

This ratio of structure function is useful to extract the heavy quark structure function from the reduced heavy quark cross section [3] at HERA. We have used this ratio R^h to determine the heavy quark reduced cross section at small-x.

Now the reduced cross section in terms of heavy quark structure function is given by

$$\begin{aligned}\sigma_r^h &= \frac{d^2\sigma^h}{dxdQ^2}\cdot\frac{xQ^4}{2\pi\alpha^2 Y_+} \\ &= F_2^h(x,Q^2,m_h^2) - \frac{y^2}{Y_+}F_L^h(x,Q^2,m_h^2) \\ &= F_2^h(x,Q^2,m_h^2)\Big(1-\frac{y^2}{Y_+}R^h\Big). \end{aligned} \tag{6.15}$$

Here $y=\frac{Q^2}{sx}$ is the inelasticity, with s the ep center-of-mass energy squared and $Y_+ = 1+(1-y)^2$. The above equation (6.15) relates the charm quark structure function to the reduced cross section via the ratio R^c. Thus, the behaviour of the ratio R^c and reduced cross section σ_r^c can be studied using the expressions (6.13), (6.14) and (6.15) with respect to the Bjorken variable x.

Again, the heavy quark content of the proton longitudinal structure function $K_L^h(x,Q^2,m_h^2)$ at small-x is determined using the relation [12]

$$K_L^h(x,Q^2,m_h^2) = \frac{F_L^h(x,Q^2,m_h^2)}{F_L^h(x,Q^2,m_h^2)+F_L^g(x,Q^2)}. \tag{6.16}$$

Here we have used the results of F_L^g from chapter 4 to calculate the quantity K_L^h.

6.1.2 Heavy quark contribution to F_L structure function using Regge approach

In the small-x region, the heavy quark structure function is given by [7–9]

$$F_k^h(x,Q^2,m_h^2) = e_h^2\frac{\alpha_s(\mu^2)}{\pi}\int_{ax}^1\frac{dw}{w}C_{k,g}^h(w,\zeta)G\Big(\frac{x}{w},\mu^2\Big), \tag{6.17}$$

where a, $m_h; (h = c, b)$, μ and $C^h_{k,g}; (k = 2, L)$ are mentioned in the previous subsection i.e., (6.1.1).

Now, the Regge like behaviour of the gluon distribution function can be expressed as [13]

$$G(x, \mu^2) = f(\mu^2) x^{-\lambda_g}, \tag{6.18}$$

where $f(\mu^2)$ is a function of μ^2 and λ_g is the Regge exponent. Now, $G\Big(\frac{x}{w}, \mu^2\Big)$ can be written as

$$G\Big(\frac{x}{w}, \mu^2\Big) = G(x, \mu^2) w^{\lambda_g}. \tag{6.19}$$

Using equations (6.18) and (6.19) in equation (6.17) we get

$$F^h_k(x, Q^2, m^2_h) = e^2_h \frac{\alpha_s(\mu^2)}{\pi} \int_{ax}^1 \frac{dw}{w} C^h_{k,g}(w, \zeta) w^{\lambda_g} G(x, \mu^2). \tag{6.20}$$

Using the above equation we have calculated the charm and beauty quark structure function in LO and NLO using the respective co-efficient functions and the low x gluon density from DL model [2]. We have also calculated the heavy quark DIS cross section ratio R^h and reduced cross section σ^h_r using the expressions (6.12) and (6.15) with the help of the results of F^h_k obtained from the equation (6.20). Lastly, to evaluate the quantities K^c_L and K^b_L using relation (6.16), we have used the results of F^g_L from chapter 5.

6.2 Results and Discussions

In this chapter, we have determined the charm and beauty quark structure functions $F^h_k(k = 2, L; h = c, b)$, ratio of heavy quark structure function R^h and reduced cross section σ^h_r in NLO approximation using Taylor expansion method and Regge like behaviour of structure function. Here we have compared our calculated results with

recent experimental H1, ZEUS data, results of DL, CD model, MSTW08 parameterization and results obtained by other author. Inclusive charm and beauty cross sections are measured in e^-p and e^+p neutral current collisions at HERA in the kinematic range $2 \times 10^{-4} \leq x \leq 0.05$ and $5 \leq Q^2 \leq 2000 GeV^2$. In our analysis, we have studied the behaviour of our results in the range $10^{-4} \leq x \leq 0.1$ and $20 \leq Q^2 \leq 600 GeV^2$.

6.2.1 Charm quark contribution to structure functions

(A)Results using Taylor expansion method

The charm structure functions F_L^c and F_2^c have been determined from the expressions (6.6) and (6.9) using the respective charm quark co-efficient functions in LO, NLO and the gluon distribution function of DL model. Here the gluon distribution function is expanded at $z = 0.8$ using the Taylor expansion method.

Figures 6.1 and 6.2 describe the behaviour of F_L^c and F_2^c structure functions with respect to x. Here the results of F_2^c structure functions are compared with recent H1 and ZEUS data. Both the charm quark components of the structure function increase towards small values of x for fixed Q^2 values. To confirm the behaviour of these structure functions we have also calculated the ratio of charm quark structure function R^c and the charm quark reduced cross section σ_r^c using the relations (6.13), (6.14) and (6.15). Figure 6.3 shows the behaviour of the predicted ratio R^c as a function of x for fixed values of Q^2. It is observed that this ratio is almost independent of x at small values of x irrespective of Q^2 values. The plots in figure 6.4 show the results of reduced cross section σ_r^c in comparison with H1 [3] and ZEUS [4] data. We have also compared our results of charm quark component of structure functions F_L^c and F_2^c with the DL, colour dipole model (CDM) [5] and results obtained by Boroun et al (GRB) [14] which are depicted in figures 6.5 and 6.6. In color dipole model the excitation of heavy flavors in DIS at small-x is described in terms of interaction of small size quark-antiquark color dipoles in the photon [5]. In a recent paper [14], Boroun et al have reported

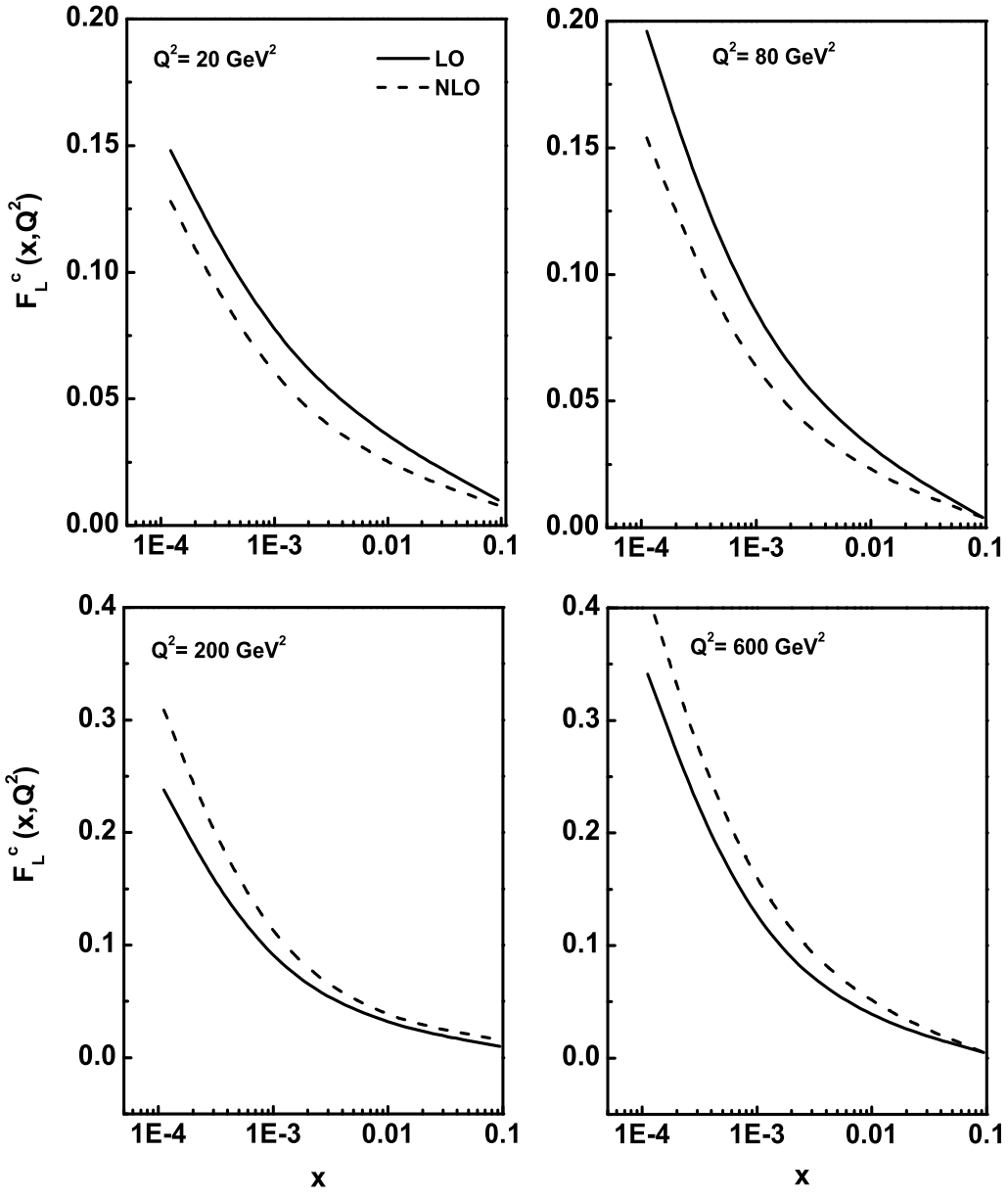

Figure 6.1: x-evolution results of F_L^c structure function using Taylor expansion method with the input gluon distribution from DL model.

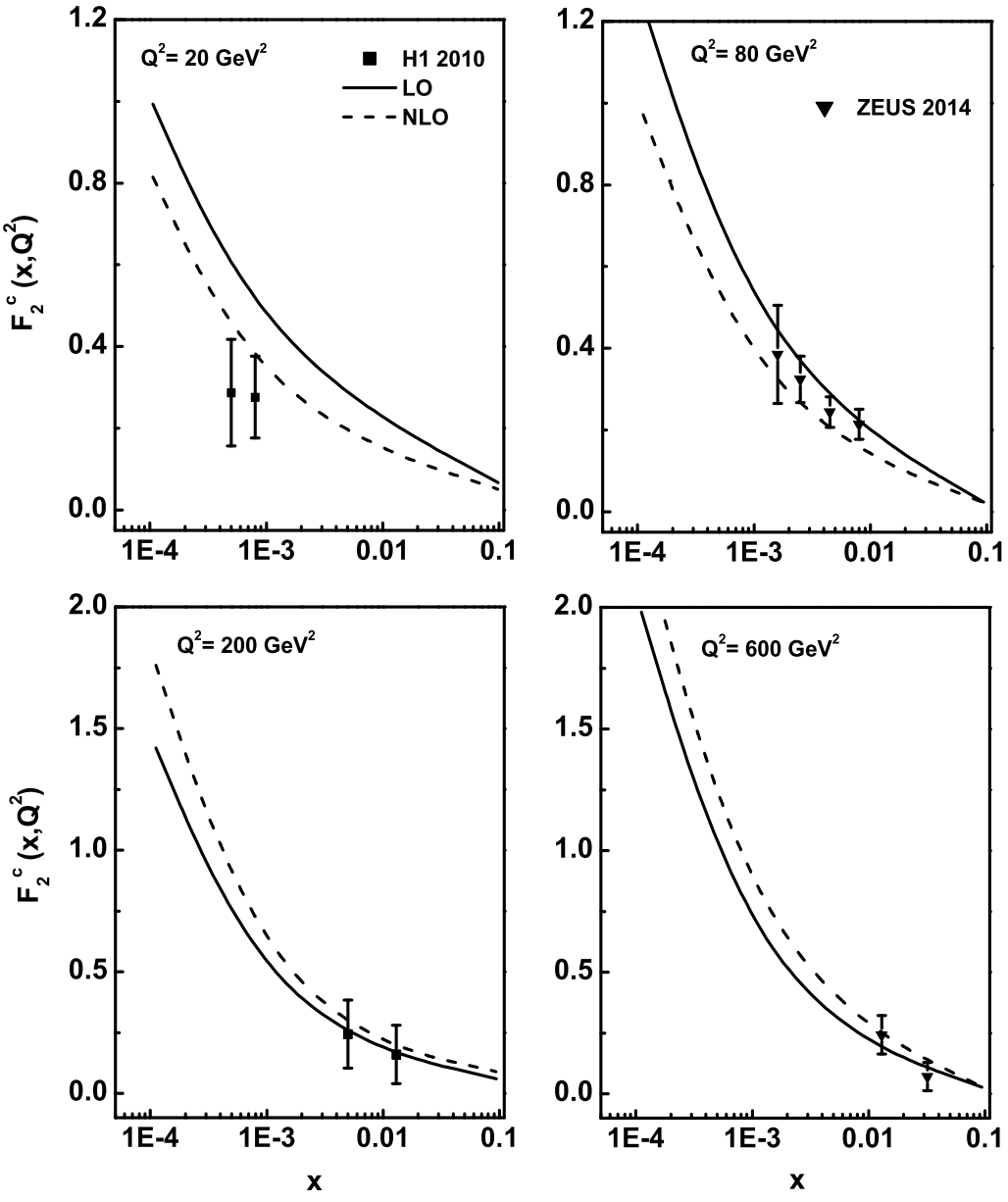

Figure 6.2: x-evolution results of F_2^c structure function using Taylor expansion method in comparison with the H1, ZEUS data.

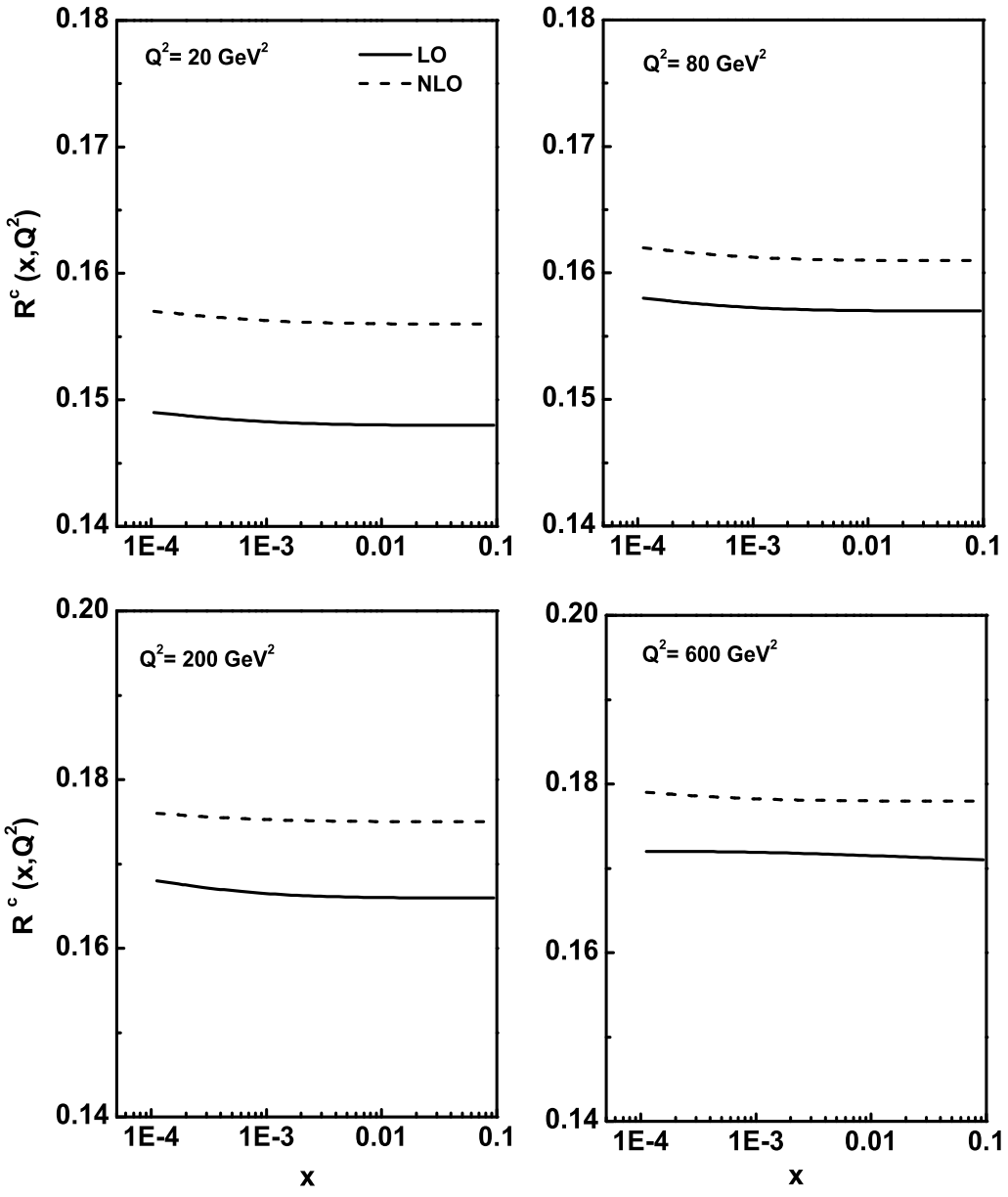

Figure 6.3: x-evolution results of the ratio of the charm quark structure functions R^c using Taylor expansion method.

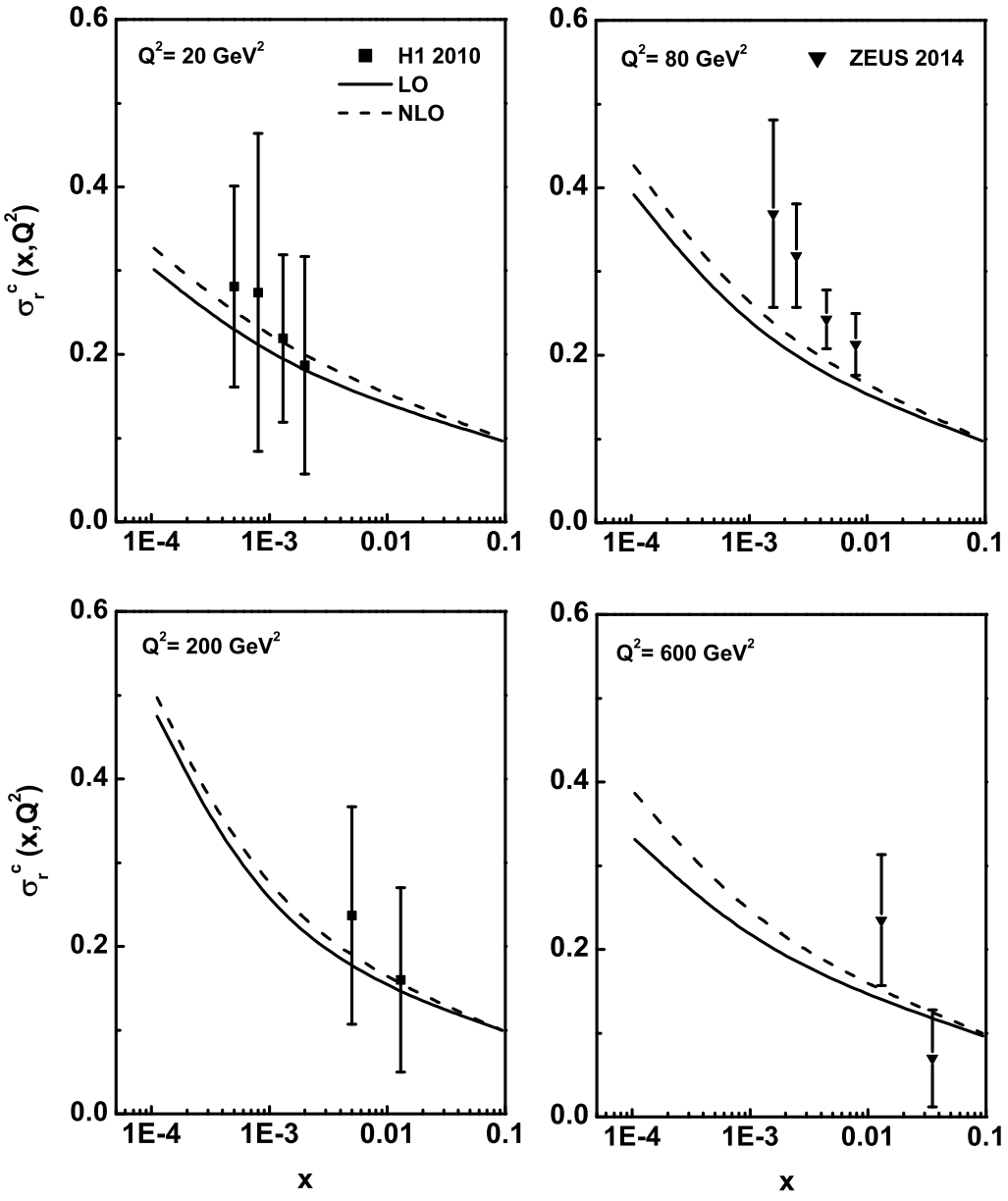

Figure 6.4: x-evolution results of charm quark reduced cross section σ_r^c using Taylor expansion method in comparison with the H1, ZEUS data.

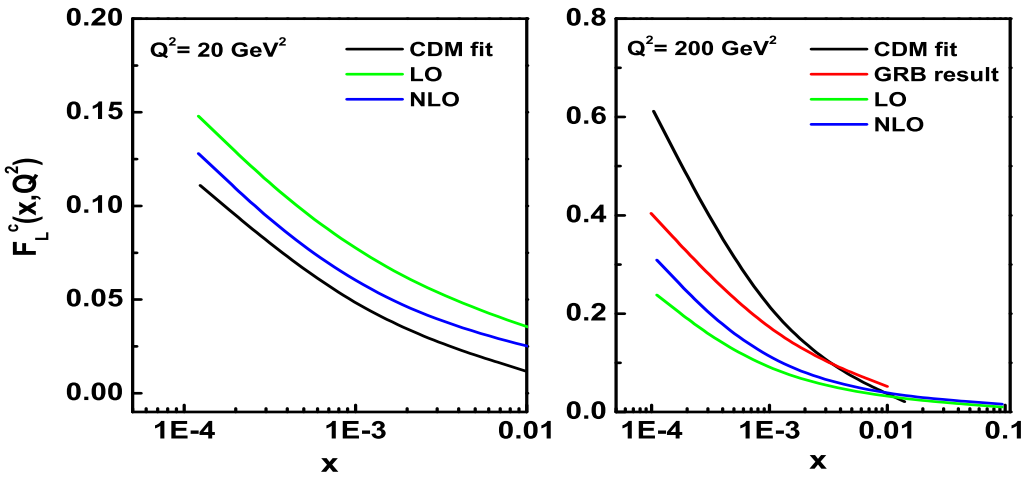

Figure 6.5: Comparison of our results of F_L^c at $Q^2 = 20, 200GeV^2$ using Taylor expansion method with the results of colour dipole model (CDM) and Boroun et al (GRB).

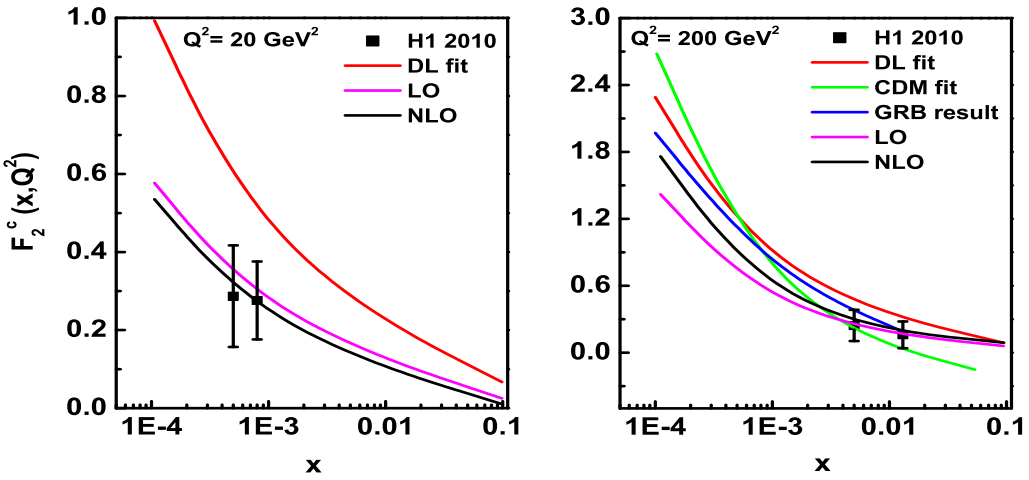

Figure 6.6: Comparison of our results of F_2^c at $Q^2 = 20, 200GeV^2$ using Taylor expansion method with the results of DL, colour dipole model (CDM) and Boroun et al (GRB).

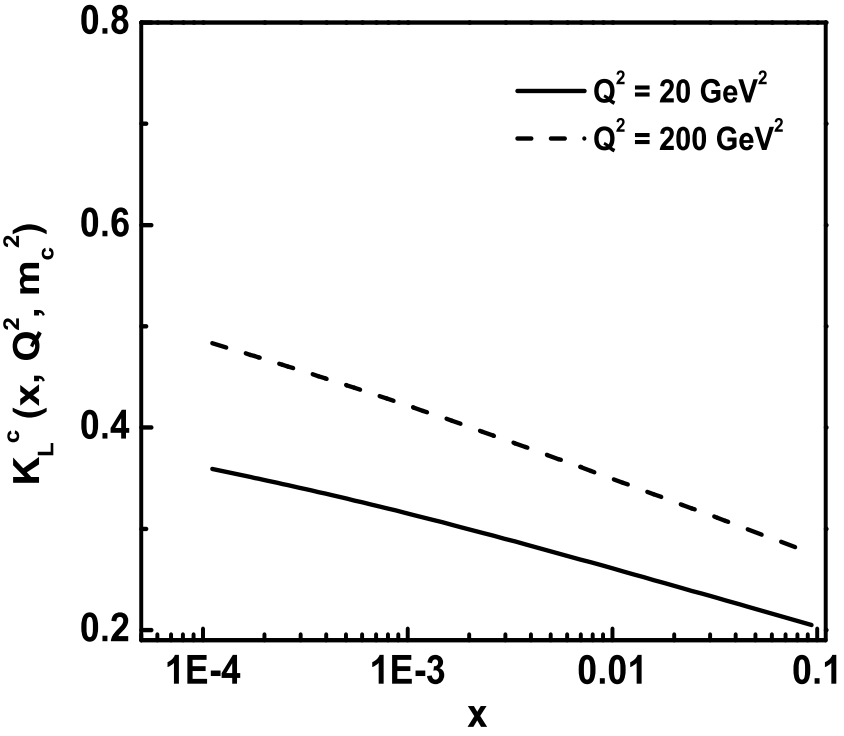

Figure 6.7: Results of the charm content of F_L structure function K_L^c with respect to x at $Q^2 = 20, 200 GeV^2$ using Taylor expansion method.

that the charm quark structure function F_k^c have a hard pomeron behaviour at low x which shows good agreement with data. In all the cases in our calculations we take the value of $m_c = 1.2GeV$ and renormalization scale μ as $\mu^2 = 4m_c^2 + Q^2$. We observed that our results for charm quark structure functions show good agreement with the data at this renormalization scale. Finally we present the charm content of the proton longitudinal structure function $K_L^c(x, Q^2, m_c^2)$ at small-x in figure 6.7. It is observed from the figure that charm content of the structure function grows towards small-x and increasing values of Q^2.

(B) Results using Regge behaviour of structure function

The charm quark structure functions F_L^c and F_2^c have been determined from the expression (6.20) using the respective charm quark co-efficient function in LO, NLO and the results of gluon distribution function obtained using the Regge behaviour of structure function in chapter 5. Here the input distribution of gluon is taken from the DL model. Figures 6.8 and 6.9 describe the behaviour of F_L^c and F_2^c structure function with respect to x. Here the results of F_2^c structure function are compared with recent H1 and ZEUS data. In both the cases, charm quark components of the structure function increases towards small values of x for fixed Q^2 values. To confirm the behaviour of these structure functions we have also calculated the ratio of charm quark structure function R^c and the charm quark reduced cross section σ_r^c using the relations (6.12) and (6.15). The behaviour of the predicted ratio R^c as a function of x for fixed values of Q^2 is depicted in figure 6.10. It is observed that this ratio is independent of x at small values of x irrespective of Q^2 values. The plots in figure 6.11 shows the results of reduced cross section σ_r^c in comparison with H1 [3] and ZEUS [4] data.

We have also compared our results of charm quark component of structure functions F_L^c and F_2^c with the DL, colour dipole model (CDM) [5] and results obtained by Boroun et al (GRB) which are depicted in figures 6.12 and 6.13. In color dipole model (CDM) the excitation of heavy flavors in DIS at small-x is described in terms of interaction of small size quark-antiquark color dipoles in the photon [5]. In all the cases in our calculations using Regge behaviour of structure function, we take the value of $m_c = 1.2GeV$ and renormalization scale μ as $\mu^2 = 4m_c^2 + Q^2$. We observed that our results for charm quark structure functions show good agreement with the data at this renormalization scale. We have also presented the charm content of the proton longitudinal structure function $K_L^c(x, Q^2, m_c^2)$ at small-x in figure 6.14. It is observed from the figure that charm content of the structure function grows towards small-x and increasing values of Q^2.

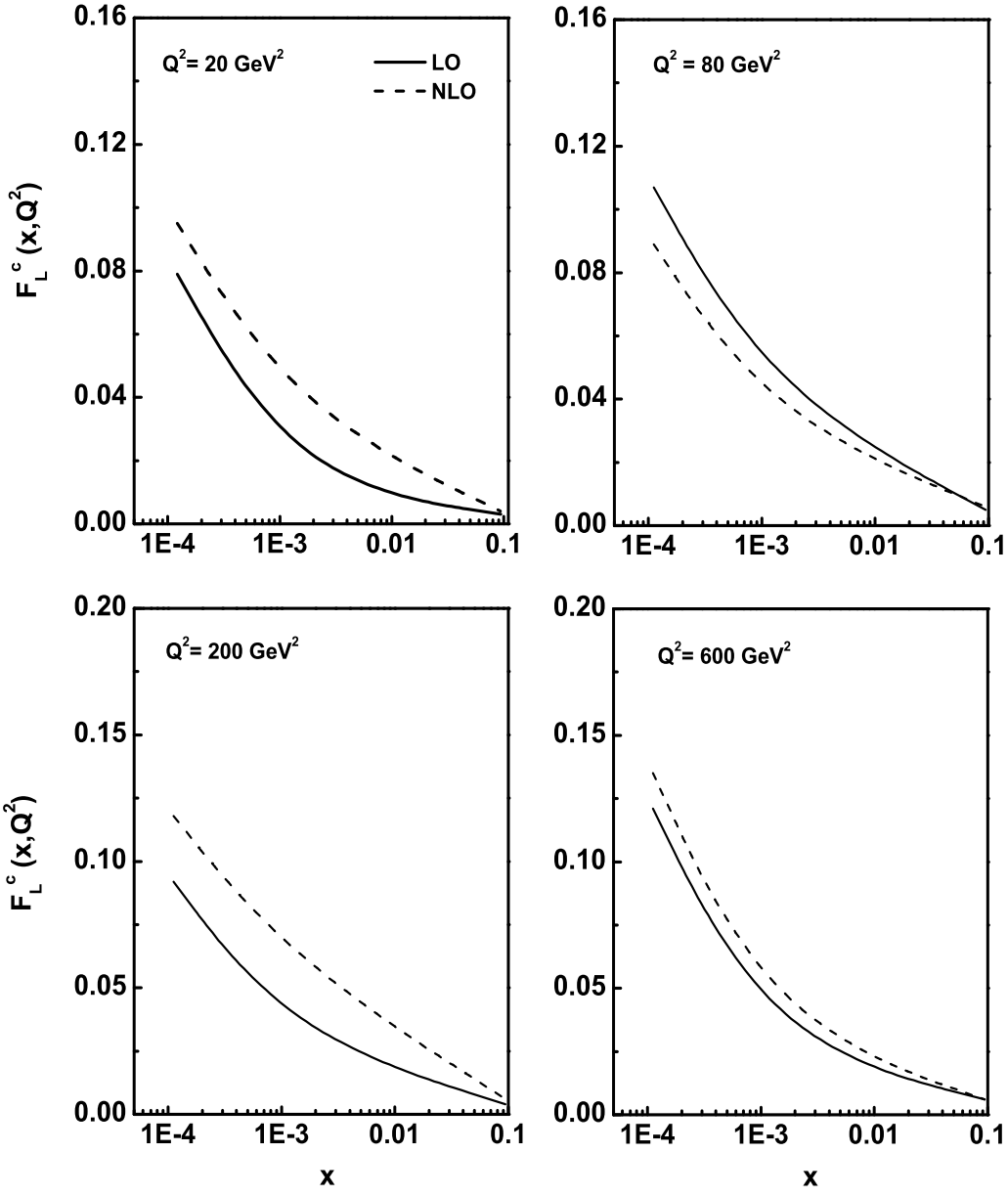

Figure 6.8: x-evolution results of F_L^c structure function using Regge theory with the input gluon distribution from DL model.

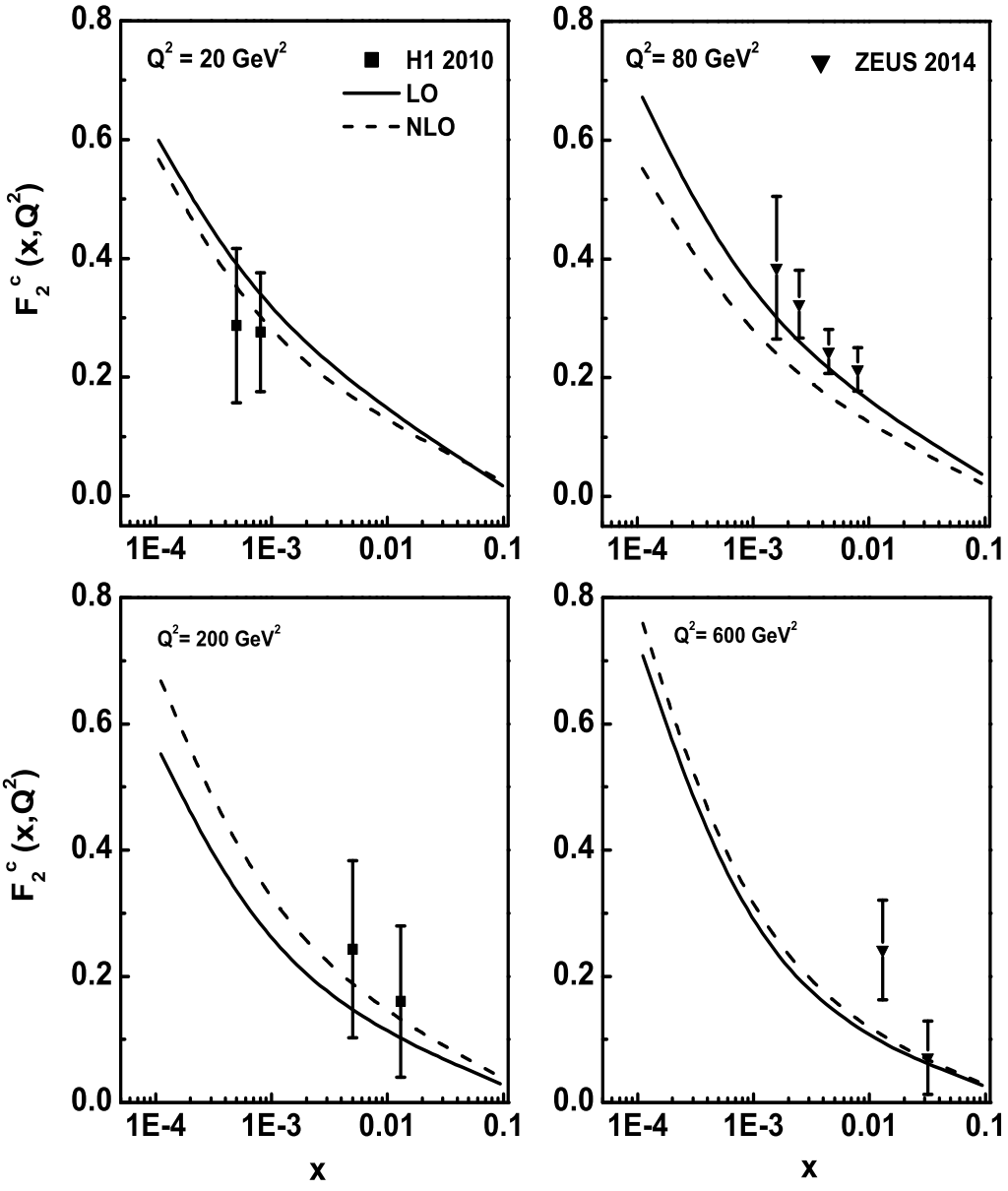

Figure 6.9: x-evolution results of F_2^c structure function using Regge theory in comparison with the H1, ZEUS data.

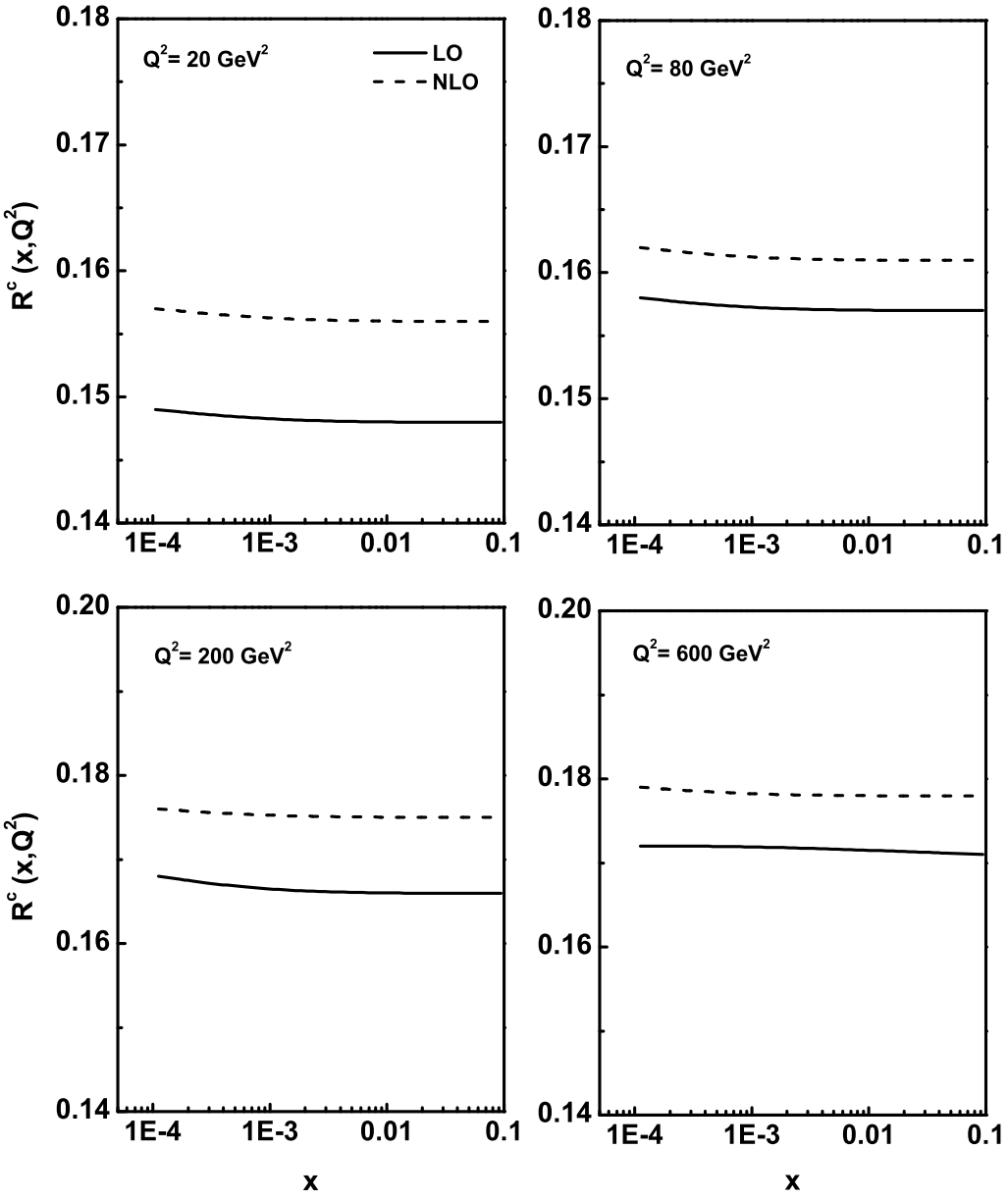

Figure 6.10: x-evolution results of the ratio of the charm quark structure function R^c using Regge theory.

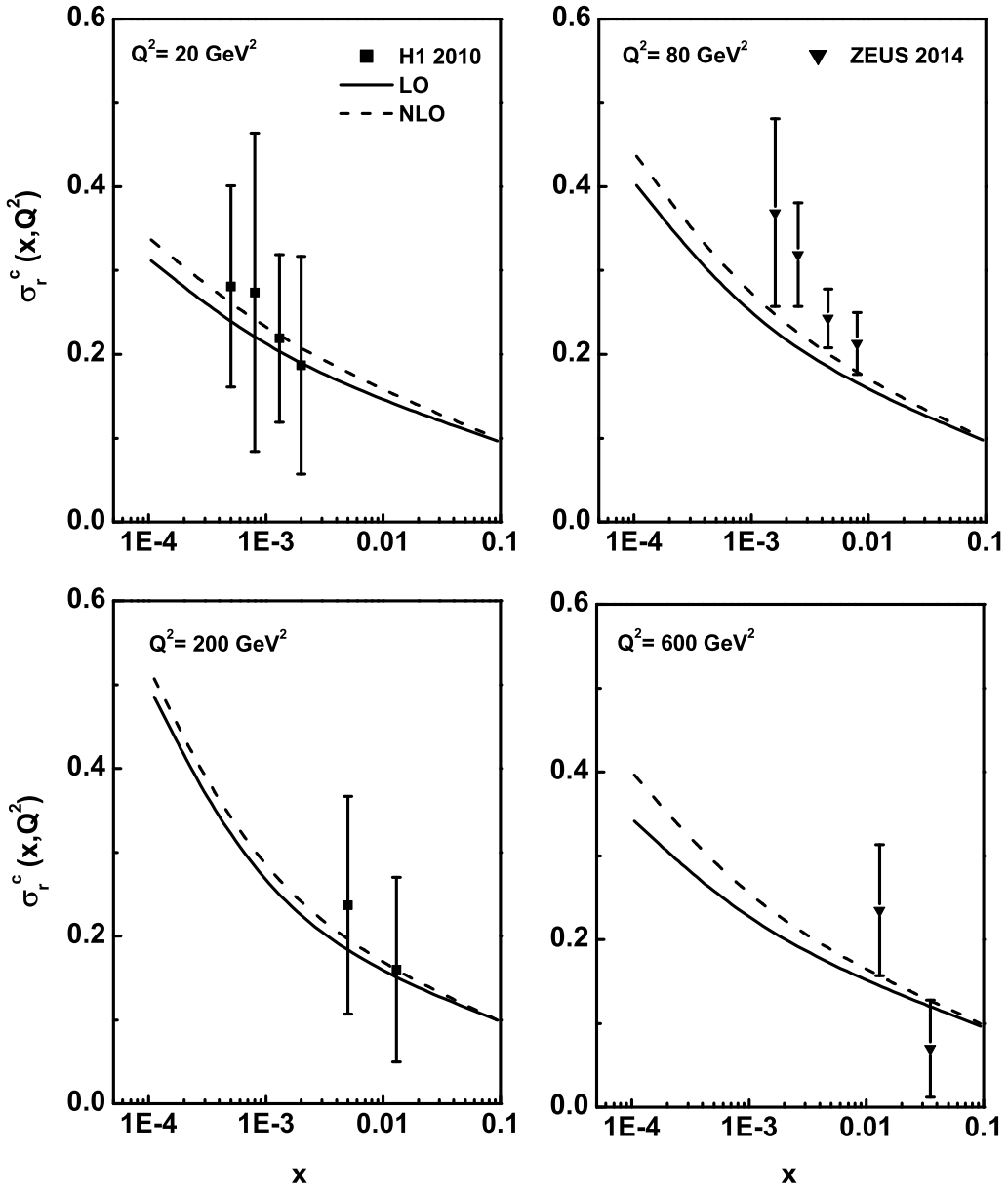

Figure 6.11: x-evolution results of the charm quark reduced cross section σ_r^c using Regge theory in comparison with the H1, ZEUS data.

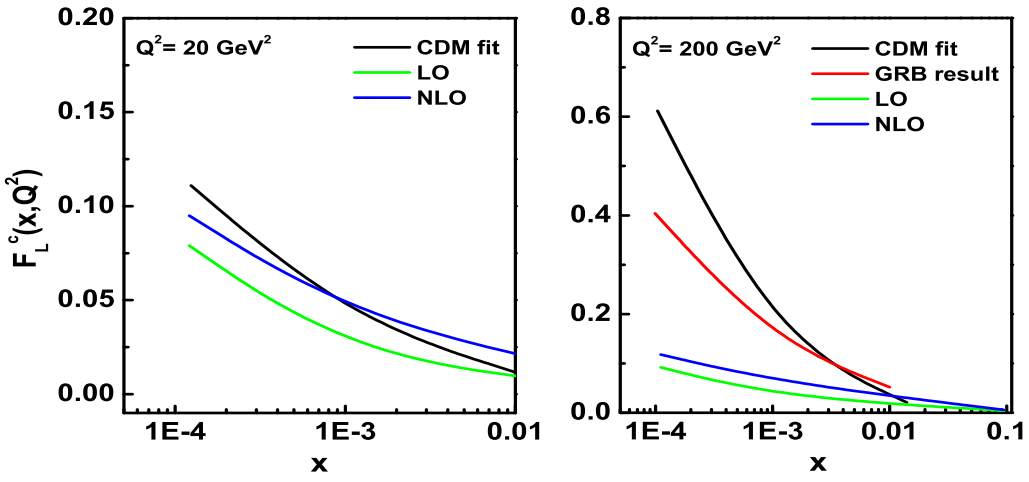

Figure 6.12: Comparison of our results of F_L^c at $Q^2 = 20, 200 GeV^2$ using Regge theory with the results of CD model and Boroun et al (GRB).

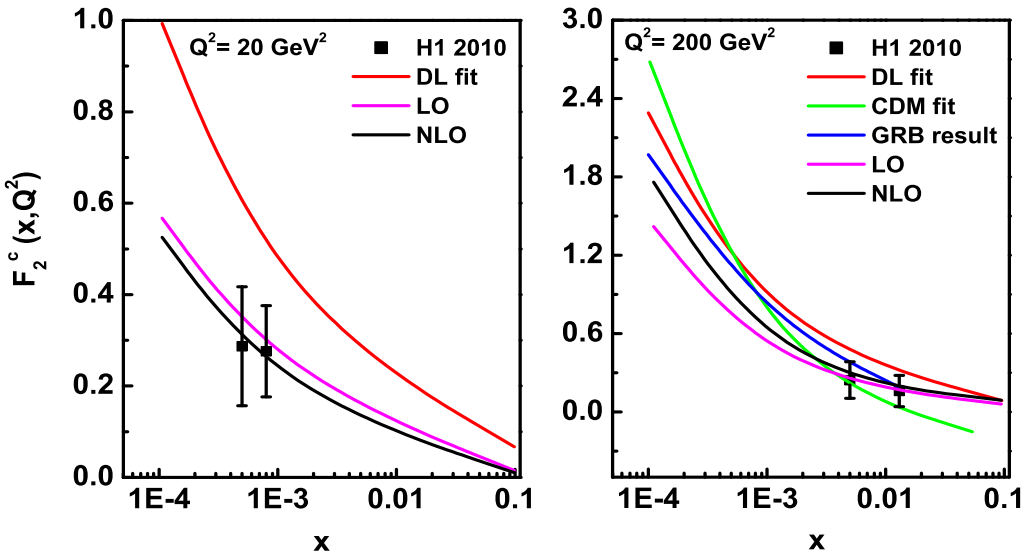

Figure 6.13: Comparison of our results of F_2^c at $Q^2 = 20, 200 GeV^2$ using Regge theory with the results of DL, CD model and Boroun et al (GRB).

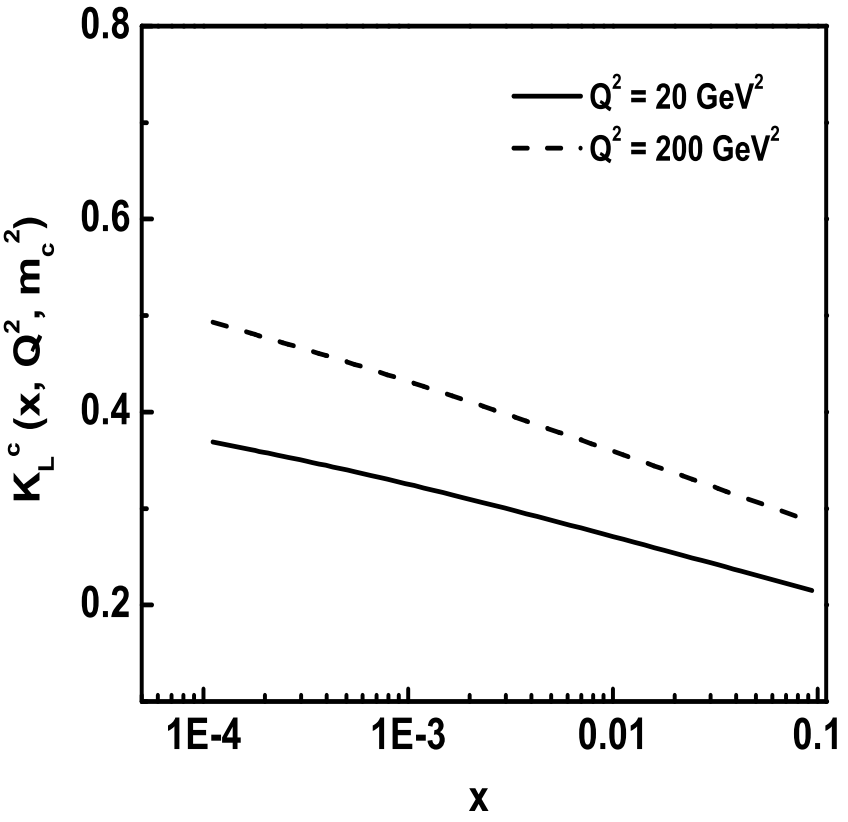

Figure 6.14: Results of the charm content of F_L structure function K_L^c with respect to x at $Q^2 = 20, 200 GeV^2$ using Regge theory.

6.2.2 Beauty quark contribution to structure functions

(A)Results using Taylor expansion method

The beauty quark structure functions F_L^b and F_2^b have been determined from the expressions (6.6) and (6.9) using the respective beauty quark co-efficient functions in LO, NLO and the gluon distribution function of DL model. Here the gluon distribution function is expanded at $z = 0.8$ using the Taylor expansion method. Figures 6.15 and 6.16 describe the behaviour of F_L^b and F_2^b structure functions with respect to x. Here

the results of F_2^b structure function are compared with recent H1 and ZEUS data. Both the beauty quark components of the structure function increase towards small values of x for fixed Q^2 values. To confirm the behaviour of these structure functions we have also calculated the ratio of beauty quark structure function R^b and the beauty quark reduced cross section σ_r^b using the relations (6.13), (6.14) and (6.15). Figure 6.17 shows the behaviour of the predicted ratio R^b as a function of x for fixed values of Q^2. It is observed that this ratio is independent of x at small values of x irrespective of Q^2 values. The plots in Figure 6.18 shows the results of reduced cross section σ_r^b in comparison with H1 [3] and ZEUS [4] data. In these plots also our results show good agreement with the experimental data.

We have also compared our results of beauty quark component of structure functions F_2^b with the results of MSTW08 parameterization which are depicted in figure 6.19. In all the cases in our calculations we take the value of $m_b = 4.2GeV$ and renormalization scale μ as $\mu^2 = 4m_b^2 + Q^2$. We observed that our results for beauty quark structure function show good agreement with the data at this renormalization scale. Finally we present the beauty content of the proton longitudinal structure function $K_L^b(x, Q^2, m_b^2)$ at small-x in figure 6.20. It is observed from the figure that beauty content of the structure function grows towards small-x and increasing values of Q^2.

(B) Results using Regge behaviour of structure function

The beauty quark structure functions F_L^b and F_2^b have been determined from the expression (6.20) using the respective beauty quark co-efficient functions in LO, NLO and the results of gluon distribution function obtained using the Regge behaviour of structure function in chapter 5. Here the input distribution of gluon is taken from the DL model. Figures 6.21 and 6.22 describe the behaviour of F_L^b and F_2^b structure function with respect to x. Here the results of F_2^b structure function are compared with recent H1 and ZEUS data. In both the cases, beauty quark components of the

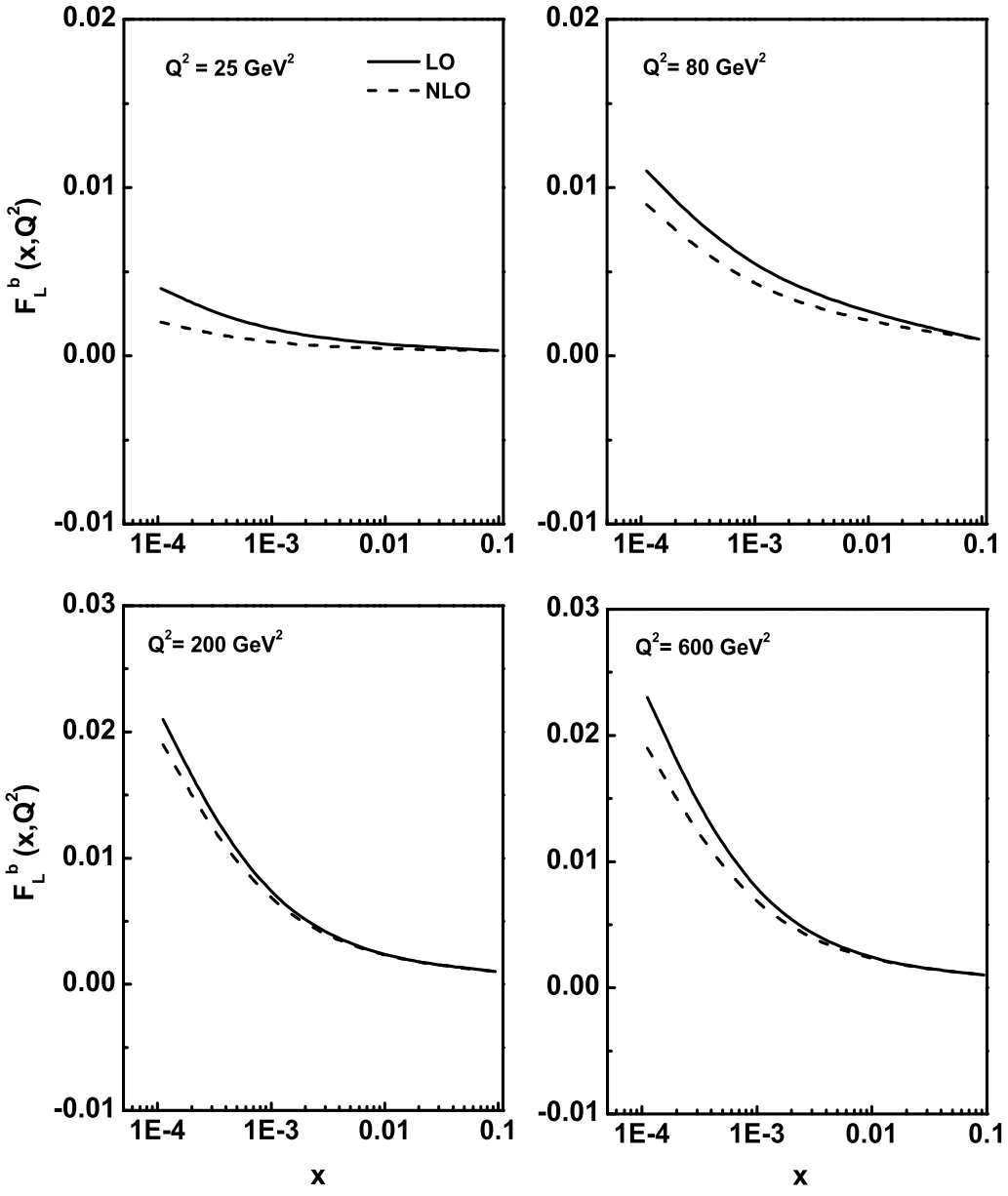

Figure 6.15: x-evolution results of F_L^b structure function using Taylor expansion method with the input gluon distribution from DL model.

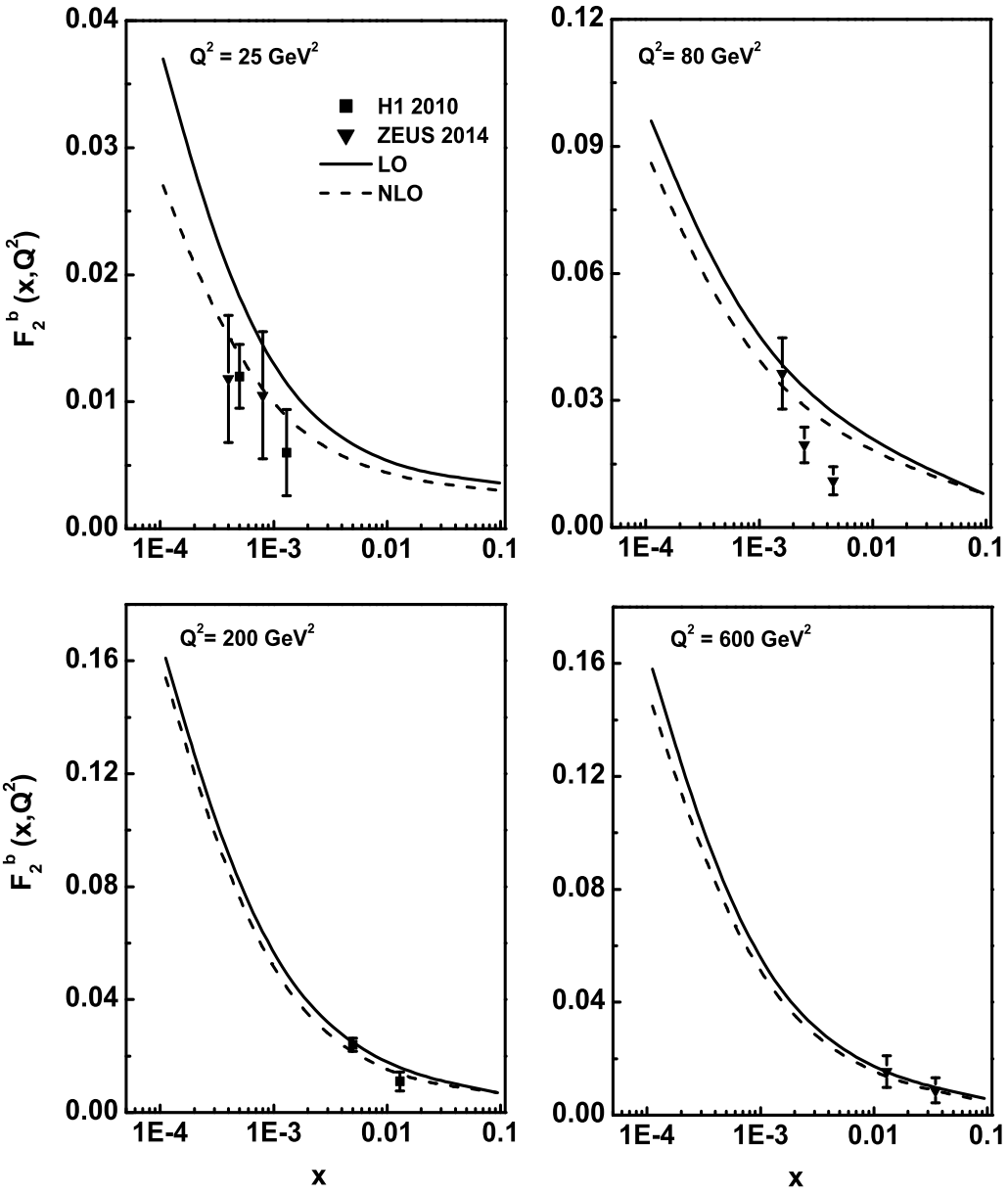

Figure 6.16: x-evolution results of F_2^b structure function using Taylor expansion method in comparison with the H1, ZEUS data.

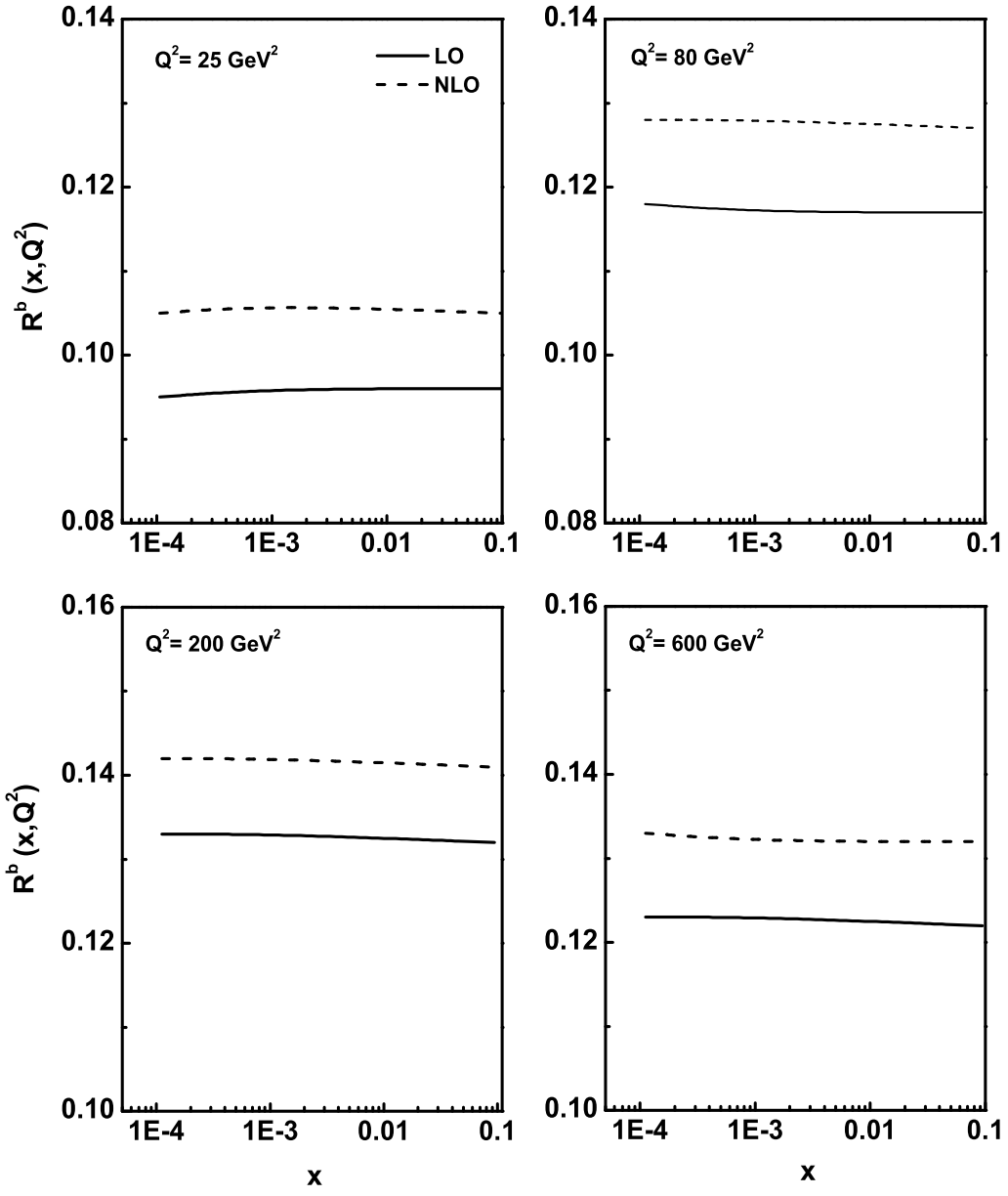

Figure 6.17: x-evolution results of the ratio of the beauty quark structure functions R^b using Taylor expansion method .

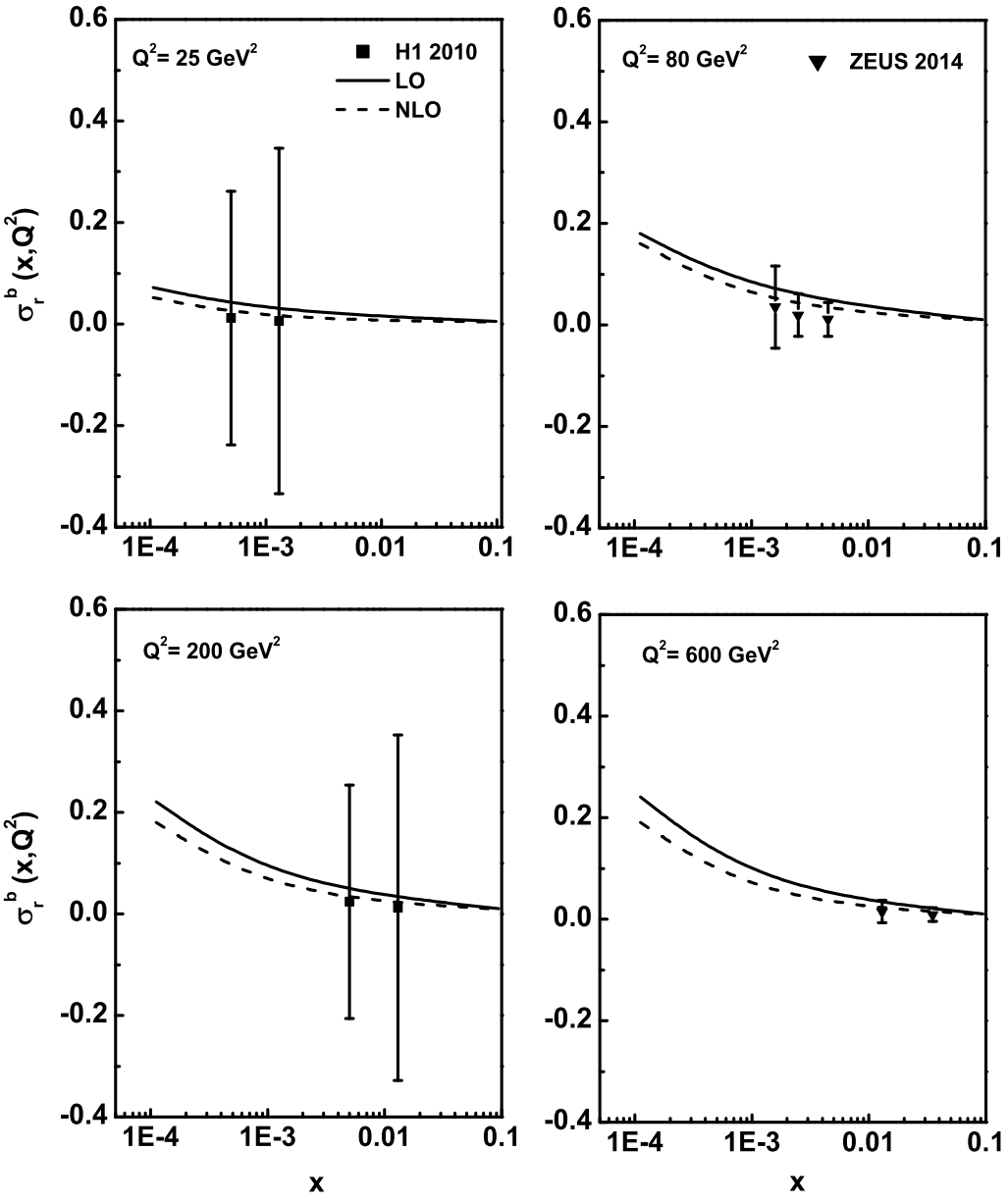

Figure 6.18: x-evolution results of the beauty quark reduced cross section σ_r^b using Taylor expansion method in comparison with the H1, ZEUS data.

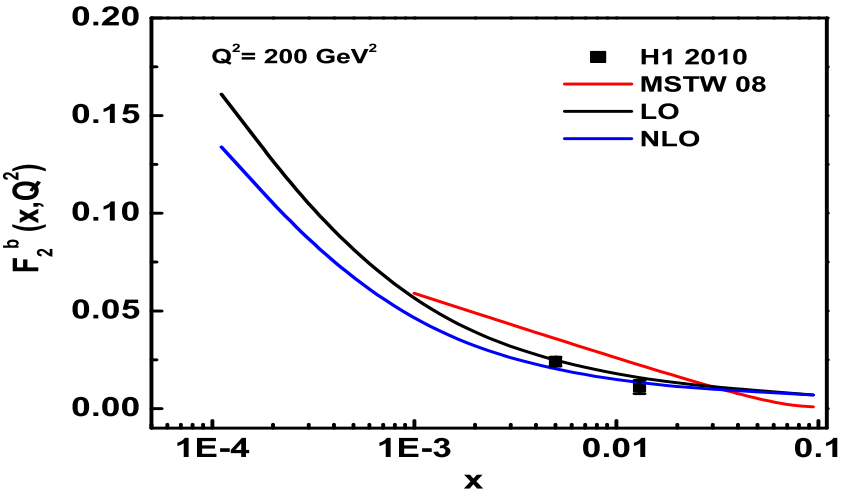

Figure 6.19: Comparison of our results of F_2^b at $Q^2 = 200GeV^2$ using Taylor expansion method with the results of MSTW 08.

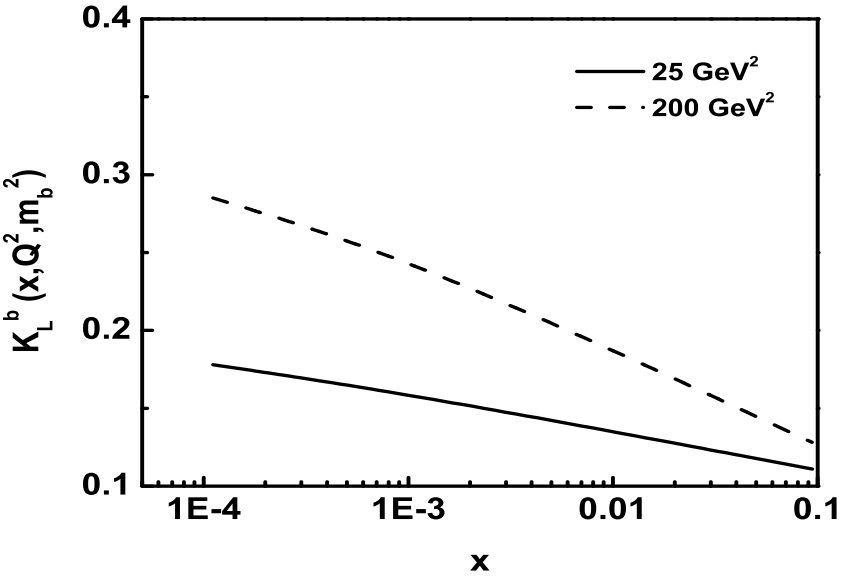

Figure 6.20: Results of the beauty content of F_L structure function K_L^b with respect to x at $Q^2 = 25, 200GeV^2$ using Taylor expansion method.

structure function increase towards small values of x for fixed Q^2 values. To confirm the behaviour of these structure functions we have also calculated the ratio of beauty quark structure function R^b and the beauty quark reduced cross section σ_r^b using the relations (6.12) and (6.15) respectively. The behaviour of the predicted ratio R^b as a function of x for fixed values of Q^2 is depicted in figure 6.23. It is observed that this ratio is independent of x at small values of x irrespective of Q^2 values. The plots in figure 6.24 show the results of reduced cross section σ_r^b in comparison with H1 [3] and ZEUS [4] data.

We have also compared our results of beauty quark structure functions F_2^b with the results of MSTW08 parameterization which are depicted in figure 6.25. We have also presented the beauty content of the proton longitudinal structure function $K_L^b(x, Q^2, m_b^2)$ at small-x in figure 6.26. It is observed from the figure that beauty content of the structure function grows towards small-x and increasing values of Q^2.

(C) Comparative study of the results of the heavy quark reduced cross section obtained by both the methods

The results of heavy quark structure functions, their ratio and the reduced cross section obtained by both the methods i.e., Taylor expansion method and Regge theory show good agreement with the available experimental data, model fit and parameterization. The heavy quark reduced cross section is calculated using the heavy quark structure function and their ratio. The behaviours of ratio of heavy quark structure functions in both the cases are same as these are independent of the distribution of gluons inside proton. Here we have presented the comparative analysis of the behaviours of charm and beauty quark reduced cross sections σ_r^c and σ_r^b with respect to x for different values of Q^2 obtained by both the methods which are depicted in figures 6.27 and 6.28. Both the figures show that our results are in good agreement with the experimental results. Figure 6.29 shows the sensitivity of our results of σ_r^c and σ_r^b with the mass

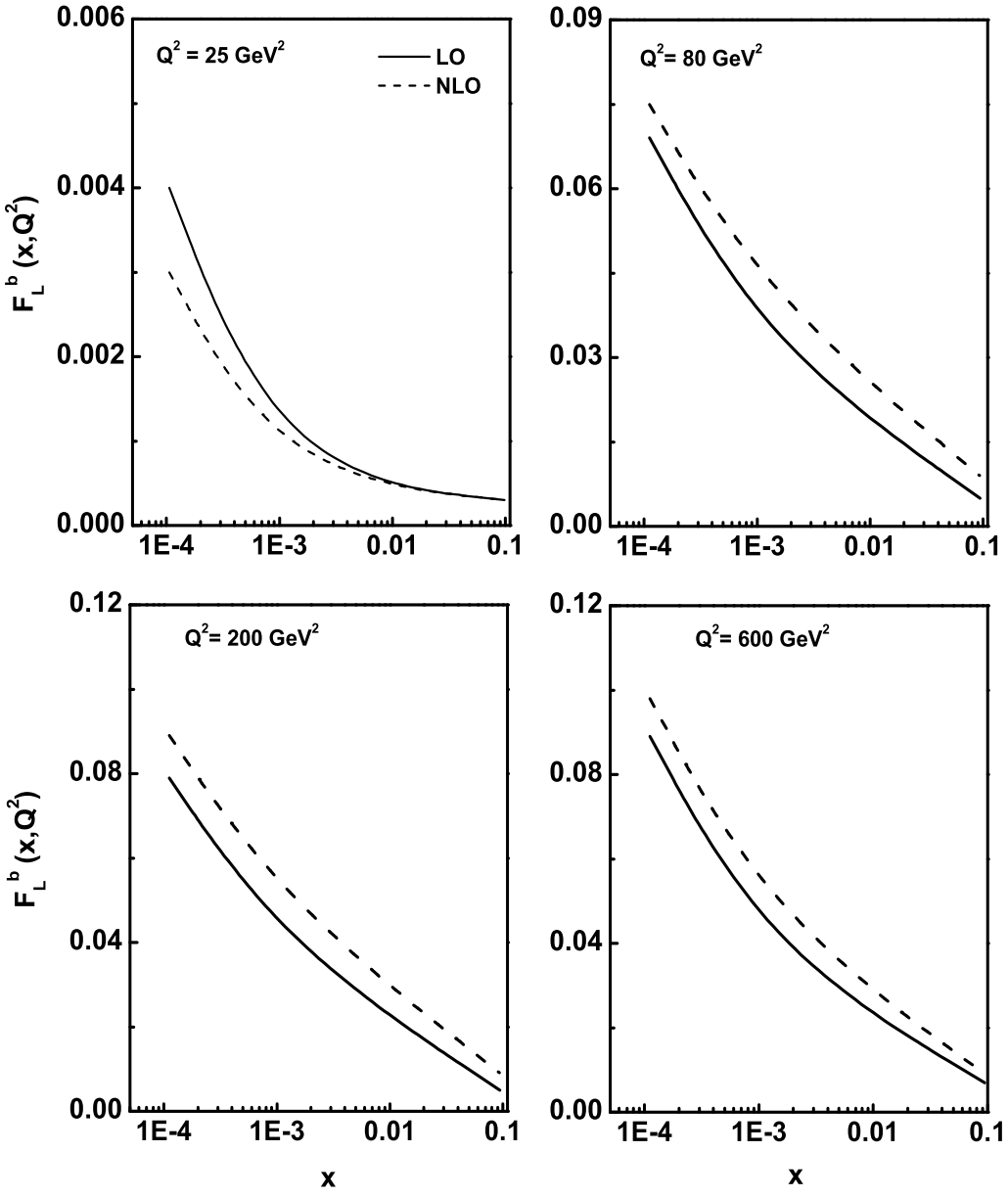

Figure 6.21: x-evolution results of F_L^b structure function using Regge theory with the input gluon distribution from DL model.

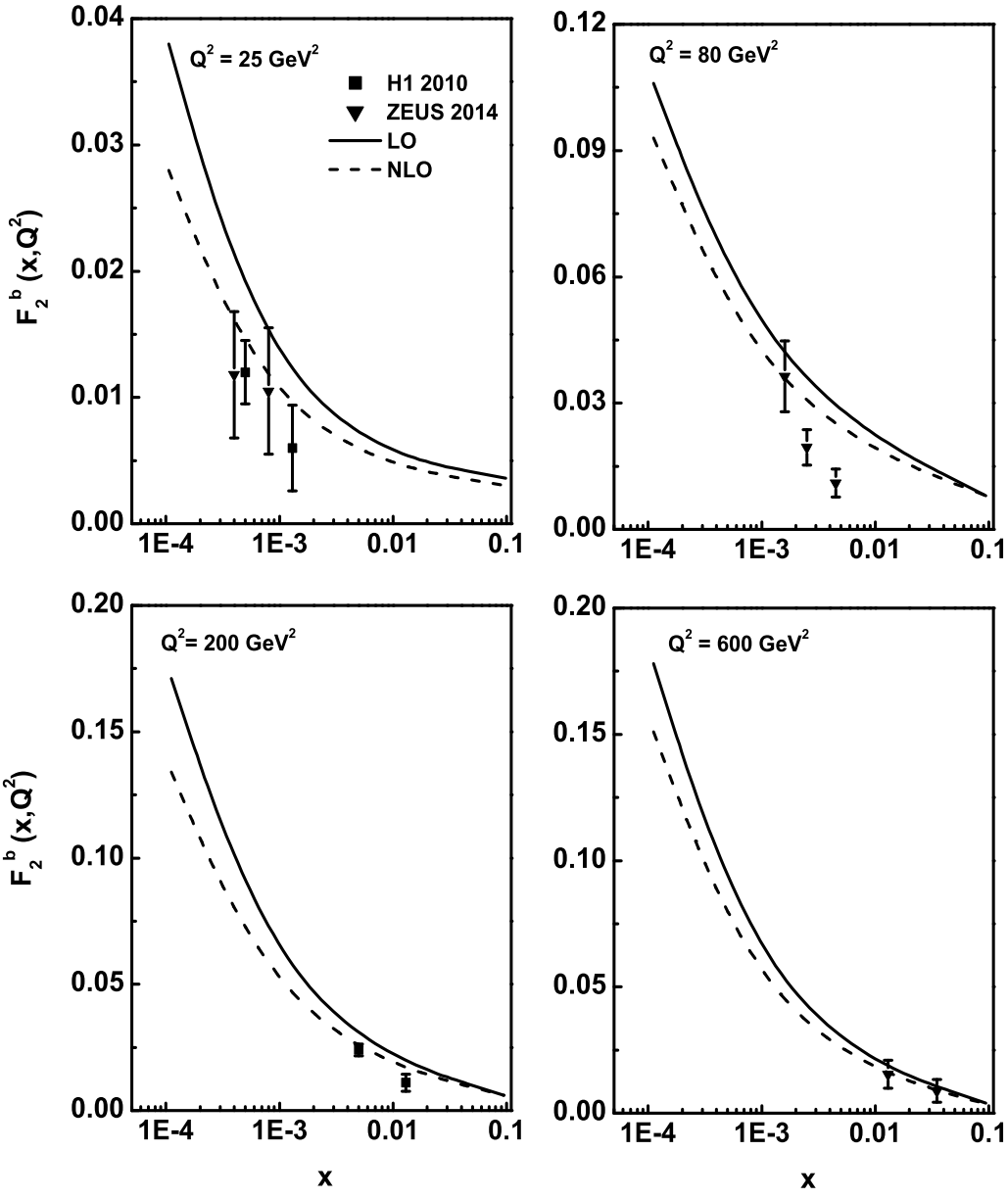

Figure 6.22: x-evolution results of F_2^b structure function using Regge theory in comparison with the H1, ZEUS data.

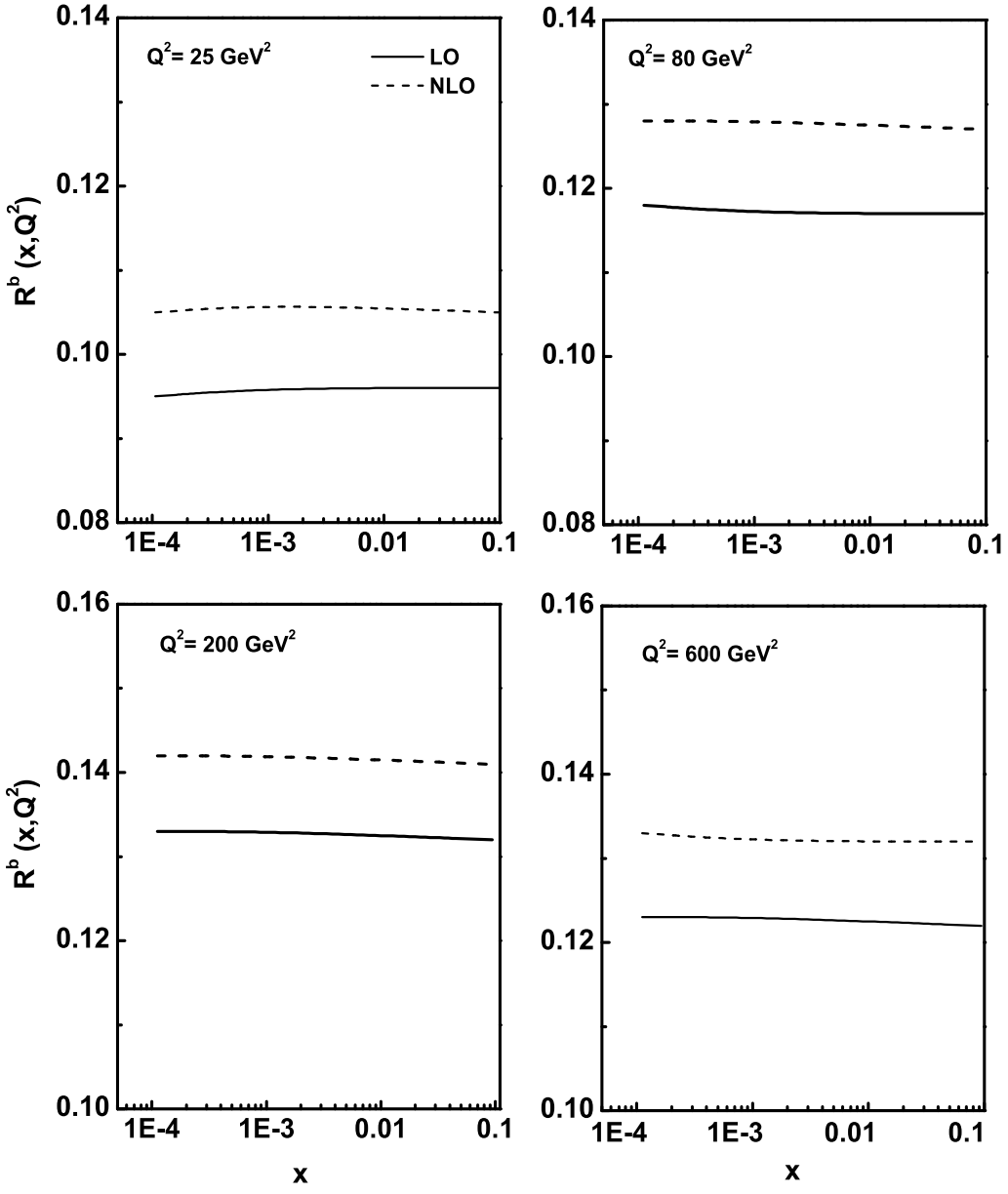

Figure 6.23: x-evolution results of the ratio of the beauty quark structure functions R^b using Regge theory.

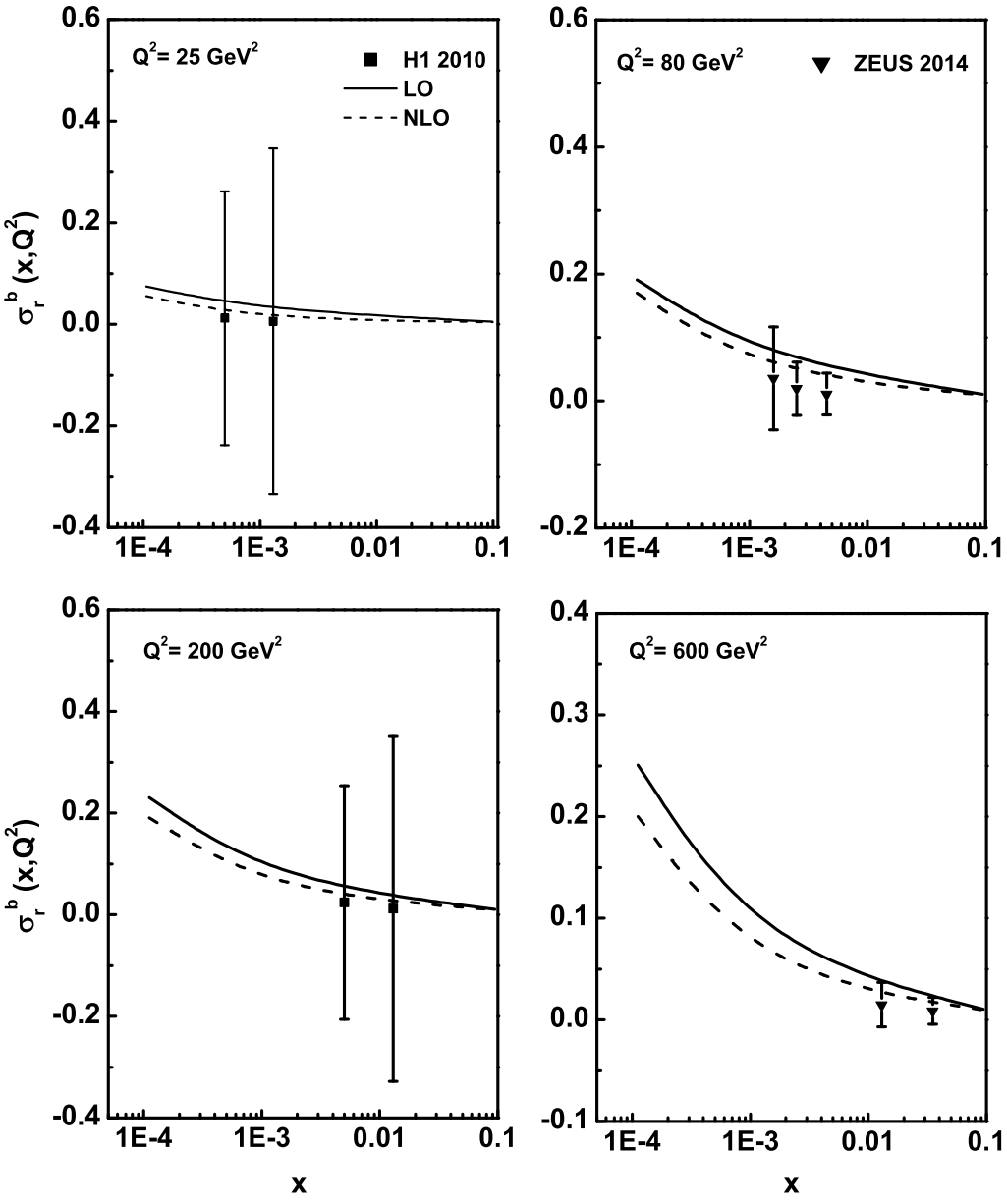

Figure 6.24: x-evolution results of the beauty quark reduced cross section σ_r^b using Regge theory in comparison with the H1, ZEUS data.

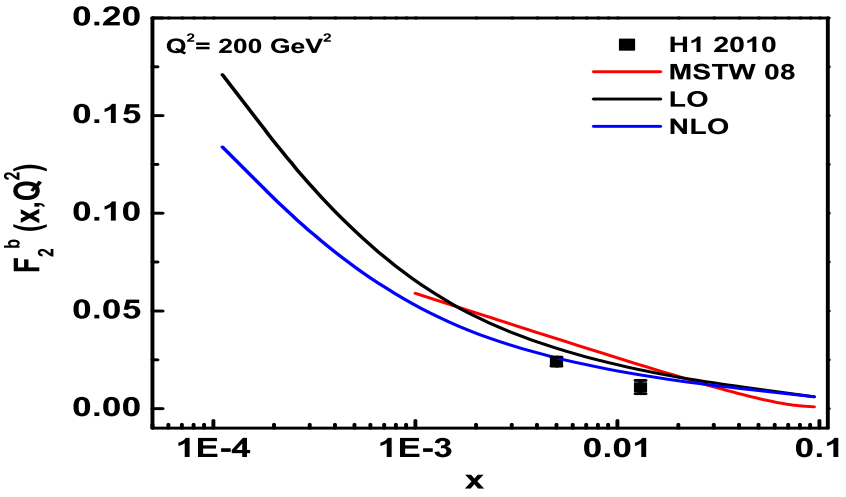

Figure 6.25: Comparison of our results of F_2^b at $Q^2 = 200GeV^2$ using Regge theory with the results of MSTW08 parameterization.

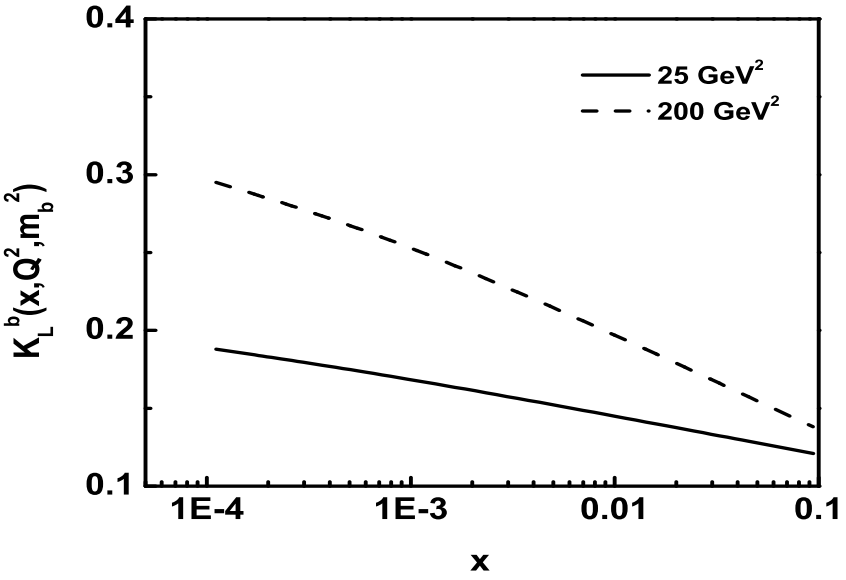

Figure 6.26: Results of the beauty content of F_L structure function K_L^b with respect to x at $Q^2 = 25, 200GeV^2$ using Regge theory.

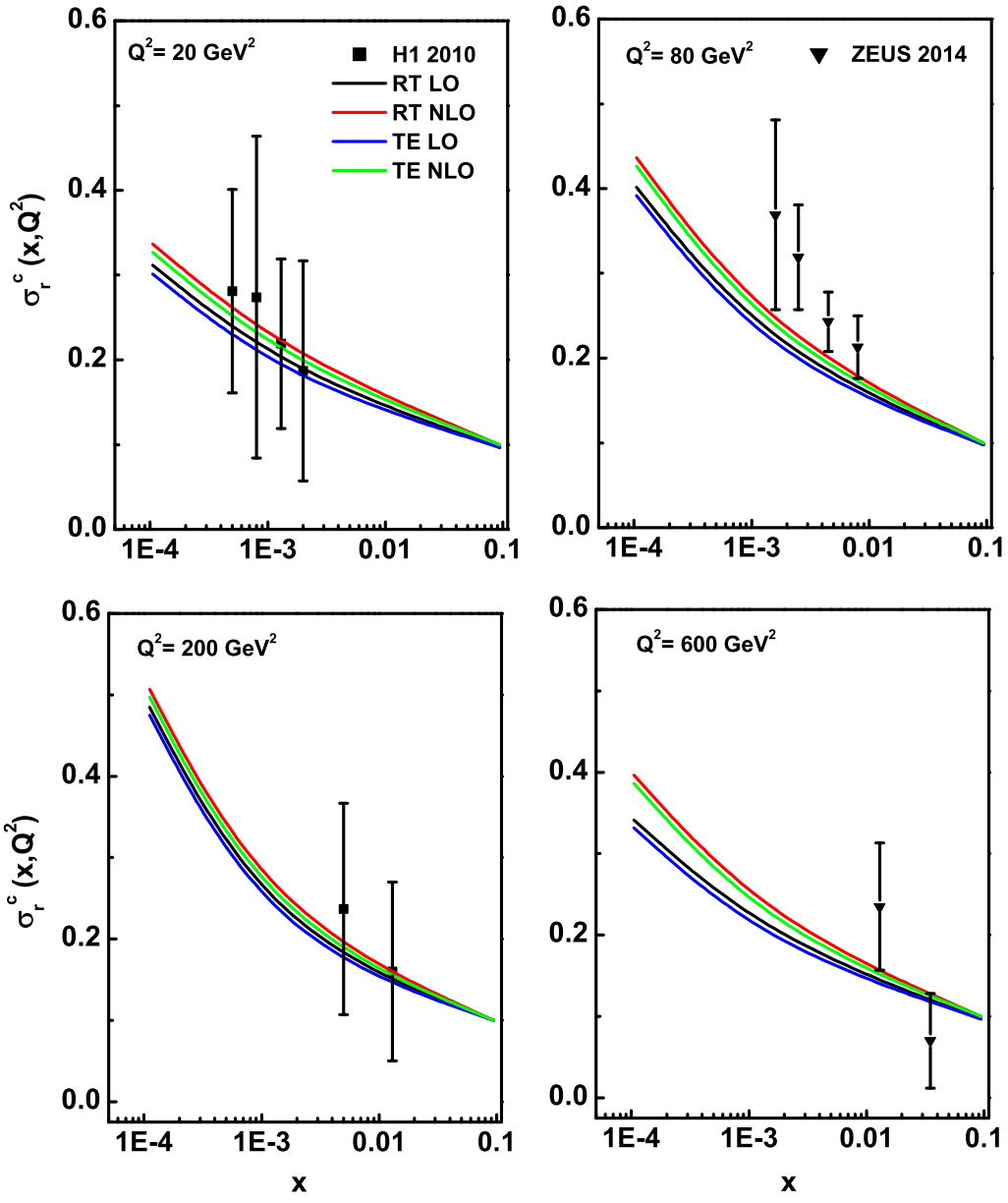

Figure 6.27: Comparison of our results of σ_r^c obtained by Taylor expansion (TE) method and Regge theory (RT).

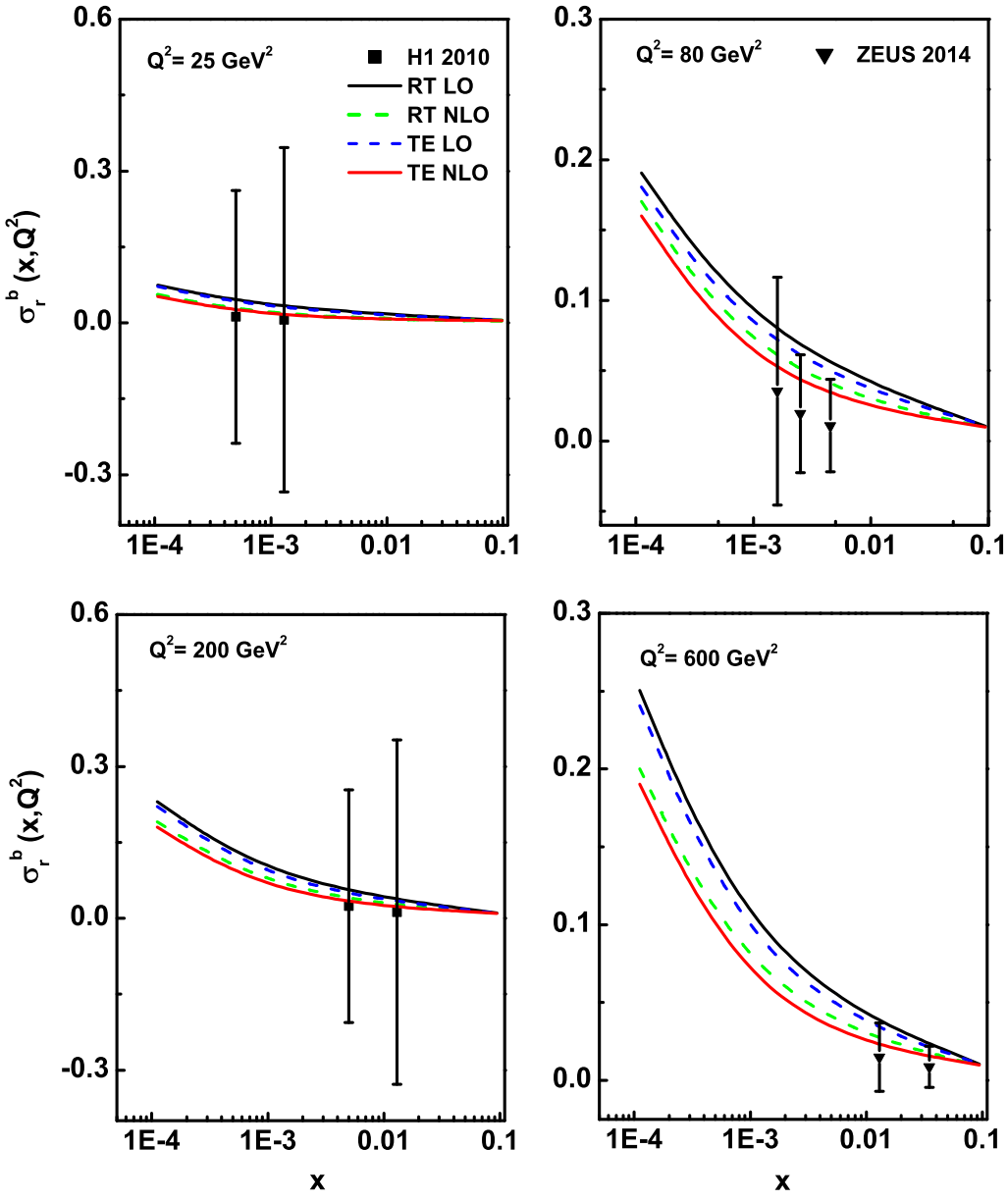

Figure 6.28: Comparison of our results of σ_r^b obtained by Taylor expansion (TE) method and Regge theory (RT).

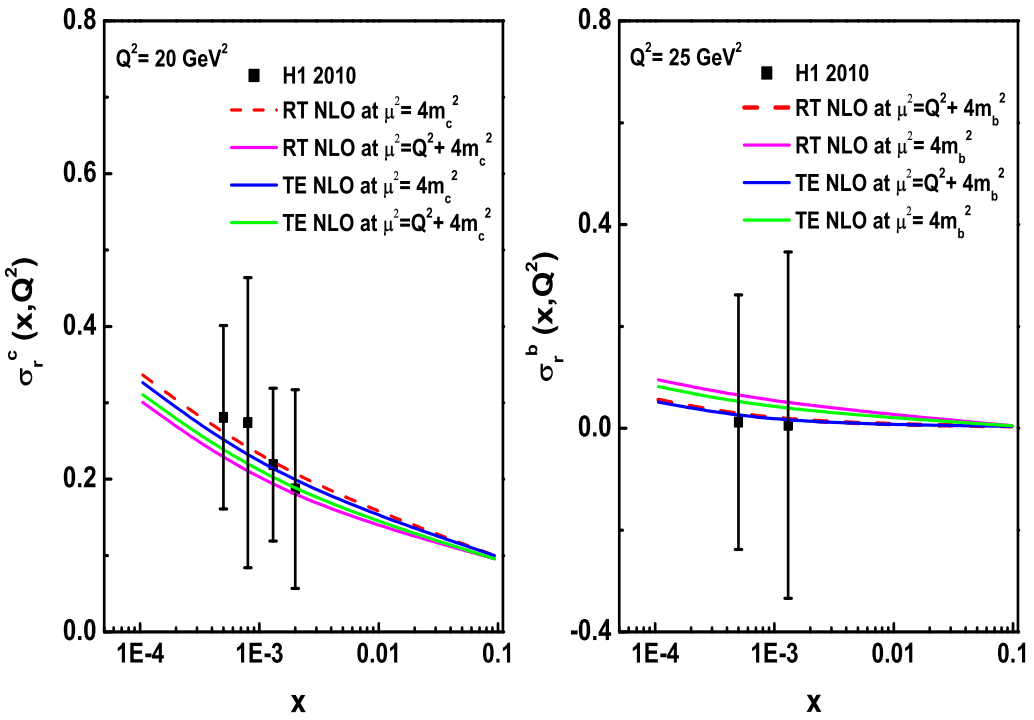

Figure 6.29: Sensitivity of our results of σ_r^b and σ_r^c with mass renormalization scale μ obtained by Taylor expansion (TE) method and Regge theory (RT).

renormalization scale μ obtained by both the methods i.e., Taylor expansion method and Regge theory method. This figure indicates that the sensitivity of our results with mass renormalization scale $\mu^2 = 4m_h^2 + Q^2$, shows good agreement with the experimental data. From the figure it is observed that the sensitivity of the choice of scale μ is relatively large in case of the small-x region than that of the high x region as in the small-x region the production of heavy quark is large compared to that in the high x region. In figure 6.29, in both the plots the behaviour of σ_r^c and σ_r^b with respect to x shows increasing behaviour towards small values of x. But in case of the charm quark the increase of the cross section is more sharp than that of the cross section in case of beauty quark. The reason for this is that the density of heavy beauty quark is less than

that of the charm quark in the small-x region. So, the charm cross section increases more sharply with respect to x than that of the beauty quark cross section.

6.3 Conclusions

In this chapter, we have calculated the heavy quark structure functions $F_k^h(k = 2, L; h = c, b)$ using gluon distribution function in NLO analysis with the help of Taylor expansion (TE) method and the Reege (RT) like behaviour of the structure function. The obtained results are compared with the experimental H1, ZEUS data, results of DL, CD model and MSTW08 parameterization which reflect compatibility of our results with the data and model fits. All the gluon dominating heavy quark structure functions show increasing behaviour towards small values of x. To confirm the validity of our calculations we have also analysed the behaviour of heavy quark structure function ratio R^h and reduced heavy quark cross section σ_r^h with respect to x which also shows good agreement with experimental data. We have also analysed the behaviour of heavy quark content of the longitudinal structure function with respect to x which reflects increasing behaviour towards small-x and high Q^2 region. In our calculations we have considered the value of the mass renormalization scale μ as $\mu^2 = 4m_h^2 + Q^2$. The sensitivity of our results of charm and beauty quark structure function with mass renormalization scale μ shows that at $\mu^2 = 4m_h^2 + Q^2$, our predicted results are compatible with the experimental data. Our predicted results in both the methods show good agreement with the experimental data, model fits and parameterization. Thus we can conclude that both the methods can be used to study the behaviour of the heavy quark structure functions.

References

[1] Carvalho, F., et al. Charm and longitudinal structure functions within the Kharzeev-Levin-Nardi model, *Phys. Rev. C* **79** (3), 035211-1–6, 2009.

[2] Donnachie, A. and Landshoff, P. V. The protons gluon distribution, *Phys. Lett. B* **550** (3-4), 160–165, 2002.

[3] Aaron, F. D., et al. Measurement of the charm and beauty structure functions using the H1 vertex detector at HERA, *Eur. Phys. J. C* **65** (1-2), 89–109, 2010.

[4] Abramowicz, H., et al. Measurement of beauty and charm production in deep inelastic scattering at HERA and measurement of the beauty-quark mass, *J. High Energy Phy.* **2014** (09), 127-1–55, 2014.

[5] Nikolaev, N. N. and Zoller, V. R. How open charm production and scaling violations probe the rightmost hard BFKL pole exchange, *Phys. Lett. B* **509** (3-4), 283–293 2001.

[6] Martin, A. D., et al. Parton distributions for the LHC, *Eur. Phys. J. C* **63** (2), 189–285, 2009.

[7] Gluck, M., Reya, E. and Vogt, A. Dynamical parton distributions of the proton and small x physics, *Z. Phys. C* **67** (3), 433–447, 1995.

[8] Gluck, M., Reya, E. and Vogt, A. Dynamical parton distributions revisited, *Eur. Phys. J. C* **5** (3), 461–470, 1998.

[9] Catani, S., Ciafaloni, M. and Hautmann, F. High energy factorization and small-x heavy flavour production, *Nucl. Phys. B* **366** (1), 135–188, 1991.

[10] Illarionov, A. Y., Kniehl, B. A. and Kotikov, A. V. Heavy-quark contributions to the ratio F_L/F_2 at low x, *Phys. Lett. B* **663** (1-2), 66–72, 2008.

[11] Baishya, R. and Sarma, J. K. Semi numerical solution of non-singlet Dokshitzer-GribovLipatovAltarelliParisi evolution equation up to next-to-next-to-leading order at small x, *Eur. Phys. J. C* **60** (4), 585–591, 2009.

[12] Laenen, E., et al. Complete $O(\alpha_S)$ corrections to heavy-flavour structure functions in electroproduction, *Nucl. Phys. B* **392** (1), 162–228, 1993.

[13] Kotikov, A. V. and Parente, G. The gluon distribution as a function of F_2 and $dF_2/dlnQ^2$ at small x. The next-to-leading analysis, *Phys. Lett. B* **379** (1-4), 195–201, 1996.

[14] Boroun, G. R. and Rezaei, B. NLO corrections to the hard pomeron behavior of the charm structure functions $F_k^c(k = 2, L)$ at low x, *Nucl. Phys. B* **857** (2), 143-152, 2012. □

Chapter 7

Conclusions

In this thesis, we solved the QCD evolution equation for F_L structure function in next-next-to-leading order (NNLO) at small values of Bjorken variable x using Taylor expansion method. The same evolution equation is used to study the behaviour of F_L structure function up to NLO at small-x using Regge like behaviour of structure function. We determined t and x-evolutions of proton longitudinal structure function F_L for both the cases. Of course in most of the cases we look into gluon dominated longitudinal structure function F_L^g as at small-x, gluon contribution dominates over the quark contribution to F_L structure function. At small-x F_L structure function is directly related to the gluon distribution inside the proton. We have determined an approximate relation between the F_L structure function and gluon distribution function in NNLO approximation using Taylor expansion method. Here in our analysis, we have used the Altarelli-Martinelli equation for F_L structure function in terms of co-efficient functions. The x-evolution of F_L structure function is studied using this relation. We have calculated the t- and x-evolutions of the gluon dominating longitudinal structure function F_L up to NNLO approximation using the gluon distribution function obtained as a result of solution of the DGLAP evolution equation for gluon distribution using Regge behaviour of structure function at small-x. Along with the light flavour structure function we have also analysed the behaviour of heavy flavour (charm and beauty)

structure function $F_k^h(k = 2, L; h = c, b)$, their ratio R^h and the heavy quark reduced cross section σ_r^h with respect to x for different values of Q^2 using both Taylor expansion and Regge theory approach. The results obtained in all the cases are compared with the available experimental data, theoretical prediction of different parameterizations, results of model fit and results with numerical method with satisfactory phenomenological success. We have also presented a comparative analysis of the our results obtained by both the methods Taylor expansion and Regge theory. All the results show good agreement with the experimental data, model fit and parameterizations and can be described within the framework of pQCD, i.e., all the structure functions increases towards small values of x and high-Q^2.

We have observed that t- and x-evolution results of F_L structure function obtained as a solution of QCD evolution equation for F_L structure function using both Taylor expansion method and Regge behaviour of structure function are in good agreement with H1, ZEUS data, results of DL model and theoretical predictions of MSTW08, CT10, ABM11 and NNPDF2.3 parameterizations. From the comparative study of evolution of F_L structure function predicted by Regge theory approach and Taylor expansion method it is observed that results obtained by both the methods are in good agreement with data and parameterizations. The evolutions of F_L structure function obtained using the approximate relation between F_L and gluon distribution function shows similar behaviour with the data and results of model fit, parameterizations. The calculated results of t- and x-evolutions of F_L structure function using the gluon distribution function obtained as a solution of the DGLAP evolution equation show compatibility with the experimental data and results of model fit and parameterizations. We have also analysed the behaviour of DIS cross section ratio R with respect to x which shows that it is independent of x irrespective of Q^2 values at small-x. The comparative study of the F_L structure function results obtained by these two method also reflects similar behaviour with the data and other results. The behaviour of the

heavy quark (charm and beauty quark) structure function with respect to x shows similar behaviour with the experimental H1, ZEUS data and results of DL, CD model, MSTW08 parameterization. To confirm our method and behaviour of these structure functions we have also analysed the behaviours of the ratio of the heavy quark structure function R^h and heavy quark reduced cross section σ_r^h with respect to x which reflect good agreement with the data. The ratio of heavy quark structure function with respect to x is also independent of x for the Q^2 values which shows that it is independent of the distribution of gluons in the proton. The heavy quark content to the F_L structure function with respect to x increases with Q^2 towards small values of x. In our analysis, while solving the evolution equations we have considered two numerical parameters T_0 and T_1, such that $T^2(t) = T_0.T(t)$ and $T^3(t) = T_1.T(t)$ with $T(t) = \frac{\alpha_s(t)}{2\pi}$. These two parameters are chosen in such a way that the difference between $T^2(t)$, $T_0.T(t)$ and $T^3(t)$, $T_1.T(t)$ are negligible in our required range of Q^2. Thus both the methods used in our analysis are simple ones and less time consuming on the numerical calculations with less number of numerical parameters compared to the other methods where several parameters are included in the input function. So, these methods may be a good alternative to other methods.

In DIS, at moderate values of x, the linear QCD evolution equation led to a good description of the behaviour of gluon distribution function. But at small values of x and low-Q^2, the problem is more complicated as recombination of the gluon in a dense system has to be taken into account. This region is better explained by non-linear evolution equations. So as future directives with the help of non-linear evolution equations one can explain the behaviour of structure functions at very small-x and thus predicts a range of onset of parton recombination. There are different theoretical models based on parton recombination and saturation which describe low-x and low-Q^2 region well. But till today this saturated gluon density regime has not been clearly observed. With the help of a new collider, Electron Ion Collider (EIC), physicist from different

parts of the world try to explain the unanswered questions about the structure of matter. The main unanswered questions are: What are the nuclear gluon and sea quark densities? To what extent are they modified by nuclear binding, quantum-mechanical interference, and other collective effects? These questions are the key to understanding the QCD origins of the nucleon-nucleon interaction at different energies, the role of non-nucleonic degrees of freedom, and the approach to a new regime of high gluon densities and saturation at high energies. This collider would be the first ever high-energy electron-nucleus collider and open up qualitatively new possibilities to study QCD in the nuclear environment. It would represent the natural next step after the high-luminosity fixed-target ep/eA experiments and the high-energy HERA ep collider. □

Appendices

Appendix A

The analytical expressions for the gluon splitting kernel $K_G^0(x)$ and $K_G^1(x)$ are given by:

$$K_G^0(x) = \sum_{i=1}^{N_f} e_i^2 8x^2(1-x) \tag{A.1}$$

$$\begin{aligned} K_G^1(x) = \Big[\sum_{i=1}^{N_f} e_i^2\Big] 16C_A x^2 & \left[\begin{array}{c} 4Li_2(x) - 2(1-x)lnxln(1-x) + 2(1+x)Li_2(-x) \\ +3ln^2x + 2(x-2)\zeta(2) + (1-x)ln^2(1-x) \\ +2(1+x)lnxln(1+x) + \dfrac{24+192x-317x^2}{24x}lnx \\ +\dfrac{1-3x-27x^2+29x^3}{3x^2}ln(1-x) \\ +\dfrac{-8+24x+501x^2-517x^3}{72x^2} \end{array}\right] \\ -16C_F x^2 & \left[\begin{array}{c} \dfrac{5+12x^2}{30}ln^2x - (1-x)ln(1-x) \\ +\dfrac{-2+10x^3-12x^5}{15x^3}[Li_2(-x) + lnxln(1+x)] \\ +2\dfrac{5-6x^2}{30}\zeta(2) + \dfrac{4-2x-27x^2-6x^3}{30x^2} \\ +\dfrac{(1-x)(-4-18x+105x^2)}{30x^2} \end{array}\right] \end{aligned} \tag{A.2}$$

Here the colour factors $C_A = 3$ and $C_F = \dfrac{4}{3}$ associated with the colour group SU(3). $Li_2(x)$ and $\zeta(2)$ are dilogarithmic function and Riemann Zeta function respectively.

The function $f(w)$ used in chapter 2 and 3 is defined as

$$f(w) = C_A w^2 \left[\begin{array}{c} 4Li_2(w) - 2(1-w)lnwln(1-w) + 2(1+w)Li_2(-w) \\ +3ln^2 w + 2(w-2)\zeta(2) + (1-w)ln^2(1-w) \\ +2(1+w)lnwln(1+w) + \frac{24+192w-317w^2}{24w}lnw \\ +\frac{1-3w-27w^2+29w^3}{3w^2}ln(1-w) + \frac{-8+24w+501w^2-517w^3}{72w^2} \end{array} \right]$$
$$-C_F w^2 \left[\begin{array}{c} \frac{5+12w^2}{30}ln^2 w - (1-w)ln(1-w) \\ +\frac{-2+10w^3-12w^5}{15w^3}[Li_2(-w) + lnwln(1+w)] \\ +2\frac{5-6w^2}{30}\zeta(2) + \frac{4-2w-27w^2-6w^3}{30w^2} \\ +\frac{(1-w)(-4-18w+105w^2)}{30w^2} \end{array} \right] \quad \text{(A.3)}$$

The analytical expressions of gluon co-efficient functions for F_L structure function are given by :

$$C^1_{L,g}(w) = 8N_f w(1-w) \quad \text{(A.4)}$$

$$\begin{aligned} C^2_{L,g}(w) \;\cong\; & N_f\{(94.74 - 49.20w)L_1^2 + 864.8w_1L_1 + 1161wL_1L_0 \\ & +60.06wL_0^2 + 39.66w_1L_0 - 5.333(w^{-1}-1)\} \end{aligned} \quad \text{(A.5)}$$

$$
\begin{aligned}
C^3_{L,g}(w) \;\cong\; & N_f\Big\{\Big(144L_1^4-\frac{47024}{27}L_1^3+6319L_1^2+53160L_1\Big)w_1+72549L_0L_1 \\
& +88238L_0^2L_1+(3709-33514w-9533w^2)w_1+66773wL_0^2 \\
& -1117L_0+45.37L_0^2-\frac{5360}{27}L_0^3-(2044.70w_1+409.506L_0)w^1\Big\} \\
& +N_f^2\Big\{\Big(\frac{32}{3}L_1^3-\frac{1216}{9}L_1^2-592.3L_1+1511wL_1\Big)w_1+311.3L_0L_1 \\
& +14.24L_0^2L_1+(577.3-729.0w)w_1+30.78wL_0^3+366.0L_0 \\
& +\frac{1000}{9}L_0^2+\frac{160}{9}L_0^3+88.5037w^{-1}w_1\Big\} \\
& +fl_{11}^gN_f^2\Big\{(-0.0105L_1^3+1.550L_1^2+19.72wL_1-66.745w \\
& +0.615w^2)w_1+\frac{20}{27}wL_0^4+\Big(\frac{280}{81}+2.260w\Big)wL_0^3-(15.40 \\
& -2.201w)wL_0^2-(71.66-0.121w)wL_0\Big\}. \qquad \text{(A.6)}
\end{aligned}
$$

In equation (A.5) and (A.6), $w_1 = 1-w$, $L_0 = lnw$, $L_1 = lnw_1$ and fl_{11}^g denote the charge factor which is defined as $fl_{11}^g = \dfrac{< e >^2}{< e^2 >}$.

The expression for gluon splitting function at small-x are written as :

$$
\begin{aligned}
P^1_{gg}(w) \;=\; & 2C_A\Big\{\frac{w}{(1-w)_+}+\frac{1-w}{w}+w(1-w)\Big\} \\
& +\delta(1-w)\frac{(11C_A-4N_fT_R)}{6}, \qquad \text{(A.7)}
\end{aligned}
$$

$$
\begin{aligned}
P^2_{gg}(w) \;=\; & \frac{12C_FN_fT_R-46C_AN_fT_R}{9w}+N_fT_R\Big\{\frac{-61}{9}C_F+\frac{172}{27}C_A\Big\} \\
& +C_A^2\Big\{\frac{1643}{54}-\frac{22}{3}\xi(2)-8\xi(3)\Big\}, \qquad \text{(A.8)}
\end{aligned}
$$

$$
P^3_{gg}(w) = \frac{224C_AT_RN_f}{27w^2}(-C_A), \qquad \text{(A.9)}
$$

where the Casimir operators of color group $SU(3)$ are defined as $C_A = 3$, $C_F = \dfrac{4}{3}$ and $T_R = \dfrac{1}{2}$.

The expressions for gluon co-efficient function for F_2 structure function in LO, NLO and NNLO are given by :

$$C^1_{2,g}(w) = N_f\{(2-4ww_1)(L_1-L_0)-2+16ww_1\}, \tag{A.10}$$

$$\begin{aligned} C^2_{2,g}(w) &= \{(6.445+209.4(1-w))L_1^3-24L_1^2+(149w^{-1}-1483)L_1 \\ &+L_1L_0(-871.8L_1-724.1L_0)+5.319L_0^3-59.48L_0^2-284.8L_0 \\ &+11.90w^{-1}+392.4-0.28\delta(1-w) \end{aligned} \tag{A.11}$$

and

$$\begin{aligned} C^3_{2,g}(w) &= N_f\Big\{\frac{966}{81}L_1^5-\frac{1871}{18}L_1^4+89.31L_1^3+979.2L_1^2-2405L_1+1372x_1L_1^4 \\ &-15729-310510x+331570x^2-244150xL_0^2-253.3xL_0^5 \\ &+L_0L_1(138230-237010L_0)-11860L_0-700.8L_0^2-1440L_0^3 \\ &+\frac{4951}{162}L_0^4-\frac{134}{9}L_0^5-x^{-1}(6362.54-932.089L_0)+0.625\delta(x_1)\Big\} \\ &+N_f^2\Big\{\frac{131}{81}L_1^4-14.72L_1^3+3.607L_1^2-226.1L_1+4.762-190x \\ &-818.4x^2-4019xL_0^2-L_0L_1(791.5+4646L_0)+739L_0+418L_0^2 \\ &+104.3L_0^3+\frac{809}{81}L_0^4+\frac{12}{9}L_0^5+84.423x^{-1}\Big\}+fl^g_{11}N_f^2\Big\{3.211L_1^2 \\ &+19.04xL_1+0.623x_1L_1^3-64.47x+121.6x^2-45.82x^3 \\ &-xL_0L_1(31.68+37.24L_0)+11.27x^2L_0^3-82.40xL_0-16.08xL_0^2 \\ &+\frac{520}{81}xL_0^3+\frac{20}{27}xL_0^4\Big\} \end{aligned} \tag{A.12}$$

respectively.

Appendix B

In the LO analysis, the heavy quark co-efficient functions used in chapter 6 are written as

$$C_{2,g}^{(0)}(w,\zeta) = \frac{1}{2}\Big([w^2+(1-w)^2 4w\zeta(1-3w)-8\zeta^2 w^2]ln\frac{1+\beta}{1-\beta} + \beta[-1+8w(1-w)-4z\zeta(1-w)]\Big) \quad \text{(B.1)}$$

and

$$C_{L,g}^{(0)}(w,\zeta) = -4w^2\zeta ln\frac{1+\beta}{1-\beta} + 2\beta w(1-w), \quad \text{(B.2)}$$

where $\beta^2 = 1-\frac{4z\zeta}{1-z}$. In NLO, we have used the compact form of the co-efficient functions in high energy regime ($\zeta << 1$). The NLO co-efficient functions $C_{k,g}^{(1)}$ and $\overline{C}_{k,g}^{(1)}$ are given by

$$C_{k,g}^{(1)} = \frac{8}{3}C_A e_h^2 ln^2(Q^2/m_h^2) \quad \text{(B.3)}$$

and

$$\overline{C}_{k,g}^{(1)} = \frac{16}{3}C_A e_h^2 ln^2(Q^2/m_h^2), \quad \text{(B.4)}$$

where $k = 2, L$ and $h = c, b$. Here the colour factor $C_A = 3$, e_h is the charge of the heavy quark and m_h is the mass of the heavy quark. $\square$

List of publications

Papers published/ accepted for publication:

1. Baruah, N., Nath, N. M. and Sarma, J. K. "Solution of Evolution Equation for Longitudinal Structure Function F_L up to next-to-next-to leading order and its t-evolution at small-x", *Int. J. Theor. Phys.* **52** (7), 2464–2476, 2013.

2. Baruah, N. and Sarma, J. K. "Evolutions of Longitudinal Structure Function F_L up to Next-to-Next-to-Leading Orders at Small-x", *Int. J. Theor. Phys.* **53** (7), 2492–2504, 2014.

3. Baruah, N., Das, M. K. and Sarma, J. K."Longitudinal Structure Function F_L of Proton from Regge Like Behaviour of Structure Function at small-x", *Few. Body. Syst.* **55** (11), 1061–1071, 2014.

4. Baruah, N., Das, M. K. and Sarma, J. K. "Longitudinal Structure Function F_L of Proton from Regge Like Behaviour of Gluon Distribution Function up to next-next-to-leading order at small-x", *Eur. Phys. J. Plus* **129** (10), 229-1–10, 2014.

5. Baruah, N., Das, M. K. and Sarma, J. K. "Analysis of small-x behaviour of Longitudinal and heavy flavour structure functions of Proton", *Int. J. Theor. Phys.* **54** (10), 3596-3611, 2015.